STRUCTURE-GUIDED DESIGN, SYNTHESIS, X-RAY CRYSTALLOGRAPHY, AND BIOCHEMICAL AND IN VIVO EVALUATION OF NOVEL SERIES OF VIRAL 3CL PROTEASE INHIBITORS OF NOROVIRUS (NV) AND MIDDLE EAST RESPIRATORY DISTRESS SYNDROME CORONAVIRUS (MERS-COV)

A Dissertation by

Anushka Chathuranga Galasiti Kankanamalage

Bachelor of Science University of Colombo, Sri Lanka, 2010

Submitted to the Department of Chemistry
and the Faculty of the Graduate School of
Wichita State University
in partial fulfilment of
the requirements for the degree of
Doctor of Philosophy

July 2017

© Copyright 2017 by Anushka Chathuranga Galasiti Kankanamalage

All Rights Received

STRUCTURE-GUIDED DESIGN, SYNTHESIS, X-RAY CRYSTALLOGRAPHY, AND BIOCHEMICAL AND IN VIVO EVALUATION OF NOVEL SERIES OF VIRAL 3CL PROTEASE INHIBITORS OF NOROVIRUS (NV) AND MIDDLE EAST RESPIRATORY DISTRESS SYNDROME CORONAVIRUS (MERS-COV)

The following faculty members have examined the final copy of this dissertation for form and content, and recommend that it be accepted in partial fulfillment of the requirements for the degree of Doctor of Philosophy with a major in Chemistry.

William C. Groutas, Committee Chair

Douglas S. English, Committee Member

James G. Bann, Committee Member

Maojun Gong, Committee Member

Li Yao, Committee Member

Accepted for the College of Liberal Arts and Sciences

Ron Matson, Dean

Accepted for the Graduate School

Dennis Livesay, Dean

DEDICATION

To My Beloved Parents, Sisters

&

My Mentor Distinguished Professor William C. Groutas

First, there is a mountain, then there is no mountain, then there is.

ACKNOWLEDGEMENTS

It is a genuine pleasure to express my deepest appreciation to my mentor, philosopher, and advisor, distinguished professor William C. Groutas. His dedication and keen interest and above all his overwhelming attitude to help me had been solely and mainly responsible for completing my work. His patience, motivation, enthusiasm, meticulous scrutiny and scholarly advice have constantly and continually inspired me in my most difficult time. Without his guidance and persistent help, this dissertation would not have been possible.

I would like to express my gratitude to my committee members Dr. Douglas S. English, Dr. James G. Bann, Dr. Maojun Gong and Dr. Li Yao for their advice and support.

I owe a deep sense of gratitude to Dr. Keyong-Ok Chang and Dr. Yunjeong Kim, Department of Diagnostic Medicine and Pathology, Kansas State University, for their kind help and collaboration in all my projects (cell-based and small animal studies).

Sincere thanks to Dr. Scott Lovell, The University of Kansas (X-ray crystallography), Linda Saif, The Ohio State University (large animal studies), Dr. Jerry Lushington, LiS Consulting (computational and modeling studies), and Dr. Terry Bowling and Dr. Mitchell Butler, Microbiotix Inc. (phramcokinetic studies) for their help.

I would like to extend my appreciation to all of my past and present colleagues in my research group, all faculty, staff, friends and colleagues of the Department of Chemistry, Wichita State University.

Finally, but not least, recognition goes out to my beloved parents, sisters, brother-in-laws, my lovely nephews and nieces and my girlfriend for their love and encouragement during my graduate studies.

ABSTRACT

Norovirus infection constitutes the primary cause of acute viral gastroenteritis. There are currently no vaccines or norovirus-specific antiviral therapeutics available for the management of norovirus infection. Norovirus 3C-like protease is essential for viral replication, consequently, inhibition of this enzyme is a fruitful avenue of investigation that may lead to the emergence of anti-norovirus therapeutics.

This dissertation describes the structure-based discovery and optimization of a novel series of dipeptidyl inhibitors of norovirus 3C-like protease using X-ray crystallography, iterative structure-activity relationship (SAR) studies, enzyme and cell-based replicon system studies, as well as efficacy studies using small and large animal models. In addition, based on the hypothesis that the S_4 subsite of the protease may provide an effective means of designing potent and cell permeable inhibitors, a structure-guided approach was used to identify lead compounds and validate the aforementioned hypothesis. A lead compound identified during the course of these studies was shown to have efficacy in the murine model of norovirus infection. Furthermore, multiple series of novel prodrugs (ester and carbamate) of transition state latent inhibitors and transition state mimics with optimal pharmacological activity and pharmacokinetics were designed, synthesized and evaluated. A series of norovirus 3CL protease inhibitors that embody an α-ketophosphonate warhead is also reported for the first time. Finally, a serendipitous discovery resulted in the identification of a feline infection peritonitis virus (FIPV) inhibitor shown in clinical trials to be effective in the treatment of FIP.

TABLE OF CONTENTS

Chapter **Page**

1. **CHAPTER I** (Introduction)…… 1-2

1.1 Norovirus…… 2
- 1.1.1 Norovirus Epidemiology ……2-4
- 1.1.2 Symptoms Risk Factors, Modes and Setting of Transmission …... 4-5
- 1.1.3 Prevention, Control and Prophylaxis ……....5-6
- 1.1.4 Norovirus Genetic Diversity ……..6-9
- 1.1.5 Norovirus Genome ……9-11
- 1.1.6 Norovirus Replication Cycle ……..11-14
- 1.1.7 Norovirus Biology and Pathogenesis ……..14-15
  - 1.1.7.1 Norovirus Binding and Entry …….…….. 15-16
- 1.1.8 Norovirus 3CL Protease ……16-18
- 1.1.9 Substrate Specificity of Norovirus 3CLpro …….. 18-19
- 1.1.10 Norovirus Active Site Mechanism of Action (MoA) …….. 19-21
- 1.1.11 Norovirus Therapeutics …….…… 22
  - 1.1.11.1 3CL Protease Inhibitors……..……..... 22-23
  - 1.1.11.2 RdRp Inhibitors ……..…. 23
  - 1.1.11.3 Entry Blockers ……..……23-24
  - 1.1.11.4 Host Factors ……..…… 24
  - 1.1.11.5 Norovirus Drugs in Clinical Development …..…….. 24-25

1.2 Middle East Respiratory Syndrome Coronavirus (MERS-CoV) ..…....…… 26
- 1.2.1 MERS-CoV Epidemiology ……..…….. 26-27
- 1.2.2 Symptoms, Risk Factors, Modes and Setting of Transmission... 27-29
- 1.2.3 Prevention, Control and Prophylactic ……... 29
- 1.2.4 MERS-CoV Genetic Diversity ……..……... 29-30
- 1.2.5 MERS-CoV Genome and Replication Cycle ……. 31-34
- 1.2.6 MERS-CoV 3CL protease and Substrate Specificity of 3CLpro...34-36
- 1.2.7 MERS-CoV Therapeutics ……. 36-37

1.3 Types of Enzyme Inhibitors ……..…… 38-40
- 1.3.1 Transition State Inhibitors and Transition State Mimics……..... 41-43

1.4 Research Objectives ……..…… 44-45

2. **CHAPTER II** (Structure-guided design and optimization of dipeptidyl inhibitors of norovirus 3CL protease. structure-activity relationships and biochemical, X-ray crystallographic, cell-based, and in vivo studies)

2.1 Inhibitor Design Rationale …….. 46-49
2.2 Chemistry …….. 49-50
2.3 Experimental Section…… 51
- 2.3.1 General ……51-67
- 2.3.2 FRET Protease Assays ……..…… 68

TABLE OF CONTENTS (continued)

Chapter **Page**

2.3.3 Cell-Based Inhibition Assays 69
2.3.4 X-ray Crystallographic studies 70-71
2.3.5 Structure Solution and Refinement 71
2.3.6 Studies with murine norovirus (MNV) 72
2.3.7 Animal Studies 73
2.4 Results and Discussion 74-77
2.4.1 X-ray Crystallography 78-82
2.4.2 Animal Studies 82-83
2.5 Conclusions 84

3. CHAPTER III (Structure-based exploration and exploitation of the S_4 subsite of norovirus 3CL protease in the design of potent and permeable inhibitors)

3.1 Inhibitor Design Rationale 85-86
3.2 Chemistry 86-87
3.3 Experimental Section 88
3.3.1 General 88-116
3.3.2 FRET Protease Assays 117
3.3.3 Cell-Based Inhibition Assays 117
3.3.4 Nonspecific Cytotoxicity Effects 117
3.3.5 X-ray Crystallographic Studies 117-118
3.3.6 Structure Solution and Refinement 118
3.4 Results and Discussion 119-131
3.5 Conclusions 132

4. CHAPTER IV (Design, synthesis and evaluation of novel prodrugs of transition state inhibitors of norovirus 3CL protease)

4.1 Inhibitor Design Rationale 133-135
4.2 Chemistry 135-136
4.3 Experimental Section 137
4.3.1 General 137-146
4.3.2 FRET Protease Assays 147
4.3.3 Cell-Based Inhibition Assays 148
4.3.4 Cytotoxicity Studies 148
4.3.5 Liver Microsomes Stability 148
4.3.6 Plasma Protein Binding 149
4.3.7 High Performance Liquid Chromatography (HPLC) 149
4.4 Results and Discussion 150-152
4.4.1 Hydrolysis of Ester Prodrugs to the Aldehyde in Mouse and Human Serum 153-155

TABLE OF CONTENTS (continued)

Chapter **Page**

4.4.2 Cytotoxicity 156
4.4.3 Liver Microsomes Stability 157-158
4.4.4 Plasma Protein Binding 159
4.5 Conclusions 160

5. CHAPTER V (Peptidyl ketophosphonate inhibitors of norovirus 3CL protease: SAR, biochemical, structural and in vitro cell-based studies)

5.1 Inhibitor Design Rationale 161-162
5.2 Chemistry 162-163
5.3 Experimental Section 164
5.3.1 General 164-171
5.3.2 FRET Protease Assays 172
5.3.3 Cell-Based Inhibition Assays 172
5.3.4 Nonspecific Cytotoxicity Effect 172
5.4 Results and Discussion 173-174
5.5 Conclusions 175

6. CHAPTER VI (Conclusions)..... 176-177

REFERENCES 178-194

LIST OF FIGURES

Figure **Page**

1.1 Norovirus Outbreaks in U.S. 2009-2012 ..……..……..……...3

1.2 Classification of *Caliciviridae* Family ……..……..…… 8

1.3 Classification of Norovirus Genogroups ……..……..…. 9

1.4 Norovirus Genome ……..……..…….. 10

1.5 The Replication Cycle of Human Norovirus ……..……..…… 13

1.6 Model of Norovirus Intestinal Infection ……..……..…….. 16

1.7 Norovirus X-ray Crystal Structure ……..……..……... 17

1.8 General Substrate and Substrate Binding Sites for Proteases……..……..… 18

1.9 Cysteine 3CL Protease Enzyme Mechanism ……..……..……... 21

1.10 A Map of the Countries Where Laboratory-Confirmed Cases of MERS-CoV Infection ……..……..……. 27

1.11 Reservoirs and Transmission of MERS-CoV ……..……..……..… 28

1.12 Classification of Subfamily Coronavirinae ……..……..… 30

1.13 MERS-CoV Genome ……..……... 32

1.14 The Replication Cycle of MERS-CoV ……..…. 33

1.15 Crustal Structure of the MERS-CoV RBD-DPP4 Receptor Complex ……..…. 35

1.16 Kinetics of Competitive Inhibitors ……..……..…….. 39

1.17 Dixon Plots for Determination of K_i …….. ….…… 40

1.18 Transition State for the Hydrolysis of a Peptide Bond ……..……..…… 42

1.19 Transition State Tetrahedral Adduct ……..……..…… 42

2.1 Interaction of a Cysteine Protease (E-Cys-SH) with a Peptidyl Transition State Inhibitor ……..……..…… 46

LIST OF FIGURES (continued)

Figure **Page**

2.2 Hydrogen Bonding Interactions Between the Inhibitor and Chain B for NV 3CLpro ……..…….... 48

2.3 Residues Spanning Ala159-Lys162 Located Near the Benzyl Ring of Precursor Aldehyde of Inhibitor ***44*** ……..... 49

2.4 $F_o - F_c$ Map of Compound ***17*** Bound to NV 3CLpro Contoured at 3σ …….... 78

2.5 Hydrogen Bond Interactions Between NV 3CLpro Compound ***17*** ……. 79

2.6 Surface Representation of Compound ***17*** Bound to NV 3CLpro …….……. 80

2.7 In vivo Efficacy Data for MNV …….. 83

3.1 $F_o - F_c$ Omit Map of Inhibitor ***7l*** ……..……..…….. 122

3.2 Electrostatic Surface Representation of NV 3CLpro and Inhibitor ***7l*** ……..... 123

3.3 Hydrogen Bond Interactions Between NV 3CLpro and Inhibitor ***7l*** …….. 124

3.4 Surface Representation of NV 3CLpro:***7l*** …..…….. 125

3.5 $F_o - F_c$ Omit Map of Inhibitor ***7m*** ……..……126

3.6 Surface Representation of NV 3CLpro:***7m*** ……..……..…….. 127

3.7 Superposition of Inhibitor ***7l*** and ***7m*** …… 128

3.8 Hydrogen Bond Interactions (dashed lines) for NV 3CLpro:***7m*** ……..…….. 128

3.9 Electrostatic Surface Representation of NV 3CLpro Showing the Aliphatic Chain of Inhibitor ***7m*** Positioned in a Hydrophobic S_4 Pocket……..…….. 129

4.1 General Structures of Prodrugs (I-II) ……..……..…….. 134

4.2 Postulated Mechanism of Action of Prodrugs (I-II) ……..……..…….. 134

4.3 Structures of Compounds ***24-26*** ……..…… 153

4.4 Time-Dependent Hydrolysis of Prodrugs ***9, 10*** and ***11*** and Conversion to the Aldehyde form in 55% Human Serum …..……..……..…… 155

LIST OF FIGURES (continued)

Figure **Page**

5.1 General Structure (I) of 3CL Protease Inhibitor …….…..…….…. 161

5.2 Transition State Tetrahedral Adduct of α-Ketophosphonates……162

LIST OF TABLES

Table **Page**

1.2 Substrate Specificity of Norovirus 3CLpro …….…….. 19

1.3 Substrate Specificity of MERS-CoV 3CLpro ……..……... 36

1.4 Possible Drug Candidate for Treatment of MERS-CoV Infection ……..……... 37

2.1 Inhibitory Activity of Compounds ***13−44*** against NV 3CLpro ……..….. 76

2.2 Selectivity of Selected Compounds Against a Panel of Proteases ……..…… 77

2.3 Crystallographic Data for NV 3CLpro:Inhibitor Structures ……..…... 81-82

3.1 Inhibitory Activity of Compounds ***6a-m*** and ***7a-m*** against NV 3CLpro ……... 120

3.2 Inhibitory Activity of Compounds ***11a-c*** and ***12a-c*** against NV 3CLpro …..... 121

3.3 Crystallographic Data for NV 3CL Protease-Inhibitor Structures ……..... 130-131

4.1 Inhibitory Activity of Compounds ***1-17*** Against NV 3CLpro ……..…..... 151

4.2 Inhibitory Activity of Compounds ***18-23*** Against NV 3CLpro ……...….. 152

4.3 Hydrolysis of Compounds in Mouse or Human Serum …..……..…….. 154

4.4 Cytotoxicity and Selectivity of Compounds ***9-11*** and ***24-26*** ……..…… 156

4.5 Metabolic Stability of Compounds ***9-11*** and ***24-26*** in Human and Mouse liver microsomes ……..……..…… 157

4.6 Plasma Protein Binding of Compounds ***9-11*** and ***24-26*** ...……..……..…… 159

5.1 Inhibitory Activity of Compounds ***9a-9h*** Against NV 3CLpro ……...….. 174

LIST OF SCHEMES

Scheme **Page**

2.1 Synthesis of Inhibitors ***13-44***. ……..……..…..... 50

3.1 Synthesis of Inhibitors ***16a-m*** and ***7a-m*** …… 87

3.2 Synthesis of Inhibitors ***11a-c*** and ***12a-c*** …… 87

4.1 Synthesis of Inhibitors ***1-8*** and ***18-24*** ……..…... 136

4.2 Synthesis of Inhibitors ***9-17*** and ***21-23*** ……..…... 136

5.1 Synthesis of Inhibitors ***9a-h*** ……...…..…. 163

COMMON ABBREVIATIONS

µM	Micromolar
3CLpro	3C-like Protease
AIDS	Acquired Immunodeficiency Syndrome
Ala	Alanine
Boc	tert-Butoxycarbonyl
C_2H_5OH	Ethanol
CC_{50}	Cytotoxic Concentration (in 50% cells)
CDC	Centers for Disease Control and Prevention
$CDCl_3$	Deuterated Chloroform
CH_3CN	Acetonitrile
CH_3OH	Methanol
Cha	Cyclohexyl alanine
Cys	Cysteine
d	Doublet
DCM	Dichloromethane
DDT	Dithiothreitol
DIEA	N,N-Diisopropylethylamine
DMEM	Dulbecco’s Minimum Essential Medium
DMF	N,N-Dimethylfornamide
DMSO	Dimethyl Sulfoxide
ds	double strand

EC_{50}	Half Maximal Effective Concentration
EDCI	1-Ethyl-3-(3-dimethylaminopropyl)carbodiimide
EDTA	Ethylenediaminetetraacetic acid
ER	Endoplasmic Reticulum
ESI	Electron Spray Ionization
EtOAc	Ethyl Acetate
FCV	Feline Calicivirus
FDA	Food and Drug Administration
FRET	Fluorescence Resonance Energy Transfer
FUT	Fucosyltransferase
GI	Genogroup I
GII	Genogroup II
GIII	Genogroup III
GIV	Genogroup IV
Gln	Glutamine
Glu	Glutamic acid
Gly	Glycine
GV	Genogroup V
GVI	Genogroup VI
GVII	Genogroup VII
HBGA	Histo-Blood Group Antigen
HCl	Hydrochloric acid
hCoV	Human Coronavirus

His	Histidine
HIV	Human Immunodeficiency Virus
HNE	Human Neutrophil Elastase
HOAc	Acetic acid
HOBt	Hydroxybenzotriazole
HPLC	High Performance Liquid Chromatography
HRMS	High Resolution Mass Spectrometry
HT	High Throughput
IACUC	Institutional Animal Care and Use Committee
IC_{50}	Half Maximal Inhibitory Concentration
INFs	Interferons
K_2CO_3	Potassium Carbonate
kDa	kilo Dalton
K_m	Michaelis-Menten constant
LC/MS	Liquid Chromatography/ Mass Spectroscopy
LCT	Liquid Chromatography of Time of Flight
Leu	Leucine
Leu	Leucine
$LiBH_4$	Lithium Borohydride
lle	Isoleucine
Lys	Lysine
m	Multiplet
MERS-CoV	Middle East Respiratory Syndrome Coronavirus

MHz	Mega hertz
mL	Milliliter
mmol	Millimolar
MNV	Murine Norovirus
MoA	Mechanism of Action
MOI	Multiplicity of Infection
mp	Melting Point
M^{pro}	Main protease
NaCl	Sodium chloride
NADPH	Nicotinamide Adenine Dinucleotide Phosphate (reduced form)
$NaHCO_3$	Sodium bicarbonate
$NaHSO_3$	Sodium Bisulfite
nM	Nanomolar
NMR	Nuclear Magnetic Resonance Spectroscopy
NS	Non-Structural
NTPase	Nucleoside Triphosphatase
NV	Norovirus
ORF	Open Reading Frame
PDB	Protein Data Bank
PEG	Polyethylene Glycol
Phe	Phenyl alanine
PK	Pharmacokinetics
PLpro	Papain-like Protease

Pol	Polymerase
pp	Polyprotein
Pro	Proline
Pro	Protease
RB	Round Bottom
RBD	Receptor Binding Domain
RdRp	RNA dependent RNA polymerase
RNA	Ribonucleic acid
RT	Room Temperature
RT-PCR	Reverse Transcription Polymerase Chain Reaction
s	Singlet
SAR	Structure-Activity Relationship
SARS	Severe Acute Respiratory Syndrome
SI	Selectivity Index (SI) ($SI=CC_{50}/IC_{50}$)
$SOCl_2$	Thionyl chloride
t	Triplet
$TCID_{50}$	Tissue Culture Infectious Dose (Half Maximal)
TEA	Triethylamine
THF	Tetrahydrofuran
Thr	Threonine
TLC	Thin Layer Chromatography
TS	Transition State
UV	Ultraviolet

Val	Valine
V_{max}	Maximum Velocity
VP	Viral Protein
VPg	Viral Protein Genome-linked
WHO	World Health Organization
XDS	X-ray Diffraction Spectroscopy

CHAPTER I

INTRODUCTION

The human body is a very complex and thriving ecosystem that contains trillions of microbes called normal flora. Usually these microbes are limited to certain areas of the body, including skin, mouth, large intestine and vagina. Normal microbial inhabitants are a threat to health only when the immune system is weakened or when they invade generally sterile parts of the body. In contrast, pathogens do not require the host to be immunocompromised or injured to initiate infection. There are four different pathogenic agents that cause disease in humans: viruses, bacteria, fungi, and parasites. Defense against these pathogens is mediated by both innate and specific immunity.

Viruses are the smallest pathogens comprised of capsules containing genetic material. They are generally contagious and are the causative agents of many common viral diseases, including influenza, HIV, hepatitis C, and many others. Mosquito-borne viruses, such as the Dengue, West Nile, and Zika viruses, are a particular worldwide health concern. The World Health Organization estimates that ~390 million cases of Dengue infection occur every year, many of them progressing to severe illness and complications, such as hemorrhagic fever. Emerging viral diseases, such as Severe Acute Respiratory Syndrome (SARS) and Middle East Respiratory Syndrome (MERS) are also a potential threat and are associated with high mortality.

Viral diseases cannot be cured by antibiotics, which can only cure bacterial diseases and infections. Moreover, some viral diseases, such as norovirus infections, are generally self-limiting in healthy individuals, lasting a few days. Finally, norovirus infection

can lead to serious and potentially life-threatening complications in individuals with co-morbidities, a suppressed or compromised immune system, and the very young and elderly.

1.1 Noroviruses

Noroviruses are the most common cause of nonbacterial epidemic gastroenteritis in humans. They are highly contagious and can infect anyone. Noroviruses belong to the family *Caliciviridae* and are subdivided into seven genogroups (GI to GVII). Noroviruses in genogroups GI, GII, and GIV are the primary cause of human acute gastroenteritis, with the GII.4 variants being more prevalent and the cause most norovirus outbreaks.[1-4]

1.1.1. Norovirus Epidemiology

A significant biological feature of noroviruses is their genetic diversity and rapid, immune selection-driven evolution. There is a lack of studies from developing countries on the epidemiology and molecular diversity of norovirus. Yet, studies in high incidence settings in the developing world may be crucial for understanding and anticipating strain emergence, and for predicting potential strains for vaccine development.[5]

Globally, norovirus infection is associated with a high economic burden, resulting in $4.2 billion in societal costs per year. In developing countries, norovirus disease results in >70,000 deaths amongst children <5 years and a societal cost of $39.8 billion, compared to $20.4 billion for all other age groups combined. Based on both age and region, costs for norovirus illness varies and is highest among adults ≥ 55 years.[6]

Norovirus infection has received considerably less attention in comparison to other viruses. There are several possible reasons for this: first, it has been challenging to estimate disease burden, in part because of sub-optimal diagnostic tests and their limited

availability; secondly, some norovirus cases are associated primarily with cruise ships and healthcare facilities[7-8] and of the estimated 20 million annual cases of norovirus infection in the United States, only a small fraction (<1%) are associated with reported outbreaks (Figure 1.1);[8-9] thirdly, although norovirus infection is perceived to only cause self-limiting, mild gastroenteritis that rarely requires medical care, there are an estimated 70000 norovirus-associated deaths among children <5 years annually in developing countries.[10]

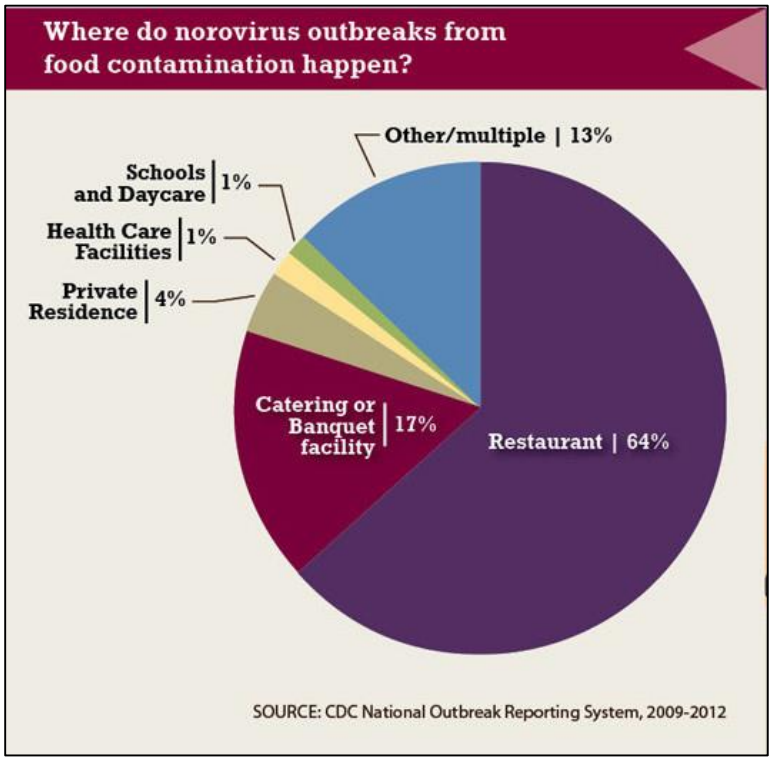

Figure 1.1 Norovirus outbreaks in U.S. 2009-2012 (reproduced from ref 7).

To date, economic studies related to norovirus infection have quantified the impact of several outbreaks in hospital settings and community cases, and have determined the cost-effectiveness of a hypothetical norovirus vaccine in high income countries (including

the Unites States, Switzerland, and Scotland). Yet there has not been a systematic international assessment of the cost of norovirus infection.[5]

1.1.2. Symptoms, Risk Factors, and Modes and Setting of Transmission

As stated earlier, for most people norovirus illness is self-limiting with diarrhea, nausea and vomiting resolved in 1-3 days,[8] however, children, older people (≥ 55 years) and immunocompromised patients develop several complications. If symptoms are severe, dehydration can occur necessitating immediate medical attention. Mild dehydration is common and can easily be reversed by drinking lots of fluids. Symptoms in adults may be different from the symptoms in children. Young children and babies may not complain of thirst but may appear listless or lethargic as they become dehydrated. Symptoms may be more severe in debilitated, elderly patients or pregnant women.[8]

Individuals with type O phenotype have been found to be most susceptible to norovirus infection. Those with B and AB phenotypes have decreased risk of infection. When B and AB phenotypes are infected, they are more likely to be asymptomatic, however, they are still contagious and can spread the virus to others.[11]

Human noroviruses (HuNoV) are highly contagious and humans are the only known reservoir. They can spread by several modes of transmission, such as, fecal-oral and vomit-oral pathways by four general routes: direct person-to-person, foodborne, waterborne or through environmental fomites. Since humans are the only known source of all human norovirus infections, all transmission is ultimately person-to-person.[12]

The strongest risk factors for community diseases is contact with an infected person. Foreign travel is also a risk factor,[13] with increased risk likely attributable to changes in behavior while traveling or exposure to a different spectrum of norovirus

strains. Risk factors data on endemic disease in developing countries is extremely limited.[13-15]

The explosive nature of some NV outbreaks in which a large number of persons become ill within 24-48 h, indicates that infection is often acquired from a common source. This was suggested in the original norovirus outbreak, but a common-source exposure could not be identified.[16] NV outbreaks have been reported in a variety of settings uniquely suited to areas of close living quarters, such as shared dining facilities, hospitals, nursing homes, schools, day care settings, military training centers and fields of operation, cruise ships and resorts.[16] In highly developed countries, healthcare facilities, including nursing homes and hospitals, are the most common settings of norovirus outbreaks. These outbreaks are highly disruptive and costly to health services.[17]

The lower incidence of disease from food, water and environmentally-transmitted disease, with a decreasing proportion of disease transmitted directly from person-to-person in higher income settings is coincident with improved sanitation and hygiene.[18] In contrast, individuals living in poor sanitation and hygiene settings likely have more exposure to norovirus through various routes.[19]

1.1.3. Prevention, Control and Prophylaxis

HuNoVs are one of the major causes of food borne gastroenteritis. They are highly contagious with a low infectious inoculum of <100 viral particles.[20] Noroviruses are able to survive in water and are relatively resistant to chlorination.[20] Thus, it is important to identify the causative agents involved in an acute gastroenteritis outbreak. Effective hand washing procedures are essential for the prevention of norovirus spread and for contamination of food. Fecal contamination of large body reservoirs of water used for

drinking or recreational activities such as swimming pools may serve as a prime source of an outbreak. Ingestion of inadequately cleaned and cooked shellfish and fresh salads from washing in contaminated water or from food handlers with symptomatic or asymptomatic norovirus infection are often implicated in large foodborne outbreaks.[20,22] Alcohol-based sanitizers are more popular in healthcare sectors, however, they often have limited efficacy against noroviruses, suggesting a risk of norovirus outbreaks in hospitals, although this is currently controversial.[23] Noroviruses remain viable on contaminated surfaces for extended periods of time and can transfer between surfaces with relative ease.[23] Therefore, it is of vital importance to have effective decontamination of norovirus-contaminated surfaces. The CDC recommends decontamination with a dilute solution of sodium hypochlorite (bleach) in the home. However, for the decontamination of larger areas following an outbreak newer approaches, such as the use of hydrogen peroxide vapor, are under investigation.[24]

In summary, the prevention and control of spread of norovirus infection requires appropriate precautions for containing and slowing norovirus outbreaks, such as hand hygiene with use of soap and water before and after contact with patients and/or inanimate objects that can be contaminated. Common control procedures during outbreaks include quarantining of infected individuals and enhanced environmental decontamination.[23] There are no commercially available prophylactics against noroviruses and glycosylated hydrogel is the only one strategy currently being explored.[25]

1.1.4. Norovirus Genetic Diversity

Norovirus belongs to the *Caliciviridae* family and is a diverse group of non-enveloped, icosahedral viruses that possess a linear, positive-sense, single-stranded

RNA (sssRNA) viruses that can infect a wide range of species.[16] The virus family is divided into at least five genera: *Lagovirus*, *Vesivirus*, *Nebovirus*, *Sapovirus*, and *Norovirus*, and an additional four genera, *Recovirus*, *Valovirus*, *Nacovirus*, and *Bavovirus* have been proposed (Figure 1.2).[26,27]

The major medical pathogens in the family are the noroviruses and sapoviruses, which cause acute gastroenteritis. Important veterinary pathogens include vesiviruses such as feline calicivirus (FCV), which causes a respiratory disease in cats, and lagoviruses such as rabbit hemorrhagic disease in rabbits.[16]

As mentioned earlier, noroviruses are subdivided into seven genogroups (GI to GVII). Human noroviruses are genetically diverse, and three distinct groups (GI, GII, and GIV) contain a prototype human norovirus (Figure 1.3).[28,29] Norovirus genogroup GII.4 has caused the majority of norovirus outbreaks and sporadic cases worldwide since the mid-1990s. Every 2-3 years this genotype evolves with new GII.4 strains by replacing previously dominant strains, a process driven by evasion of immunity in the human population.[5]

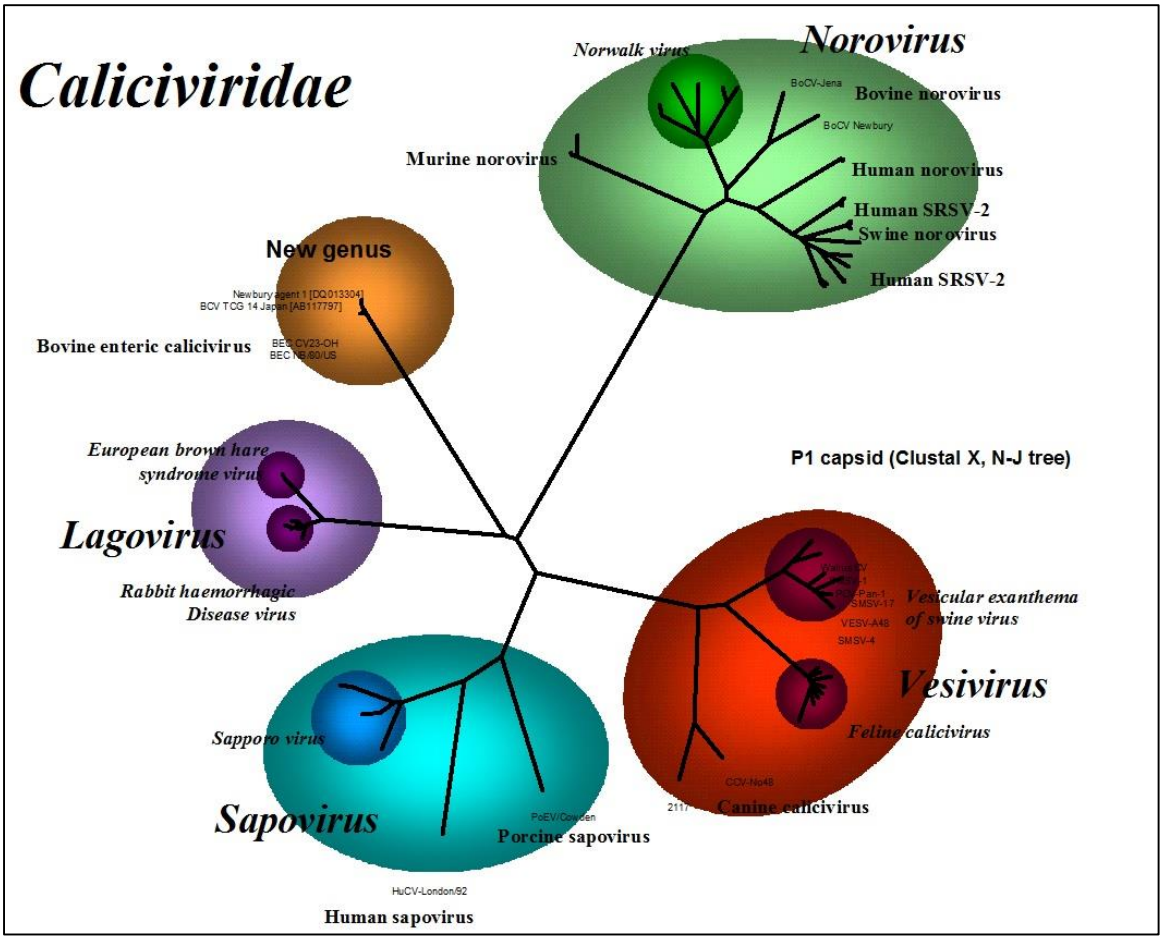

Figure 1.2 Classification of the Caliciviridae family.
(reproduced from Knowles, N.J. http://www.caliciviridae.com.)

Evolution of norovirus GII.4 strain and emergence of new epidemic strains is primarily driven by mutation in the P2 domain of ORF2, which is the domain most exposed to the host cells via the hypervariable region of the capsid.[30-33]

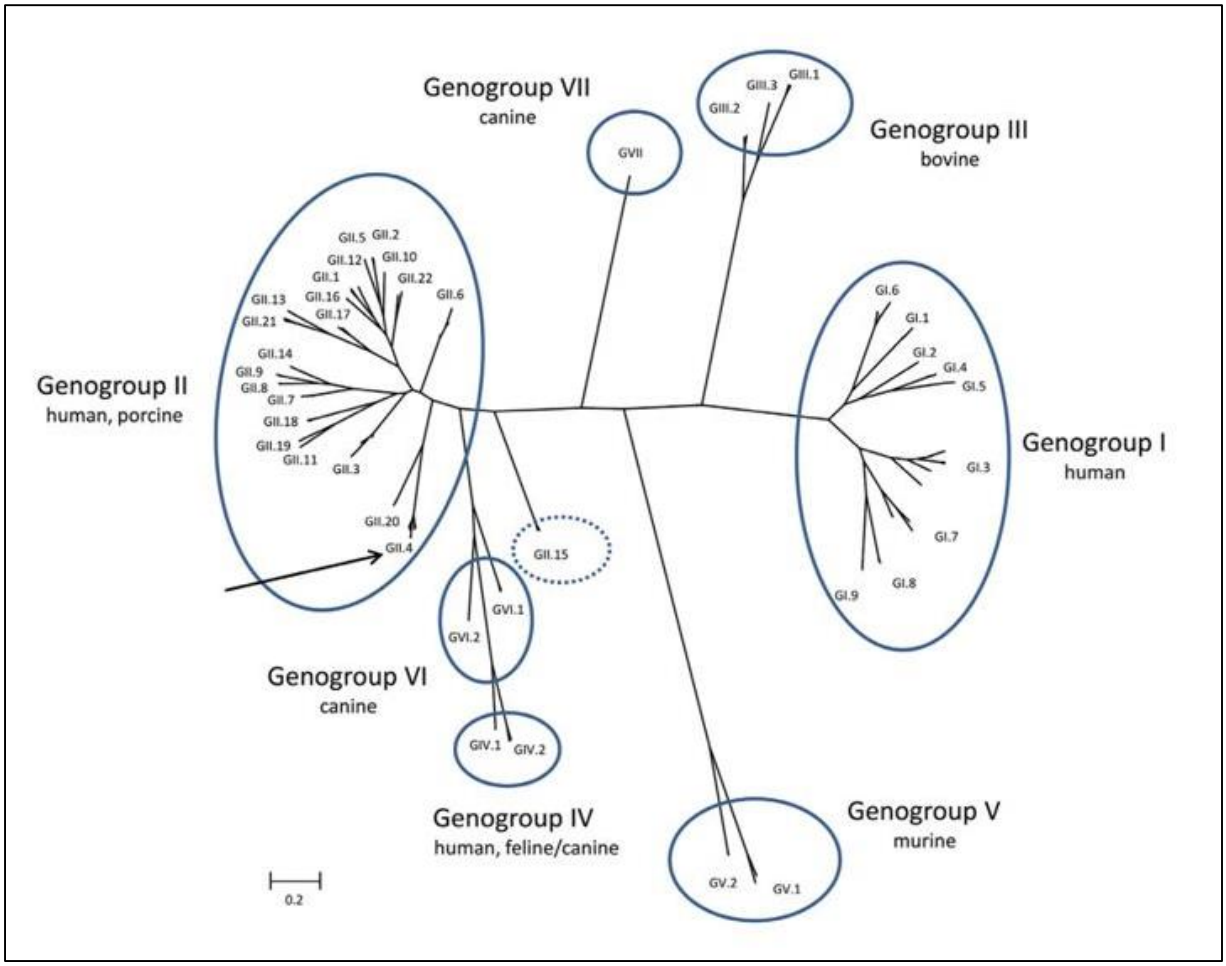

Figure 1.3 Classification of Norovirus genogroups (reproduced from ref 32).

1.1.5. Norovirus Genome

The norovirus genome is a single-stranded positive sense RNA that is ~7.5 kb long and is comprised of three open reading frames (ORF1–3).[16] The genome is polyadenylated at the 3' end and is covalently linked to the nonstructural protein viral protein genome-linked (VPg) at the 5' end. ORF1 encodes a nonstructural protein and ORF2, and ORF3 encode structural proteins, the major capsid protein (VP1), and the minor capsid protein (VP2), respectively (Figure 1.4).[34] The nonstructural protein is essential for viral replication. Cleavage of ORF1 polyprotein by the viral-encoded 3C-like

protease (3CLpro) generates six mature nonstructural proteins designated p48 (N-terminal protein), p41 (NTPase), p22, VPg, Pro (3CLpro), and Pol (RNA dependent RNA polymerase (RdRp)).[35]

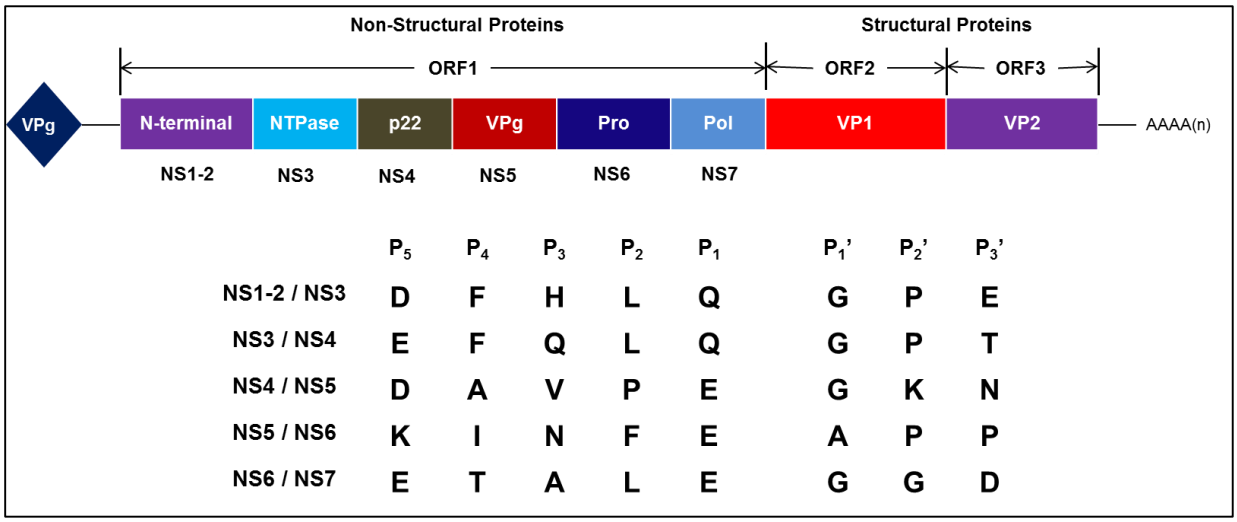

Figure 1.4 Norovirus genome and NV 3CLpro cleavage sites.

The generated proteins display an array of functions, including facilitating the anchoring and assembly of the membrane-associated replication complex (p48, p41, and p22), infectivity and viral genome translation initiation (VPg), polyprotein cleavage (3CLpro), and genome replication (RdRp).[34] 3CLpro and RdRp play essential roles in viral replication, consequently, they are particularly well suited as targets for antiviral drug development.

A major capsid protein VP1 (ORF2) which contains antigenic and cell binding determinants VP1 is comprised of a shell (S) domain and a protruding (P) domain, which is further subdivided into two subdomains (P1 and P2).[16,34,35,37] The many functions associated with the hypervariable region in P2 include interactions with individual

oligosaccharide residues of the histo-blood group antigen (HBGA) receptors[38-40] and sialic acid-containing glycosphingolipids. ORF3 encodes a small basic protein VP2, which is believed to enhance the stability and structural integrity of VP1.[16,35]

The mature polyprotein is processed by a virus-encoded 3C-like cysteine protease (3CLpro) to generate six nonstructural proteins: p48 (NS1/2), NTPase/RNA helicase (NS3), p22 (NS4), VPg (NS5), a protease (NS6), and an RNA-dependent RNA polymerase (RdRp) (NS7) (Figure 1.4).[16,34-35] Co- and post-translational processing of the polyprotein by norovirus 3CLpro is essential for virus replication. As mentioned previously, the functions of p48 and p22 have not been fully elucidated, however, the 15 kDa VPg protein is covalently linked to genomic and subgenomic mRNAs and its covalent linkage to the 5′ end of norovirus RNA is essential for virus infectivity.[34,41]

1.1.6. Norovirus Replication Cycle

Norovirus infection is a complex disease that involves the interplay of multiple host and viral factors and mediators, including a variance in genetic susceptibility to norovirus infections arising from different binding affinities of norovirus strains and blood antigens (HBGAs).

The mechanism of internalization of human noroviruses after binding to HBGAs is not yet known, however, it may be dependent on dynamin and cholesterol, as has been shown for murine noroviruses.[34,42] Replication of the virus occurs in the cytoplasm in close association with host-derived membrane complexes (Figure 1.5). The mechanisms of assembly and release of human noroviruses remain largely unknown. The genome, in the form of a positive-sense RNA strand ((+)RNA), is encapsulated in a capsid that is formed by VP1 and VP2. The capsid attaches to the cell surface through interactions

between VP1 and host histo-blood group antigens (HBGAs) (step 1), and is subsequently internalized, uncoated and disassembled (step 2). The (+)RNA is then transcribed and translated in the cytoplasm of the host cell. Translation is mediated by host translation factors that are recruited by the non-structural virus protein VPg. VPg is covalently bound to the 5′ end of the genome and the polyprotein that is encoded by ORF1 is post-translationally cleaved (step 3) by the virus-encoded protease, Pro (also known as NS6 or 3C‑like), into individual proteins: p48 (also known as NS1/2 or N‑term), NTPase (also known as NS3 or 2C‑like), p22 (also known as NS4 or 3A‑like), VPg, Pro and RNA-dependent RNA polymerase (RdRp).

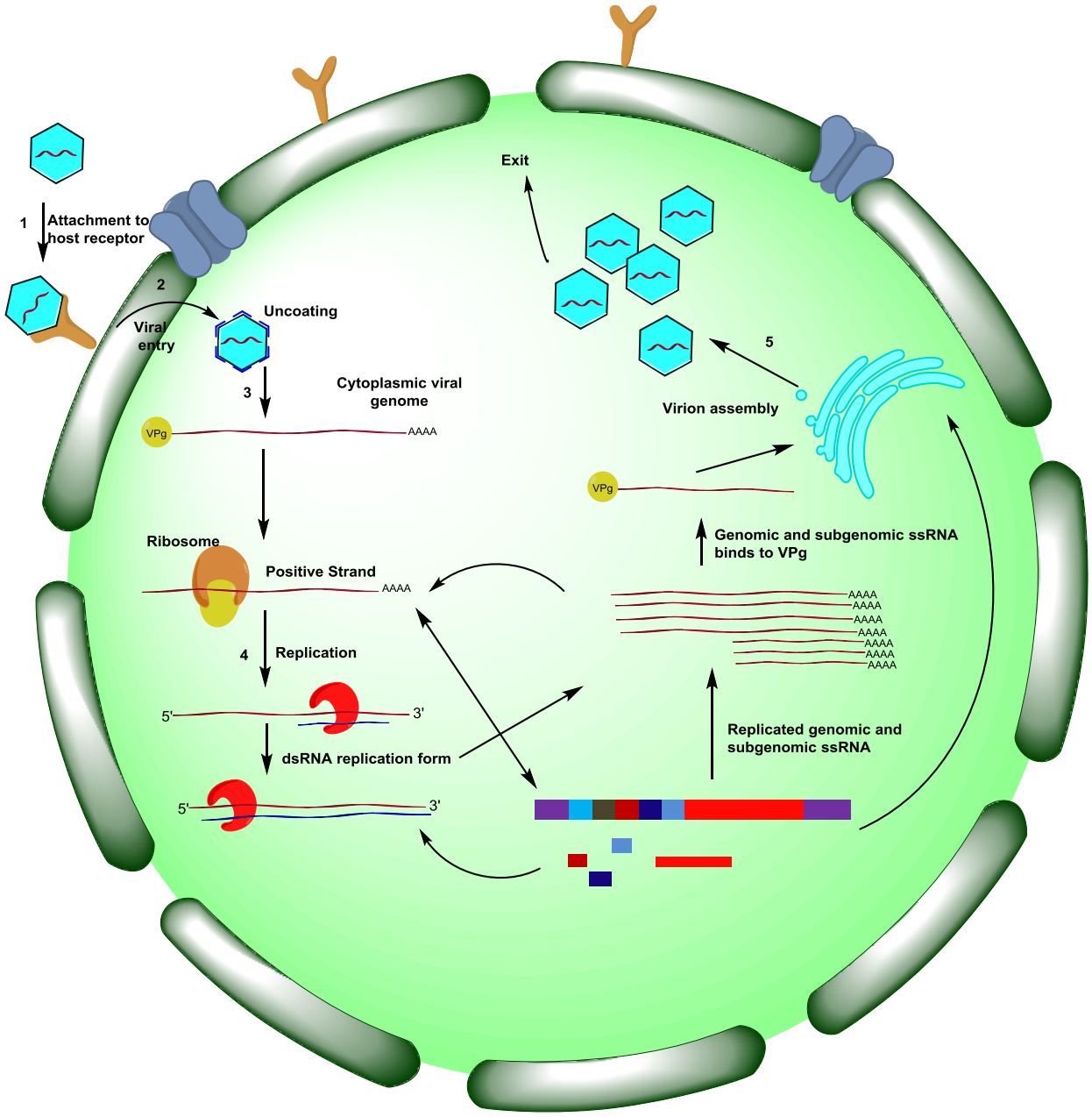

Figure 1.5 The replication cycle of human norovirus. (reproduced from ref 43).

During genome replication, (+)RNA is transcribed into negative-sense RNAs ((–)RNAs), which are used as templates for the synthesis of new genomic and subgenomic (+)RNAs, respectively (step 4). Subgenomic (+)RNAs contain only ORF2 and ORF3, and are used for the production of VP1 and VP2. During encapsidation (step

5), genomic-and possibly subgenomic- (+)RNAs are packaged into new virions, which are subsequently released from the infected host cell, although the mechanism by which release occurs remains largely unknown.

1.1.7. Norovirus Biology and Pathogenesis

Recent groundbreaking advances in our understanding of norovirus biology such as, for example, infection of immune cells (B cells, macrophages, dendritic cells, T cells),[45, 51] as well as epithelial cells (enterocytes) in the gastrointestinal tract by noroviruses; promotion of infection of enterocytes by bile acids;[46a-d] the role of the gut microbiome in enhancing norovirus infection and, finally, the identification of a proteinaceous receptor that mediates binding to the cell surface and is both necessary and sufficient for viral entry and replication in vitro and in vivo, have greatly illuminated norovirus pathobiology. Nevertheless, there are currently no norovirus-specific antivirals or vaccines to combat infection. Main obstacles for making progress toward the discovery of norovirus therapeutics include the lack of a human norovirus cell culture and the lack of optimal animal models. With respect to the latter, currently available animal models of NV cause gastroenteritis without enterocyte infection. This suggests that other mechanisms may play a role in the infection such as, for example, infection of immune cells could trigger the release of pathogenic levels of pro-inflammatory cytokines.[54] Alternatively, NV may encode a viral enterotoxin from infected immune cells which could act on enterocytes basally to cause epithelium dysfunction.[55] Additional gaps in our understanding of human noroviruses include the need for a detailed understanding of the function of cellular proteins required for NV genome translation and replication and the impact of virus infection on cellular processes. In summary, the development of effective

solutions for norovirus prevention, treatment, and control will largely depend on advances in our understanding of norovirus pathobiology.

1.1.7.1. Norovirus Binding and Entry

Generally, NV infection of susceptible target cells takes place via a multistep process, which starts with the binding of viral particles to host cell receptors, namely, histo-blood group antigens (HBGAs) and/or the recently-identified proteinaceous receptor, followed by active uptake of virus. This initiates conformational changes in the viral capsid, activating cellular signaling, promoting endocytosis, or direct driving penetration.[47-48,53] A working model for NV intestinal infection has been proposed that incorporates our current understanding of the mechanisms used by human noroviruses to cross the intestinal epithelial cell barrier (Figure 1.6).[49] In this model, noroviruses bind HBGA on the surface of specific members of the intestinal microbiota and/or enterocytes. Indeed, numerous studies have demonstrated that NV particles bind to carbohydrates expressed on enterocytes and secreted into the gut lumen. NV may bind to enteric bacteria since they also can express similar carbohydrates (1). Transcytosis of NV across the intestinal epithelium via M cells is followed by infection of dendritic cells, macrophages, and B cells (3). As mentioned earlier, the recent identification of a proteinaceous receptor suggests that several potential mechanisms of promoting infection are possible, and the precise role of HABAs and other entry receptors (CD36, CD98 transferrin receptors etc.)[50] remain to be addressed.

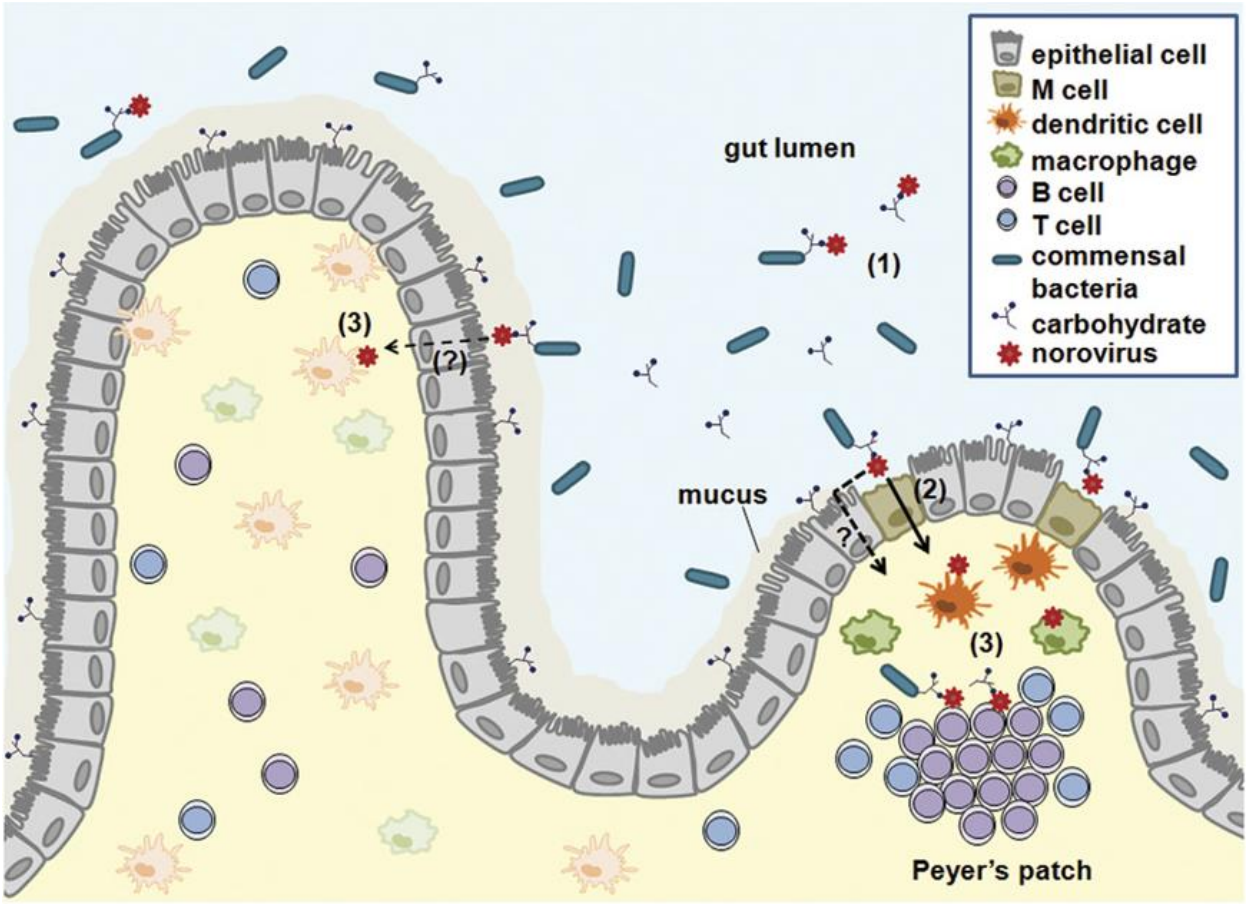

Figure 1.6 A working model of norovirus intestinal infection (reproduced from ref. 49).

1.1.8. Norovirus 3CL Protease

Norovirus 3CLpro is a chymotrypsin-like cysteine protease with an active site comprised of a prototypical catalytic triad/diad (Cys139 acts as nucleophile, His30 acts as general base, and Glu54 helps His30 maintain a correct orientation) that is located at the interface of a β-sheet domain and a β-barrel domain.[34,37] Norovirus 3CLpro is an induced fit enzyme with an extended binding cleft. When a substrate docks to the active site of the enzyme it does so in an extended β-strand conformation in which the substrate backbone hydrogen bonds with the backbone carbonyl and amide groups of the e**II** β-strand of the protease, forming an antiparallel β-sheet (Figure 1.7). These interactions

allow correct positioning of the terminal residue (P1) of the substrate for proteolytic cleavage. The terminal carboxyl group of P1 is properly aligned with the substrate/inhibitor for nucleophilic attack by Cys139, reminiscent of the tetrahedral intermediate state. The backbone amide groups of the C139 and G137 are correctly positioned facing the negatively charged oxygen of the tetrahedral adduct.[28,59-60]

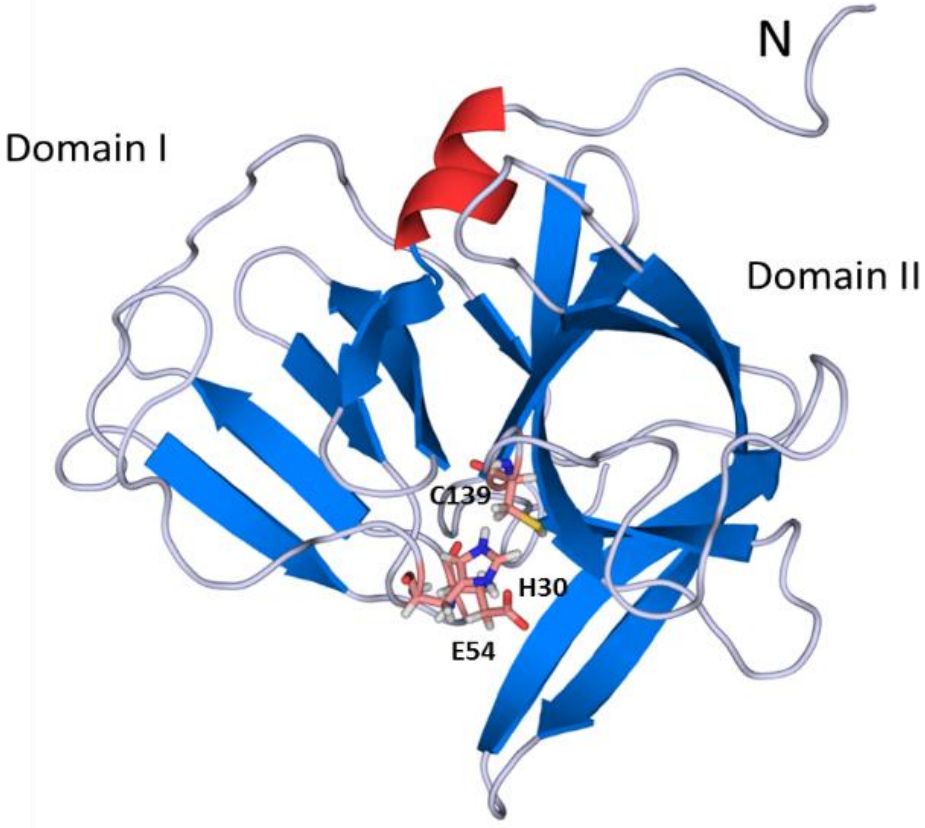

Figure 1.7 Norovirus X-ray crystal structure. Ribbon representation of the solution structure of NV 3CLpro (2LNC)[43] with the catalytic residues shown as sticks and the very short strand shown in green color.

Like all (+) strand RNA viruses, replication of the viral genome is effected by the virally encoded RdRp. Genomic and subgenomic RNA synthesis by the viral RdRp entails

two different mechanisms: a de novo-initiated mechanism and a VPg-dependent mechanism.[16,34] The central roles played by 3CLpro and RdRp in virus replication render them attractive targets for the development of norovirus-specific antivirals.

1.1.9. Substrate Specificity of Norovirus 3CLpro

Analysis of the protease structures with bound substrates has provided insight into how amino acid variations are accommodated by proteases in general and norovirus 3CL protease in paticular. The specific subsites (pockets) in the protease that line the substrate binding groove between the two domains (Figure 1.8) [28,59,61-62] , designated S4 to S1, interact with the P4 to P1 residues in the substrate.

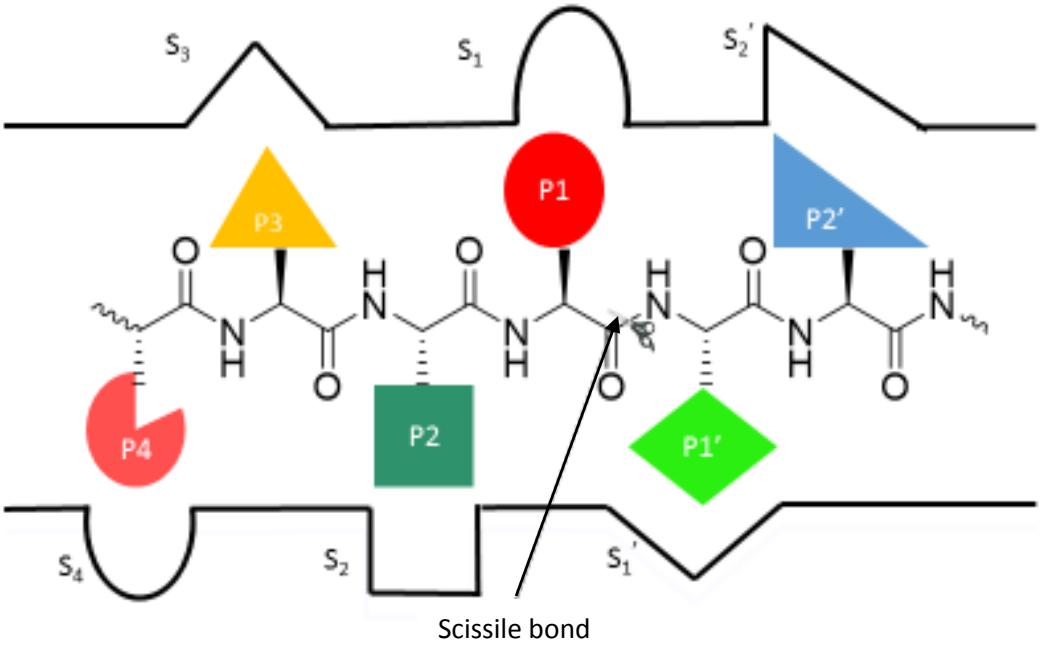

Figure 1.8 General substrate and protease active site subsites (pockets). The cleavage site is the P_1-P_1' amide bond (scissile bond), as shown with a scissor. From the scissile bond toward the N-terminus, substrate residues are designated as P_1, P_2, P_3, P_4, etc and from the scissile bond to the C-terminus the residues are designated P_1', P_2' etc. The corresponding protease binding pockets are designated S_1, S_2, S_3, S_4, etc. and S_1', S_2', etc, respectively.

The primary substrate specificity of NV 3CLpro is determined by the P_1 residue. The scissile bonds (P_1-P_1') cleaved by the NV 3CLpro within its 200 kDa polyprotein substrate are within the dipeptide recognition sequences Glu-Gly, Gln-Gly, or Gln-Ala. The S_1 subsite that accommodates the P_1 substrate (Glu or Gln) is sufficiently large enough to fill fully the glutamine side chain, whereas the S_1' subsite is shallow and can accommodate only small amino acids (Gly or Ala). The preferred amino acids at the P_3, P_2, and P_1 positions are X-Leu-Gln, respectively, where X is Gln, Glu or His. The S2 subsite is considerably large and hydrophobic (Table 1.1).[63]

TABLE 1.1 SUBSTRATE SPECIFICITY OF VIRAL 3C AND 3CL PROTEASES NOROVIRUS AND SOME OTHER VIRUSES

Viral 3Cpro or 3CLpro	P_5	P_4	P_3	P_2	P_1	P_1'	P_2'
NV	D/E	F/Y	H/Q/E	L	Q	G	P
EV71	E	A	V/L/T	L/F	Q	G	P
CVA16	E	A	L	F	Q	G	P
SARS-CoV	S	A	V/T/K	L	Q	A/S	G

1.1.10. Norovirus 3CLpro: Mechanism of Action (MoA)

The mechanism of action related to the hydrolysis of peptide bond by NV 3CLpro involves two main steps: (a) the first step takes place via nucleophilic attack on the carbonyl carbon by the thiolate anion of Cys139 (acylation step), which results in the formation of tetrahedral intermediate (acyl-inhibitor) followed by release of the C-terminal part of the substrate; (b) the next step is deacylation via nucleophilic attack on the

thioester bond of the acyl-enzyme complex by a water molecule, thereby releasing free enzyme. The deacylation step proceeds through a tetrahedral transition state and isaccompanied by the release of a peptidyl fragment and free enzyme (Figure 1.9).

High-resolution X-ray crystal structures of NV 3CLpro and inhibitors provide detailed information on how NV 3CLpro recognizes peptide inhibitors or substrates. When an inhibitor (or substrate) is correctly positioned within the active site cleft, Cys139 facilitates nucleophilic attack on the carbonyl carbon of the scissile bond which is located in sufficiently close proximity to the thiolate (formed between His30 and Cys139), by yielding an unstable covalently-bound tetrahedral intermediate. The negative charge on the carbonyl oxygen of the substrate generated during the nucleophilic attack is located in the oxyanion hole and is stabilized by hydrogen bonds involving the backbone amide nitrogen of Cys139 and Gly137.

The sulfur atom of Cys139 is covalently bound to substrate and the His30 side chain adopts a favorable conformation by pointing away from Cys139 and Glu54. The His30 side chain appears to interact electrostatically with the C-terminal carboxylate of the hydrolyzed substrate. In the absence of the substrate, the His30 side chain would most likely adopt a conformation in which the imidazole is within hydrogen-bonding distance with both Cys139 and Glu54. This agrees with biochemical and structural studies of a related enzyme[59-60] which showed that it is indeed His30 and not His157 (which is also close to Cys139) that participates in catalysis.

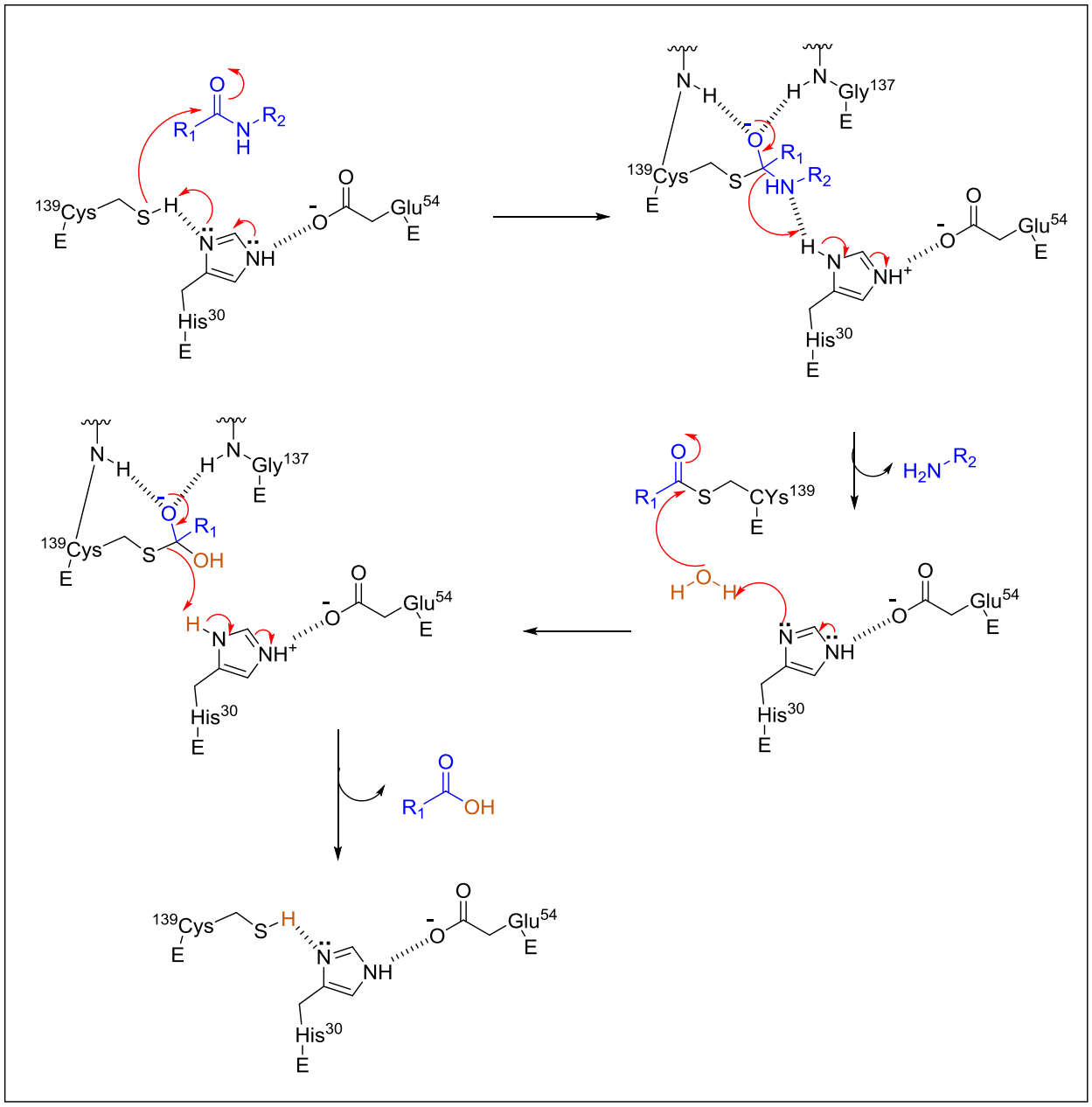

Figure 1.9 Cysteine 3CL protease enzyme mechanism.

.

1.1.11. Norovirus Therapeutics

Besides supportive fluid therapy,[64] treatment options available to individuals suffering from acute gastroenteritis are currently limited because no norovirus-specific antiviral agent has yet been approved by the FDA. Thus, the availability of an efficacious and safe norovirus therapeutic or prophylactic would have a major impact on the control of norovirus infection.

In principle, both viral and host factors can serve as potential targets for antiviral drug discovery and, furthermore, any step in the viral replication cycle can be targeted (Figure 1.5). The advent of a robust and highly sensitive FRET-based assay for norovirus 3CLpro and a cell-based replicon system has greatly facilitated the identification and evaluation of anti-norovirus hits.[65] As is generally true for other viruses, antivirals aimed at targeting viral components (attachment, entry, and uncoating inhibitors, as well as protease and polymerase inhibitors) of norovirus may result in the selection of resistant mutants, while unwanted side effects from inhibiting host factors involved in bodily functions are a concern for antivirals targeting host factors. In either case, a non-toxic norovirus therapeutic that rapidly reduces viral load and is effective as a prophylactic would constitute a major advance in the field.

1.1.11.1. 3CL Protease inhibitors

Direct-acting protease inhibitors have been the subject of intense studies and several drugs that act by inhibiting proteases are currently in the clinic for the treatment of HIV/AIDs and hepatitis C. Furthermore, the involvement of proteases in a multitude of diseases, including parasitic, inflammatory, cardiovascular, and respiratory, has led to the

approval of several drugs, including thrombin inhibitors for the treatment of deep vein thrombosis, pulmonary embolism, and atrial fibrillation.

1.1.11.2. RdRp Inhibitors

The inhibition of viral RNA dependent RNA polymerases has been a highly successful endeavor that has resulted in the introduction of several RdRp inhibitors in the clinic. The central role played by norovirus RdRp in virus replication and the lack of human homologs renders RdRp an attractive target for antiviral drug discovery. Several X-ray crystal structures of human and murine norovirus RdRp that are well-suited to serving as a launching pad for the design of RdRp inhibitors have been reported, including complexes with 5-fluorouracil,[66] 2-thiouridine and ribavirin,[67] and suramin-related compounds.[68]. Importantly, it has been shown that the RdRp inhibitor 2'-C-methylcytidine is effective against norovirus-induced diarrhea and mortality in the murine model of norovirus infection.[69-70] Favipiravir has also been shown to inhibit norovirus replication in vitro.[71] Future developments related to RdRp inhibitors are likely to identify additional promising nucleoside and nonnucleoside direct acting antivirals.

1.1.11.3. Entry Blockers

There has been a flurry of activity related to the design and discovery of inhibitors of norovirus attachment, entry, and/or uncoating. Because HBGA-binding sites are conserved in human noroviruses, molecules that block the HBGA binding site are of potential therapeutic value.[72-74] Screening of carbohydrate libraries and small molecule libraries has resulted in the identification of multiple binding blockers.[75-77] The recent demonstration that the endosomal cysteine protease cathepsin L is required for calicivirus

replication, offers another promising avenue of investigation for identifying molecules of potential therapeutic value.[78]

1.1.11.4. Host Factors

Despite impressive progress in our understanding of the norovirus life cycle,[33,41,54,79-80] there is a need for a sharper definition of how the virus exploits host factors for survival, propagation, and infectivity. As mentioned earlier, multiple host cell factors, including a network of host proteins that interact with the 5' and 3' ends of the human and murine norovirus genome, play critical roles in viral RNA replication.[33,41,80-81] Moreover, studies have shown that the cholesterol pathway, as well as the molecular chaperone Hsp90, a component of the ribonucleoprotein complex, could also serve as potential targets for novel therapeutic options.[82-83]

1.1.11.5. Norovirus Drugs in Clinical Development

Nitazoxanide, an antiprotozoal prodrug used in the treatment of infectious diarrhea caused by *C. parvum* and *G. lamblia* has demonstrated efficacy against norovirus infection in clinical trials.[84] There is limited information on its anti-noroviral effects and mechanism of action.[85] Nitazoxanide provides strong validation of drug repurposing[83] as a means of identifying compounds that inhibit norovirus.

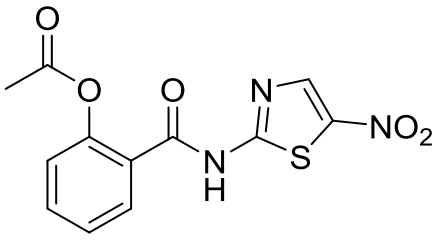

Nitazoxanide[84]

In summary, NV 3CL protease is an attractive target for the development of anti-norovirus therapeutics and prophylactics, therefore, the thrust of the studies described herein is centered on this enzyme.

1.2. Middle East Respiratory Syndrome Coronavirus (MERS-CoV)

Middle East Respiratory Syndrome (MERS) is an emerging respiratory illness recently recognized in humans. It is caused by MERS coronavirus (MERS-CoV) and was first reported in Saudi Arabia in 2012. MERS-CoV has continued to emerge and spread to countries outside of the Arabian Peninsula, such as South Korea and 27 other countries, including the United States, as a result of travel of infected individuals or close contact with infected persons.[86] Thus, MERS-CoV has become a global threat due to continuous outbreaks in Middle Eastern countries and the potential of spread to other countries.

1.2.1 MERS-CoV Epidemiology

The origin of MERS-CoV was originally thought to be bats as the reservoir based on phylogenetic similarities with certain bat coronaviruses.[87] However, the MERS-CoV strain found in humans was not an exact match with bat species, instead dromedary camels have been found to harbor the same MERS-CoV and MERS-CoV-like antibodies as infected humans. Currently, dromedary camels are recognized as the main animal reservoir for MERS-CoV.[88]

The first outbreak of MERS-CoV among humans was reported in 2012 when eight healthcare workers from one intensive care unit in Jordan, however, the source was unknown at that time until July 2012, when a Saudi Arabian patient contracted acute pneumonia with renal failure, which eventually led to his death.[89-90] According to the World Health Organization (WHO) report published in April 2016, there have been 1,728 confirmed cases of MERS-CoV infection in 27 countries with approximately 36% of case-

fatality (Figure 1.10).[86] The emergence of MERS-CoV and SARS-CoV underscores the threat of infectious diseases from animal reservoirs.

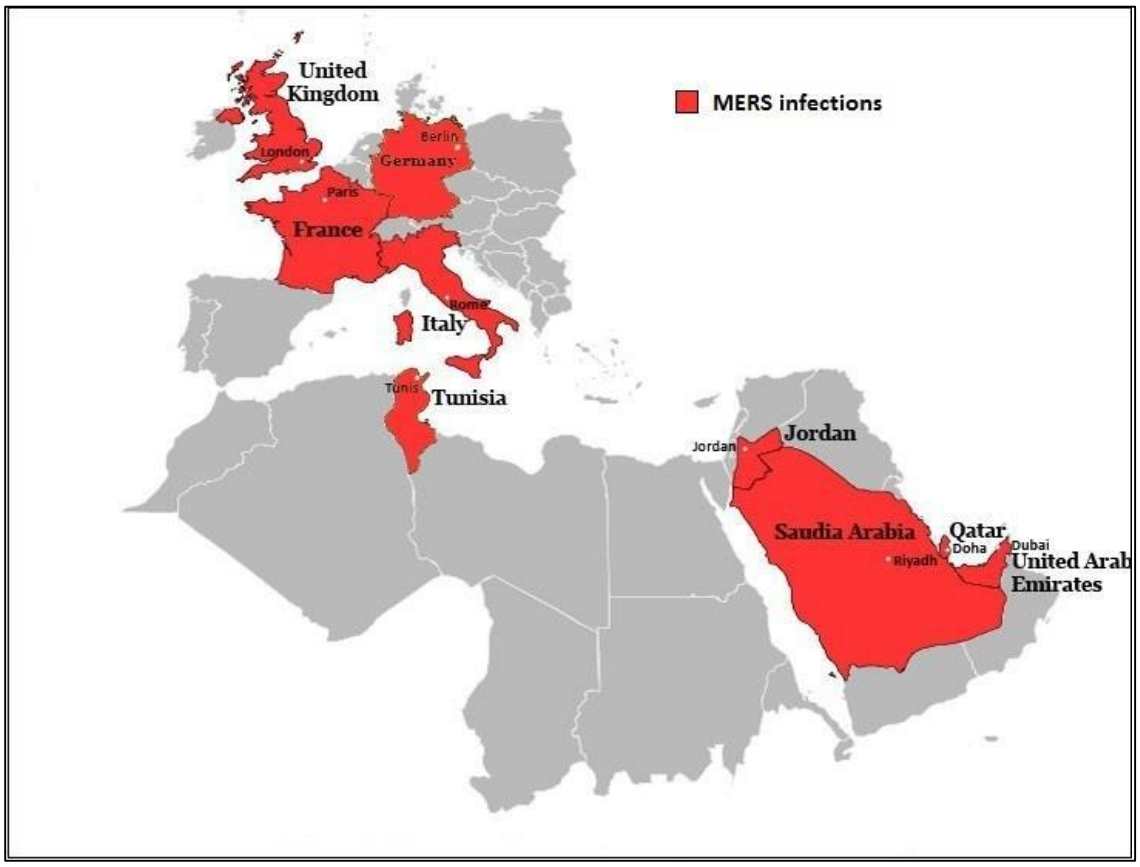

Figure 1.10 A map of the countries where laboratory-confirmed cases of MERS-CoV infection (countries highlighted with red) (reproduced from http://www.uq.edu.au/vdu/VDUMERSCoronavirus.htm).

1.2.2 Symptoms, Risk Factors, Mode and Setting of Transmission

MERS-CoV has a median incubation period of ~5 days. Most of the infected people remain asymptomatic during the incubation period, however, 95% of patients develop disease within 13 days of exposure, ranging from no symptoms to mild upper respiratory symptoms, such as fever, chills, coughing, headache and myalgia to severe pneumonitis,

or respiratory failure. Less common symptoms include abdominal pain, nausea, loss of appetite, vomiting and diarrhea.[91-94]

Risk factors associated with MERS-CoV infection in humans are not yet fully understood. Some studies have suggested that several risk factors are associated with poor MERS-CoV infection outcome, such as hypertension, chronic heart disease, and diabetes, old age, and male sex.[92,95] Most of the outbreaks are primarily based on transmission in healthcare settings, however, sustained human-to-human transmission case has not been documented as yet. [95-96]

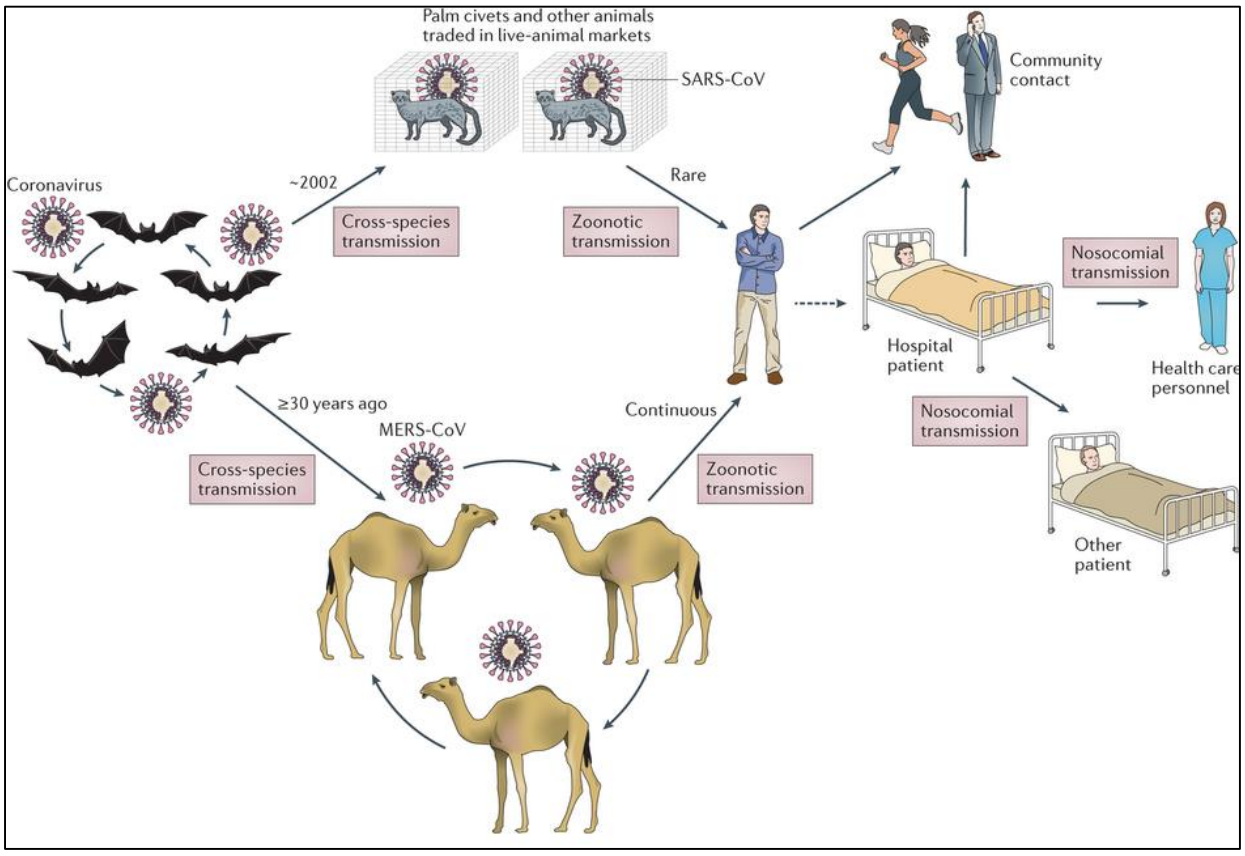

Figure 1.11 Reservoirs and transmission of MERS-CoV (reproduced from ref 98).

A serological survey in dromedary camels from Oman and the Canary Islands showed a high pervasiveness of MERS-CoV neutralizing antibodies in these animals. The

ubiquity of infected dromedary camels close to humans and continuation of zoonotic transmission may explain why MERS-CoV continues to cause infections in humans.[97-98] MERS-CoV transmission of human-to-human is mainly through nosocomial transmission. Transmission of MERS between family members and transmission between patient-to-patient are the most common routes of infection (Figure1.11).[98]

1.2.3 Prevention, Control, and Prophylaxis

The emergence of MERS-CoV infection and the lack of specific therapeutics demand implementation of a new plan and strategy in combating MERS-CoV infection. Public health surveillance and contact management, such as careful field visit of every confirmed case and monitoring exposed individuals for 14 days after the last exposure, building sufficient laboratory and diagnostic capacities, including training of laboratory personnel, case management, and risk communication, are of paramount importance.

The Centers for Disease Control have introduced guidelines and precautionary recommendations regarding MERS-CoV to prevent and contain the transmission of all suspected cases and air-borne transmission from surrounding environment and people. Direct healthcare workers should place all suspected patients in an isolated negative-pressure room and take adequate safety precautions by wearing a safety disposable gown, two pairs of gloves, a face shield, and donning an N-95 respirator while they are in direct contact with infected or suspected patients.[99-100]

1.2.4 MERS-CoV Genetic Diversity

MERS-CoV belongs to the *Coronaviridae* family. The virus family is divided into two subfamilies, *Coronavirinae* and *Torovirinae*. The *Coronavirinae* subfamily is divided into four genera, α-coronavirus, β-coronavirus, ɣ-coronavirus, and δ-coronavirus. MERS-

CoV, as well as SARS-CoV, belong to the genus β-coronavirus. There are four different lineages, A, B, C and D, in the *β*-coronavirus genus. MERS-CoV, as well as SARS-CoV, belong to the genus β-coronavirus, lineage B and C, respectively. Human coronaviruses are implicated in respiratory infection, otitis media, diarrhea, myocarditis and neurological disease. Coronaviruses are also important pathogens in animals and are associated with respiratory and enteric illnesses, including transmissible gastroenteritis virus (TGV), feline infectious peritonitis virus (FIPV), and bovine coronavirus. The genera *γ*- and *δ*-coronavirus contain only viruses that infect animals (Figure 1.12).

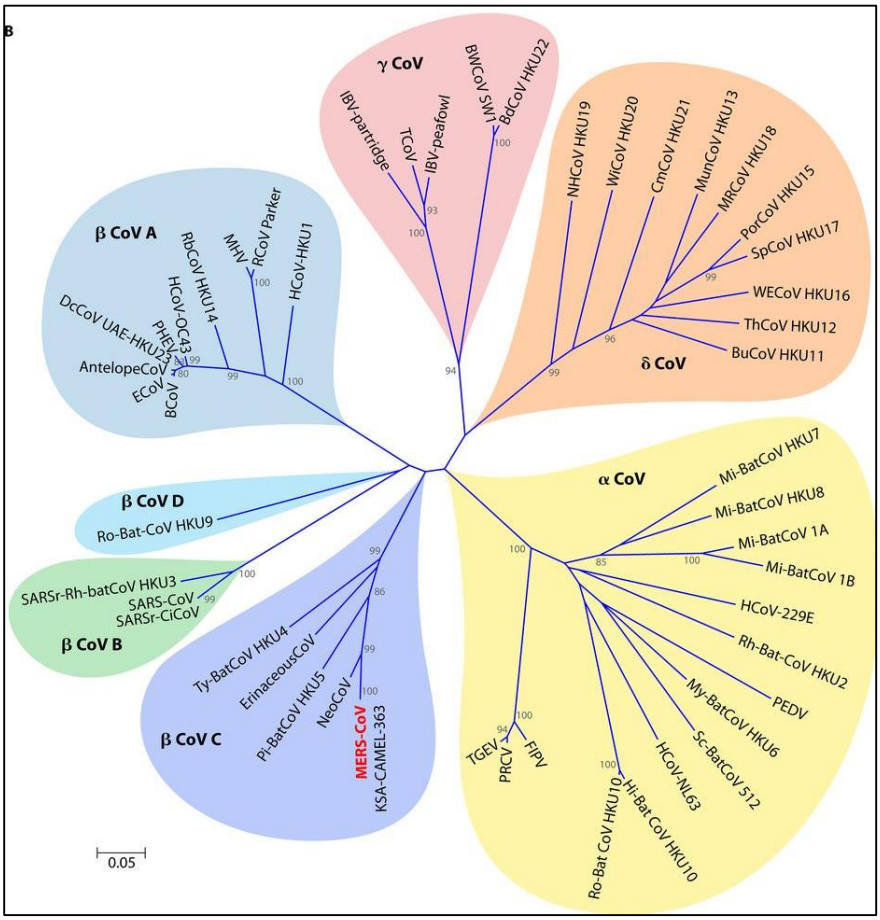

Figure 1.12 Classification of subfamily *Coronavirinae* (reproduced from ref 101).

1.2.5 MERS-CoV Genome and Replication Cycle

MERS-CoV is an enveloped virus with a single-stranded positive sense RNA genome of ~30 kb. The two large open reading frames (ORF1a and ORF1b) on the 5' end of the MERS-CoV genome encode nonstructural proteins, while those on the 3' end encode the spike glycoprotein (S), the small envelope protein (E), the membrane glycoprotein (M), the nucleocapsid structural proteins, and several accessory proteins (Figure 1.13). Translation of the genomic mRNA of ORF1a yields polyprotein pp1a. A second polyprotein (pp1b) is the product of a ribosomal frame that joins ORF1a together with ORF1b. ORF1a encodes a papain-like protease (PLpro) and a 3C-like protease (3CLpro). Polyproteins pp1a and pp1b are processed by 3CLpro (11 cleavage sites) and PLpro (3 cleavage sites) resulting in 16 mature nonstructural proteins.[101-103] Both proteases are essential for viral replication, making them attractive targets for drug development.

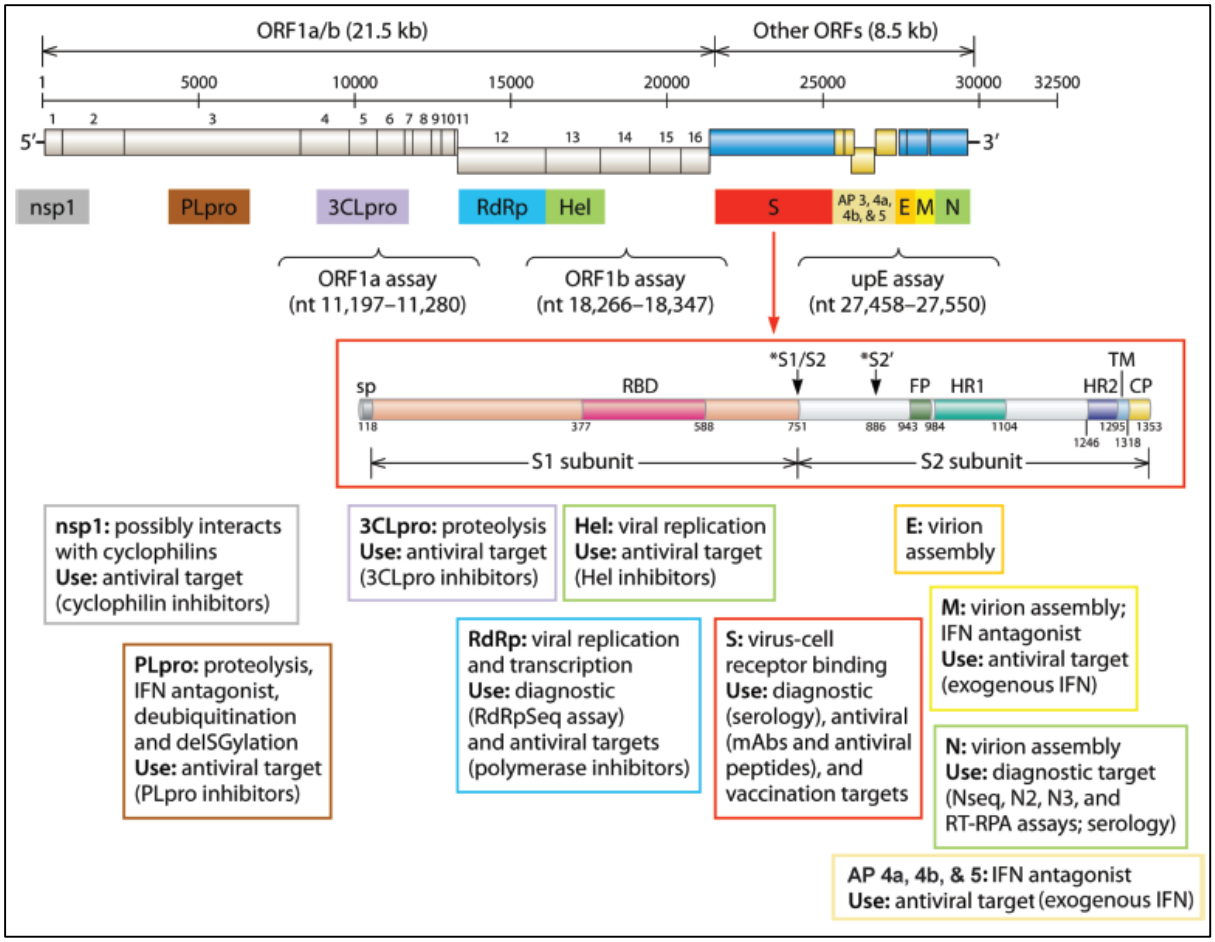

Figure 1.13 MERS-CoV genome (reproduced from ref 101).

MERS-CoV entry is initiated by the binding of S protein to cell receptors, human dipeptidyl peptidase 4 (hDDP4). In the endosome, the fusion peptide in the S protein induces fusion to endosomal membranes leading to viral RNA entry into the cytoplasm.[98,104] Once pathogenic viral (+)RNA genome is released in the cytoplasm, ORF1a initiates translation and continues in ORF1b, thereby producing the two major polyproteins (pp1a and pp1b).

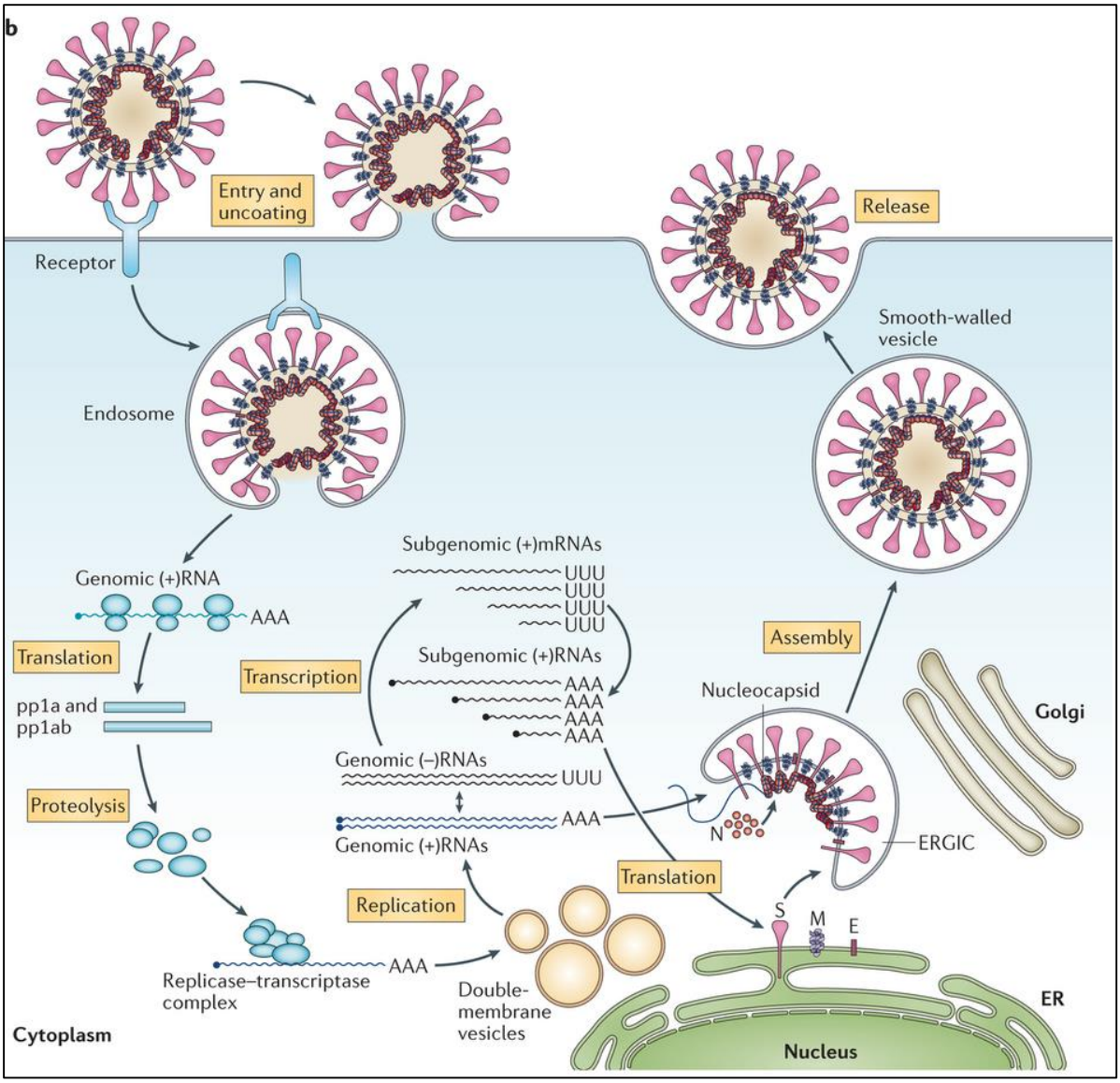

Figure 1.14 The replication cycle of MERS-CoV (reproduced from ref 98).

ORF1ab comprises two-thirds of the viral genome and encodes16 nonstructural proteins (nsp). The remaining one-third of the genome encodes five accessory proteins and structural proteins E, N, S and M. As mentioned above, the virus genome encodes two proteases PLpro and 3CL pro which cleave the pp1a and pp1ab proteins at 3 and 11 different sites respectively.[105-107]

Encapsidation of freshly synthesized (+)sense RNA genome takes place in the cytoplasm by the N protein and then transported to the ER-Golgi compartment for further

assembly of the virion with several proteins such as protein S, M and E through the cell membrane of the rough endoplasmic reticulum (ER). Finally, the double-stranded RNAs (dsRNAs) generated during viral replication with the support of interferons (IFNs) (Figure 1.14).[93,98,108]

1.2.6 MERS-CoV 3CL Protease and Substrate Specificity

The MERS-CoV 3CL protease (3CLpro), also referred to as “main protease”, is essential for viral replication. Due to its vital role in viral replication, MERS-CoV 3CLpro has emerged as an attractive drug target.[109-111] MERS-CoV 3CLpro is a chymotrypsin-like cysteine protease. It has two N-terminal domains containing two β-barrel chymotrypsin-like folds with the active site in the cleft between the two domains, and a globular cluster comprising five helices (Figure 1.15). MERS-CoV 3CLpro has a catalytic Cys-148-His41 dyad in the active site. The Cys148 thiolate anion serves as the principal nucleophile and His41 serves as general base. Kinetic studies indicate that MERS-CoV 3CLpro is less efficient in processing peptide substrates, as compared to other β-CoV proteases, presumably because MERS-CoV 3CLpro is a weakly associated dimer.[112-113]

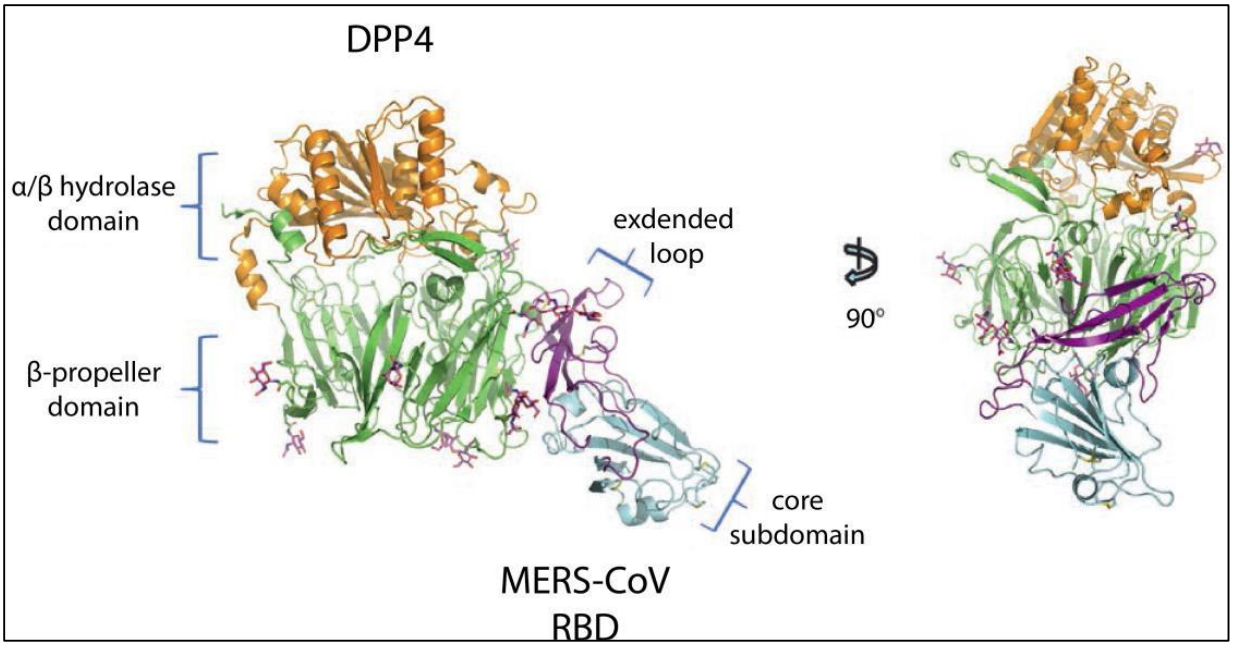

Figure 1.15 Crustal structure of the MERS-CoV RBD-DPP4 receptor complex. The RBD consists of a core subdomain (light blue) and a long extended loop (purple). The extracellular domain of the DPP4 receptor contains a β-propeller domain (green) and an α/β hydrolase domain (orange). The RBD-receptor contact is mediated via the extended loop of the RBD and the β-propeller domain of the receptor. (reproduced from ref. 104).

MERS-CoV 3CLpro has a well-defined substrate specificity. The substrate binding site of 3CLpro has two deeply buried S_1 and S_2 subsites and shallow S_1', S_3, and S_4 subsites.[114-115] The enzyme has a primary substrate specificity for a P1 Gln residue which is held tightly in the S1 pocket by an array of hydrogen bonds. The largely hydrophobic S2 subsite shows a strong preference for a P2 Leu residue, although Phe and Met are also accommodated. The P3 residue side chain is oriented toward the solvent, thus P3 can be highly diverse (Val, Thr, Lys),[115] while the S4 pocket is somewhat shallow. In general, the preferred amino acids at the P_3, P_2, P_1, and P_1' positions are Val, Leu, Gln, and Glu respectively (Table 1.2).[116] Functional and structural studies have revealed the

similarities between the 3CLpro of coronaviruses which may be exploited in the design of broad spectrum inhibitors. Furthermore, the absolute requirement for a P1 residue provides a measure of confidence that inhibitors of MERS-CoV 3CLpro may display high selectivity since no host-cell proteases are known to have this type of substrate specificity.

TABLE 1.2 SUBSTRATE SPECIFICITY OF CORONAVIRUS 3CLPRO

Viral 3CLpro	P_5	P_4	P_3	P_2	P_1	P_1'	P_2'
	S_5	S_4	S_3	S_2	S_1	S_1'	S_2'
MERS-CoV	D	V	V	L	Q	G	L
SARS-CoV	S	A	V/T/K	L	Q	A/S	G

1.2.7 MERS-CoV Therapeutics

Although MERS-CoV 3CLpro has been identified as a potential target in drug discovery, there are currently no FDA-approved therapeutics that target this protease. Therefore, MERS-CoV infection is currently managed by focusing on organ support for respiratory and renal failure. Use of broad-spectrum antibacterial and antiviral agents, such as a regimen consisting of a β-lactam, a macrolide and an antiviral against influenza, has also been recommended.[98,101,117] A plethora of studies evaluating different drugs and regimens for the treatment of MERS-CoV infection have been reported, however, these have met with limited success (Table 1.3).[98,117-128]

TABLE 1.3 POSSIBLE DRUG CANDIDATES FOR THE TREATMENT OF MERS-COV INFECTION

Drug candidate	Observed effect	Study references
Interferons (α, β, λ3, α2b)	Effective in a non-human primate model's kidney cell lines, HAE cultures, lung epithelial by reducing RNA levels (Monkeys).	118,119,120, 121
Ribavirin	Reduction of the MERS-CoV-induced CPE and the viral protein levels in monkey kidney cell lines (more efficient when combined with INF-α2b)	121
Corticosteroids	Significant improvement of the respiratory condition of a MERS-CoV patient (no direct effect has been proved)	122
Cyclosporin A	Inhibition of the MERS-CoV-induced CPE in monkey kidney and a human liver cell lines	120
SB203580	Reduction of the viral load in a human lung epithelial cell line	123
ADS-J1, HP-HAS	Inhibition of MERS-CoV pseudo-virus infection in human liver and mink lung cell lines	124
MDL28170, Camostat	Inhibition of MERS-CoV-S-mediated transduction of a human fetal lung fibroblast cell line and human colon cell line.	125
N3 , CE-10	Inhibition of the proteolytic activity of MERS-CoV 3CLpro	126, 127
MERS-CoV RBD	Reduction of the viral load in a MERS-CoV-infected monkey kidney cell line	128

1.3 Types of Enzyme Inhibitors

Enzyme inhibitors are generally classified into covalent and noncovalent inhibitors. Covalent inhibitors are sub-classified into affinity labels, which have a chemically reactive group as part of their structure (chloromethyl ketone, epoxide, isocyanate, etc), and mechanism-based inhibitors, which are relatively unreactive molecules that contain a masked or latent reactive group as part of their structure. In the case of mechanism-based inhibitors, binding to the active site of an enzyme is followed by unmasking of the latent reactive group via the enzyme's catalytic machinery. Subsequent reaction with an active site nucleophilic residue leads to irreversible inactivation of the enzyme. Covalent inhibitors are time-dependent, namely, loss of enzyme activity is a function of time. The high chemical reactivity of covalent inhibitors frequently results in decreased selectivity, consequently, only a small number of drugs function as covalent inhibitors due to the high likelihood of potential toxicity arising from off-target effects.

Noncovalent inhibitors interact with a target enzyme via an array of non-covalent binding interactions that include hydrogen bonds, ion-ion interactions, ion-dipole or dipole-dipole interactions, and hydrophobic interactions. Most drugs on the market that act by inhibiting an enzyme are noncovalent inhibitors, specifically, reversible competitive inhibitors. Such an inhibitor, once bound to the active site of the enzyme, blocks the substrate from binding, since the inhibitor and substrate resemble each other structurally and geometrically (Figure 1.16).

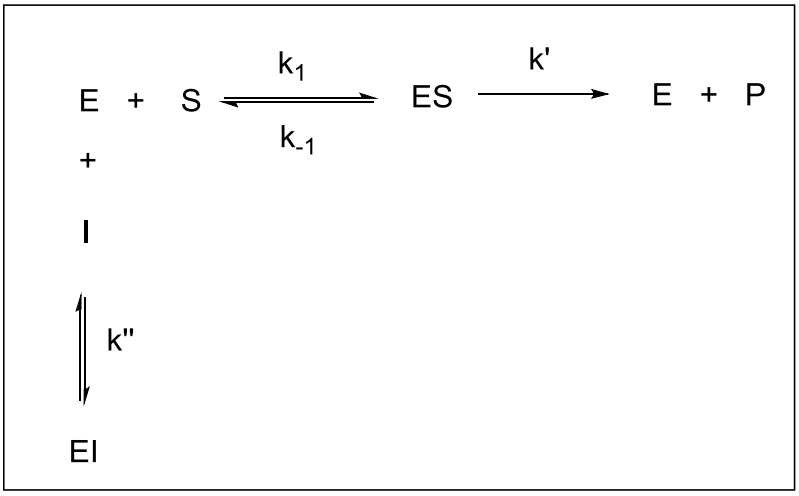

Figure 1.16 Kinetics of reversible competitive inhibitors.

The potency of noncovalent inhibitors can be rapidly evaluated by determining their IC_{50} values (concentration of inhibitor that reduces enzyme activity by 50%). Active compounds are rank-ordered in terms of target potency. Nonspecific cytotoxic effects by the compounds are also assessed in various cells to determine CC_{50} values (cell cytotoxicity) and therapeutic indices (Selectivity Index (SI) = CC_{50}/IC_{50}). Typical benchmarks to be attained for gauging success would be a $CC_{50} > 100$ and a selectivity index (TI) > 1000 for $IC_{50} < 0.1$ μM. Inhibitors are subsequently evaluated in replicon-harboring cells by determining their ED_{50} (half maximal effective concentration) values. Submicromolar ED_{50} values are desirable and reflect high potency and cellular permeability. An approximate value for the inhibition constant (K_I), a measure of the potency of an inhibitor, can be estimated using the Chang-Prusoff equation.

$$K_i = \frac{IC_{50}}{\left(1 + \frac{[S]}{K_m}\right)}$$

IC_{50} values do not provide any information about the mechanism of action (MoA) of an inhibitor, consequently, the MoA of a select number of inhibitors is routinely investigated in detail. The inhibition constant (K_I) of compounds behaving as simple reversible competitive inhibitors can be determined using Dixon plots (Figure 1.17)[129]. In this method the initial rate is measured as a function of inhibitor concentration at two different fixed concentrations of substrate. The data are then plotted as 1/v vs [I] for each substrate concentration and the value of K_i is determined from the x-axis value (where the two lines intersect)

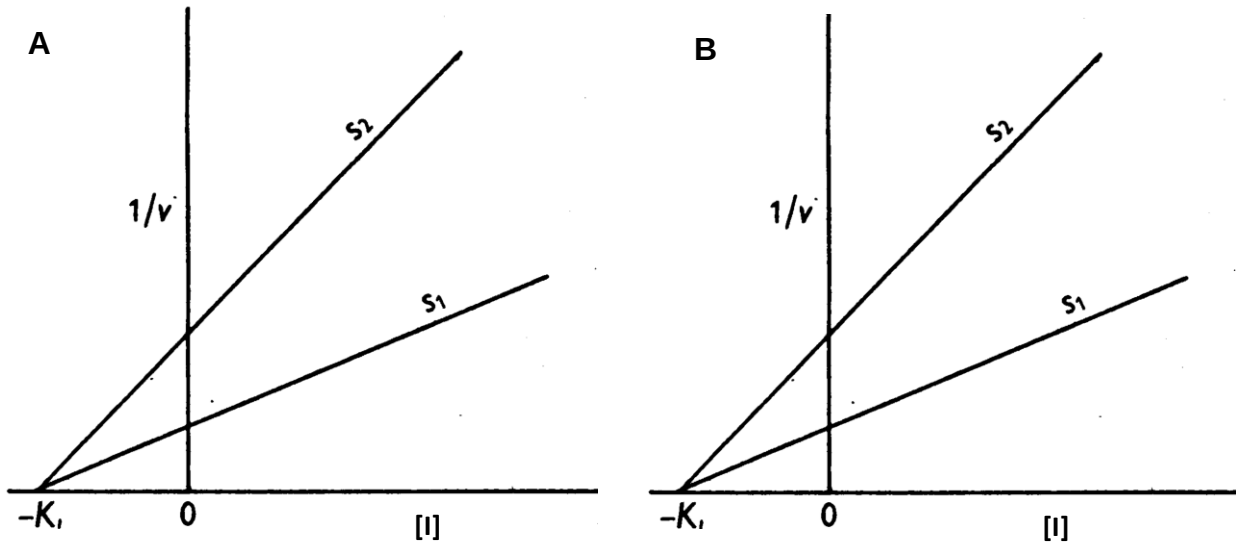

Figure 1.17 Dixon plots for determination of K_i of A) reversible competitive inhibitor and B) Noncompetitive inhibitor (reproduced from ref. 129).

1.3.1 Transition State Inhibitors and Transition State Mimics

The types of inhibitors described in this thesis are transition state (TS) inhibitors and transition state mimics. Linus Pauling first advanced the notion that enzymes bind their substrates most tightly in the geometry of the transition state of the reaction they catalyze. Thus, when the structure of a molecule resembles the transition state geometry assumed by the substrate during catalysis, or when a molecule can assume the same transition state geometry upon nucleophilic attack by an active site residue, such a molecule would be expected to exhibit a much higher affinity for the target enzyme than the substrate itself and can be a powerful inhibitor of the enzyme by forming a highly stable enzyme-inhibitor complex. In other words, inhibitor molecules resembling the transition state species would be much more tightly bound to the enzyme than would be the substrate. Although TS inhibitors frequently form a covalent bond with an active site catalytic residue, the inhibition is reversible. Many drugs on the market behave as transition state inhibitors (or analogs).

By way of illustration, the TS for the hydrolysis of a peptide bond is illustrated in Figure 1.18. A TS inhibitor of a protease that incorporates an sp2-hybridized center in its structure (aldehyde, alpha-ketoamide, trifluomethylketone, etc) would proceed through a TS that resembles that of the enzymatic reaction in forming a tetrahedral adduct (Figure 1.19).

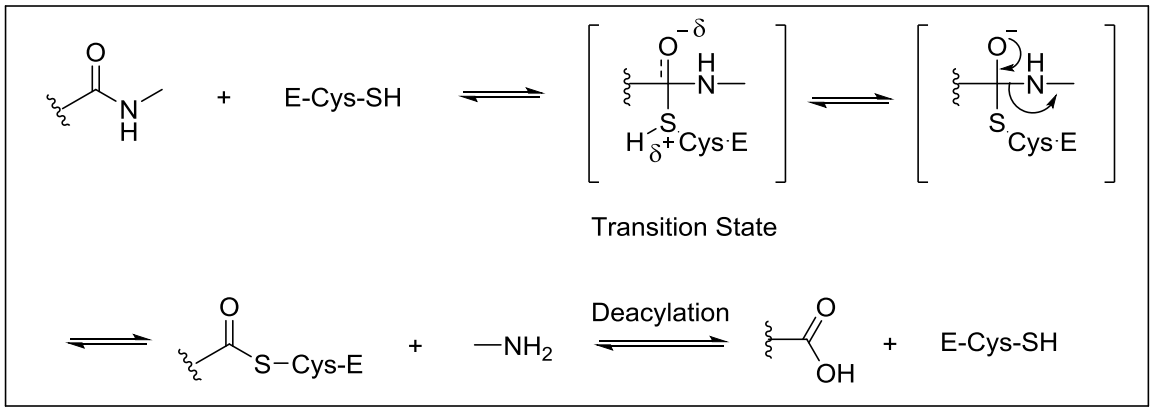

Figure 1.18 Transition state for the hydrolysis of peptide bond.

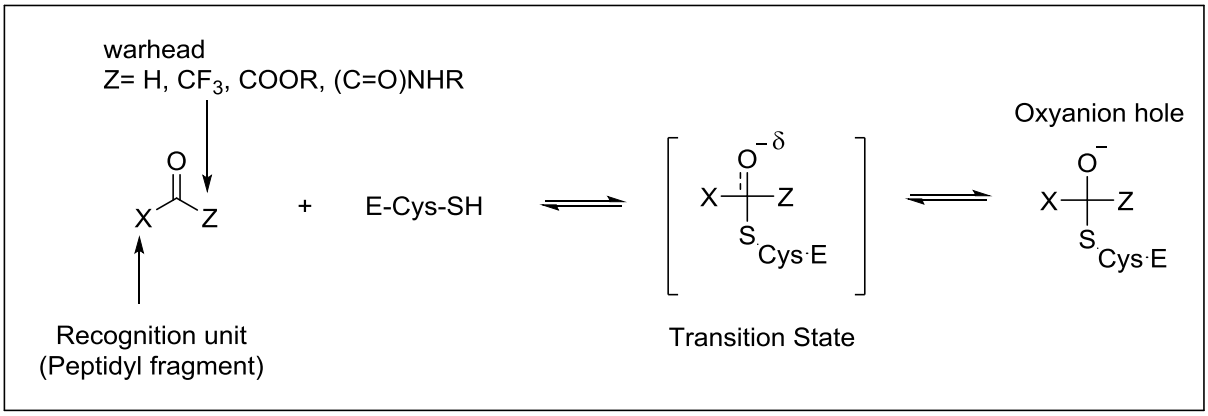

Figure 1.19 Transition state tetrahedral adduct.

Transition state inhibitors frequently behave as slow-binding inhibitors, namely, the equilibrium between the enzyme and inhibitor is established slowly and, consequently, the inhibition is time-dependent (this is in sharp contrast to ordinary reversible inhibitors where the equilibrium is established rapidly).[130-131]

$$E + I \underset{k_{off}}{\overset{k_{on}}{\rightleftharpoons}} EI$$

Slow-binding enzyme inhibition can be monitored continuously by adding enzyme to a solution of a fluorogenic substrate in buffer solution and increasing concentrations of the inhibitor, and monitoring the increase in fluorescence as a function of time. The generated progress curves are typically nonlinear least squares-fitted to eq 1 below, where v_o represents the initial rate, v_s the steady state rate, k_{obs} is the apparent first-order rate constant characterizing the formation of the steady-state enzyme-inhibitor complex, and F_o is the initial fluorescence. Association and dissociation constants (k_{on} and k_{off}, respectively) for a one-step association mechanism can be obtained from the slope and intercept, respectively, of plots of the apparent first rate constant k_{obs} *versus* [I] according to eq 2 below, where S is the fluorogenic peptide substrate used. The inhibition constant, K_I, is given by k_{off}/k_{on} and is an index of the potency of an inhibitor.

$$F = V_s t + \frac{(V_o - V_s)\left(1 - e^{(-k_{obs}t)}\right)}{k_{obs}} + F_o \qquad \text{Eq 1}$$

$$k_{obs} = k_{off} + k_{on}[I]/(1 + \frac{[S]}{K_m}) \qquad \text{Eq 2}$$

Alternatively, a two-step mechanism is possible,[132] where an initial complex (EI) is formed and then slowly converts to a more stable state (EI*). The one-step and two-step mechanisms can be differentiated on the basis of an analysis of progress curves obtained in the presence of increasing inhibitor concentrations and the kinetics of enzyme inactivation. In both mechanisms, the steady-state for enzyme-initiated reactions is predicted to be dependent on inhibitor concentration, however, the initial rates of the one- and two-step binding mechanisms are predicted to be independent and dependent on inhibitor concentration, respectively.[133-134]

1.4 Research Objectives

The primary research goals of the work described in this thesis were the following:

(a) Validate the hypothesis that a structure-based approach can be used to design and synthesize multiple novel series of transition state inhibitors of norovirus and MERS coronavirus 3CL proteases;

(b) Conduct biochemical, crystallographic, computational, in vitro, and cell-based studies to unravel the mechanism of action of the inhibitors.

(c) Establish the validity of the hypothesis that NV 3CL protease is a druggable target by demonstrating efficacy in animal models of norovirus and MERS-CoV infection.

(d) Optimize the drug-like and pharmacokinetic characteristics of identified inhibitors using novel prodrugs;

(e) Engage in the structure-guided design of NV and MERS-CoV 3CL protease inhibitors that incorporate in their structures novel design elements for optimizing pharmacological activity and PK characteristics and assess the validity and scope of the approach with respect to applicability to other proteases of clinical relevance;

(f) Conduct exploratory studies to assess the potential use of novel tunable warheads in the design of transition state inhibitors and transition state mimics.

(g) Evaluate in clinical trials an identified drug candidate for the treatment of feline infectious peritonitis virus.

(h) Identify and evaluate drug candidates for NV and MERS-CoV infection that can be further optimized to identify clinical candidates suitable for further advancement.

(i) Validate the hypothesis that the structure-based design of broad-spectrum antiviral agents that act by inhibiting the essential 3C or 3CL protease of several related viruses

is feasible (these include the phylogenetically related *Caliciviridae* (noroviruses), *Picornaviridae* (human rhinovirus, enteroviruses) and *Coronaviridae* (FIPV, SARS-CoV and MERS-CoV families). Because the 3C and 3CL proteases of these viruses share several common characteristics, including a chymotrypsin-like fold, structurally-similar active sites, a cysteine (Cys) residue as an active site nucleophile and histidine (His) as a general base catalyst in the catalytic triad or dyad, and a primary substrate specificity for a glutamine (Gln) residue at the P1 position, we hypothesized using the X-ray crystal structures of the target proteases, that a drug-like entity can be fashioned that inhibits the 3Cpro or 3CLpro of multiple viruses. Such an entity would be expected to function as a broad-spectrum antiviral agent. An array of tools and methodologies, including hit identification, hit-to-lead optimization, structure-activity relationships, scaffold hopping, multi-step organic synthesis, heterocyclic and peptide chemistry, X-ray crystallography; structure-based design of peptidyl transition state inhibitors and transition state mimics and, finally, prodrugs of transition state inhibitors, were employed to assess the validity of this hypothesis.

CHAPTER II

STRUCTURE-GUIDED DESIGN AND OPTIMIZATION OF DIPEPTIDYL INHIBITORS OF NOROVIRUS 3CL PROTEASE. STRUCTURE-ACTIVITY RELATIONSHIPS AND BIOCHEMICAL, X-RAY CRYSTALLOGRAPHIC, CELL-BASED, AND IN VIVO STUDIES

2.1 Inhibitor Design Rationale

We initially focused on the design of peptidyl transition state inhibitors of NV 3CLpro that incorporate in their structure a recognition element (a peptidyl fragment) that is congruent with the known substrate specificity of the enzyme (*vide supra*) and a warhead (aldehyde or α-ketoamide), latent warhead (bisulfite adduct) or transition state mimic (α-hydroxyphosphonate). In the case of inhibitors incorporating an aldehyde or α-ketoamide functionality in their structure, interaction with the active site cysteine (Cys139) leads to the formation of a reversible adduct (Figure 2.1).[135]

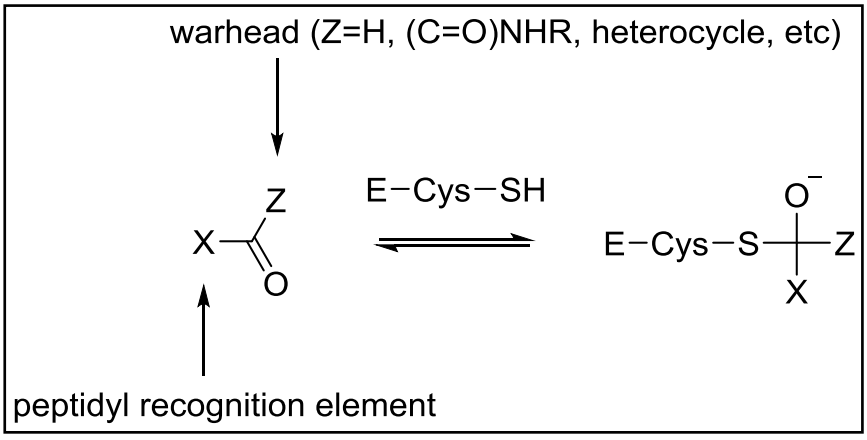

Figure 2.1 Interaction of a cysteine protease (E-Cys-SH) with a peptidyl transition state inhibitor.

Furthermore, in previous studies we demonstrated that norovirus 3CLpro shows a strong preference for a P2 cyclohexylalanine and, consequently, a P_2 cyclohexyl alanine residue, as well as a glutamine surrogate,[136] were incorporated in the structures of the inhibitors. The key binding interactions between norovirus 3CLpro and inhibitor were revealed by determining the high resolution X-ray crystal structure of NV 3CLpro with bound inhibitor (I) (R_1=cyclohexylmethyl, R_2=H, X=CH(OH)SO_3Na).

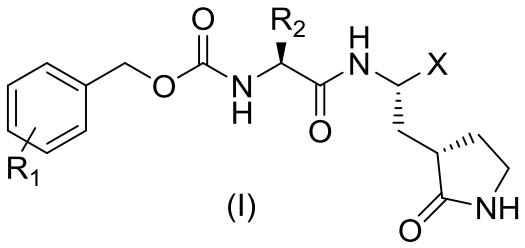

(I)

The co-crystal structure of the complex showed that, under the crystallization conditions used, the bisulfite reverted to the precursor aldehyde which subsequently formed a tetrahedral adduct with the active site cysteine (Cys139) (Figure 2.2). Inspection of the co-crystal structure revealed opportunities for additional binding interactions with a more efficient use of chemical structure. Specifically, one such opportunity was recognized by observing that there is a particular stretch of residues spanning Ala159, Ala160, Thr161 and Lys162 that are within 4.0 Å from the benzyl ring (Figure 2.3). Thus, it was envisaged that the incorporation of an appropriate functional group into the phenyl ring could serve as a locus for the formation of a hydrogen bond with the Thr161 or Lys162 backbone and/or side chains, stabilizing the flexible benzyl segment and increasing binding affinity. The formation of a halogen bond also appeared plausible.[137] Thus, a small

focused library of compounds was synthesized to evaluate these hypotheses, the ultimate goal being the identification of a dipeptidyl lead candidate suitable for conducting preclinical studies.

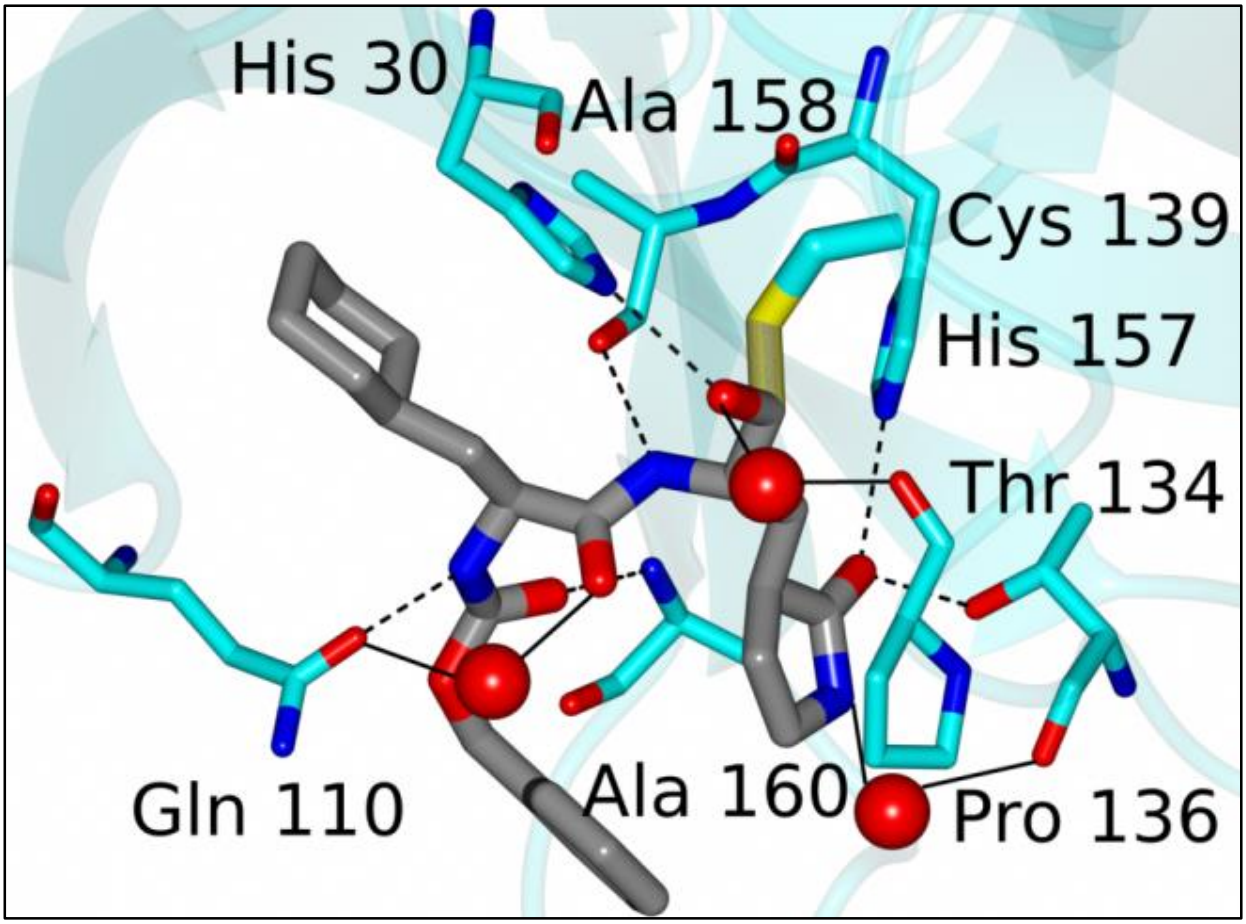

Figure 2.2 Hydrogen bonding interactions between the inhibitor and chain B for NV 3CLpro:ligand (precursor aldehyde of inhibitor ***44*)** Side chain residues are colored cyan, inhibitor is colored gray, and water molecules are represented as red spheres. Hydrogen bonds are represented as dashed lines and water mediated contacts as solid lines

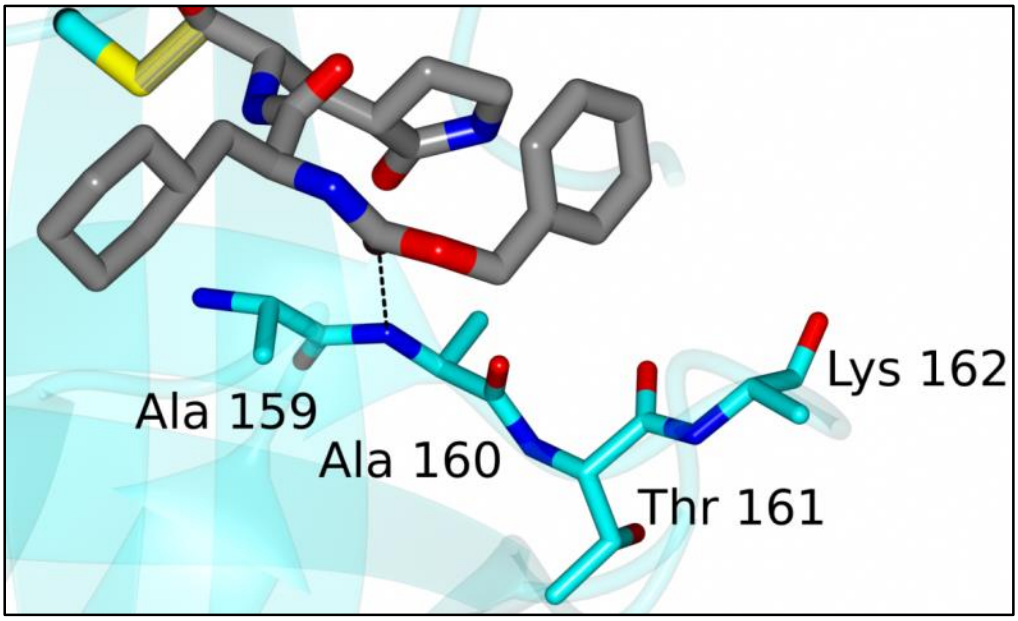

Figure 2.3 Residues spanning Ala159-Lys162 located near the benzyl ring of precursor aldehyde of inhibitor ***44.***

2.2 Chemistry

The synthesis of compounds ***13-44*** is outlined in Scheme 2.1. Refluxing cyclohexylalanine methyl ester hydrochloride (or leucine methyl ester hydrochloride) with trichloromethyl chloroformate yielded the corresponding isocyanate which was reacted with an appropriately substituted benzyl alcohol to yield a carbamate adduct methyl ester that was hydrolyzed to the corresponding acid with lithium hydroxide in aqueous THF. Subsequent coupling with glutamine surrogate methyl ester hydrochloride[124] afforded the desired dipeptidyl ester which was then reduced to the corresponding alcohol with lithium borohydride. Dess-Martin oxidation followed by flash chromatography purification yielded pure dipeptidyl aldehyde. The enantiomeric purity of the aldehyde was consistently high, with the amount of epimerized aldehyde ranging between 0-10%, depending on the

structure of the dipeptidyl aldehyde. Further reaction of the aldehyde with diethyl phosphite in the presence of diisopropyl ethyl amine yielded the corresponding α-hydroxyphosphonate as a mixture of epimers.[138] The corresponding bisulfite adducts were readily obtained as white solids by stirring the aldehydes with sodium bisulfite in an ethyl acetate/water mixture.[139] Reaction of the aldehyde with cyclopropyl isonitrile followed by Dess-Martin oxidation of the α-hydroxy cyclopropyl amide yielded the desired α-ketoamides. The synthesized compounds are listed in Table 2.1.

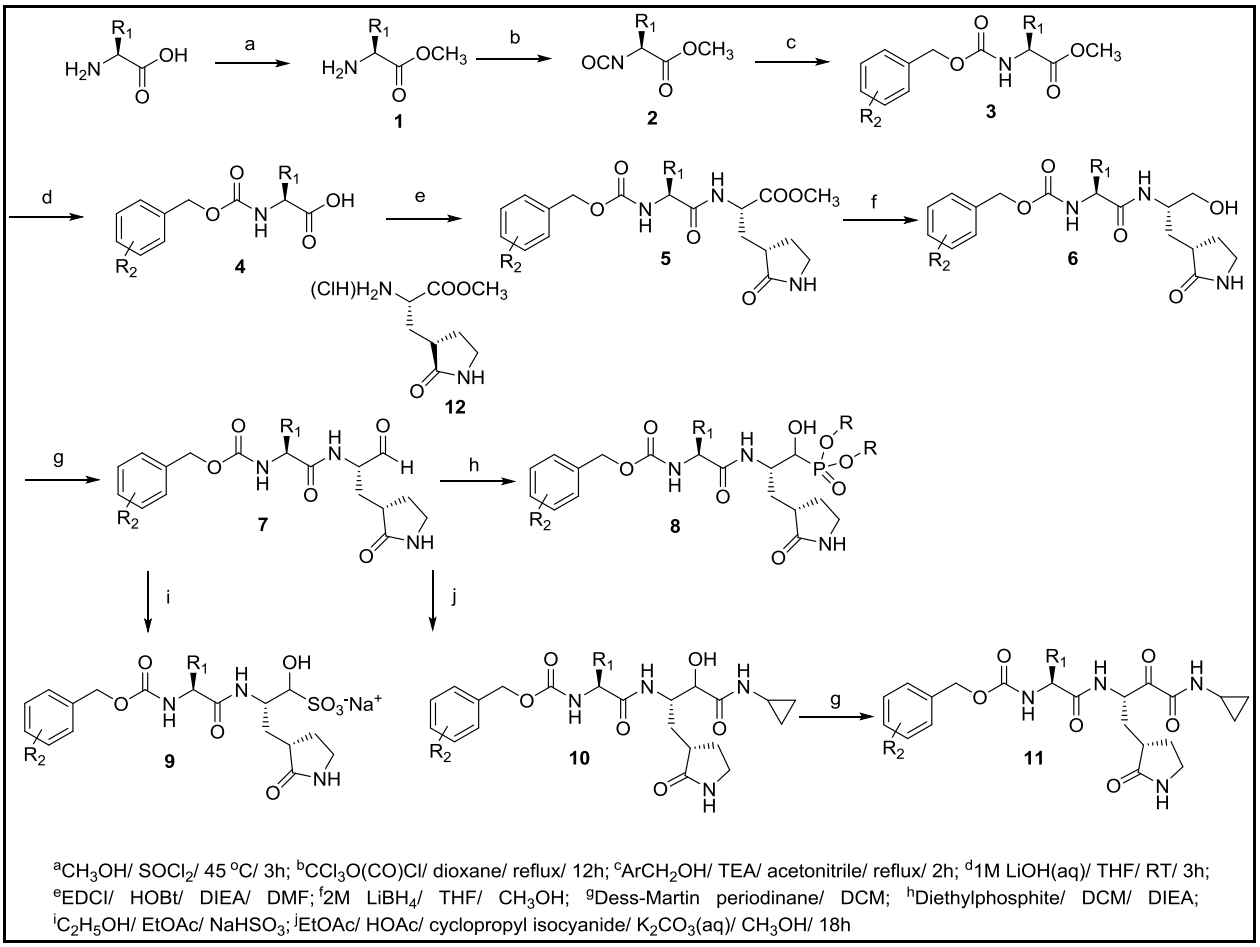

Scheme 2.1 Synthesis of inhibitors ***13-44***.

2.3 Experimental Section

2.3.1 General

Reagents and dry solvents were purchased from various chemical suppliers (Aldrich, Acros Organics, Chem-Impex, TCI America, and Bachem) and were used as obtained. Silica gel (230-450 mesh) used for flash chromatography was purchased from Sorbent Technologies (Atlanta, GA). Thin layer chromatography was performed using Analtech silica gel plates. Visualization was accomplished using UV light and/or iodine. NMR spectra were recorded in $CDCl_3$ or DMSO-d_6 using a Varian XL-400 spectrometer. Melting points were recorded on a Mel-Temp apparatus and are uncorrected. High resolution mass spectrometry (HRMS) was performed at the University of Kansas Mass Spectrometry lab using an LCT Premier mass spectrometer (Waters, Milford, MA) equipped with a time of flight mass analyzer and an electrospray ion source. The purity of the compounds was established using HPLC and was >95%.

Synthesis of amino acid methyl esters 1. General procedure. To a 250 mL RB flask (oven dried and purged with nitrogen) was added absolute methanol (30 mL) and the solution was cooled to 0 ^{0}C in an ice bath while kept under a nitrogen atmosphere. Thionyl chloride (8 mL) was added to the cooled methanol with stirring, followed by the addition of the amino acid (100 mmol). The ice bath was replaced by a water bath and the reaction mixture was heated to ~50 ^{0}C for 3 h with stirring. Removal of the solvent left a white residue which was washed with diethyl ether (250 mL) and collected by vacuum filtration to yield the amino acid methyl ester hydrochloride ***1*** as a white solid.

Synthesis of amino acid methyl ester isocyanates 2. General procedure. Amino acid methyl ester hydrochloride (100 mmol) was placed in a dry 500-mL RB flask and then dried overnight on the vacuum pump. The flask was flushed with nitrogen and dry dioxane (200 mL) was added followed by trichloromethyl chloroformate (29.67 g, 150 mmol), and the reaction mixture was refluxed for 10 h. The solvent was removed on the rotary evaporator and the residue was vacuum distilled to yield pure isocyanate ***2*** as a colorless oil.

Synthesis of substituted benzyl carbamates 3. General procedure. A solution of substituted benzyl alcohol (20 mmol) in dry acetonitrile (15 mL) was treated with triethylamine (4.05 g, 40 mmol) followed by the amino acid methyl ester isocyanate (20 mmol). The resulting solution was refluxed for 2 h and then allowed to cool to room temperature. The solution was concentrated and the residue was taken up in ethyl acetate (75 mL). The organic layer was washed with 5% HCl (2 x 20 mL) and brine (20 mL). The organic layer was dried over anhydrous sodium sulfate, filtered and concentrated, leaving a colorless oil (compound ***3***).

Synthesis of acids 4. General procedure. A solution of ester ***3*** (20 mmol) in tetrahydrofuran (30 mL) was treated with 1M LiOH (40 mL). The reaction mixture was stirred for 3 h at room temperature and the disappearance of the ester was monitored by TLC. Most of the solvent was evaporated off and the residue was diluted with water (25 mL). The solution was acidified to pH ~3 using 5% hydrochloride acid (20 mL) and the aqueous layer was extracted with ethyl acetate (3 x 100 mL). The combined organic layers were dried over anhydrous sodium sulfate, filtered, and concentrated to yield compound **4** as a colorless oil.

Synthesis of compounds 5. General Procedure. To a solution of compound ***4*** (10 mmol) in dry DMF (20 mL) was added EDCI (2.40 g, 12.5 mmol, 1.25 eq), HOBt (1.92 g, 12.5 mmol, 1.25 eq) and the mixture was stirred for 30 minutes at room temperature. In a separate flask, a solution of deprotected glutamine surrogate *12* (2.23 g, 10 mmol) in DMF (15 mL) cooled to 0-5 ^{o}C was treated with diisopropylethylamine (DIEA) (9.5 g, 40 mmol, 4 eq), stirred for 30 minutes, and then added to the reaction mixture containing acid. The reaction mixture was stirred for 12 h while monitoring the reaction by TLC. The solvent was removed and the residue was partitioned between ethyl acetate (200 mL) and 10% citric acid (2 x 40 mL). The ethyl acetate layer was further washed with saturated aqueous $NaHCO_3$ (40 mL), followed by saturated NaCl (50 mL). The organic layer was dried over anhydrous sodium sulfate, filtered and concentrated to yield a yellow-colored oily product. Purification by flash chromatography yielded ester ***5*** as a white solid.

Synthesis of alcohols 6. General procedure. To a solution of ester ***5*** (5 mmol) in anhydrous THF (30 mL) was added lithium borohydride (2M in THF, 7.5 mL, 15 mmol) dropwise, followed by absolute ethyl alcohol (15 mL), and the reaction mixture was stirred at room temperature overnight. The reaction mixture was then acidified by adding 5% HCl and the pH adjusted to ~2. Removal of the solvent left a residue which was taken up in ethyl acetate (100 mL). The organic layer was washed with brine (25 mL), dried over anhydrous sodium sulfate, filtered, and concentrated to yield compound **6** as a white solid.

Synthesis of aldehydes 7. General procedure. Compound ***6*** (5 mmol) was dissolved in anhydrous dichloromethane (50 mL) under a nitrogen atmosphere and cooled to 0^{o}C. Dess-Martin periodinane reagent (3.18 g, 7.5 mmol, 1.5 eq) was added to the reaction

mixture with stirring. The ice bath was removed and the reaction mixture was stirred at room temperature for 3 h (monitoring by TLC indicated complete disappearance of the starting material). A solution of 10% aqueous sodium thiosulfate (20 mL) was added and the solution was stirred for another 15 minutes. The aqueous layer was removed and the organic layer was washed with 10% aqueous sodium thiosulfate (20 mL), followed by saturated aqueous sodium bicarbonate (2 x 20 mL), water (2 x 20 mL) and brine (20 mL). The organic layer was dried over anhydrous sodium sulfate, filtered and concentrated. The yellow residue was purified by flash chromatography (silica gel/methylene chloride/ethyl acetate/methanol) to yield a white solid ***7***.

2-Chlorobenzyl ((S)-3-cyclohexyl-1-oxo-1-(((S)-1-oxo-3-((S)-2-oxopyrrolidin-3-yl)propan-2-yl)amino)propan-2-yl)carbamate (13): Yield (78%), mp 58-60 ^{o}C. ^{1}H NMR (400 MHz, DMSO-d_6) δ 9.41 (s, 1H), 8.47 - 8.52 (m, 1H), 7.57 - 7.69 (m, 1H), 7.44 - 7.51 (m, 2H), 7.32 - 7.40 (m, 2H), 5.74 - 5.77 (m, 1H), 5.02 - 5.19 (m, 2H), 4.06 - 4.22 (m, 2H), 3.00 - 3.17 (m, 2H), 2.19 - 2.31 (m, 1H), 2.08 - 2.17 (m, 1H), 1.84 - 1.94 (m, 1H), 1.54 - 1.76 (m, 8H), 1.39 - 1.52 (m, 3H), 1.08 - 1.19 (m, 2H), 0.81 - 0.93 (m, 2H). HRMS (ESI) calcd for $C_{24}H_{32}ClN_3O_5Na$: $[M+Na]^+$: 500.1928. Found: 500.1914.

3-Chlorobenzyl ((S)-3-cyclohexyl-1-oxo-1-(((S)-1-oxo-3-((S)-2-oxopyrrolidin-3-yl)propan-2-yl)amino)propan-2-yl)carbamate (16): Yield (86%), mp 54-56 ^{o}C. ^{1}H NMR (400 MHz, $CDCl_3$) δ 9.46 (s, 1H), 8.35 (d, *J* = 5.47 Hz, 1H), 7.33 (br. s., 1H), 7.27 - 7.31 (m, 1H), 7.22 - 7.27 (m, 1H), 7.16 - 7.21 (m, 1H), 6.36 - 6.49 (m, 1H), 5.60 (d, *J* = 8.20 Hz, 1H), 5.05 (s, 2H), 4.17 - 4.41 (m, 2H), 3.15 - 3.38 (m, 2H), 2.24 - 2.50 (m, 2H), 1.84 - 2.06 (m, 2H), 1.74 - 1.83 (m, 2H), 1.45 - 1.73 (m, 6H), 1.30 - 1.43 (m, 1H), 1.02 - 1.27 (m,

3H), 0.76 - 1.01 (m, 2H). HRMS (ESI) calcd for $C_{24}H_{32}ClN_3O_5Na$: $[M+Na]^+$: 500.1928. Found: 500.1917.

3-Chlorobenzyl ((S)-1-cyclohexyl-2-oxo-2-(((S)-1-oxo-3-((S)-2-oxopyrrolidin-3-yl)propan-2-yl)amino)ethyl)carbamate (21): Yield (81%), mp 51-53 ^oC. ^1H NMR (400 MHz, $CDCl_3$) δ 9.49 (s, 1H), 8.49 - 8.56 (m, 1H), 7.38 (br. s., 1H), 7.27 - 7.30 (m, 2H), 7.23 (d, *J* = 4.30 Hz, 1H), 5.71 - 5.78 (m, 1H), 5.44 - 5.51 (m, 1H), 5.08 (d, *J* = 13.28 Hz, 2H), 4.25 - 4.33 (m, 1H), 4.14 - 4.21 (m, 1H), 3.37 (d, *J* = 9.37 Hz, 2H), 2.36 - 2.52 (m, 2H), 1.95 (d, *J* = 6.64 Hz, 1H), 1.88 (br. s., 1H), 1.76 (d, *J* = 10.94 Hz, 2H), 1.68 (br. s., 2H), 1.58 (s, 4H), 1.21 - 1.34 (m, 2H), 1.13 (d, *J* = 12.89 Hz, 2H). HRMS (ESI) calcd for $C_{23}H_{30}ClN_3O_5Na$: $[M+Na]^+$: 486.1772. Found: 486.1758.

3-Chlorobenzyl ((S)-4-methyl-1-oxo-1-(((S)-1-oxo-3-((S)-2-oxopyrrolidin-3-yl)propan-2-yl)amino)pentan-2-yl)carbamate (22): Yield (82%), mp 53-55 ^oC. ^1H NMR (400 MHz, $CDCl_3$) δ 9.45 (s, 1H), 8.51 - 8.54 (m, 1H), 7.90 - 7.94 (m, 1H), 7.36 - 7.43 (m, 1H), 7.13 - 7.33 (m, 3H), 5.26 - 5.32 (m, 1H), 5.02 - 5.15 (m, 2H), 4.25 - 4.37 (m, 2H), 3.29 - 3.41 (m, 2H), 2.39 - 2.47 (m, 1H), 1.83 - 1.99 (m, 2H), 1.66 - 1.78 (m, 3H), 1.57 (m, 2H), 0.97 (d, *J* = 6.16 Hz, 6H).. HRMS (ESI) calcd for $C_{21}H_{28}ClN_3O_5Na$: $[M+Na]^+$: 460.1615. Found: 460.1611.

4-Chlorobenzyl ((S)-3-cyclohexyl-1-oxo-1-(((S)-1-oxo-3-((S)-2-oxopyrrolidin-3-yl)propan-2-yl)amino)propan-2-yl)carbamate (24): Yield (67%), mp 56-58 ^oC. ^1H NMR (400 MHz, $CDCl_3$) δ 9.48 (s, 1H), 8.31 (d, J = 5.47 Hz, 1H), 7.27 - 7.35 (m, 4H), 6.01 (br. s., 1H), 5.34 (d, J = 8.20 Hz, 1H), 5.03 - 5.11 (m, 2H), 4.28 - 4.39 (m, 2H), 3.35 (t, J = 8.20 Hz, 2H), 2.35 - 2.51 (m, 2H), 1.90 - 1.98 (m, 1H), 1.79 - 1.90 (m, 2H), 1.60 - 1.76 (m,

5H), 1.53 (ddd, J = 5.47, 8.98, 14.06 Hz, 1H), 1.23 - 1.30 (m, 2H), 1.08 - 1.22 (m, 2H), 0.81 - 1.03 (m, 3H). HRMS (ESI) calcd for $C_{24}H_{32}ClN_3O_5Na$: $[M+Na]^+$: 500.1928. Found: 500.1917.

2-Fluorobenzyl ((S)-3-cyclohexyl-1-oxo-1-(((S)-1-oxo-3-((S)-2-oxopyrrolidin-3-yl)propan-2-yl)amino)propan-2-yl)carbamate (25): Yield (81%), mp 61-63 ^oC. ^1H NMR (400 MHz, $CDCl_3$) δ 9.49 (s, 1H), 8.35 - 8.53 (m, 1H), 8.24 - 8.30 (m, 1H), 7.40 (t, *J* = 7.23 Hz, 1H), 7.27 - 7.34 (m, 1H), 7.10 - 7.17 (m, 1H), 7.05 (t, *J* = 9.18 Hz, 1H), 5.82 (br. s., 1H), 5.27 - 5.34 (m, 1H), 5.14 - 5.25 (m, 2H), 4.25 - 4.43 (m, 2H), 3.26 - 3.44 (m, 2H), 2.31 - 2.57 (m, 2H), 1.93 - 2.00 (m, 2H), 1.79 - 1.91 (m, 2H), 1.47 - 1.76 (m, 5H), 1.38 (d, *J* = 2.73 Hz, 1H), 1.07 - 1.29 (m, 3H), 0.84 - 1.03 (m, 2H). HRMS (ESI) calcd for $C_{24}H_{32}FN_3O_5Na$: $[M+Na]^+$: 484.2224. Found: 484.2214.

3-Fluorobenzyl ((S)-3-cyclohexyl-1-oxo-1-(((S)-1-oxo-3-((S)-2-oxopyrrolidin-3-yl)propan-2-yl)amino)propan-2-yl)carbamate (27): Yield (66%), mp 53-55 ^oC. ^1H NMR (400 MHz, $CDCl_3$) δ 9.48 (s, 1H), 8.40 (d, *J* = 5.08 Hz, 1H), 7.27 - 7.35 (m, 1H), 7.06 - 7.14 (m, 1H), 6.99 (dt, *J* = 2.34, 8.59 Hz, 2H), 5.97 (br s, 1H), 5.41 (d, *J* = 8.20 Hz, 1H), 5.06 - 5.14 (m, 2H), 4.25 - 4.41 (m, 2H), 3.29 - 3.41 (m, 2H), 2.27 - 2.54 (m, 2H), 1.90 - 2.00 (m, 1H), 1.79 - 1.89 (m, 2H), 1.60 - 1.78 (m, 6H), 1.48 - 1.58 (m, 1H), 1.32 - 1.46 (m, 1H), 1.08 - 1.30 (m, 3H), 0.85 - 1.04 (m, 2H). HRMS (ESI) calcd for $C_{24}H_{32}FN_3O_5Na$: $[M+Na]^+$: 484.2224. Found: 484.2207.

3-Bromobenzyl ((S)-3-cyclohexyl-1-oxo-1-(((S)-1-oxo-3-((S)-2-oxopyrrolidin-3-yl)propan-2-yl)amino)propan-2-yl)carbamate (29): Yield (83%), mp 52-55 ^oC. ^1H NMR (400 MHz, $CDCl_3$) δ 9.48 (s, 1H), 8.24 - 8.67 (m, 1H), 7.53 (br s, 1H), 7.35 - 7.47 (m, 1H),

7.25 - 7.29 (m, 2H), 7.22 (d, *J* = 7.42 Hz, 1H), 5.66 - 5.74 (m, 1H), 5.08 (br s, 2H), 4.23 - 4.40 (m, 2H), 3.36 (d, *J* = 8.59 Hz, 2H), 2.32 - 2.53 (m, 2H), 1.95 (br. s., 1H), 1.84 (br. s., 2H), 1.69 (d, *J* = 9.37 Hz, 5H), 1.57 (br. s., 3H), 1.32 - 1.46 (m, 1H), 1.08 - 1.28 (m, 2H), 0.84 - 1.05 (m, 2H). HRMS (ESI) calcd for $C_{24}H_{32}BrN_3O_5Na$: $[M+Na]^+$: 544.1423. Found: 544.1410.

3-Iodobenzyl ((S)-3-cyclohexyl-1-oxo-1-(((S)-1-oxo-3-((S)-2-oxopyrrolidin-3-yl)propan-2-yl)amino)propan-2-yl)carbamate (33): Yield (80%), mp 56-58 ^oC. ^1H NMR (400 MHz, $CDCl_3$) δ 9.48 (s, 1H), 8.38 - 8.44 (m, 1H), 7.73 (br s, 1H), 7.64 (d, *J* = 7.81 Hz, 1H), 7.31 (d, *J* = 7.81 Hz, 1H), 7.05 - 7.11 (m, 1H), 5.86 (br s, 1H), 5.34 (d, *J* = 7.81 Hz, 1H), 5.05 (s, 2H), 4.27 - 4.39 (m, 2H), 3.31 - 3.40 (m, 2H), 2.32 - 2.53 (m, 2H), 1.91 - 1.99 (m, 2H), 1.79 - 1.90 (m, 2H), 1.69 (d, *J* = 7.81 Hz, 6H), 1.47 - 1.58 (m, 1H), 1.38 (br s, 1H), 1.09 - 1.29 (m, 2H), 0.84 - 1.04 (m, 2H). HRMS (ESI) calcd for $C_{24}H_{32}IN_3O_5Na$: $[M+Na]^+$: 592.1284. Found: 592.1295.

2-Methoxybenzyl ((S)-3-cyclohexyl-1-oxo-1-(((S)-1-oxo-3-((S)-2-oxopyrrolidin-3-yl)propan-2-yl)amino)propan-2-yl)carbamate (35): Yield (64%), mp 56-58 ^oC. ^1H NMR (400 MHz, $CDCl_3$) δ 9.49 (br. s., 1H), 8.16 - 8.24 (m, 1H), 7.30 - 7.37 (m, 2H), 7.29 (s, 1H), 6.93 (t, *J* = 7.42 Hz, 1H), 6.88 (d, *J* = 8.20 Hz, 1H), 5.80 (br s, 1H), 5.11 - 5.24 (m, 2H), 4.28 - 4.40 (m, 2H), 3.83 (s, 3H), 3.27 - 3.39 (m, 2H), 2.40 (d, *J* = 12.89 Hz, 2H), 1.96 (br s, 2H), 1.78 - 1.90 (m, 2H), 1.64 - 1.76 (m, 4H), 1.60 (s, 1H), 1.53 (dd, *J* = 4.10, 9.57 Hz, 1H), 1.39 (br s, 1H), 1.08 - 1.30 (m, 3H), 0.85 - 1.04 (m, 2H). HRMS (ESI) calcd for $C_{25}H_{35}N_3O_6Na$: $[M+Na]^+$: 496.2424. Found: 496.2432.

3-Methoxybenzyl ((S)-3-cyclohexyl-1-oxo-1-(((S)-1-oxo-3-((S)-2-oxopyrrolidin-3-yl)propan-2-yl)amino)propan-2-yl)carbamate (36): Yield (76%), mp 60-62 ^{o}C. ^{1}H NMR (400 MHz, $CDCl_3$) δ 9.48 (s, 1H), 8.32 (d, *J* = 5.95 Hz, 1H), 7.22 - 7.26 (m, 1H), 6.88 - 6.95 (m, 2H), 6.84 (d, *J* = 8.24 Hz, 1H), 6.48 (br s, 1H), 5.56 (d, *J* = 8.39 Hz, 1H), 5.08 (s, 2H), 4.22 - 4.44 (m, 2H), 3.80 (s, 3H), 3.24 - 3.36 (m, 2H), 2.29 - 2.51 (m, 2H), 1.87 - 2.08 (m, 2H), 1.76 - 1.86 (m, 1H), 1.59 - 1.75 (m, 6H), 1.46 - 1.58 (m, 1H), 1.38 (br. s., 1H), 1.06 - 1.28 (m, 3H), 0.82 - 1.04 (m, 2H). HRMS (ESI) calcd for $C_{25}H_{35}N_3O_6Na$: $[M+Na]^+$: 496.2424. Found: 496.2418.

3-Cyanobenzyl ((S)-3-cyclohexyl-1-oxo-1-(((S)-1-oxo-3-((S)-2-oxopyrrolidin-3-yl)propan-2-yl)amino)propan-2-yl)carbamate (37): Yield (73%), mp 58-60 ^{o}C. ^{1}H NMR (400 MHz, $CDCl_3$) δ 9.45 (s, 1H), 8.53 (d, *J* = 5.47 Hz, 1H), 7.65 - 7.76 (m, 2H), 7.54 - 7.62 (m, 1H), 7.43 - 7.50 (m, 1H), 6.24 - 6.50 (m, 1H), 5.60 - 5.75 (m, 1H), 5.02 - 5.35 (m, 2H), 4.45 - 4.56 (m, 1H), 4.24 - 4.41 (m, 1H), 3.18 - 3.43 (m, 2H), 2.29 - 2.59 (m, 2H), 2.07 - 2.25 (m, 2H), 1.49 - 1.99 (m, 6H), 1.30 - 1.46 (m, 1H), 1.08 - 1.23 (m, 4H), 0.83 - 1.01 (m, 3H). HRMS (ESI) calcd for $C_{25}H_{32}N_4O_5Na$: $[M+Na]^+$: 491.2270. Found: 491.2258.

3-((tert-Butoxycarbonyl)amino)benzyl ((S)-3-cyclohexyl-1-oxo-1-(((S)-1-oxo-3-((S)-2-oxopyrrolidin-3-yl)propan-2-yl)amino)propan-2-yl)carbamate (38): Yield (65%), mp 106-110 ^{o}C. ^{1}H NMR (400 MHz, $CDCl_3$) δ 9.52 (s, 1H), 9.41 - 9.46 (m, 1H), 8.40 - 8.46 (m, 1H), 7.32 - 7.38 (m, 1H), 7.24 (br s, 1H), 7.22 (s, 1H), 7.20 (s, 1H), 6.92 - 6.98 (m, 1H), 5.42 - 5.51 (m, 1H), 4.98 (s, 2H), 4.22 - 4.41 (m, 2H), 3.30 (d, *J* = 7.20 Hz, 2H), 2.22 - 2.50 (m, 2H), 2.03 (s, 1H), 1.86 - 1.94 (m, 1H), 1.76 (d, *J* = 8.09 Hz, 3H), 1.56 - 1.72 (m, 4H), 1.48 (s, 9H), 1.30 - 1.40 (m, 1H), 1.04 - 1.25 (m, 4H), 0.91 (br s, 2H). HRMS (ESI) calcd for $C_{29}H_{42}N_4O_7Na$: $[M+Na]^+$: 581.2951. Found: 581.2957.

3-Nitrobenzyl ((S)-3-cyclohexyl-1-oxo-1-(((S)-1-oxo-3-((S)-2-oxopyrrolidin-3-yl)propan-2-yl)amino)propan-2-yl)carbamate (39): Yield (70%), mp 52-54 ^{o}C. ^{1}H NMR (400 MHz, $CDCl_3$) δ 9.45 (s, 1H), 8.67 (d, *J* = 5.08 Hz, 1H), 8.30 (s, 1H), 8.16 (d, *J* = 8.20 Hz, 1H), 7.66 (d, *J* = 7.81 Hz, 1H), 7.50 - 7.55 (m, 1H), 5.85 (br s, 1H), 5.38 (d, *J* = 8.20 Hz, 1H), 5.11 - 5.30 (m, 2H), 4.31 - 4.40 (m, 1H), 4.24 (d, *J* = 6.25 Hz, 1H), 3.37 (dd, *J* = 6.05, 8.79 Hz, 2H), 2.33 - 2.52 (m, 2H), 1.86 - 1.97 (m, 2H), 1.47 - 1.84 (m, 6H), 1.31 - 1.44 (m, 2H), 1.06 - 1.28 (m, 3H), 0.82 - 1.04 (m, 3H). HRMS (ESI) calcd for $C_{24}H_{32}N_4O_7Na$: $[M+Na]^+$: 511.2169. Found: 511.2153.

Benzyl ((S)-4-methyl-1-oxo-1-(((S)-1-oxo-3-((S)-2-oxopyrrolidin-3-yl)propan-2-yl)amino)pentan-2-yl)carbamate (40): Yield (83%), mp 57-59 ^{o}C. ^{1}H NMR (400 MHz, $CDCl_3$) δ 9.53 (br s, 1H), 8.32 - 8.45 (m, 1H), 7.32 - 7.46 (m, 5H), 5.78 - 5.85 (m, 1H), 5.34 (br s, 1H), 5.09 - 5.18 (m, 2H), 4.35 (br s, 2H), 3.30 - 3.45 (m, 2H), 2.30 - 2.59 (m, 2H), 1.99 (d, *J* = 6.64 Hz, 1H), 1.83 - 1.93 (m, 1H), 1.69 - 1.81 (m, 1H), 1.58 - 1.69 (m, 2H), 1.23-1.30 (m, 1H), 0.94 (d, J= 6.15 Hz, 6H). HRMS (ESI) calcd for $C_{21}H_{29}N_3O_5Na$: $[M+Na]^+$: 426.2005. Found: 426.1997.

Benzyl ((S)-3-cyclohexyl-1-oxo-1-(((S)-1-oxo-3-((S)-2-oxopyrrolidin-3-yl)propan-2-yl)amino)propan-2-yl)carbamate (43): Yield (74%), mp 53-56 ^{o}C. ^{1}H NMR (400 MHz, $CDCl_3$) δ 9.48 (s, 1H), 8.31 (d, *J* = 5.86 Hz, 1H), 7.73 (br s, 1H), 7.34 (br s, 5H), 5.50 - 5.59 (m, 1H), 5.04 - 5.15 (m, 2H), 4.20 - 4.53 (m, 2H), 3.20 - 3.41 (m, 2H), 2.23 - 2.51 (m, 2H), 1.88 - 2.03 (m, 1H), 1.74 - 1.86 (m, 2H), 1.66 (d, *J* = 5.86 Hz, 6H), 1.45 - 1.58 (m, 1H), 1.30 - 1.43 (m, 1H), 1.18 (d, *J* = 16.12 Hz, 3H), 0.79 - 1.03 (m, 2H). HRMS (ESI) calcd for $C_{24}H_{33}N_3O_5Na$: $[M+Na]^+$: 466.2318. Found: 466.2299.

Synthesis of α-Hydroxyphosphonates *8*. General procedure. To a solution of diethylphosphite (135 mg, 1 mmol) in dry dichloromethane (3.5 mL) was added DIEA (129 mg, 1 mmol) followed by a solution of aldehyde ***7*** (1 mmol) in dichloromethane (5 mL). The reaction mixture was stirred at room temperature for 20 h. The reaction mixture was diluted with dichloromethane (100 mL) and washed with 5% HCl (2 x 20 mL), and brine (30 mL). The organic layer was dried over anhydrous sodium sulfate, filtered and concentrated, leaving a light yellow solid which was purified by flash chromatography to yield compound ***8*** as a white solid.

2-Chlorobenzyl ((2S)-3-cyclohexyl-1-(((2S)-1-(diethoxyphosphoryl)-1-hydroxy-3-((S)-2-oxopyrrolidin-3-yl)propan-2-yl)amino)-1-oxopropan-2-yl)carbamate (14): Yield (79%), mp 103-106 ^{o}C. ^{1}H NMR (400 MHz, $CDCl_3$) δ 7.66 - 7.71 (m, 1H), 7.41 (d, *J* = 3.12 Hz, 1H), 7.33 - 7.37 (m, 1H), 7.28 - 7.32 (m, 1H), 7.21 - 7.26 (m, 3H), 5.49 - 5.57 (m, 1H), 5.15 - 5.24 (m, 2H), 4.06 - 4.21 (m, 4H), 3.97 - 4.04 (m, 1H), 3.86 - 3.95 (m, 1H), 3.41 - 3.52 (m, 1H), 1.77 - 1.86 (m, 2H), 1.56 - 1.71 (m, 6H), 1.50 - 1.56 (m, 1H), 1.25 - 1.37 (m, 7H), 1.23 (s, 2H), 1.17 (dt, *J* = 2.15, 7.13 Hz, 4H), 0.86 (br s, 4H). HRMS (ESI) calcd for $C_{28}H_{43}ClN_3O_8PNa$: $[M+Na]^+$: 638.2374. Found: 638.2379.

3-Chlorobenzyl ((2S)-3-cyclohexyl-1-(((2S)-1-(diethoxyphosphoryl)-1-hydroxy-3-((S)-2-oxopyrrolidin-3-yl)propan-2-yl)amino)-1-oxopropan-2-yl)carbamate (17): Yield (81%), mp 58-61 ^{o}C. ^{1}H NMR (400 MHz, $CDCl_3$) δ 7.77 - 7.83 (m, 1H), 7.30 - 7.38 (m, 1H), 7.24 - 7.29 (m, 2H), 7.16 - 7.23 (m, 1H), 6.39 - 6.48 (m, 1H), 5.86 - 5.94 (m, 1H), 5.33 - 5.42 (m, 1H), 4.98 - 5.12 (m, 2H), 4.22 - 4.42 (m, 2H), 4.07 - 4.20 (m, 4H), 3.91 - 4.01 (m, 1H), 3.17 - 3.35 (m, 2H), 2.30 - 2.47 (m, 2H), 2.10 - 2.23 (m, 2H), 1.66 (d, *J* =

11.33 Hz, 6H), 1.41 - 1.54 (m, 2H), 1.28 - 1.36 (m, 6H), 1.05 - 1.22 (m, 3H), 0.79 - 1.00 (m, 3H). HRMS (ESI) calcd for $C_{28}H_{43}ClN_3O_8PNa$: $[M+Na]^+$: 638.2374. Found: 638.2367.

2-Fluorobenzyl ((2S)-3-cyclohexyl-1-(((2S)-1-(diethoxyphosphoryl)-1-hydroxy-3-((S)-2-oxopyrrolidin-3-yl)propan-2-yl)amino)-1-oxopropan-2-yl)carbamate (26): Yield (73%), mp 98-101 ^oC. ^1H NMR (400 MHz, DMSO-d_6) δ 7.80 (br s, 1H), 7.65 (d, *J* = 8.98 Hz, 1H), 7.49 - 7.57 (m, 1H), 7.33 - 7.48 (m, 2H), 7.14 - 7.25 (m, 2H), 5.90 - 5.97 (m, 1H), 5.71 - 5.84 (m, 1H), 5.07 (d, *J* = 6.35 Hz, 2H), 3.95 - 4.09 (m, 5H), 3.75 - 3.93 (m, 1H), 2.96 - 3.24 (m, 3H), 2.00 - 2.26 (m, 2H), 1.50 - 1.75 (m, 7H), 1.36 - 1.47 (m, 2H), 1.19 - 1.33 (m, 6H), 1.01 - 1.15 (m, 3H), 0.84 (d, *J* = 7.91 Hz, 3H). HRMS (ESI) calcd for $C_{28}H_{43}FN_3O_8PNa$: $[M+Na]^+$: 622.2670. Found: 622.2658.

3-Bromobenzyl ((2S)-3-cyclohexyl-1-(((2S)-1-(diethoxyphosphoryl)-1-hydroxy-3-((S)-2-oxopyrrolidin-3-yl)propan-2-yl)amino)-1-oxopropan-2-yl)carbamate (30): Yield (78%), mp 48-52 ^oC. ^1H NMR (400 MHz, $CDCl_3$) δ 8.35 - 8.40 (m, 1H), 7.46 (d, *J* = 3.32 Hz, 1H), 7.33 - 7.39 (m, 1H), 7.21 (br s, 1H), 7.11 - 7.18 (m, 2H), 5.88 (s, 1H), 5.26 - 5.31 (m, 1H), 5.01 (d, *J* = 3.32 Hz, 2H), 4.02 - 4.15 (m, 6H), 3.27 (d, *J* = 6.44 Hz, 3H), 1.88 (br. s., 1H), 1.76 (d, *J* = 9.37 Hz, 2H), 1.60 (br s, 7H), 1.46 (d, *J* = 1.95 Hz, 1H), 1.23 - 1.34 (m, 6H), 1.19 (s, 1H), 0.98 - 1.16 (m, 3H), 0.75 - 0.96 (m, 3H). HRMS (ESI) calcd for $C_{28}H_{43}BrN_3O_8PNa$: $[M+Na]^+$: 682.1869. Found: 682.1896.

Synthesis of bisulfite adducts *9*. General procedure. To a solution of aldehyde ***7*** (5 mmol) in dry ethyl acetate (20 mL) was added absolute ethanol (12 mL) with stirring, followed by a solution of sodium bisulfite (540 mg; 5 mmol) in water (5 mL). The reaction mixture was stirred for 3 h at 50 ^0C. The reaction mixture was allowed to cool to room

temperature and then vacuum filtered. The solid was thoroughly washed with absolute ethanol and the filtrate was dried over anhydrous sodium sulfate, filtered, and concentrated to yield yellowish oil. The oily product was treated with ethyl ether (2 x 50 mL) to form white solid. The white solid was stirred with ethyl ether (30 mL) and ethyl acetate (15 mL) for 5 minutes. Careful removal of the solvent using a pipette left compound ***9*** as a white solid.

Sodium (2S)-2-((S)-2-((((2-chlorobenzyl)oxy)carbonyl)amino)-3-cyclohexylpropanamido)-1-hydroxy-3-((S)-2-oxopyrrolidin-3-yl)propane-1-sulfonate (15): Yield (60%), mp 128-132 ^{o}C. ^{1}H NMR (400 MHz, $CDCl_3$) δ 7.51 - 7.53 (m, 1H), 7.40 - 7.45 (m, 1H), 7.35 - 7.39 (m, 1H), 7.26 (s, 3H), 6.99 - 7.00 (m, 1H), 5.18 - 5.29 (m, 2H), 3.68 - 3.78 (m, 2H), 3.48 (d, *J* = 7.03 Hz, 3H), 3.29 - 3.40 (m, 1H), 1.92 - 1.98 (m, 1H), 1.80 - 1.91 (m, 2H), 1.71 (br s, 7H), 1.24 - 1.28 (m, 5H), 0.79 - 0.96 (m, 2H), 0.68 - 0.76 (m, 1H). HRMS (ESI) calcd for $C_{24}H_{33}ClN_3O_8S$: [M-]: 558.1677. Found: 558.1648.

Sodium (2S)-2-((S)-2-((((3-chlorobenzyl)oxy)carbonyl)amino)-3-cyclohexylpropanamido)-1-hydroxy-3-((S)-2-oxopyrrolidin-3-yl)propane-1-sulfonate (18): Yield (67%), mp 124-126 ^{o}C. ^{1}H NMR (400 MHz, DMSO-d_6) δ 7.66 (d, *J* = 8.98 Hz, 1H), 7.58 (dd, *J* = 9.18, 11.52 Hz, 1H), 7.49 (d, *J* = 8.20 Hz, 1H), 7.42 (d, *J* = 4.30 Hz, 1H), 7.40 (d, *J* = 1.95 Hz, 1H), 7.30 - 7.39 (m, 2H), 5.41 (d, *J* = 5.86 Hz, 1H), 5.25 (d, *J* = 5.86 Hz, 1H), 5.03 (s, 2H), 4.17 - 4.26 (m, 1H), 3.89 - 3.99 (m, 2H), 3.81 - 3.87 (m, 1H), 3.10 (t, *J* = 9.96 Hz, 1H), 2.95 - 3.05 (m, 1H), 2.01 - 2.25 (m, 3H), 1.51 - 1.78 (m, 6H), 1.37 - 1.48 (m, 1H), 1.28 (br s, 1H), 1.15 - 1.21 (m, 1H), 1.08 - 1.14 (m, 2H), 0.74 - 0.94 (m, 2H). HRMS (ESI) calcd for $C_{24}H_{33}ClN_3O_8S$: [M-]: 558.1677. Found: 558.1656.

Sodium(2S)-2-((S)-2-((((3-bromobenzyl)oxy)carbonyl)amino)-3-cyclohexylpropanamido)-1-hydroxy-3-((S)-2-oxopyrrolidin-3-yl)propane-1-sulfonate (31): Yield (86%), mp 132-135 ^{o}C. ^{1}H NMR (400 MHz, DMSO-d_6) δ 7.68 (d, *J* = 8.98 Hz, 1H), 7.60 (d, *J* = 9.37 Hz, 1H), 7.53 - 7.58 (m, 1H), 7.50 (d, *J* = 7.81 Hz, 1H), 7.45 (d, *J* = 4.30 Hz, 1H), 7.29 - 7.41 (m, 2H), 5.54 (d, *J* = 5.47 Hz, 1H), 5.36 (d, *J* = 5.08 Hz, 1H), 5.03 (s, 2H), 4.18 - 4.27 (m, 1H), 3.91 - 4.10 (m, 1H), 2.96 - 3.15 (m, 2H), 2.05 - 2.23 (m, 2H), 1.89 - 2.05 (m, 1H), 1.49 - 1.75 (m, 6H), 1.38 - 1.47 (m, 1H), 1.23 - 1.35 (m, 1H), 1.02 - 1.21 (m, 5H), 0.75 - 0.95 (m, 2H). HRMS (ESI) calcd for $C_{24}H_{33}BrN_3O_8S$: [M-]: 602.1172. Found: 602.1168.

Sodium (2S)-2-((S)-3-cyclohexyl-2-((((3-iodobenzyl)oxy)carbonyl)amino)propanamido)-1-hydroxy-3-((S)-2-oxopyrrolidin-3-yl)propane-1-sulfonate (34): Yield (78%), mp 135-137 ^{o}C. ^{1}H NMR (400 MHz, DMSO-d_6) δ 8.48 - 8.52 (m, 1H), 7.73 (br s, 1H), 7.66 (d, *J* = 7.62 Hz, 1H), 7.51 - 7.59 (m, 1H), 7.45 (d, *J* = 3.52 Hz, 1H), 7.36 (br s, 1H), 7.13 - 7.21 (m, 1H), 5.45 - 5.52 (m, 1H), 5.28 - 5.35 (m, 1H), 4.92 - 5.14 (m, 2H), 4.13 - 4.29 (m, 1H), 3.88 - 4.08 (m, 1H), 2.97 - 3.19 (m, 2H), 1.91 (s, 3H), 1.37 - 1.78 (m, 7H), 1.02 - 1.24 (m, 5H), 0.73 - 0.97 (m, 3H). HRMS (ESI) calcd for $C_{24}H_{33}IN_3O_8S$: [M-]: 650.1033. Found: 650.1019.

Sodium (2S)-2-((S)-2-(((benzyloxy)carbonyl)amino)-4-methylpentanamido)-1-hydroxy-3-((S)-2-oxopyrrolidin-3-yl)propane-1-sulfonate (41): Yield (73%), mp 109-113 ^{o}C. ^{1}H NMR (400 MHz, DMSO-d_6) δ 7.57 - 7.62 (m, 1H), 7.47 - 7.52 (m, 1H), 7.26 - 7.40 (m, 5H), 5.47 - 5.51 (m, 1H), 5.31 - 5.36 (m, 1H), 4.96 - 5.05 (m, 3H), 4.19 - 4.28 (m, 1H), 3.83 - 4.06 (m, 2H), 3.07 - 3.16 (m, 1H), 2.97 - 3.06 (m, 1H), 2.04 - 2.23 (m, 2H),

1.71 - 1.81 (m, 1H), 1.52 - 1.68 (m, 2H), 1.39 - 1.50 (m, 2H), 0.85 (ddd, *J* = 3.03, 6.52, 9.40 Hz, 6H). HRMS (ESI) calcd for $C_{21}H_{30}N_3O_8S$: [M-]: 484.1754. Found: 484.1754.

Sodium (2S)-2-((S)-2-(((benzyloxy)carbonyl)amino)-3-cyclohexylpropanamido)-1-hydroxy-3-((S)-2-oxopyrrolidin-3-yl)propane-1-sulfonate (44): Yield (78%), mp 131-133 ^oC. ^1H NMR (400 MHz, DMSO-d_6) δ 7.62 - 7.69 (m, 1H), 7.43 - 7.51 (m, 1H), 7.27 - 7.40 (m, 5H), 5.82 - 5.86 (m, 1H), 5.52 (d, *J* = 6.25 Hz, 1H), 5.36 (d, *J* = 5.96 Hz, 1H), 5.02 (s, 2H), 3.83 - 4.08 (m, 2H), 2.97 - 3.20 (m, 3H), 1.86 - 2.25 (m, 3H), 1.51 - 1.82 (m, 6H), 1.37 - 1.48 (m, 2H), 1.29 (br s, 1H), 1.02 - 1.22 (m, 3H), 0.75 - 0.94 (m, 2H). HRMS (ESI) calcd for $C_{24}H_{34}N_3O_8S$: [M-]: 524.2067. Found: 524.2045.

Synthesis of compound 10. General procedure. A solution of aldehyde ***7*** (5 mmol) in ethyl acetate (30 mL) kept at 0 ^oC was treated with acetic acid (0.34 g; 5.75 mmol) followed by cyclopropyl isocyanide (0.37 g; 5.5 mmol), and the reaction mixture was stirred at room temperature for 18 h. The solution was concentrated in vacuo and the residue was dissolved in methanol (30 mL) and treated with a solution of K_2CO_3 (1.72 g; 12.5 mmol) in water (25 mL). The reaction mixture was stirred at room temperature for 2 h. Methanol was evaporated off and the aqueous layer was extracted with ethyl acetate (3 x 100 mL). The combined organic layers were washed with 5% HCl (2 x 50 mL) and brine (75 mL). The organic layer was dried over anhydrous sodium sulfate and the solvent was removed to yield compound ***10*** as a white solid. This was used in the next step without further purification.

Synthesis of α-ketoamides 11. General procedure. To a solution of **c**ompound **10** (5 mmol) in anhydrous dichloromethane (50 mL) cooled to 0 ^oC and kept under a nitrogen atmosphere was added Dess-Martin periodinane reagent (3.18 g, 7.5 mmol, 1.5 eq) with

stirring. The ice bath was removed and the reaction mixture was stirred at room temperature for 3 h. The reaction was monitored by TLC until the starting material disappeared. A solution of 10% aqueous sodium thiosulfate (20 mL) was added and the solution was stirred for 15 minutes. The solution was poured into a separatory funnel and the aqueous layer was removed. The organic layer was washed with 10 % aqueous sodium thiosulfate (20 mL), followed by saturated aqueous sodium bicarbonate (2 x 20 mL), water (2 x 20 mL) and brine (20 mL). The organic layer was dried over anhydrous sodium sulfate, filtered and concentrated leaving a yellow solid which was purified by flash chromatography (silica gel/methylene chloride/ethyl acetate/methanol) to yield **11** as a white solid.

3-Chlorobenzyl ((S)-3-cyclohexyl-1-(((S)-4-(cyclopropylamino)-3,4-dioxo-1-((S)-2-oxopyrrolidin-3-yl)butan-2-yl)amino)-1-oxopropan-2-yl)carbamate (19): Yield (88%), mp 135-138 ^{o}C. ^{1}H NMR (400 MHz, $CDCl_3$) δ 8.42 (br s, 1H), 7.36 (br s, 1H), 7.27 - 7.29 (m, 2H), 7.19 - 7.24 (m, 2H), 6.97 (br s, 1H), 5.97 (br s, 1H), 5.08 (d, *J* = 4.30 Hz, 2H), 4.24 - 4.42 (m, 2H), 3.27 - 3.40 (m, 2H), 2.76 (dd, *J* = 3.52, 7.42 Hz, 1H), 2.35 - 2.60 (m, 2H), 2.07 (dd, *J* = 3.32, 5.27 Hz, 1H), 1.89 - 1.99 (m, 2H), 1.77 - 1.87 (m, 2H), 1.59 - 1.75 (m, 4H), 1.43 - 1.56 (m, 1H), 1.38 (br s, 1H), 1.09 - 1.28 (m, 3H), 0.86 - 1.04 (m, 2H), 0.81 - 0.85 (m, 2H), 0.56 - 0.66 (m, 2H). HRMS (ESI) calcd for $C_{28}H_{37}ClN_4O_6Na$: $[M+Na]^+$: 583.2299. Found: 583.2293.

3-Chlorobenzyl ((S)-1-(((S)-4-(cyclopropylamino)-3,4-dioxo-1-((S)-2-oxopyrrolidin-3-yl)butan-2-yl)amino)-4-methyl-1-oxopentan-2-yl)carbamate (23): Yield (72%), mp 66-68 ^{o}C. ^{1}H NMR (400 MHz, $CDCl_3$) δ 8.40 (d, *J* = 5.47 Hz, 1H), 7.24 (br s, 1H), 7.16 - 7.22 (m, 1H), 7.11 (br s, 2H), 6.75 (br s, 1H), 5.63 - 5.75 (m, 1H), 5.10 - 5.21 (m, 1H),

4.93 - 5.05 (m, 2H), 4.22 - 4.36 (m, 2H), 3.15 - 3.30 (m, 2H), 2.69 (d, *J* = 3.12 Hz, 1H), 2.39 - 2.51 (m, 1H), 2.31 (d, *J* = 3.91 Hz, 1H), 1.80 - 2.01 (m, 5H), 1.50 - 1.72 (m, 3H), 1.38 - 1.49 (m, 2H), 0.86 (d, *J* = 4.69 Hz, 2H), 0.74 (d, *J* = 7.42 Hz, 2H), 0.54 (br s, 2H). HRMS (ESI) calcd for $C_{25}H_{33}ClN_4O_6Na$: $[M+Na]^+$: 543.1986. Found: 543.1989.

3-Fluorobenzyl ((S)-3-cyclohexyl-1-(((S)-4-(cyclopropylamino)-3,4-dioxo-1-((S)-2-oxopyrrolidin-3-yl)butan-2-yl)amino)-1-oxopropan-2-yl)carbamate (28): Yield (74%), mp 95-98 ^oC. ^1H NMR (400 MHz, $CDCl_3$) δ 8.41 - 8.49 (m, 1H), 7.28 - 7.36 (m, 2H), 7.25 (d, *J* = 2.34 Hz, 1H), 7.10 (t, *J* = 7.42 Hz, 2H), 6.90 - 7.02 (m, 1H), 5.83 (br s, 1H), 5.04 - 5.13 (m, 2H), 4.25 - 4.39 (m, 2H), 3.36 (dd, *J* = 4.49, 8.79 Hz, 2H), 2.76 (dd, *J* = 3.52, 7.42 Hz, 1H), 2.51 - 2.61 (m, 1H), 2.39 - 2.50 (m, 1H), 2.06 - 2.14 (m, 1H), 1.94 (d, *J* = 10.94 Hz, 2H), 1.80 (br s, 1H), 1.58 - 1.74 (m, 6H), 1.48 (br s, 1H), 1.31 - 1.42 (m, 1H), 1.07 - 1.29 (m, 3H), 0.79 - 1.03 (m, 3H), 0.61 (ddd, *J* = 1.56, 4.00, 5.76 Hz, 2H). HRMS (ESI) calcd for $C_{28}H_{37}FN_4O_6Na$: $[M+Na]^+$: 567.2595. Found: 567.2592.

3-Bromobenzyl ((S)-3-cyclohexyl-1-(((S)-4-(cyclopropylamino)-3,4-dioxo-1-((S)-2-oxopyrrolidin-3-yl)butan-2-yl)amino)-1-oxopropan-2-yl)carbamate (32): Yield (70%), mp 124-127 ^oC. ^1H NMR (400 MHz, $CDCl_3$) δ 8.39 - 8.45 (m, 1H), 7.52 (br s, 1H), 7.43 (d, *J* = 7.62 Hz, 1H), 7.27 (br s, 1H), 7.22 (d, *J* = 7.62 Hz, 2H), 6.90 - 6.95 (m, 1H), 5.71 - 5.75 (m, 1H), 5.18 - 5.27 (m, 1H), 5.07 (s, 2H), 4.28 - 4.35 (m, 1H), 3.35 (dd, *J* = 4.10, 8.98 Hz, 3H), 2.72 - 2.81 (m, 2H), 2.06 - 2.15 (m, 2H), 1.86 - 2.01 (m, 2H), 1.69 (d, *J* = 10.94 Hz, 5H), 1.58 (s, 3H), 1.25 (s, 2H), 0.87 - 1.02 (m, 2H), 0.84 (d, *J* = 7.42 Hz, 2H), 0.55 - 0.67 (m, 2H). HRMS (ESI) calcd for $C_{28}H_{37}BrN_4O_6Na$: $[M+Na]^+$: 627.1794. Found: 627.1791.

Benzyl ((S)-1-(((S)-4-(cyclopropylamino)-3,4-dioxo-1-((S)-2-oxopyrrolidin-3-yl)butan-2-yl)amino)-4-methyl-1-oxopentan-2-yl)carbamate (42): Yield (78%), mp 75-78 ^{o}C. ^{1}H NMR (400 MHz, $CDCl_3$) δ 8.43 (d, *J* = 5.68 Hz, 1H), 7.33 (s, 5H), 7.08 (d, *J* = 3.48 Hz, 1H), 6.57 (s, 1H), 5.53 (d, *J* = 8.79 Hz, 1H), 5.19 - 5.26 (m, 1H), 5.08 (s, 2H), 4.40 (dt, *J* = 5.49, 8.88 Hz, 1H), 3.22 - 3.36 (m, 2H), 2.71 - 2.80 (m, 1H), 2.48 - 2.58 (m, 1H), 2.35 - 2.46 (m, 1H), 1.88 - 2.10 (m, 3H), 1.59 - 1.79 (m, 2H), 1.45 - 1.55 (m, 1H), 0.95 (d, *J* = 6.41 Hz, 6H), 0.79 - 0.86 (m, 2H), 0.57 - 0.66 (m, 2H). HRMS (ESI) calcd for $C_{25}H_{34}N_4O_6Na$: $[M+Na]^+$: 509.2376. Found: 509.2364.

2.3.2 FRET Protease Assays

The FRET protease assay was performed by preparing stock solutions of the substrate (Edans-DFHLQ/GP-Dabcyl and inhibitor in DMSO and diluting into assay buffer which was comprised of 20mM HEPES buffer, pH 8, containing NaCl (200 mM), 0.4 mM EDTA, glycerol (60%), and 6 mM dithiothreitol (DTT). The protease was mixed with serial dilutions of each compound or with DMSO in 25 µL of assay buffer and incubated at 37^{o}C for 30 min, followed by the addition of 25 µL of assay buffer containing substrate. Fluorescence readings were obtained using an excitation wavelength of 360 nm and an emission wavelength of 460 nm on a fluorescence microplate reader (FLx800; Biotec, Winoosk, VT) 1 h following the addition of substrate. Relative fluorescence units (RFU) were determined by subtracting background values (substrate-containing well without protease) from the raw fluorescence values, as described previously.[140,158,160] The dose-dependent FRET inhibition curves were fitted with a variable slope by using GraphPad Prism software (GraphPad, La Jolla, CA) in order to determine the IC_{50} values of the inhibitors.

2.3.3 Cell- Based Inhibition Assays

The effects of each inhibitor on virus replication were examined in cell culture systems. Virus-infected cells were incubated at 37^{o}C using the H23 cell line. Briefly, confluent and semi-confluent cells were inoculated with virus at a multiplicity of infection of 0.05 for 1 h, and the inoculum was replaced with medium containing DMSO (<0.1%) or each compound (up to 100 μM). The virus-infected cells were further incubated for up to 168 h, and the replication of virus was measured by the 50% tissue culture infective dose ($TCID_{50}$)[140] method and/or real-time quantitative RT-PCR (qRT-PCR). The $TCID_{50}$ method was used for titration of viruses showing apparent cell cytopathic effects, which included MNV-1. Real-time qRT-PCR was performed for titration of NV (replicon harboring cells). For real-time qRT-PCR, RNA was extracted from each sample (cell lysates for HG23 cells) by use of an RNeasy kit (Qiagen, Valencia, CA), followed by amplification in a Cepheid SmartCycler with the following parameters: 45^{o}C for 30 min and 95^{o}C for 10 min followed by 40 cycles of denaturation at 95^{o}C for 30 s, annealing at 50^{o}C for 1 min, and elongation at 72^{o}C for 30 s. The primers and probes used for real-time qRT-PCR for NV included 5'-CGYTGGATGCGNTTYCATGA-3', 5'-CTTAGACGCCATCATCATTYAC-3' and 6-carboxyfluorescein(FAM)-5'-AGATYGCGATCYCCTGTCCA-3'-6-carboxytetramethylrhodamine (TAMRA). The IC_{50}s were determined by GraphPadPrism software.

2.3.4 X-ray Crystallographic Studies. Crystallization and Data Collection

Purified NV 3CLpro in 100 mM NaCl, 50 mM PBS pH 7.2, 1 mM DTT at a concentration of 10 mg/mL was used for preparation of the norovirus 3CL protease-compound ***17*** complex. A stock solution of 100 mM compound ***17*** or ***44*** was prepared in DMSO and each NV 3CLpro:inhibitor complex was prepared by mixing 12 µL of ***17*** or ***44*** (3 mM) with 388 µL (0.49 mM) of NV 3CLpro and incubating on ice for 1 h. The mixture was loaded onto a Superdex 75 10/300 GL column equilibrated with 100 mM NaCl, 20 mM Tris pH 8.0 and the sample was concentrated to 8.0 mg/mL in a Vivaspin-20 (Vivaproducts, Inc.) concentrator for crystallization screening. All crystallization experiments were conducted Compact Jr. (Rigaku Reagents) sitting drop vapor diffusion plates at 20 ^{o}C using equal volumes of protein and the crystallization solution were equilibrated against 75 µL of the latter. Crystals of NV 3CLpro-ligand ***17*** that displayed a needle morphology were obtained overnight from the Proplex HT screen (Molecular Dimensions) condition D4 (20% (w/v) PEG 5000 MME, 100 mM Tris pH 7.5, 200 mM ammonium sulfate). Samples were transferred to a fresh drop composed of 80% crystallization solution and 20% PEG glycerol and stored in liquid nitrogen. Two crystal forms of the NV 3CLpro:***44*** complex that displayed a prismatic morphology were observed in 2 days from the Wizard 3 & 4 screen (Emerald Biosystems). The primitive hexagonal (NV 3CLpro:***44***-h) form was obtained from condition A1 (20% w/v PEG3350, 200 mM ammonium citrate) and a primitive orthorhombic (NV 3CLpro:***44***-o) from A10 (20% w/v PEG3350, 200 mM sodium thiocyanate). Samples were transferred to a fresh drop composed of 80% crystallization solution and 20% PEG 400 and stored in liquid nitrogen

prior to data collection. X-ray diffraction data were collected at the Advanced Photon Source beamline 17-ID using a Dectris Pilatus 6M pixel array detector.

2.3.5 Structure Solution and Refinement

Intensities were integrated using XDS[141-142] and the Laue class analysis and data scaling were performed with Aimless[143] which suggested that the highest probability Laue class was 6/*mmm* and possible space groups was $P6_122$ or $P6_522$ for NV 3CLpro, NV 3CLpro:***17*****,** and NV 3CLpro:***44***-h. The Matthew's coefficient[144] suggested that there was a single molecule in the asymmetric unit (Vm=2.8 $Å^3$/Da, % solvent=56%). Structure solution was conducted by molecular replacement with Phaser[145] using a previously determined structure of inhibitor bound NV 3CLpro (PDB: 3UR9)[140] as the search model and all space groups with 622 point symmetry were tested. The top solution was obtained in the space group $P6_522$ which was used from this point forward. NV 3CLpro:***44***-o was isomorphous with PDB 3UR9. Structure refinement using and manual model building were conducted with Phenix[146] and Coot[147] respectively. Disordered side chains were truncated to the point for which electron density could be observed. Structure validation was conducted with Molprobity[148] and figures were prepared using the CCP4MG package[149].

2.3.6 Study with MNV[42]

RAW264.7 cells, mouse macrophage cell line, were maintained in Dulbecco's Minimum Essential Medium (DMEM) containing antibiotics of chlortetracycline (25 µg/ml), penicillin (250 U/ml), and streptomycin (250 µg/ml) in the presence of 2~5% fetal bovine serum. MNV-1 was obtained from H. Virgin at Washington University (St. Louis, MO). Antiviral activity of each compound against MNV-1 in cell culture was determined with RAW264.7 cells. Each compound was dissolved in DMSO to make a 10 mM stock solution. The amount of DMSO in cell culture did not exceed 0.5%. The stock solution was serially diluted with cell culture media prior to addition to confluent monolayer of RAW264.7 cells in 24-well plates. Cells were immediately infected with virus at a multiplicity of infection (MOI) of 0.05 ~0.1. After further incubation of the cells at 37°C for 48 h, cells were frozen and thawed and virus titers were determined by the 50% tissue culture infectious dose ($TCID_{50}$) method. The 50% effective concentration (EC_{50}) values were determined by GraphPad Prism (GraphPad Software, San Diego, CA) by nonlinear regression analyses of dose-response curves of the inhibition of virus replication against log inhibitor concentration (variable slope).

2.3.7 Animal Experiments[150]

The animal study was performed in accordance with a protocol approved by the Institutional Animal Care and Use Committee (IACUC) at Kansas State University. BALB/c mice were purchased from Charles River Lab (Wilmington, MA). Seven to eight week-old female BALB/c mice were inoculated intraperitoneally with MNV-1 at $2x10^6$ $TCID_{50}$/mouse. Mice were peritoneally given 50 µl of drug vehicle (10% EtOH and 90% PEG400) or compound ***16*** (20 mg/kg/day) divided into two doses per day. Compound administration started 4 h prior to virus infection and continued daily until mice were euthanized. At 3 days post infection (dpi), mice were sacrificed and the small and large intestinal tracts were collected. The intestines were placed in PBS and the intestinal contents were gently removed by squeezing. The tissues were homogenized in PBS (5 or 3 mL for small and large intestines, respectively) and frozen at -70C until ready to use. Virus titers of the homogenized supernatant were determined by the $TCID_{50}$ method and statistical analysis was performed on log-transformed $TCID_{50}$ values using a two-tailed Student t-test ($p<0.05$). Fold changes in the geometric mean liver virus titers in each group were calculated by dividing virus titers in control group by the treated group.

2.4. Results and Discussion

The synthesized compounds were evaluated for their inhibitory activity against NV 3CLpro, as well as their anti-norovirus activity in a cell-based replicon system, as previously described.[151] The IC_{50} and ED_{50} values are the average of at least two determinations and are listed in Table 2.1. The enzyme selectivity of a select number of inhibitors was evaluated against a panel of representative proteases and the results are summarized in Table 2.2. The methodologies employed in conducting the enzyme assays and inhibition studies were as described previously by us[151] and others.[152] The in vivo efficacy of compound ***16*** was evaluated in the murine model of norovirus infection.

Inspection of the results shown in Table 2.1 reveals that, in general, dipeptidyl inhibitors that incorporate in their structure an aldehyde or aldehyde bisulfite adduct (masked aldehyde) display lower ED_{50} values than the corresponding compounds bearing an α-hydroxyphosphonate or α-ketoamide moiety. Furthermore, the aldehyde and aldehyde bisulfite adduct-derived inhibitors had comparable ED_{50} values. These results are consistent with previous studies which showed that the activity of the aldehyde bisulfite adducts parallels the activity of the precursor aldehydes.[151c,e] Other things being equal, inhibitors having a cyclohexyl alanine P_2 residue are more potent than the corresponding t-butyl glycine or leucine inhibitors (compare compounds ***16***, ***21*** and ***22*****).** As revealed by the X-ray crystal structure (Figure 2.6), the cyclohexyl alanine side chain optimally fills the hydrophobic S_2 subsite, while the leucine and t-butyl alanine side chains do not. A range of ring substituents were explored to enhance pharmacological activity. Compounds with a halogen at the meta position were particularly effective (compounds ***16***, ***27***, ***29***, ***33***). These observations are suggestive of the involvement of a halogen bond

between the halogen and the C=O of Ala160, however, this could not be demonstrated with absolute certainty because of the partially disordered m-chlorobenzyl moiety.

In order to evaluate the specific interactions between the enzyme and the α-hydroxyphosphonate inhibitors, inhibitor ***17*** was incubated with NV 3CLpro in Tris buffer, pH 8.0. Surprisingly, the enzyme-inhibitor complex formed corresponded to the complex formed between aldehyde ***16*** and 3CL protease. The formation of this complex indicates initial non-enzymatic (buffer)- or enzyme-catalyzed conversion of α-hydroxyphosphonate ***17*** to the corresponding aldehyde ***16*****,** followed by the formation of a tetrahedral adduct with the active site cysteine (Cys139). Studies aimed at ascertaining the validity of this hypothesis are in progress. The ensemble of hydrogen bonding and hydrophobic interactions in the enzyme-ligand complex are near identical to those observed with aldehyde inhibitor (I), where R_1= H, R_1= cyclohexylmethyl, X=CHO) (Figure 2.2).

TABLE 2.1. ACTIVITY OF COMPOUNDS 13−44 AGAINST NV 3CL PROTEASE AND NOROVIRUS IN CELL-BASED REPLICON CELLS

Compound	R_1	R_2	X	IC50 (μM)	ED50 (μM)
13	*o*-Cl	Cha	CHO	0.8	0.08
14			$CH(OH)P(O)(OC_2H_5)_2$	>10	0.2
15			$CH(OH)(SO_3^-Na^+)$	0.7	0.07
16	*m*-Cl	Cha	CHO	0.1	0.02
17			$CH(OH)P(O)(OC_2H_5)_2$	>10	0.06
18			$CH(OH)(SO_3^-Na^+)$	0.1	0.02
19			C(O)C(O)NH(Cyc-Prop)	0.25	0.085
20			$C(O)NHSO_2CH_3$	>10	>2
21		Chg	CHO	5.1	0.15
22		Leu	CHO	0.9	0.1
23			C(O)C(O)NH(Cyc-Prop)	5.5	0.3
24	*p*-Cl	Cha	CHO	0.71	0.08
25	*o*-F	Cha	CHO	0.9	0.08
26			$CH(OH)P(O)(OC_2H_5)_2$	>10	>2
27	*m*-F	Cha	CHO	1.2	0.09
28			C(O)C(O)NH(Cyc-Prop)	3.5	0.3
29	*m*-Br	Cha	CHO	0.3	0.03
30			$CH(OH)P(O)(OC_2H_5)_2$	6.5	0.15
31			$CH(OH)(SO_3^-Na^+)$	0.15	0.03
32			C(O)C(O)NH(Cyc-Prop)	1.5	0.2
33	*m*-I	Cha	CHO	0.35	0.05
34			$CH(OH)(SO_3^-Na^+)$	0.15	0.04
35	*o*-OCH3	Cha	CHO	>10	0.1
36	*m*-OCH3	Cha	CHO	1.4	0.15
37	*m*-CN	Cha	CHO	>10	0.2
38	*m*-NHBoc	Cha	CHO	4.5	1.5
39	*m*-NO2	Cha	CHO	0.6	0.15
40	H	Leu	CHO	0.6	0.2
41			$CH(OH)(SO_3^-Na^+)$	0.8	0.3
42			C(O)C(O)NH(Cyc-Prop)	3.4	1.1
43		Cha	CHO	0.3	0.06
44			$CH(OH)(SO_3^-Na^+)$	0.4	0.06

An initial evaluation of selectivity was carried out using a panel of proteases and four representative inhibitors (***16, 17, 29*** and ***30).*** As shown in Table 2.2, these compounds displayed minimal activity toward the proteases of the digestive and blood coagulation cascade systems. Selectivity was uniformly lower against the serine protease human neutrophil elastase (HNE).

TABLE 2.2. SELECTIVITY OF SELECTED COMPOUNDS AGAINST A PANEL OF PROTEASES

Enzyme[25]	**I/E**	**Compound (% inhibition)**				**$[I]_f$ (μM)**
		16	**17**	**29**	**30**	
HNE	50	15	86.5	26.5	63	15.4
Chymotrypsin	250	0	2.4	0	0	2.5
Trypsin	250	5	8.8	0	1	125
Thrombin	250	0	0	0	0	2.75
Factor Xa	250	1	0	0	6	1.23
Plasmin	250	0	15	7	13	2.5
Carboxypeptidase A	250	12	14.3	11.6	0	43

2.4.1. X-ray Crystallography

X-ray crystallography was used to elucidate the nature of the interaction of compound ***17*** with NV 3CLpro. The X-ray crystal structure of NV 3CLpro revealed the presence of prominent difference electron density with the substructure of **17** that is equivalent to precursor aldehyde inhibitor ***16*** covalently bound to Cys 139. However, no electron density was observed for the hydroxyphosphonate group that should be present for inhibitor ***17*** (Figure 2.4). Instead, the structure of the NV 3CLpro-ligand complex was found to correspond to the covalent adduct of precursor aldehyde inhibitor ***16*** and NV 3CLpro. In addition, the m-chlorobenzyl ring was partially disordered so the electron density for this region of the inhibitor was somewhat ambiguous. The interactions between NV 3CLpro and inhibitor ***16*** are shown in Figure 2.5.

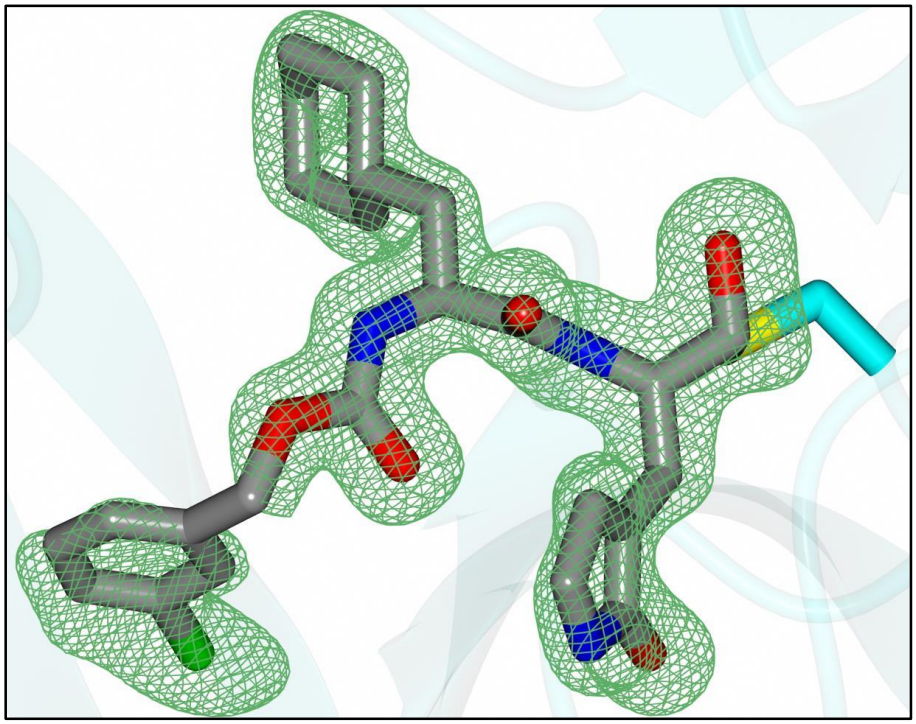

Figure 2.4. $F_o - F_c$ map (green mesh) of precursor aldehyde derived from compound ***17*** bound to NV 3CLpro contoured at 3σ.

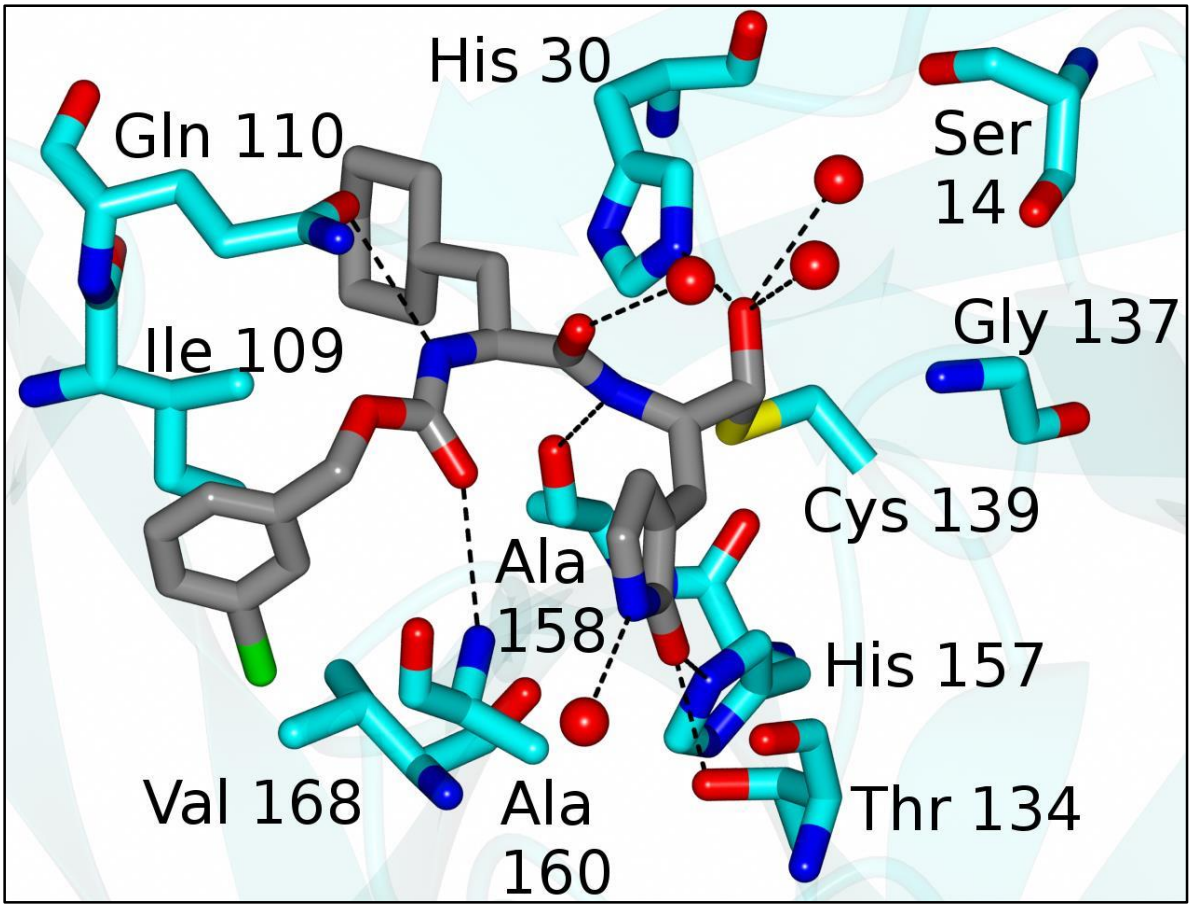

Figure 2.5. Hydrogen bond interactions between NV 3CLpro and precursor aldehyde derived from compound ***17.*** Hydrogen bonds are represented as dashed lines and water mediated contacts are shown as solid lines.

The m-chlorophenyl ring of inhibitor ***16*** occupies a hydrophobic pocket near Ile 109 and Val 168. Van der Waals and electrostatic surface representations of the inhibitor and NV 3CLpro are shown in Figure 2.6.

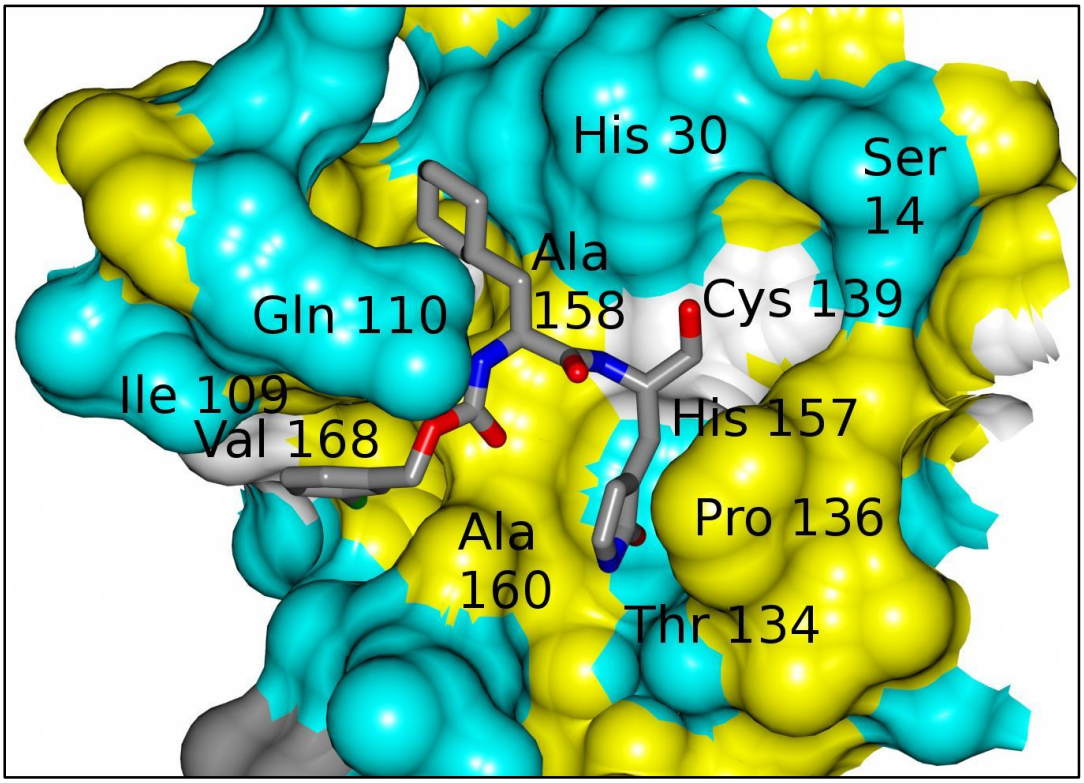

Figure 2.6. Surface representation of precursor aldehyde of compound ***17*** bound to NV 3CLpro. Neighboring residues of NV 3CLpro are colored yellow (nonpolar), white (weakly polar) and cyan (polar).

TABLE 2.3. CRYSTALLOGRAPHIC DATA FOR NV 3CLPRO:INHIBITOR STRUCTURES

	NV 3CLpro:17	NV 3CLpro:44-h	NV 3CLpro:44-o
Data Collection			
Unit-cell parameters (Å, °)	*a*=124.23, *c*=49.97	*a*=121.85, *c*=51.50	*a*=37.47 *b*=66.91 *c*=126.4
Space group	$P6_522$	$P6_522$	$P2_12_12_1$
Resolution (Å)[1]	45.32-1.85 (1.89-1.85)	46.28-1.60 (1.63-1.60)	45.94-1.45 (1.48-1.45)
Wavelength (Å)	1.0000	1.0000	1.0000
Temperature (K)	100	100	100
Observed reflections	384,657	579,016	371,208
Unique reflections	19,899	30,219	57,354
$\langle I/\sigma(I)\rangle$[1]	14.9 (2.4)	16.3 (2.0)	18.9 (1.8)
Completeness (%)[1]	100 (100)	100 (100)	100 (100)
Multiplicity[1]	19.3 (18.5)	19.2 (16.9)	6.5 (6.5)
R_{merge} (%)[1, 2]	19.7 (150.5)	16.6 (169.2)	4.7 (105.4)
R_{meas} (%)[1, 4]	20.3 (154.7)	17.0 (174.5)	5.1 (114.5)
R_{pim} (%)[1, 4]	4.6 (35.8)	3.9 (42.3)	2.0 (44.4)
$CC_{1/2}$ [1, 5]	0.998 (0.763)	99.9 (71.1)	100 (63.5)
Refinement			
Resolution (Å) [1]	45.32-1.85	36.85-1.60	35.65-1.45
Reflections (working/test)[1]	18,907/968	28,660/1,530	54,369/2,905
R_{factor} / R_{free} (%)[1,3]	16.3/19.7	16.3/17.5	17.3/19.9
No. of atoms (Protein/Ligand/Water)	1,236/33/129	1,319/32/160	2,444/58/218
Model Quality			
R.m.s deviations			
Bond lengths (Å)	0.009	0.009	0.008
Bond angles (°)	1.229	1.234	1.020
Average *B*-factor (Å^2)			
All Atoms	21.1	17.2	24.3
Protein	19.9	15.6	23.6
Ligand	25.7	18.5	25.4
Water	29.9	19.0	32.1
Coordinate error (maximum likelihood) (Å)	0.16	0.18	0.15
Ramachandran Plot			
Most favored (%)	98.8	98.3	98.5
Additionally allowed (%)	1.2	1.7	1.5

TABLE 2.3 (continued)

1) Values in parenthesis are for the highest resolution shell.
2) $R_{merge} = \Sigma_{hkl}\Sigma_i \ |I_i(hkl) - \langle I(hkl)\rangle| \ / \ \Sigma_{hkl}\Sigma_i \ I_i(hkl)$, where $I_i(hkl)$ is the intensity measured for the *i*th reflection and $\langle I(hkl)\rangle$ is the average intensity of all reflections with indices hkl.
3) $R_{factor} = \Sigma_{hkl} \ ||F_{obs} \ (hkl)| - |F_{calc} \ (hkl)|| \ / \ \Sigma_{hkl} \ |F_{obs} \ (hkl)|$; Rfree is calculated in an identical manner using 5% of randomly selected reflections that were not included in the refinement.
4) R_{meas} = redundancy-independent (multiplicity-weighted) R_{merge}[143,153]. R_{pim} = precision-indicating (multiplicity-weighted) R_{merge}[154-155].
5) $CC_{1/2}$ is the correlation coefficient of the mean intensities between two random half-sets of data [156-157].

2.4.2. Animal Studies

Compound ***16*** was used to obtain a preliminary indication of in vivo efficacy. All compounds that were effective against NV in cell culture were also effective against MNV-1 in the range 0.08 to 5 µM. Among them compound ***16*** was found to be the most effective with an EC_{50} value of 80 nM. It is noted that compound ***16*** was also most effective against NV (Table 2.1). In mice, treatment with compound ***16*** significantly reduced the virus titers in the small and large intestines at 3 days post virus infection by 42.12- and 7.98-fold, respectively, compared to the untreated control group (Figure 2.7). The overall virus titers in the small intestine were higher than those in the large intestine, and the reduction of viral titers was also greater in the small intestine than the large intestine.

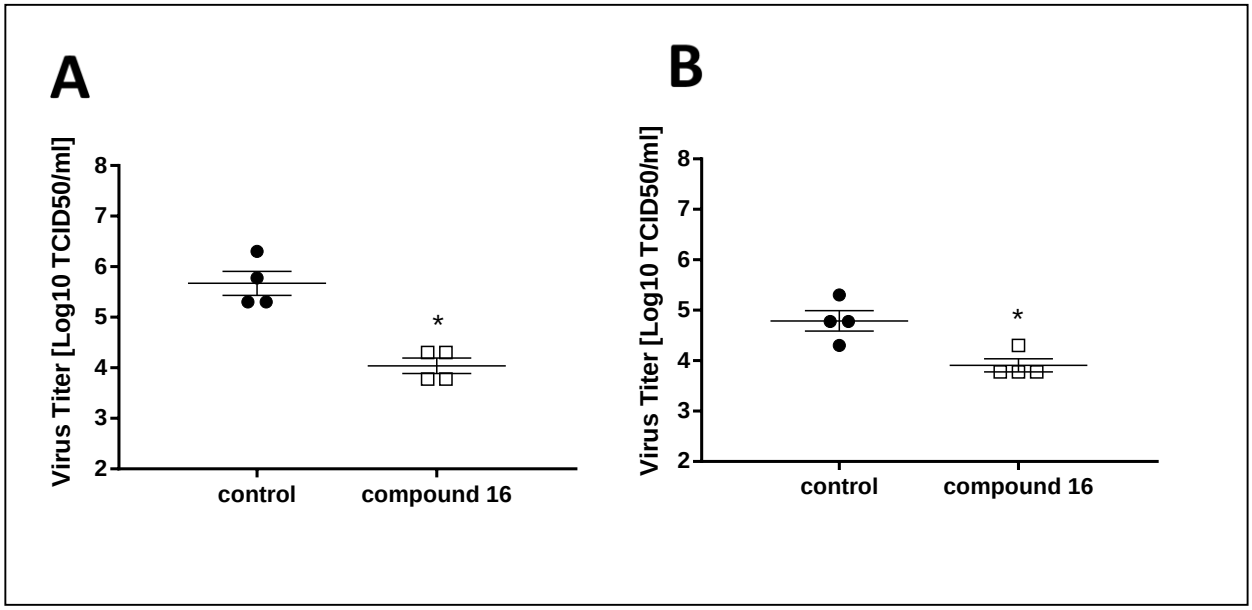

Figure 2.7. Protease inhibitor suppresses norovirus replication in the intestinal tract in mice (effects of a 3CLpro inhibitor treatment on murine norovirus titers in the intestinal tracts of mice). Balb/c mice were orally infected with MNV-1 at $2x10^6$ $TCID_{50}$ and intraperitoneally given compound ***16*** at 10 mg/kg twice daily with the first dose starting 4 hrs prior to virus infection. At 72 h post virus infection, the intestinal tract tissues were harvested and processed for determination for virus titers by the $TCID_{50}$ assay. Mean and the standard error of the mean of virus titers in the small intestine (A) or large intestine (B) at 3 day post MNV-1 infection are shown. Each filled circle indicates a control mouse that was given drug vehicle and each empty box indicates a mouse given compound ***16***. Asterisk indicates $P<0.01$.

2.5. Conclusions

In summary, these studies describe the optimization of the pharmacological activity and selectivity of dipeptidyl inhibitors of norovirus 3CL protease by employing iterative medicinal chemistry/SAR studies, X-ray crystallography, *in vitro* and cell-based screening, and *in vivo* efficacy studies. Importantly, these studies have identified lead compounds that show efficacy in the murine model of norovirus infection and, consequently, are suitable for conducting further pre-clinical studies.

CHAPTER III

STRUCTURE-BASED EXPLORATION AND EXPLOITATION OF THE S_4 SUBSITE OF NOROVIRUS 3CL PROTEASE IN THE DESIGN OF POTENT AND PERMEABLE INHIBITORS

3.1 Inhibitor Design Rationale

The design and optimization of the inhibitors was informed by the utilization of available crystal structures and the parallel acquisition of additional high-resolution X-ray crystal structures. Thus, inspection of previously-determined high resolution X-ray crystal structures of dipeptidyl inhibitors bound to norovirus 3CL protease (PDB accession codes 4XBB, 4XBC and 4XBD)[158] revealed that the “cap” R group in inhibitor (I) projects toward the S_4 subsite of the enzyme and suggested that its close proximity to a string of hydrophobic amino acids (Ala158, Ala160, Val168 and Ile109) could be exploited through appropriate cap modifications, including the use of sulfonamide functionalities. Additional design considerations included the use of key recognition elements, such as a Gln surrogate[159] and a cyclohexyl methyl residue at the P_1 and P_2 positions, respectively, capable of engaging in H-bonding and hydrophobic interactions. Finally, based on the recently-demonstrated *in vivo* efficacy of aldehyde bisulfite adducts[160], this moiety was incorporated into inhibitor (I) and, for comparative purposes, the corresponding aldehyde inhibitors were also included.

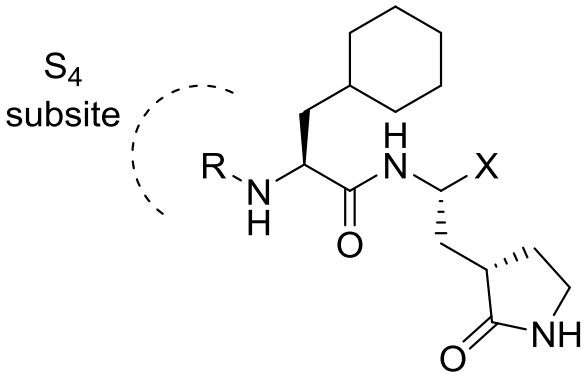

(I)

3.2 Chemistry

The synthesis of inhibitors ***6a-7m*** was accomplished using the reaction sequence shown in Scheme 3.1. Briefly, N-Boc-L-cyclohexyl methyl alanine was coupled to glutamine surrogate ***8*** [159] to obtain ***2***, followed by removal of the Boc protective group to yield intermediate ***3*** which was subsequently reacted with a series of sulfonyl chlorides to yield sulfonamide esters ***4a-m.*** Reduction with lithium borohydride generated the corresponding alcohols ***5a-m***. Dess-Martin periodinane oxidation of ***5a-m*** proceeded smoothly to yield aldehydes ***6a-m***, which were transformed to the corresponding aldehyde bisulfite adducts ***7a-m*****.** The synthesized sulfonamide derivatives are listed in Table 3.1. Carbamates ***12a-c*** were synthesized according to Scheme 2 via reaction of intermediate ***3*** with an appropriate chloroformate and further elaboration to yield the corresponding aldehydes and aldehyde bisulfite adducts, which are listed in Table 3.2.

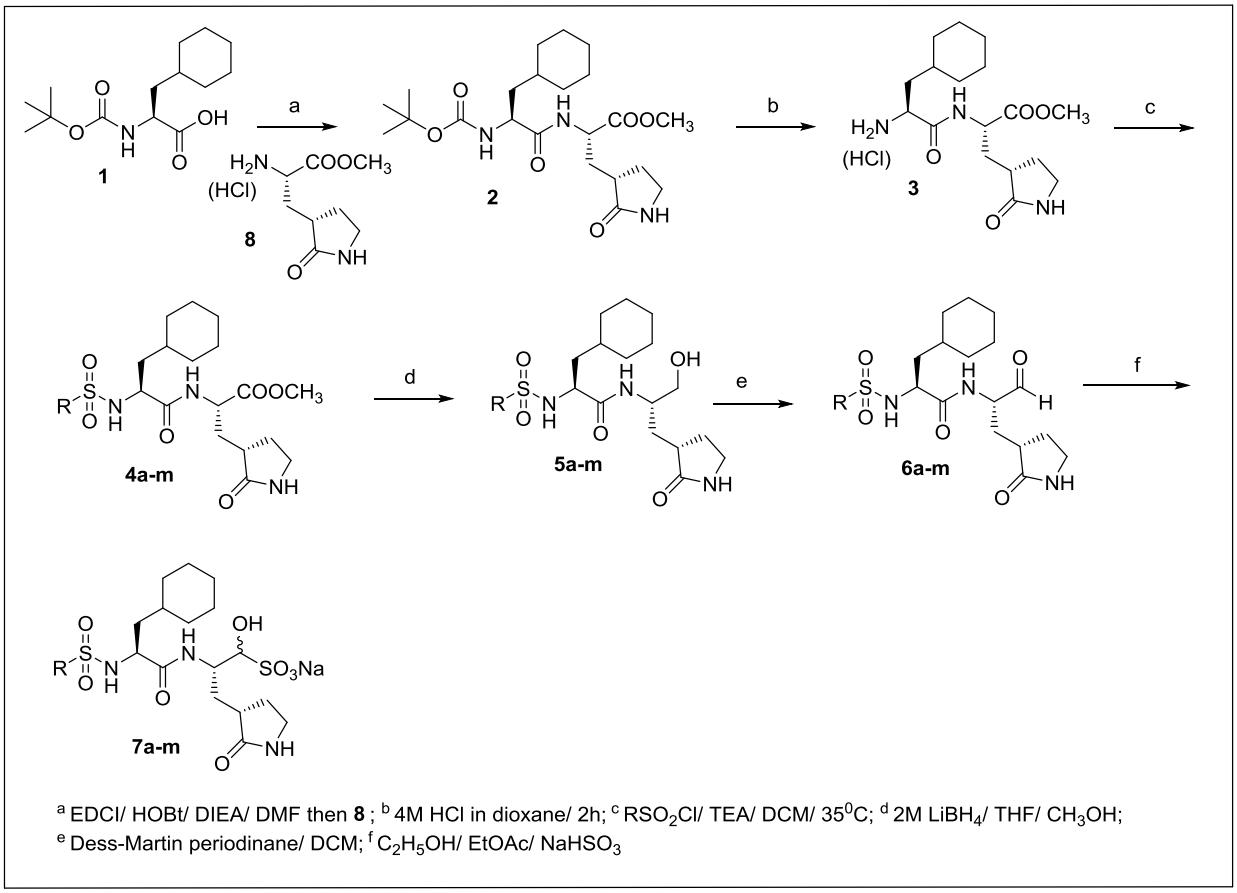

[a] EDCI/ HOBt/ DIEA/ DMF then **8** ; [b] 4M HCl in dioxane/ 2h; [c] RSO_2Cl/ TEA/ DCM/ 35^0C; [d] 2M $LiBH_4$/ THF/ CH_3OH;
[e] Dess-Martin periodinane/ DCM; [f] C_2H_5OH/ EtOAc/ $NaHSO_3$

Scheme 3.1 Synthesis of Inhibitors ***6a-m*** and ***7a-m***.

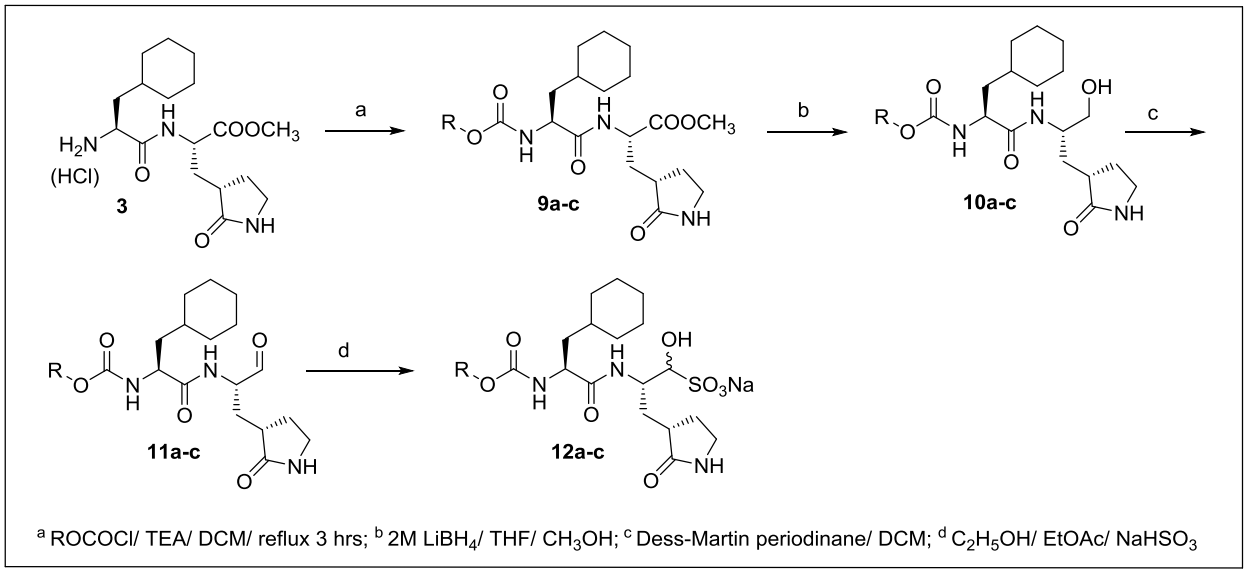

[a] ROCOCl/ TEA/ DCM/ reflux 3 hrs; [b] 2M $LiBH_4$/ THF/ CH_3OH; [c] Dess-Martin periodinane/ DCM; [d] C_2H_5OH/ EtOAc/ $NaHSO_3$

Scheme 3.2 Synthesis of Inhibitors ***11a-c*** and ***12a-c***.

3.3 Experimental Section

3.3.1 General

Reagents and dry solvents were purchased from various chemical suppliers (Chem-Impex, Acros Organics, TCI America, Aldrich, and Bachem) and were used as obtained. Silica gel (230-450 mesh) used for flash chromatography was purchased from Sorbent Technologies (Atlanta, GA). Thin layer chromatography was performed using Analtech silica gel plates (Newark, DE). Visualization was accomplished using UV light and/or iodine. NMR spectra were recorded in $CDCl_3$ or DMSO-d_6 using a Varian XL-400 spectrometer and are reported relative to TMS (δ_H= 0.00 ppm). Chemical shifts are reported in ppm and spin multiplicities are represented by the following signals: s (singlet), d (doublet), dd (doublets of doublet), t (triplet), q (quartet) and m (multiplet). Melting points were recorded on a Mel-Temp apparatus and are uncorrected. High resolution mass spectrometry (HRMS) was performed at the University of Kansas Mass Spectrometry lab using an LCT Premier mass spectrometer (Waters, Milford, MA) equipped with a time of flight mass analyzer and an electrospray ion source or in-house using a G6230B TOF MS (Agilent Technologies, Santa Clara, CA). The purity of the synthesized compounds was established using HPLC and was >95%.

Synthesis of compound 2. To a solution of compound ***1*** (10 mmol) in dry DMF (20 mL) was added EDCI (2.40 g, 12.5 mmol, 1.25 eq), HOBt (1.92 g, 12.5 mmol, 1.25 eq) and the mixture was stirred for 30 minutes at room temperature. In a separate flask, a solution of deprotected glutamine surrogate 8 (2.23 g, 10 mmol) in DMF (15 mL) cooled to 0-5 ^oC was treated with N,N-diisopropylethylamine (DIEA) (9.5 g, 40 mmol, 4 eq), stirred for 30 minutes, and then added to the reaction mixture containing (L) N-Boc cyclohexylalanine.

The reaction mixture was stirred for 12 h while monitoring the reaction by TLC. The solvent was removed and the residue was dissolved in ethyl acetate (200 mL) and washed with 10% aqueous citric acid (2 x 40 mL). The ethyl acetate layer was further washed with saturated $NaHCO_3$ (40 mL), followed by saturated NaCl (50 mL). The organic layer was dried over anhydrous sodium sulfate, filtered and concentrated to yield a yellow-colored oily product. Purification by flash chromatography yielded ester ***2*** as a white solid.

methyl (2S)-2-((S)-2-((tert-butoxycarbonyl)amino)-3-cyclohexylpropanamido)-3-(2-oxopyrrolidin-3-yl)propanoate (2). Yield (77%), mp 72-74 ^{0}C. ^{1}H NMR (400 MHz, $CDCl_3$-*d*) δ ppm 0.84 - 1.04 (m, 2 H) 1.11 - 1.31 (m, 4 H) 1.44 (s, 9 H) 1.60 - 1.75 (m, 6 H) 1.78 - 1.94 (m, 3 H) 2.15 - 2.28 (m, 1 H) 2.35 - 2.48 (m, 2 H) 3.26 - 3.40 (m, 2 H) 3.73 (s, 3 H) 4.21 - 4.34 (m, 1 H) 4.53 (ddd, *J*=11.13, 7.37, 3.91 Hz, 1 H) 5.03 (d, *J*=7.23 Hz, 1 H) 6.34 (s, 1 H) 7.55 (d, *J*=5.66 Hz, 1 H). HRMS (ESI) calcd for $C_{22}H_{37}N_3O_6$: [M-]: 439.2682. Found: 439.2866.

Synthesis of compound 3. To a solution of compound ***2*** (10 mmol) in dry DCM (5 mL) was added 4M HCl in dioxane (10 mL) and the mixture was stirred for 2 h at room temperature. The solvent was removed and the residue was dried under high vacuum to yield the hydrochloride salt as a pale white solid.

methyl (2S)-2-((S)-2-amino-3-cyclohexylpropanamido)-3-(2-oxopyrrolidin-3-yl) propanoate hydrochloride (3). Yield (100%), mp 60-62 ^{0}C. ^{1}H NMR (400 MHz, DMSO-d_6) δ ppm 0.87 (quin, *J*=10.76 Hz, 2 H) 1.09 - 1.29 (m, 3 H) 1.34 - 1.45 (m, 2 H) 1.52 - 1.60 (m, 2 H) 1.65 (d, *J*=8.25 Hz, 4 H) 1.80 (d, *J*=12.03 Hz, 1 H) 2.01 - 2.13 (m, 1 H) 2.12 - 2.24 (m, 2 H) 2.38 - 2.48 (m, 2 H) 3.07 - 3.23 (m, 2 H) 3.58 (s, 3 H) 3.79 (d, *J*=5.30 Hz,

1 H) 4.25 (br. s, 1 H) 4.36 - 4.46 (m, 1 H) 7.69 (s, 1 H) 8.33 (s, 1 H) 9.00 (d, *J*=7.74 Hz, 1 H). HRMS (ESI) calcd for $C_{17}H_{30}ClN_3O_4$: [M-]: 375.1925. Found: 375.1920.

Synthesis of compounds 4a-m. General Procedure. To a solution of compound ***3*** (5 mmol) in dry DCM (20 mL) kept at 0 ^oC was added triethylamine (TEA) (1.3 mL,11 mmol, 2.2 eq) slowly with stirring. The appropriate sulfonyl chloride derivative (5.5 mmol, 1.1 eq) was added and reaction mixture was stirred for 12 h at 35 ^oC. The solvent was removed and the residue was dissolved in ethyl acetate (50 mL) and washed with water (2 x 25 mL). The ethyl acetate layer was further washed with saturated NaCl (50 mL). The organic layer was dried over anhydrous sodium sulfate, filtered and concentrated to yield a crude product. Purification by flash chromatography yielded esters ***4a-m***.

methyl (2S)-2-((S)-3-cyclohexyl-2-(phenylsulfonamido)propanamido)-3-(2-oxopyrrolidin-3-yl)propanoate (4a). Yield (73%), mp 45-47 ^0C. ^1H NMR (400 MHz, $CDCl_3$-*d*) δ ppm 0.67 - 0.79 (m, 1 H) 0.82 - 0.94 (m, 1 H) 0.98 - 1.07 (m, 2 H) 1.10 - 1.22 (m, 1 H) 1.31 - 1.41 (m, 1 H) 1.43 - 1.65 (m, 6 H) 1.73 - 1.88 (m, 2 H) 2.02 - 2.13 (m, 2 H) 2.19 - 2.29 (m, 1 H) 2.34 (ddd, *J*=12.40, 8.40, 4.00 Hz, 1 H) 3.38 (dd, *J*=8.93, 4.74 Hz, 2 H) 3.70 (s, 3 H) 3.84 (td, *J*=9.30, 4.93 Hz, 1 H) 4.27 (ddd, *J*=11.23, 6.98, 3.86 Hz, 1 H) 5.30 (s, 1 H) 5.97 (d, *J*=9.18 Hz, 1 H) 6.44 (s, 1 H) 7.44 - 7.50 (m, 2 H) 7.51 - 7.57 (m, 1 H) 7.87 (d, *J*=7.23 Hz, 2 H). HRMS (ESI) calcd for $C_{23}H_{33}N_3O_6S$: [M+H]: 480.2168 Found: 480.2147.

methyl (2S)-2-((S)-3-cyclohexyl-2-((phenylmethyl)sulfonamido)propanamido)-3-(2-oxopyrrolidin-3-yl)propanoate (4b). Yield (77%), mp 41-43 ^0C. ^1H NMR (400 MHz, $CDCl_3$-*d*) δ ppm 0.82 - 0.98 (m, 2 H) 1.07 - 1.30 (m, 3 H) 1.42 - 1.51 (m, 2 H) 1.59 - 1.71 (m, 5 H) 1.77 (d, *J*=12.45 Hz, 1 H) 1.82 - 1.96 (m, 2 H) 2.17 (ddd, *J*=14.13, 11.74, 5.66 Hz, 1 H) 2.34 - 2.44 (m, 1 H) 2.45 - 2.54 (m, 1 H) 3.31 - 3.39 (m, 2 H) 3.73 (s, 3 H) 3.94 -

4.04 (m, 1 H) 4.22 - 4.33 (m, 2 H) 4.44 - 4.53 (m, 1 H) 5.51 (d, *J*=8.98 Hz, 1 H) 6.15 (s, 1 H) 7.33 - 7.39 (m, 3 H) 7.41 - 7.47 (m, 2 H) 7.99 (d, *J*=6.74 Hz, 1 H). HRMS (ESI) calcd for $C_{24}H_{35}N_3O_6S$: [M+H]: 494.2325 Found: 494.2302.

methyl (2S)-2-((S)-3-cyclohexyl-2-((2-phenylethyl)sulfonamido)propanamido)-3-(2-oxopyrrolidin-3-yl)propanoate (4c). Yield (82%), mp 45-47 ^{0}C. ^{1}H NMR (400 MHz, $CDCl_3$-*d*) δ ppm 0.84 - 1.06 (m, 2 H) 1.09 - 1.30 (m, 4 H) 1.47 - 1.59 (m, 2 H) 1.61 - 1.74 (m, 4 H) 1.75 - 1.94 (m, 3 H) 2.13 (ddd, *J*=14.08, 11.96, 5.69 Hz, 1 H) 2.19 - 2.29 (m, 1 H) 2.30 - 2.42 (m, 1 H) 3.06 - 3.16 (m, 2 H) 3.17 - 3.34 (m, 4 H) 3.64 (s, 3 H) 4.10 (td, *J*=9.02, 4.86 Hz, 1 H) 4.39 - 4.48 (m, 1 H) 5.68 (d, *J*=9.47 Hz, 1 H) 6.24 (s, 1 H) 7.17 - 7.25 (m, 2 H) 7.25 - 7.35 (m, 3 H) 8.15 (d, *J*=6.79 Hz, 1 H). HRMS (ESI) calcd for $C_{25}H_{37}N_3O_6S$: [M+H]: 508.2481 Found: 508.2460.

methyl (2S)-2-((S)-3-cyclohexyl-2-((4-fluorophenyl)sulfonamido)propanamido)-3-(2-oxopyrrolidin-3-yl)propanoate (4d). Yield (78%), mp 63-65 ^{0}C. ^{1}H NMR (400 MHz, $CDCl_3$-*d*) δ ppm 0.76 (d, *J*=10.40 Hz, 1 H) 0.85 - 0.96 (m, 1 H) 1.08 (d, *J*=9.52 Hz, 2 H) 1.13 - 1.22 (m, 1 H) 1.35 - 1.55 (m, 2 H) 1.55 - 1.66 (m, 5 H) 1.71 (br. s., 1 H) 1.79 - 1.92 (m, 2 H) 1.99 - 2.11 (m, 1 H) 2.19 - 2.28 (m, 1 H) 2.36 (ddd, *J*=12.55, 8.47, 4.37 Hz, 1 H) 3.39 (dd, *J*=8.93, 4.64 Hz, 2 H) 3.70 (s, 3 H) 3.81 (td, *J*=9.28, 4.93 Hz, 1 H) 4.21 - 4.29 (m, 1 H) 6.00 (d, *J*=9.23 Hz, 1 H) 6.31 (s, 1 H) 7.15 (t, *J*=8.54 Hz, 2 H) 7.86 - 7.92 (m, 2 H) 7.95 (d, *J*=6.59 Hz, 1 H). HRMS (ESI) calcd for $C_{23}H_{32}FN_3O_6S$: [M+H]: 498.2074 Found: 498.2050.

methyl (2S)-2-((S)-2-((3-chlorophenyl)sulfonamido)-3-cyclohexylpropanamido)-3-(2-oxopyrrolidin-3-yl)propanoate (4e). Yield (81%), mp 58-59 ^{0}C. ^{1}H NMR (400 MHz, $CDCl_3$-*d*) δ ppm 0.73 - 0.82 (m, 1 H) 0.84 - 0.94 (m, 1 H) 1.06 (t, *J*=8.98 Hz, 2 H) 1.13 -

1.20 (m, 1 H) 1.40 (d, *J*=16.50 Hz, 1 H) 1.44 - 1.50 (m, 1 H) 1.51 - 1.65 (m, 4 H) 1.72 (br. s., 2 H) 1.79 - 1.89 (m, 2 H) 1.97 - 2.08 (m, 1 H) 2.23 - 2.30 (m, 1 H) 2.35 (d, *J*=11.52 Hz, 1 H) 3.35 - 3.42 (m, 2 H) 3.68 (s, 3 H) 3.85 (d, *J*=4.20 Hz, 1 H) 4.15 - 4.23 (m, 1 H) 5.98 (d, *J*=9.08 Hz, 1 H) 6.27 (s, 1 H) 7.40 - 7.45 (m, 1 H) 7.47 - 7.53 (m, 1 H) 7.75 (d, *J*=7.62 Hz, 1 H) 7.83 (s, 1 H) 8.16 (d, *J*=5.96 Hz, 1 H). HRMS (ESI) calcd for $C_{23}H_{32}ClN_3O_6S$: [M+H]: 514.1779 Found: 514.1738.

methyl (2S)-2-((S)-2-((4-chlorophenyl)sulfonamido)-3-cyclohexylpropanamido)-3-(2-oxopyrrolidin-3-yl)propanoate (4f). Yield (76%), mp 52-54 ^{0}C. ^{1}H NMR (400 MHz, $CDCl_3$-*d*) δ ppm 0.70 - 0.83 (m, 1 H) 0.89 (q, *J*=11.00 Hz, 1 H) 1.03 - 1.12 (m, 1 H) 1.13 - 1.22 (m, 1 H) 1.37 - 1.54 (m, 2 H) 1.57 - 1.68 (m, 5 H) 1.71 (br. s., 1 H) 1.80 - 1.91 (m, 2 H) 1.97 - 2.09 (m, 2 H) 2.17 - 2.26 (m, 1 H) 2.32 - 2.45 (m, 1 H) 3.36 - 3.46 (m, 2 H) 3.70 (s, 3 H) 3.80 (td, *J*=9.25, 4.98 Hz, 1 H) 4.16 - 4.25 (m, 1 H) 6.00 (d, *J*=9.28 Hz, 1 H) 6.30 (s, 1 H) 7.44 (d, *J*=8.59 Hz, 2 H) 7.81 (d, *J*=8.59 Hz, 2 H) 8.04 (d, *J*=6.35 Hz, 1 H). HRMS (ESI) calcd for $C_{23}H_{32}ClN_3O_6S$: [M+H]: 514.1779 Found: 514.1770.

methyl (2S)-2-((S)-2-(((4-chlorophenyl)methyl)sulfonamido)-3-cyclohexylpropanamido)-3-(2-oxopyrrolidin-3-yl)propanoate (4g). Yield (71%), mp 38-39 ^{0}C. ^{1}H NMR (400 MHz, $CDCl_3$-*d*) δ ppm 0.83 - 0.98 (m, 2 H) 1.08 - 1.29 (m, 3 H) 1.40 - 1.52 (m, 2 H) 1.60 - 1.71 (m, 5 H) 1.77 (d, *J*=12.30 Hz, 1 H) 1.84 - 1.98 (m, 2 H) 2.09 - 2.20 (m, 1 H) 2.34 - 2.45 (m, 1 H) 2.46 - 2.53 (m, 1 H) 3.37 (dd, *J*=8.81, 4.66 Hz, 2 H) 3.73 (s, 3 H) 3.95 - 4.03 (m, 1 H) 4.18 - 4.31 (m, 2 H) 4.40 - 4.48 (m, 1 H) 5.67 (d, *J*=8.93 Hz, 1 H) 6.21 (s, 1 H) 7.32 - 7.35 (m, 2 H) 7.38 - 7.42 (m, 2 H) 8.10 (d, *J*=6.49 Hz, 1 H). HRMS (ESI) calcd for $C_{24}H_{34}ClN_3O_6S$: [M+H]: 528.1835 Found: 528.1879.

methyl (2S)-2-((S)-2-((2-(3-chlorophenyl)ethyl)sulfonamido)-3-cyclohexylpropanamido)-3-(2-oxopyrrolidin-3-yl)propanoate (4h). Yield (71%), mp 63-65 ^{0}C. ^{1}H NMR (400 MHz, $CDCl_3$-*d*) δ ppm 0.85 - 1.05 (m, 2 H) 1.12 - 1.31 (m, 3 H) 1.49 - 1.58 (m, 2 H) 1.62 - 1.75 (m, 6 H) 1.79 - 1.96 (m, 2 H) 2.13 (ddd, *J*=14.10, 12.00, 5.79 Hz, 1 H) 2.25 - 2.34 (m, 1 H) 2.36 - 2.45 (m, 1 H) 3.03 - 3.16 (m, 2 H) 3.21 - 3.29 (m, 2 H) 3.30 - 3.39 (m, 2 H) 3.68 (s, 3 H) 4.05 - 4.16 (m, 1 H) 4.39 - 4.47 (m, 1 H) 5.80 (d, *J*=9.52 Hz, 1 H) 6.28 (s, 1 H) 7.10 (d, *J*=6.83 Hz, 1 H) 7.19 - 7.26 (m, 3 H) 8.24 (d, *J*=6.69 Hz, 1 H). HRMS (ESI) calcd for $C_{25}H_{36}ClN_3O_6S$: [M+H]: 542.2092 Found: 542.2033.

methyl (2S)-2-((S)-3-cyclohexyl-2-(thiophene-3-sulfonamido)propanamido)-3-(2-oxopyrrolidin-3-yl)propanoate (4i). Yield (62%), mp 45-47 ^{0}C. ^{1}H NMR (400 MHz, $CDCl_3$-*d*) δ ppm 0.72 - 0.85 (m, 1 H) 0.86 - 0.95 (m, 1 H) 1.04 - 1.15 (m, 2 H) 1.16 - 1.27 (m, 1 H) 1.35 - 1.46 (m, 1 H) 1.50 (dd, *J*=9.45, 4.76 Hz, 1 H) 1.54 - 1.67 (m, 5 H) 1.79 - 1.92 (m, 3 H) 2.04 - 2.18 (m, 1 H) 2.28 - 2.42 (m, 2 H) 3.35 - 3.41 (m, 2 H) 3.71 (s, 3 H) 3.95 (td, *J*=9.19, 4.91 Hz, 1 H) 4.34 (ddd, *J*=11.28, 7.08, 3.81 Hz, 1 H) 6.17 (d, *J*=8.93 Hz, 1 H) 6.53 (br. s., 1 H) 7.04 (dd, *J*=4.83, 3.91 Hz, 1 H) 7.56 (dd, *J*=4.96, 1.00 Hz, 1 H) 7.61 (dd, *J*=3.64, 1.05 Hz, 1 H) 7.89 (d, *J*=6.88 Hz, 1 H). HRMS (ESI) calcd for $C_{21}H_{31}N_3O_6S_2$: [M+H]: 486.1733 Found: 486.1785.

methyl (2S)-2-((S)-2-([1,1'-biphenyl]-4-sulfonamido)-3-cyclohexylpropanamido)-3-(2-oxopyrrolidin-3-yl)propanoate (4j). Yield (62%), mp 89-92 ^{0}C. ^{1}H NMR (400 MHz, $CDCl_3$-*d*) δ ppm 0.73 (d, *J*=10.50 Hz, 1 H) 0.81 - 0.93 (m, 1 H) 0.98 - 1.07 (m, 2 H) 1.09 - 1.18 (m, 1 H) 1.31 - 1.43 (m, 1 H) 1.45 - 1.64 (m, 6 H) 1.67 - 1.84 (m, 3 H) 1.96 - 2.05 (m, 1 H) 2.08 - 2.19 (m, 2 H) 3.01 - 3.10 (m, 1 H) 3.17 - 3.25 (m, 1 H) 3.66 (s, 3 H) 3.81 (td, *J*=9.21, 4.86 Hz, 1 H) 4.16 - 4.24 (m, 1 H) 5.92 (d, *J*=9.13 Hz, 1 H) 6.18 (s, 1 H) 7.37 -

7.42 (m, 1 H) 7.43 - 7.48 (m, 2 H) 7.57 (d, *J*=7.32 Hz, 2 H) 7.66 (d, *J*=8.40 Hz, 2 H) 7.91 (d, *J*=8.40 Hz, 2 H) 8.00 (d, *J*=6.49 Hz, 1 H). HRMS (ESI) calcd for $C_{29}H_{37}N_3O_6S$: [M+H]: 556.2481 Found: 556.2430.

methyl (2S)-2-((S)-3-cyclohexyl-2-((2-(1,3-dioxoisoindolin-2-yl)ethyl)sulfonamido) propanamido)-3-(2-oxopyrrolidin-3-yl)propanoate (4k). Yield (72%), mp 59-60 ^{0}C. ^{1}H NMR (400 MHz, $CDCl_3$-*d*) δ ppm 0.85 - 1.03 (m, 2 H) 1.09 - 1.24 (m, 3 H) 1.58 (td, *J*=9.35, 5.74 Hz, 2 H) 1.63 - 1.77 (m, 5 H) 1.79 - 1.87 (m, 2 H) 1.94 (ddd, *J*=14.26, 7.49, 3.69 Hz, 1 H) 2.20 (ddd, *J*=14.04, 11.80, 5.77 Hz, 1 H) 2.35 - 2.45 (m, 1 H) 2.48 - 2.58 (m, 1 H) 3.30 - 3.47 (m, 4 H) 3.67 (s, 3 H) 4.03 - 4.19 (m, 2 H) 4.32 (dt, *J*=14.40, 7.03 Hz, 1 H) 4.43 - 4.54 (m, 1 H) 5.91 (d, *J*=9.11 Hz, 1 H) 6.37 (s, 1 H) 7.67 - 7.76 (m, 2 H) 7.81 - 7.89 (m, 2 H) 8.23 (d, *J*=6.71 Hz, 1 H). HRMS (ESI) calcd for $C_{27}H_{36}N_4O_8S$: [M+H]: 577.2332 Found: 577.2340.

methyl (2S)-2-((S)-3-cyclohexyl-2-((3-(4-methoxyphenoxy)propyl)sulfonamido) propanamido)-3-(2-oxopyrrolidin-3-yl)propanoate (4l). Yield (67%), mp 49-51 ^{0}C. ^{1}H NMR (400 MHz, $CDCl_3$-*d*) δ ppm 0.86 - 1.02 (m, 2 H) 1.10 - 1.30 (m, 3 H) 1.47 - 1.59 (m, 2 H) 1.62 - 1.74 (m, 5 H) 1.79 - 1.90 (m, 2 H) 1.93 (dt, *J*=7.03, 3.56 Hz, 1 H) 2.13 (ddd, *J*=14.13, 11.79, 5.96 Hz, 1 H) 2.26 (dd, *J*=6.13, 3.25 Hz, 2 H) 2.31 - 2.39 (m, 1 H) 2.42 - 2.52 (m, 1 H) 3.17 - 3.26 (m, 2 H) 3.26 - 3.36 (m, 2 H) 3.70 (s, 3 H) 3.76 (s, 3 H) 4.00 (t, *J*=5.86 Hz, 2 H) 4.05 - 4.15 (m, 1 H) 4.39 - 4.50 (m, 1 H) 5.63 (d, *J*=9.42 Hz, 1 H) 6.16 (s, 1 H) 6.81 (s, 4 H) 8.23 (d, *J*=6.59 Hz, 1 H). HRMS (ESI) calcd for $C_{27}H_{41}N_3O_8S$: [M+H]: 568.2693 Found: 568.2633.

methyl (2S)-2-((S)-3-cyclohexyl-2-(octylsulfonamido)propanamido)-3-(2-oxo pyrrolidin-3-yl)propanoate (4m). Yield (75%), mp 56-58 ^{0}C. ^{1}H NMR (400 MHz, $CDCl_3$-*d*) δ ppm 0.88 (t, *J*=6.79 Hz, 4 H) 0.91 - 1.04 (m, 2 H) 1.09 - 1.34 (m, 9 H) 1.36 - 1.44 (m, 1 H) 1.46 - 1.56 (m, 1 H) 1.58 - 1.65 (m, 6 H) 1.69 (d, *J*=14.06 Hz, 4 H) 1.77 - 1.89 (m, 2 H) 1.90 - 1.99 (m, 1 H) 2.09 - 2.21 (m, 1 H) 2.38 - 2.54 (m, 2 H) 3.00 (t, *J*=7.96 Hz, 2 H) 3.35 - 3.43 (m, 2 H) 3.73 (s, 3 H) 3.99 - 4.09 (m, 1 H) 4.42 - 4.50 (m, 1 H) 5.34 (d, *J*=9.32 Hz, 1 H) 6.04 (s, 1 H) 8.13 (d, *J*=6.54 Hz, 1 H). HRMS (ESI) calcd for $C_{25}H_{46}N_3O_6S$: [M+H]: 516.3107 Found: 516.3112.

Synthesis of alcohols 5a-m. To a solution of ester **4** (5 mmol) in anhydrous THF (30 mL) was added dropwise lithium borohydride (2M in THF, 7.5 mL, 15 mmol), followed by absolute ethyl alcohol (15 mL), and the reaction mixture was stirred at room temperature overnight. The reaction mixture was then acidified using 5% HCl and the pH was adjusted to ~2. Removal of the solvent left a residue which was taken up in ethyl acetate (100 mL) and the organic layer was washed with brine (25 mL), dried over anhydrous sodium sulfate, filtered, and concentrated to yield compounds **5a-m.**

(2S)-3-cyclohexyl-N-((2S)-1-hydroxy-3-(2-oxopyrrolidin-3-yl)propan-2-yl)-2-(phenyl sulfonamido)propanamide (5a). Yield (95%), mp 48-51 ^{0}C. ^{1}H NMR (400 MHz, $CDCl_3$-*d*) δ ppm 0.59 - 0.73 (m, 2 H) 0.76 - 0.94 (m, 2 H) 0.96 - 1.18 (m, 3 H) 1.31 (br. s, 1 H) 1.39 - 1.64 (m, 6 H) 1.75 - 1.87 (m, 1 H) 1.96 - 2.04 (m, 2 H) 2.30 - 2.44 (m, 2 H) 3.32 - 3.40 (m, 2 H) 3.42 - 3.49 (m, 1 H) 3.57 (dd, *J*=11.25, 3.25 Hz, 1 H) 3.69 - 3.78 (m, 1 H) 3.84 - 3.93 (m, 1 H) 6.28 (d, *J*=8.10 Hz, 1 H) 6.37 (s, 1 H) 7.48 - 7.53 (m, 2 H) 7.55 - 7.60 (m, 1 H) 7.71 (d, *J*=7.32 Hz, 1 H) 7.89 (d, *J*=7.47 Hz, 2 H). HRMS (ESI) calcd for $C_{22}H_{33}N_3O_5S$: [M+H]: 452.2219 Found: 452.2210.

(2S)-3-cyclohexyl-N-((2S)-1-hydroxy-3-(2-oxopyrrolidin-3-yl)propan-2-yl)-2-((phenylmethyl)sulfonamido)propanamide (5b). Yield (94%), mp 45-47 ^{0}C. ^{1}H NMR (400 MHz, $CDCl_3$-*d*) δ ppm 0.81 - 0.96 (m, 2 H) 1.07 - 1.23 (m, 4 H) 1.37 (br. s., 1 H) 1.43 - 1.52 (m, 1 H) 1.56 (dd, *J*=13.72, 6.74 Hz, 2 H) 1.62 - 1.76 (m, 6 H) 1.77 - 1.86 (m, 1 H) 2.38 (td, *J*=5.93, 3.47 Hz, 1 H) 2.46 (d, *J*=6.40 Hz, 1 H) 3.31 (d, *J*=7.62 Hz, 2 H) 3.54 - 3.60 (m, 1 H) 3.65 (d, *J*=8.49 Hz, 1 H) 3.83 - 3.93 (m, 1 H) 3.97 - 4.06 (m, 1 H) 4.26 (s, 2 H) 5.85 (d, *J*=7.08 Hz, 1 H) 6.26 (s, 1 H) 7.32 - 7.38 (m, 3 H) 7.38 - 7.43 (m, 2 H) 7.66 (d, *J*=7.18 Hz, 1 H). HRMS (ESI) calcd for $C_{23}H_{35}N_3O_5S$: [M+H]: 466.2376 Found: 466.2360.

(2S)-3-cyclohexyl-N-((2S)-1-hydroxy-3-(2-oxopyrrolidin-3-yl)propan-2-yl)-2-((2-phenylethyl)sulfonamido)propanamide (5c). Yield (94%), mp 49-50 ^{0}C. ^{1}H NMR (400 MHz, $CDCl_3$-*d*) δ ppm 0.84 - 1.01 (m, 2 H) 1.10 - 1.23 (m, 4 H) 1.55 (d, *J*=7.23 Hz, 2 H) 1.60 - 1.74 (m, 6 H) 1.77 - 1.87 (m, 2 H) 2.20 - 2.30 (m, 1 H) 2.33 - 2.42 (m, 1 H) 3.05 - 3.15 (m, 2 H) 3.18 - 3.33 (m, 2 H) 3.59 (d, *J*=18.50 Hz, 2 H) 3.83 (br. s., 1 H) 4.01 (d, *J*=4.39 Hz, 2 H) 4.14 - 4.22 (m, 2 H) 6.11 (d, *J*=5.42 Hz, 1 H) 6.45 (s, 1 H) 7.16 - 7.23 (m, 2 H) 7.23 - 7.33 (m, 3 H) 7.79 (d, *J*=6.59 Hz, 1 H). HRMS (ESI) calcd for $C_{24}H_{37}N_3O_5S$: [M+H]: 480.2532 Found: 480.2508.

(2S)-3-cyclohexyl-2-((4-fluorophenyl)sulfonamido)-N-((2S)-1-hydroxy-3-(2-oxopyrrolidin-3-yl)propan-2-yl)propanamide (5d). Yield (96%), mp 66-68 ^{0}C. ^{1}H NMR (400 MHz, $CDCl_3$-*d*) δ ppm 0.63 - 0.77 (m, 1 H) 0.79 - 0.90 (m, 1 H) 0.91 - 1.18 (m, 3 H) 1.34 (d, *J*=11.81 Hz, 1 H) 1.42 - 1.52 (m, 2 H) 1.52 - 1.67 (m, 6 H) 1.79 - 1.89 (m, 1 H) 2.01 (d, *J*=6.40 Hz, 1 H) 2.27 - 2.42 (m, 2 H) 3.33 - 3.41 (m, 2 H) 3.46 - 3.55 (m, 2 H) 3.58 (br. s., 1 H) 3.68 - 3.78 (m, 1 H) 3.85 - 4.01 (m, 1 H) 6.33 (s, 1 H) 7.18 (t, *J*=8.28 Hz, 2 H) 7.80

(d, *J*=7.20 Hz, 1 H) 7.91 (dd, *J*=8.47, 5.00 Hz, 2 H) 8.25 (d, *J*=5.82 Hz, 1 H). HRMS (ESI) calcd for $C_{22}H_{32}FN_3O_5S$: [M+H]: 470.2125 Found: 470.2115.

(2S)-2-((3-chlorophenyl)sulfonamido)-3-cyclohexyl-N-((2S)-1-hydroxy-3-(2-oxo pyrrolidin-3-yl)propan-2-yl)propanamide (5e). Yield (94%), mp 61-63 ^{0}C. ^{1}H NMR (400 MHz, $CDCl_3$-*d*) δ ppm 0.67 - 0.80 (m, 2 H) 0.86 (q, *J*=11.23 Hz, 1 H) 0.94 - 1.19 (m, 3 H) 1.38 - 1.51 (m, 3 H) 1.52 - 1.67 (m, 4 H) 1.84 (t, *J*=8.01 Hz, 2 H) 1.93 - 2.01 (m, 1 H) 2.32 - 2.43 (m, 2 H) 3.33 - 3.42 (m, 2 H) 3.44 - 3.50 (m, 1 H) 3.54 - 3.60 (m, 1 H) 3.77 (dt, *J*=8.86, 4.60 Hz, 1 H) 3.81 - 3.88 (m, 1 H) 4.21 (br. s, 1 H) 6.28 (s, 1 H) 7.45 (t, *J*=7.79 Hz, 1 H) 7.49 - 7.56 (m, 1 H) 7.78 (d, *J*=7.57 Hz, 1 H) 7.84 - 7.89 (m, 1 H) 7.97 (d, *J*=5.57 Hz, 1 H) 8.17 (d, *J*=7.20 Hz, 1 H). HRMS (ESI) calcd for $C_{22}H_{32}ClN_3O_5S$: [M+H]: 486.1829 Found: 486.1809.

(2S)-2-((4-chlorophenyl)sulfonamido)-3-cyclohexyl-N-((2S)-1-hydroxy-3-(2-oxo pyrrolidin-3-yl)propan-2-yl)propanamide (5f). Yield (93%), mp 56-57 ^{0}C. ^{1}H NMR (400 MHz, $CDCl_3$-*d*) δ ppm 0.65 - 0.77 (m, 1 H) 0.78 - 0.93 (m, 1 H) 0.94 - 1.19 (m, 3 H) 1.34 - 1.42 (m, 1 H) 1.43 - 1.52 (m, 2 H) 1.53 - 1.64 (m, 5 H) 1.76 - 1.90 (m, 2 H) 1.91 - 2.02 (m, 1 H) 2.24 - 2.33 (m, 1 H) 2.38 (dd, *J*=8.30, 3.32 Hz, 1 H) 3.34 - 3.44 (m, 2 H) 3.45 - 3.52 (m, 1 H) 3.58 (d, *J*=8.15 Hz, 1 H) 3.82 (br. s, 1 H) 3.95 (d, *J*=3.91 Hz, 1 H) 4.17 - 4.25 (m, 1 H) 5.97 (d, *J*=5.20 Hz, 1 H) 6.33 (s, 1 H) 7.41 - 7.50 (m, 2 H) 7.79 - 7.89 (m, 2 H) 8.05 (d, *J*=7.20 Hz, 1 H). HRMS (ESI) calcd for $C_{22}H_{32}ClN_3O_5S$: [M+H]: 486.1829 Found: 486.1811.

(2S)-2-(((4-chlorophenyl)methyl)sulfonamido)-3-cyclohexyl-N-((2S)-1-hydroxy-3-(2-oxopyrrolidin-3-yl)propan-2-yl)propanamide (5g). Yield (95%), mp 47-48 ^{0}C. ^{1}H NMR (400 MHz, $CDCl_3$-*d*) δ ppm 0.82 - 0.95 (m, 2 H) 1.11 - 1.21 (m, 2 H) 1.37 (d, *J*=4.42 Hz,

1 H) 1.43 - 1.50 (m, 1 H) 1.53 - 1.61 (m, 3 H) 1.62 - 1.75 (m, 6 H) 1.83 (dd, *J*=11.42, 9.67 Hz, 1 H) 2.00 (br. s., 1 H) 2.35 - 2.52 (m, 2 H) 3.30 - 3.36 (m, 2 H) 3.55 - 3.61 (m, 1 H) 3.64 - 3.71 (m, 1 H) 3.84 - 3.93 (m, 1 H) 4.00 (d, *J*=3.56 Hz, 1 H) 4.23 (d, *J*=4.96 Hz, 2 H) 5.81 (d, *J*=8.40 Hz, 1 H) 6.11 (s, 1 H) 7.30 - 7.33 (m, 1 H) 7.34 - 7.36 (m, 3 H) 7.80 (d, *J*=7.03 Hz, 1 H). HRMS (ESI) calcd for $C_{23}H_{34}ClN_3O_5S$: [M+H]: 500.1986 Found: 500.1978.

(2S)-2-((2-(3-chlorophenyl)ethyl)sulfonamido)-3-cyclohexyl-N-((2S)-1-hydroxy-3-(2-oxopyrrolidin-3-yl)propan-2-yl)propanamide (5h). Yield (96%), mp 67-69 ^{0}C. ^{1}H NMR (400 MHz, $CDCl_3$-*d*) δ ppm 0.86 - 1.02 (m, 2 H) 1.09 - 1.21 (m, 2 H) 1.45 - 1.65 (m, 4 H) 1.70 (d, *J*=10.25 Hz, 5 H) 1.76 - 1.86 (m, 2 H) 1.99 (d, *J*=5.81 Hz, 1 H) 2.25 - 2.35 (m, 1 H) 2.35 - 2.45 (m, 1 H) 3.04 - 3.16 (m, 2 H) 3.19 - 3.28 (m, 2 H) 3.29 - 3.37 (m, 2 H) 3.49 (br. s, 1 H) 3.54 - 3.60 (m, 1 H) 3.62 - 3.69 (m, 1 H) 3.95 - 4.05 (m, 2 H) 5.87 (d, *J*=9.03 Hz, 1 H) 6.17 (s, 1 H) 7.10 (d, *J*=6.74 Hz, 1 H) 7.20 - 7.23 (m, 2 H) 7.24 (br. s., 1 H) 7.94 (d, *J*=7.03 Hz, 1 H). HRMS (ESI) calcd for $C_{24}H_{36}ClN_3O_5S$: [M+H]: 514.2142 Found: 514.2148.

(2S)-3-cyclohexyl-N-((2S)-1-hydroxy-3-(2-oxopyrrolidin-3-yl)propan-2-yl)-2-(thiophene-2-sulfonamido)propanamide (5i). Yield (96%), mp 48-50 ^{0}C. ^{1}H NMR (400 MHz, DMSO-d_6) δ ppm 0.65 - 0.84 (m, 2 H) 0.95 - 1.14 (m, 3 H) 1.29 - 1.38 (m, 4 H) 1.47 - 1.64 (m, 6 H) 1.67 - 1.78 (m, 1 H) 2.01 - 2.12 (m, 2 H) 3.04 - 3.19 (m, 2 H) 3.21 - 3.29 (m, 2 H) 3.63 (dd, *J*=6.96, 4.17 Hz, 1 H) 3.77 (q, *J*=7.53 Hz, 1 H) 4.65 (t, *J*=5.49 Hz, 1 H) 7.09 - 7.14 (m, 1 H) 7.53 - 7.54 (m, 1 H) 7.55 (s, 1 H) 7.73 (d, *J*=8.64 Hz, 1 H) 7.87 (dd, *J*=4.88, 1.03 Hz, 1 H) 8.08 (d, *J*=8.35 Hz, 1 H). HRMS (ESI) calcd for $C_{20}H_{31}N_3O_5S_2$: [M+H]: 458.1783 Found: 458.1739.

(2S)-2-([1,1'-biphenyl]-4-sulfonamido)-3-cyclohexyl-N-((2S)-1-hydroxy-3-(2-oxo pyrrolidin-3-yl)propan-2-yl)propanamide (5j). Yield (92%), mp 93-95 ^{0}C. ^{1}H NMR (400 MHz, DMSO-*d*$_6$) δ ppm 0.61 - 0.71 (m, 1 H) 0.72 - 0.82 (m, 1 H) 0.84 - 0.95 (m, 1 H) 0.98 - 1.12 (m, 2 H) 1.25 - 1.38 (m, 3 H) 1.40 - 1.53 (m, 4 H) 1.56 (d, *J*=9.28 Hz, 2 H) 1.66 - 1.79 (m, 2 H) 2.02 - 2.12 (m, 2 H) 2.86 - 2.97 (m, 1 H) 3.00 - 3.08 (m, 1 H) 3.09 - 3.16 (m, 1 H) 3.27 (dd, *J*=10.04, 4.70 Hz, 1 H) 3.56 - 3.66 (m, 1 H) 3.70 - 3.80 (m, 1 H) 4.64 (t, *J*=5.00 Hz, 1 H) 6.53 (s, 1 H) 7.41 - 7.46 (m, 1 H) 7.49 (d, *J*=5.30 Hz, 1 H) 7.51 - 7.55 (m, 2 H) 7.68 - 7.75 (m, 2 H) 7.82 - 7.89 (m, 4 H) 7.95 (d, *J*=8.37 Hz, 1 H). HRMS (ESI) calcd for $C_{28}H_{37}N_3O_5S$: [M+H]: 528.2532 Found: 528.2568.

(2S)-3-cyclohexyl-2-((2-(1,3-dioxoisoindolin-2-yl)ethyl)sulfonamido)-N-((2S)-1-hydroxy-3-(2-oxopyrrolidin-3-yl)propan-2-yl)propanamide (5k). Yield (94%), mp 65-66 ^{0}C. ^{1}H NMR (400 MHz, $CDCl_3$-*d*) δ ppm 0.83 - 1.01 (m, 2 H) 1.06 - 1.21 (m, 4 H) 1.41 - 1.74 (m, 6 H) 1.80 (d, *J*=11.74 Hz, 2 H) 1.95 - 2.02 (m, 2 H) 2.30 - 2.51 (m, 2 H) 3.24 - 3.38 (m, 2 H) 3.50 - 3.59 (m, 3 H) 3.64 (d, *J*=4.15 Hz, 1 H) 3.84 - 3.97 (m, 1 H) 4.03 (br. s., 1 H) 4.21 - 4.34 (m, 1 H) 4.64 (s, 2 H) 5.88 (s, 1 H) 7.33 - 7.41 (m, 2 H) 7.48 - 7.56 (m, 1 H) 7.59 (d, *J*=6.18 Hz, 1 H) 7.71 - 7.76 (m, 1 H) 8.22 (d, *J*=7.30 Hz, 1 H). HRMS (ESI) calcd for $C_{26}H_{36}N_4O_7S$: [M+H]: 549.2383 Found: 549.2363.

(2S)-3-cyclohexyl-N-((2S)-1-hydroxy-3-(2-oxopyrrolidin-3-yl)propan-2-yl)-2-((3-(4-methoxyphenoxy)propyl)sulfonamido)propanamide (5l). Yield (94%), mp 58-61 ^{0}C. ^{1}H NMR (400 MHz, $CDCl_3$-*d*) δ ppm 0.87 - 1.02 (m, 2 H) 1.10 - 1.23 (m, 2 H) 1.42 - 1.58 (m, 3 H) 1.59 - 1.74 (m, 6 H) 1.78 - 1.87 (m, 2 H) 2.00 - 2.09 (m, 1 H) 2.20 - 2.30 (m, 2 H) 2.36 (ddd, *J*=9.18, 6.18, 3.34 Hz, 1 H) 2.41 - 2.51 (m, 1 H) 3.16 - 3.26 (m, 2 H) 3.27 - 3.33 (m, 2 H) 3.36 (d, *J*=6.05 Hz, 1 H) 3.54 - 3.61 (m, 1 H) 3.63 - 3.71 (m, 1 H) 3.76 (s, 3 H)

3.94 - 4.05 (m, 4 H) 5.75 (d, *J*=8.84 Hz, 1 H) 6.01 (s, 1 H) 6.78 - 6.86 (m, 4 H) 7.96 (d, *J*=6.98 Hz, 1 H). HRMS (ESI) calcd for $C_{26}H_{41}N_3O_7S$: [M+H]: 540.2743 Found: 540.2773.

(2S)-3-cyclohexyl-N-((2S)-1-hydroxy-3-(2-oxopyrrolidin-3-yl)propan-2-yl)-2-(octyl sulfonamido)propanamide (5m). Yield (91%), mp 65-66 ^{0}C. ^{1}H NMR (400 MHz, $CDCl_3$-*d*) δ ppm 0.88 (t, *J*=6.71 Hz, 3 H) 0.93 - 1.03 (m, 2 H) 1.10 - 1.21 (m, 2 H) 1.22 - 1.33 (m, 10 H) 1.36 - 1.44 (m, 2 H) 1.44 - 1.51 (m, 1 H) 1.52 - 1.58 (m, 1 H) 1.59 - 1.75 (m, 5 H) 1.76 - 1.90 (m, 4 H) 2.01 - 2.11 (m, 2 H) 2.37 - 2.53 (m, 2 H) 2.99 (t, *J*=7.96 Hz, 2 H) 3.33 - 3.40 (m, 2 H) 3.54 - 3.61 (m, 1 H) 3.64 - 3.70 (m, 1 H) 3.93 (td, *J*=9.08, 5.22 Hz, 1 H) 3.97 - 4.06 (m, 1 H) 5.66 (d, *J*=8.98 Hz, 1 H) 6.12 (s, 1 H) 7.82 (d, *J*=7.27 Hz, 1 H). HRMS (ESI) calcd for $C_{24}H_{45}N_3O_5S$: [M+H]: 488.3158 Found: 488.3143.

Synthesis of aldehydes 6. General procedure. Compound ***5*** (5 mmol) was dissolved in anhydrous dichloromethane (50 mL) under a nitrogen atmosphere and cooled to 0 ^{o}C. Dess-Martin periodinane reagent (3.18 g, 7.5 mmol, 1.5 eq) was added to the reaction mixture with stirring. The ice bath was removed and the reaction mixture was stirred at room temperature for 3 h (monitoring by TLC indicated complete disappearance of the starting material). A solution of 10% aqueous sodium thiosulfate (20 mL) was added and the solution was stirred for 15 minutes. The aqueous layer was removed and the organic layer was washed with 10% aqueous sodium thiosulfate (20 mL), followed by saturated aqueous sodium bicarbonate (2 x 20 mL), water (2 x 20 mL) and brine (20 mL). The organic layer was dried over anhydrous sodium sulfate, filtered and concentrated. The yellow residue was purified by flash chromatography using silica gel (methylene chloride/ethyl acetate/methanol) to yield a white solid ***6a-m***.

(2S)-3-cyclohexyl-N-((2S)-1-oxo-3-(2-oxopyrrolidin-3-yl)propan-2-yl)-2-(phenylsulfonamido)propanamide (6a). Yield (74%), mp 69-71 ^{0}C. ^{1}H NMR (400 MHz, $CDCl_3$-*d*) δ ppm 0.73 (dd, *J*=11.52, 2.93 Hz, 1 H) 0.86 (td, *J*=11.91, 9.37 Hz, 1 H) 0.93 - 1.21 (m, 3 H) 1.24 - 1.36 (m, 1 H) 1.47 (ddd, *J*=14.16, 9.47, 4.88 Hz, 2 H) 1.51 - 1.66 (m, 4 H) 1.71 - 1.78 (m, 2 H) 1.81 - 1.92 (m, 2 H) 2.31 - 2.42 (m, 2 H) 3.34 - 3.43 (m, 2 H) 3.88 (td, *J*=9.28, 4.88 Hz, 1 H) 4.11 (dt, *J*=8.89, 6.10 Hz, 1 H) 6.14 (d, *J*=8.59 Hz, 1 H) 6.41 (s, 1 H) 7.45 - 7.58 (m, 3 H) 7.86 - 7.91 (m, 2 H) 8.36 (d, *J*=5.86 Hz, 1 H) 9.23 (d, *J*=0.78 Hz, 1 H). HRMS (ESI) calcd for $C_{22}H_{31}N_3O_5S$: [M-]: 449.1984. Found: 449.1981.

(2S)-3-cyclohexyl-N-((2S)-1-oxo-3-(2-oxopyrrolidin-3-yl)propan-2-yl)-2-((phenylmethyl)sulfonamido)propanamide (6b). Yield (76%), mp 62-64 ^{0}C. ^{1}H NMR (400 MHz, $CDCl_3$-*d*) δ ppm 0.80 - 0.97 (m, 2 H) 1.09 - 1.30 (m, 3 H) 1.36 - 1.55 (m, 2 H) 1.57 - 1.79 (m, 6 H) 1.81 - 1.90 (m, 1 H) 1.92 - 2.02 (m, 2 H) 2.34 - 2.43 (m, 1 H) 2.47 - 2.57 (m, 1 H) 3.31 - 3.39 (m, 2 H) 3.98 (td, *J*=8.50, 6.05 Hz, 1 H) 4.22 - 4.32 (m, 2 H) 4.33 - 4.41 (m, 1 H) 5.61 (d, *J*=8.59 Hz, 1 H) 6.25 (s, 1 H) 7.33 - 7.38 (m, 3 H) 7.40 - 7.45 (m, 2 H) 8.26 (d, *J*=6.25 Hz, 1 H) 9.49 (s, 1 H). HRMS (ESI) calcd for $C_{23}H_{33}N_3O_5S$: [M-]: 463.2141 Found: 463.2143.

(2S)-3-cyclohexyl-N-((2S)-1-oxo-3-(2-oxopyrrolidin-3-yl)propan-2-yl)-2-((2-phenylethyl)sulfonamido)propanamide (6c). Yield (74%), mp 60-62 ^{0}C. ^{1}H NMR (400 MHz, $CDCl_3$-*d*) δ ppm 0.84 - 1.04 (m, 2 H) 1.09 - 1.30 (m, 2 H) 1.43 - 1.61 (m, 2 H) 1.62 - 1.76 (m, 6 H) 1.78 - 1.89 (m, 2 H) 1.89 - 2.07 (m, 2 H) 2.20 - 2.33 (m, 1 H) 2.34 - 2.46 (m, 1 H) 3.02 - 3.17 (m, 2 H) 3.19 - 3.43 (m, 4 H) 4.12 (td, *J*=8.96, 5.42 Hz, 1 H) 4.33 (dt, *J*=10.23, 5.28 Hz, 1 H) 5.72 (d, *J*=9.08 Hz, 1 H) 6.30 (br. s., 1 H) 7.16 - 7.25 (m, 3 H) 7.26 - 7.34

(m, 2 H) 8.45 (d, *J*=5.96 Hz, 1 H) 9.48 (s, 1 H). HRMS (ESI) calcd for $C_{24}H_{35}N_3O_5S$: [M-]: 477.2297. Found: 477.2296.

(2S)-3-cyclohexyl-2-((4-fluorophenyl)sulfonamido)-N-((2S)-1-oxo-3-(2-oxopyrrolidin-3-yl)propan-2-yl)propanamide (6d). Yield (68%), mp 68-70 ^{0}C. ^{1}H NMR (400 MHz, $CDCl_3$-*d*) δ ppm 0.64 - 0.91 (m, 2 H) 0.95 - 1.20 (m, 3 H) 1.29 - 1.38 (m, 1 H) 1.42 - 1.66 (m, 6 H) 1.71 - 1.77 (m, 1 H) 1.81 - 1.92 (m, 2 H) 2.28 - 2.47 (m, 2 H) 3.34 - 3.44 (m, 2 H) 3.79 - 3.89 (m, 1 H) 4.12 (q, *J*=7.08 Hz, 1 H) 6.15 (d, *J*=8.69 Hz, 1 H) 6.35 (br. s., 1 H) 7.11 - 7.23 (m, 2 H) 7.87 - 7.95 (m, 3 H) 8.44 (d, *J*=5.52 Hz, 1 H) 9.33 (s, 1 H). HRMS (ESI) calcd for $C_{22}H_{30}N_3O_5FS$: [M-]: 467.1890. Found: 467.1889.

(2S)-2-((3-chlorophenyl)sulfonamido)-3-cyclohexyl-N-((2S)-1-oxo-3-(2-oxopyrrolidin-3-yl)propan-2-yl)propanamide (6e). Yield (76%), mp 52-53 ^{0}C. ^{1}H NMR (400 MHz, $CDCl_3$-*d*) δ ppm 0.70 - 0.96 (m, 3 H) 1.00 - 1.23 (m, 4 H) 1.33 - 1.43 (m, 1 H) 1.45 - 1.71 (m, 6 H) 1.80 - 1.91 (m, 2 H) 2.33 - 2.48 (m, 2 H) 3.35 - 3.45 (m, 2 H) 3.85 - 3.95 (m, 1 H) 3.99 - 4.09 (m, 1 H) 6.11 (d, *J*=8.84 Hz, 1 H) 6.27 (br. s., 1 H) 7.41 - 7.49 (m, 1 H) 7.49 - 7.57 (m, 1 H) 7.75 - 7.81 (m, 1 H) 7.85 - 7.90 (m, 1 H) 8.67 (d, *J*=4.98 Hz, 1 H) 9.27 (s, 1 H). HRMS (ESI) calcd for $C_{22}H_{30}N_3O_5ClS$: [M-]: 483.1595. Found: 483.1593.

(2S)-2-((4-chlorophenyl)sulfonamido)-3-cyclohexyl-N-((2S)-1-oxo-3-(2-oxopyrrolidin-3-yl)propan-2-yl)propanamide (6f). Yield (76%), mp 72-74 ^{0}C. ^{1}H NMR (400 MHz, $CDCl_3$-*d*) δ ppm 0.69 - 0.93 (m, 2 H) 0.97 - 1.22 (m, 4 H) 1.25 - 1.38 (m, 1 H) 1.43 - 1.72 (m, 6 H) 1.81 - 1.91 (m, 2 H) 2.02 - 2.15 (m, 1 H) 2.24 - 2.34 (m, 1 H) 2.35 - 2.44 (m, 1 H) 3.36 - 3.47 (m, 2 H) 3.83 (td, *J*=9.01, 5.18 Hz, 1 H) 4.03 - 4.15 (m, 1 H) 6.26 (d, *J*=8.69

Hz, 1 H) 6.38 (s, 1 H) 7.41 - 7.53 (m, 2 H) 7.82 (d, *J*=8.54 Hz, 2 H) 8.51 (d, *J*=5.37 Hz, 1 H) 9.33 (s, 1 H). HRMS (ESI) calcd for $C_{22}H_{30}N_3O_5ClS$: [M-]: 483.1595. Found: 483.1591.

(2S)-2-(((4-chlorophenyl)methyl)sulfonamido)-3-cyclohexyl-N-((2S)-1-oxo-3-(2-oxo pyrrolidin-3-yl)propan-2-yl)propanamide (6g). Yield (75%), mp 52-53 ^{0}C. ^{1}H NMR (400 MHz, $CDCl_3$-*d*) δ ppm 0.80 - 0.97 (m, 2 H) 1.10 - 1.31 (m, 4 H) 1.36 - 1.54 (m, 1 H) 1.56 - 1.78 (m, 6 H) 1.80 - 1.90 (m, 1 H) 1.92 - 1.98 (m, 2 H) 2.36 - 2.46 (m, 1 H) 2.47 - 2.57 (m, 1 H) 3.32 - 3.42 (m, 2 H) 3.92 - 4.00 (m, 1 H) 4.12 (q, *J*=7.14 Hz, 2 H) 4.28 - 4.37 (m, 1 H) 5.69 (d, *J*=8.59 Hz, 1 H) 6.23 (s, 1 H) 7.30 - 7.43 (m, 4 H) 8.39 (d, *J*=5.66 Hz, 1 H) 9.49 (s, 1 H). HRMS (ESI) calcd for $C_{23}H_{33}N_3O_5ClS$: [M-]: 497.1751. Found: 497.1754.

(2S)-2-((2-(3-chlorophenyl)ethyl)sulfonamido)-3-cyclohexyl-N-((2S)-1-oxo-3-(2-oxo pyrrolidin-3-yl)propan-2-yl)propanamide (6h). Yield (73%), mp 53-55 ^{0}C. ^{1}H NMR (400 MHz, $CDCl_3$-*d*) δ ppm 0.84 - 1.03 (m, 2 H) 1.08 - 1.31 (m, 4 H) 1.43 - 1.57 (m, 2 H) 1.60 - 1.86 (m, 6 H) 1.89 - 1.97 (m, 2 H) 2.24 - 2.36 (m, 1 H) 2.36 - 2.48 (m, 1 H) 3.00 - 3.13 (m, 2 H) 3.16 - 3.41 (m, 4 H) 4.06 - 4.14 (m, 1 H) 4.27 - 4.36 (m, 1 H) 5.71 (d, *J*=9.28 Hz, 1 H) 6.22 (s, 1 H) 7.08 (d, *J*=6.83 Hz, 1 H) 7.16 - 7.24 (m, 3 H) 8.56 (d, *J*=5.76 Hz, 1 H) 9.47 (s, 1 H). HRMS (ESI) calcd for $C_{24}H_{34}N_3O_5ClS$: [M-]: 511.1908. Found: 511.1907.

(2S)-3-cyclohexyl-N-((2S)-1-oxo-3-(2-oxopyrrolidin-3-yl)propan-2-yl)-2-(thiophene-2-sulfonamido)propanamide (6i). Yield (75%), mp 68-69 ^{0}C. ^{1}H NMR (400 MHz, $CDCl_3$-*d*) δ ppm 0.70 - 0.95 (m, 2 H) 1.01 - 1.25 (m, 3 H) 1.30 - 1.41 (m, 1 H) 1.46 - 1.70 (m, 6 H) 1.74 - 2.00 (m, 4 H) 2.32 - 2.51 (m, 2 H) 3.40 (d, *J*=9.08 Hz, 2 H) 3.98 (td, *J*=9.01, 4.64 Hz, 1 H) 4.15 - 4.25 (m, 1 H) 6.32 (d, *J*=8.49 Hz, 1 H) 6.48 (br. s., 1 H) 7.03 - 7.10 (m, 1 H) 7.55 - 7.60 (m, 1 H) 7.63 (dd, *J*=3.52, 0.98 Hz, 1 H) 8.35 (d, *J*=5.86 Hz, 1 H) 9.31 (s, 1 H). HRMS (ESI) calcd for $C_{20}H_{29}N_3O_5S_2$: [M-]: 455.1549. Found: 455.1546.

(2S)-2-([1,1'-biphenyl]-4-sulfonamido)-3-cyclohexyl-N-((2S)-1-oxo-3-(2-oxopyrrolidin-3-yl)propan-2-yl)propanamide (6j). Yield (75%), mp 56-58 ^{0}C. ^{1}H NMR (400 MHz, $CDCl_3$-*d*) δ ppm 0.68 - 0.80 (m, 2 H) 0.84 - 0.90 (m, 1 H) 0.91 - 0.97 (m, 1 H) 0.98 - 1.08 (m, 1 H) 1.09 - 1.20 (m, 2 H) 1.31 - 1.44 (m, 1 H) 1.45 - 1.68 (m, 6 H) 1.72 - 1.81 (m, 1 H) 1.81 - 1.89 (m, 1 H) 1.90 - 2.00 (m, 1 H) 2.17 - 2.37 (m, 2 H) 3.15 - 3.25 (m, 1 H) 3.27 - 3.38 (m, 1 H) 3.87 (td, *J*=9.00, 4.91 Hz, 1 H) 4.04 - 4.16 (m, 1 H) 6.13 (d, *J*=8.45 Hz, 1 H) 6.37 (br. s., 1 H) 7.39 - 7.44 (m, 1 H) 7.45 - 7.51 (m, 1 H) 7.58 (d, *J*=7.13 Hz, 2 H) 7.68 (d, *J*=8.35 Hz, 2 H) 7.94 (d, *J*=8.35 Hz, 2 H) 8.44 (d, *J*=5.61 Hz, 1 H) 9.30 (s, 1 H). HRMS (ESI) calcd for $C_{28}H_{35}N_3O_5S$: [M-]: 525.2297. Found: 525.2297.

(2S)-3-cyclohexyl-2-((2-(1,3-dioxoisoindolin-2-yl)ethyl)sulfonamido)-N-((2S)-1-oxo-3-(2-oxopyrrolidin-3-yl)propan-2-yl)propanamide (6k). Yield (73%), mp 59-61 ^{0}C. ^{1}H NMR (400 MHz, $CDCl_3$-*d*) δ ppm 0.80 - 1.04 (m, 2 H) 1.09 - 1.28 (m, 3 H) 1.43 - 1.73 (m, 6 H) 1.80 (br. s., 2 H) 1.93 - 2.02 (m, 1 H) 2.16 - 2.23 (m, 1 H) 2.31 - 2.46 (m, 2 H) 2.48 - 2.62 (m, 1 H) 3.24 - 3.55 (m, 4 H) 3.63 - 3.76 (m, 1 H) 4.04 - 4.19 (m, 2 H) 4.25 - 4.40 (m, 1 H) 5.81 (d, *J*=8.69 Hz, 1 H) 6.23 (t, *J*=7.64 Hz, 1 H) 7.45 - 7.61 (m, 1 H) 7.67 - 7.79 (m, 1 H) 7.84 (dd, *J*=5.37, 3.03 Hz, 1 H) 7.94 (d, *J*=7.62 Hz, 1 H) 8.57 (d, *J*=5.86 Hz, 1 H) 9.48 (s, 1 H). HRMS (ESI) calcd for $C_{26}H_{34}N_4O_7S$: [M-]: 546.2148. Found: 546.2144.

(2S)-3-cyclohexyl-2-((3-(4-methoxyphenoxy)propyl)sulfonamido)-N-((2S)-1-oxo-3-(2-oxopyrrolidin-3-yl)propan-2-yl)propanamide (6l). Yield (73%), mp 47-49 ^{0}C. ^{1}H NMR (400 MHz, $CDCl_3$-*d*) δ ppm 0.85 - 1.03 (m, 2 H) 1.06 - 1.31 (m, 2 H) 1.44 - 1.60 (m, 2 H) 1.62 - 1.76 (m, 6 H) 1.79 - 1.88 (m, 2 H) 1.91 - 2.00 (m, 2 H) 2.22 - 2.31 (m, 2 H) 2.31 - 2.41 (m, 1 H) 2.44 - 2.55 (m, 1 H) 3.15 - 3.28 (m, 2 H) 3.28 - 3.39 (m, 2 H) 3.76 (s, 3 H) 3.96 - 4.03 (m, 2 H) 4.09 (td, *J*=9.01, 5.42 Hz, 1 H) 4.29 - 4.37 (m, 1 H) 5.58 (d,

J=9.18 Hz, 1 H) 6.11 (s, 1 H) 6.77 - 6.87 (m, 4 H) 8.53 (d, *J*=5.66 Hz, 1 H) 9.49 (s, 1 H). HRMS (ESI) calcd for $C_{26}H_{39}N_3O_7S$: [M-]: 537.2509. Found: 537.2508.

(2S)-3-cyclohexyl-2-(octylsulfonamido)-N-((2S)-1-oxo-3-(2-oxopyrrolidin-3-yl)propan-2-yl)propanamide (6m). Yield (74%), sticky solid. ^{1}H NMR (400 MHz, $CDCl_3$-*d*) δ ppm 0.84 - 1.03 (m, 4 H) 1.11 - 1.35 (m, 8 H) 1 Yield (%), mp 43-45 ^{0}C..38 (d, *J*=6.44 Hz, 2 H) 1.48 - 1.61 (m, 3 H) 1.62 - 1.77 (m, 8 H) 1.77 - 1.89 (m, 4 H) 1.94 - 2.02 (m, 2 H) 2.38 - 2.48 (m, 1 H) 2.48 - 2.59 (m, 1 H) 3.00 (t, *J*=7.96 Hz, 2 H) 3.34 - 3.43 (m, 2 H) 4.05 (td, *J*=9.01, 5.22 Hz, 1 H) 4.33 - 4.41 (m, 1 H) 5.52 (d, *J*=9.18 Hz, 1 H) 6.21 (s, 1 H) 8.38 (d, *J*=5.96 Hz, 1 H) 9.51 (s, 1 H). HRMS (ESI) calcd for $C_{24}H_{43}N_3O_5S$: [M-]: 485.2923. Found: 485.2922.

Synthesis of bisulfite adducts *7a-m.* General procedure. To a solution of aldehyde ***6*** (5 mmol) in dry ethyl acetate (20 mL) was added absolute ethanol (12 mL) with stirring, followed by a solution of sodium bisulfite (540 mg; 5 mmol) in water (5 mL). The reaction mixture was stirred for 3 h at 50 ^{0}C and then allowed to cool to room temperature. The precipitate was vacuum filtered and the solid was thoroughly washed with absolute ethanol. The filtrate was dried over anhydrous sodium sulfate, filtered, and concentrated to yield a yellowish oil which was treated with ethyl ether (2 x 50 mL) to form a white solid. The white solid was stirred with ethyl ether (30 mL) and ethyl acetate (15 mL) for 5 minutes. Careful removal of the solvent using a pipette yielded compounds ***7a-m.***

Sodium (2S)-2-((S)-3-cyclohexyl-2-(phenylsulfonamido)propanamido)-1-hydroxy-3-(2-oxopyrrolidin-3-yl)propane-1-sulfonate (7a). Yield (68%), mp 154-156 ^{0}C. ^{1}H NMR (400 MHz, DMSO-d_6) δ ppm 0.57 - 0.82 (m, 2 H) 0.91 (d, *J*=9.18 Hz, 1 H) 1.00 - 1.14 (m, 2 H) 1.16 - 1.25 (m, 1 H) 1.29 (d, *J*=8.40 Hz, 1 H) 1.51 (d, *J*=11.33 Hz, 6 H) 1.68

- 1.87 (m, 1 H) 1.89 - 2.10 (m, 2 H) 2.95 - 3.15 (m, 2 H) 3.71 - 3.81 (m, 2 H) 3.87 (d, *J*=3.91 Hz, 1 H) 4.07 (t, *J*=9.23 Hz, 1 H) 5.35 (d, *J*=5.57 Hz, 1 H) 5.41 (d, *J*=5.86 Hz, 1 H) 7.45 (br. s., 1 H) 7.49 - 7.65 (m, 4 H) 7.71 - 7.93 (m, 3 H). HRMS (ESI) calcd for $C_{22}H_{32}N_3O_8S_2Na$: [M-]: 553.1529. Found: 553.1531.

Sodium (2S)-2-((S)-3-cyclohexyl-2-((phenylmethyl)sulfonamido)propanamido)-1-hydroxy-3-(2-oxopyrrolidin-3-yl)propane-1-sulfonate (7b). Yield (76%), mp 137-139 ^{0}C. ^{1}H NMR (400 MHz, DMSO-d_6) δ ppm 0.85 (br. s., 2 H) 1.01 - 1.28 (m, 3 H) 1.31 - 1.48 (m, 2 H) 1.51 - 1.83 (m, 6 H) 1.86 - 2.26 (m, 4 H) 2.90 - 3.03 (m, 1 H) 3.11 (d, *J*=5.86 Hz, 1 H) 3.84 - 4.03 (m, 2 H) 4.19 - 4.30 (m, 1 H) 4.33 (s, 1 H) 5.46 (d, *J*=5.47 Hz, 1 H) 5.57 (d, *J*=6.25 Hz, 1 H) 7.35 (br. s., 5 H) 7.46 (d, *J*=8.20 Hz, 1 H) 7.51 (br. s., 1 H) 7.73 (d, *J*=8.98 Hz, 1 H) 7.97 (d, *J*=8.98 Hz, 1 H). HRMS (ESI) calcd for $C_{23}H_{34}N_3O_8S_2Na$: [M-]: 567.1685. Found: 567.1682.

Sodium (2S)-2-((S)-3-cyclohexyl-2-((2-phenylethyl)sulfonamido)propanamido)-1-hydroxy-3-(2-oxopyrrolidin-3-yl)propane-1-sulfonate (7c). Yield (65%), mp 74-76 ^{0}C. ^{1}H NMR (400 MHz, DMSO-d_6) δ ppm 0.78 - 0.98 (m, 2 H) 1.04 - 1.29 (m, 4 H) 1.44 (br. s., 3 H) 1.65 (br. s., 4 H) 1.76 - 1.93 (m, 2 H) 2.00 (br. s., 1 H) 2.16 (br. s., 1 H) 2.69 (d, *J*=8.40 Hz, 1 H) 2.90 (d, *J*=9.96 Hz, 2 H) 3.05 (br. s., 4 H) 3.84 (br. s., 1 H) 3.96 (br. s., 1 H) 4.17 - 4.30 (m, 1 H) 7.26 (d, *J*=4.59 Hz, 5 H) 7.47 (br. s., 1 H) 7.59 - 7.64 (m, 1 H) 7.94 (br. s., 1 H) 8.64 (d, *J*=7.03 Hz, 1 H). HRMS (ESI) calcd for $C_{24}H_{36}N_3O_8S_2Na$: [M-]: 581.1842. Found: 581.1841.

Sodium (2S)-2-((S)-3-cyclohexyl-2-((4-fluorophenyl)sulfonamido)propanamido)-1-hydroxy-3-(2-oxopyrrolidin-3-yl)propane-1-sulfonate (7d). Yield (78%), mp 75-77 ^{0}C.

^{1}H NMR (400 MHz, DMSO-d_6) δ ppm 0.64 - 0.84 (m, 2 H) 0.88 - 0.99 (m, 1 H) 1.04 - 1.13 (m, 3 H) 1.16 - 1.26 (m, 2 H) 1.28 - 1.39 (m, 2 H) 1.55 (d, *J*=9.57 Hz, 4 H) 1.69 - 1.85 (m, 1 H) 1.89 - 1.96 (m, 1 H) 2.05 - 2.14 (m, 1 H) 3.00 - 3.16 (m, 2 H) 3.54 - 3.63 (m, 1 H) 3.70 - 3.81 (m, 1 H) 3.98 - 4.08 (m, 1 H) 5.31 (dd, *J*=16.23, 5.93 Hz, 1 H) 7.32 - 7.46 (m, 2 H) 7.53 (d, *J*=4.74 Hz, 1 H) 7.63 - 7.70 (m, 1 H) 7.74 (s, 1 H) 7.79 - 7.90 (m, 2 H) 7.95 (br. s., 1 H). HRMS (ESI) calcd for $C_{22}H_{31}N_3O_8FS_2Na$: [M-]: 571.1434. Found: 571.1435.

Sodium (2S)-2-((S)-2-((3-chlorophenyl)sulfonamido)-3-cyclohexylpropanamido)-1-hydroxy-3-(2-oxopyrrolidin-3-yl)propane-1-sulfonate (7e). Yield (78%), mp 74-75 ^{0}C. ^{1}H NMR (400 MHz, DMSO-d_6) δ ppm 0.64 - 0.84 (m, 3 H) 0.91 (d, *J*=6.40 Hz, 1 H) 1.01 - 1.21 (m, 4 H) 1.28 - 1.37 (m, 1 H) 1.42 - 1.63 (m, 4 H) 1.67 - 1.87 (m, 2 H) 1.88 - 2.14 (m, 2 H) 3.01 - 3.21 (m, 2 H) 3.75 - 3.90 (m, 1 H) 4.01 - 4.15 (m, 1 H) 4.26 - 4.42 (m, 1 H) 5.27 (d, *J*=5.27 Hz, 1 H) 6.02 - 6.10 (m, 1 H) 7.44 (br. s., 1 H) 7.50 - 7.60 (m, 1 H) 7.61 - 7.69 (m, 1 H) 7.70 - 7.75 (m, 1 H) 7.76 - 7.83 (m, 1 H) 8.05 - 8.17 (m, 1 H) 8.48 - 8.60 (m, 1 H). HRMS (ESI) calcd for $C_{22}H_{31}N_3O_8ClS_2Na$: [M-]: 587.1139. Found: 587.1134.

Sodium (2S)-2-((S)-2-((4-chlorophenyl)sulfonamido)-3-cyclohexylpropanamido)-1-hydroxy-3-(2-oxopyrrolidin-3-yl)propane-1-sulfonate (7f). Yield (61%), mp152-153 ^{0}C. ^{1}H NMR (400 MHz, DMSO-d_6) δ ppm 0.64 - 0.86 (m, 2 H) 1.01 - 1.12 (m, 4 H) 1.15 - 1.27 (m, 1 H) 1.29 - 1.37 (m, 2 H) 1.39 - 1.62 (m, 6 H) 1.71 - 1.93 (m, 2 H) 1.97 - 2.09 (m, 1 H) 3.01 - 3.13 (m, 2 H) 3.73 - 3.81 (m, 1 H) 3.87 (dd, *J*=5.53, 2.18 Hz, 1 H) 4.00 - 4.12 (m, 1 H) 5.28 - 5.39 (m, 1 H) 7.45 (d, *J*=1.88 Hz, 1 H) 7.56 - 7.65 (m, 2 H) 7.73 - 7.87 (m, 3 H) 8.03 (d, *J*=13.23 Hz, 1 H). HRMS (ESI) calcd for $C_{22}H_{31}N_3O_8ClS_2Na$: [M-]: 587.1139. Found: 587.1137.

Sodium (2S)-2-((S)-2-(((4-chlorophenyl)methyl)sulfonamido)-3-cyclohexylpropanamido)-1-hydroxy-3-(2-oxopyrrolidin-3-yl)propane-1-sulfonate (7g). Yield (61%), mp 76-78 ^{0}C. ^{1}H NMR (400 MHz, DMSO-d_6) δ ppm 0.84 (br. s., 2 H) 1.04 - 1.24 (m, 6 H) 1.37 (d, *J*=8.59 Hz, 2 H) 1.65 (d, *J*=8.98 Hz, 6 H) 1.84 - 1.97 (m, 1 H) 2.08 - 2.35 (m, 3 H) 2.95 (d, *J*=7.42 Hz, 1 H) 3.04 - 3.18 (m, 1 H) 3.57 (dd, *J*=13.18, 6.83 Hz, 1 H) 3.74 (q, *J*=6.77 Hz, 1 H) 3.84 - 3.99 (m, 1 H) 4.17 - 4.38 (m, 1 H) 7.41 (br. s., 3 H) 7.50 - 7.55 (m, 1 H) 7.65 (br. s., 1 H) 7.92 (d, *J*=8.69 Hz, 1 H) 8.64 (d, *J*=6.83 Hz, 1 H). HRMS (ESI) calcd for $C_{23}H_{33}N_3O_8ClS_2Na$: [M-]: 601.1295. Found: 601.1295.

Sodium (2S)-2-((S)-2-((2-(3-chlorophenyl)ethyl)sulfonamido)-3-cyclohexylpropanamido)-1-hydroxy-3-(2-oxopyrrolidin-3-yl)propane-1-sulfonate (7h). Yield (71%), mp 78-80 ^{0}C. ^{1}H NMR (400 MHz, DMSO-d_6) δ ppm 0.87 (br. s., 2 H) 1.02 - 1.23 (m, 5 H) 1.30 - 1.53 (m, 4 H) 1.54 - 1.71 (m, 4 H) 1.74 - 1.87 (m, 2 H) 1.92 - 2.10 (m, 1 H) 2.65 - 2.79 (m, 1 H) 2.86 - 3.00 (m, 2 H) 3.02 - 3.17 (m, 2 H) 3.73 (q, *J*=7.08 Hz, 1 H) 3.85 - 4.02 (m, 2 H) 4.20 (d, *J*=7.57 Hz, 1 H) 4.68 - 4.78 (m, 1 H) 7.21 - 7.37 (m, 3 H) 7.42 - 7.51 (m, 1 H) 7.55 - 7.62 (m, 1 H) 7.69 (d, *J*=8.79 Hz, 1 H) 7.90 - 7.98 (m, 1 H). HRMS (ESI) calcd for $C_{24}H_{35}N_3O_8ClS_2Na$: [M-]: 615.1452. Found: 615.1459.

Sodium (2S)-2-((S)-3-cyclohexyl-2-(thiophene-2-sulfonamido)propanamido)-1-hydroxy-3-(2-oxopyrrolidin-3-yl)propane-1-sulfonate (7i). Yield (67%), mp 156-158 ^{0}C. ^{1}H NMR (400 MHz, DMSO-d_6) δ ppm 0.64 - 0.83 (m, 2 H) 0.92 - 1.13 (m, 4 H) 1.16 - 1.25 (m, 1 H) 1.28 - 1.38 (m, 1 H) 1.55 (d, *J*=11.38 Hz, 6 H) 1.70 - 1.95 (m, 2 H) 1.97 - 2.15 (m, 2 H) 2.97 - 3.19 (m, 2 H) 3.74 - 3.84 (m, 1 H) 3.84 - 3.94 (m, 1 H) 4.05 - 4.17 (m, 1 H) 5.31 (t, *J*=6.93 Hz, 1 H) 7.09 (t, *J*=4.00 Hz, 1 H) 7.45 (s, 1 H) 7.54 - 7.60 (m, 1 H) 7.73 (d,

J=8.93 Hz, 1 H) 7.82 - 7.87 (m, 1 H) 8.05 (br. s., 1 H). HRMS (ESI) calcd for $C_{20}H_{30}N_3O_8S_3Na$: [M-]: 599.1093. Found: 599.1094.

Sodium (2S)-2-((S)-2-([1,1'-biphenyl]-4-sulfonamido)-3-cyclohexylpropanamido)-1-hydroxy-3-(2-oxopyrrolidin-3-yl)propane-1-sulfonate (7j). Yield (59%), mp 154-156 ^{0}C. ^{1}H NMR (400 MHz, DMSO-d_6) δ ppm 0.66 (d, *J*=4.98 Hz, 1 H) 0.76 (d, *J*=10.64 Hz, 1 H) 0.87 (br. s., 1 H) 1.00 - 1.13 (m, 4 H) 1.16 - 1.24 (m, 1 H) 1.29 - 1.39 (m, 3 H) 1.41 - 1.62 (m, 6 H) 1.73 - 1.84 (m, 1 H) 1.89 - 2.05 (m, 1 H) 2.85 - 2.93 (m, 1 H) 2.97 - 3.09 (m, 1 H) 3.61 (dd, *J*=10.20, 3.37 Hz, 1 H) 3.71 - 3.83 (m, 1 H) 3.87 - 3.94 (m, 1 H) 5.31 (t, *J*=5.08 Hz, 1 H) 7.38 (d, *J*=3.81 Hz, 1 H) 7.42 - 7.47 (m, 2 H) 7.51 (d, *J*=2.05 Hz, 2 H) 7.58 - 7.66 (m, 1 H) 7.69 - 7.78 (m, 2 H) 7.80 - 7.90 (m, 2 H) 7.94 (d, *J*=7.42 Hz, 1 H). HRMS (ESI) calcd for $C_{28}H_{36}N_3O_8S_2Na$: [M-]: 629.1842. Found: 629.1844.

Sodium (2S)-2-((S)-3-cyclohexyl-2-((2-(1,3-dioxoisoindolin-2-yl)ethyl)sulfonamido) propanamido)-1-hydroxy-3-(2-oxopyrrolidin-3-yl)propane-1-sulfonate (7k). Yield (76%), mp 74-76 ^{0}C. ^{1}H NMR (400 MHz, DMSO-d_6) δ ppm 0.85 (br. s., 2 H) 0.99 - 1.27 (m, 5 H) 1.41 (br. s., 2 H) 1.53 - 1.74 (m, 6 H) 1.80 - 1.92 (m, 1 H) 2.05 - 2.31 (m, 2 H) 2.96 - 3.14 (m, 2 H) 3.54 - 3.65 (m, 1 H) 3.74 (q, *J*=7.13 Hz, 2 H) 3.94 (d, *J*=6.05 Hz, 3 H) 4.31 - 4.41 (m, 1 H) 6.03 - 6.15 (m, 1 H) 6.63 (dd, *J*=9.03, 2.10 Hz, 1 H) 7.43 - 7.55 (m, 2 H) 7.59 - 7.74 (m, 1 H) 7.83 - 7.94 (m, 2 H) 8.62 - 8.71 (m, 1 H). HRMS (ESI) calcd for $C_{26}H_{35}N_4O_{10}S_2Na$: [M-]: 650.1692. Found: 650.1693.

Sodium (2S)-2-((S)-3-cyclohexyl-2-((3-(4-methoxyphenoxy)propyl)sulfonamido)propanamido)-1-hydroxy-3-(2-oxopyrrolidin-3-yl)propane-1-sulfonate (7l). Yield (63%), mp 65-67 ^{0}C. ^{1}H NMR (400 MHz, DMSO-d_6) δ ppm 0.85 (d, *J*=10.74 Hz, 2 H) 1.02 - 1.30

(m, 3 H) 1.33 - 1.50 (m, 2 H) 1.52 - 1.69 (m, 6 H) 1.71 - 1.84 (m, 2 H) 1.88 - 2.22 (m, 5 H) 2.93 - 3.04 (m, 2 H) 3.05 - 3.17 (m, 2 H) 3.69 (s, 3 H) 3.80 (br. s., 1 H) 3.85 - 3.92 (m, 1 H) 3.95 - 4.07 (m, 2 H) 4.22 (br. s., 1 H) 5.47 (d, *J*=5.86 Hz, 1 H) 6.85 (s, 4 H) 7.37 - 7.51 (m, 1 H) 7.65 (d, *J*=8.98 Hz, 1 H) 7.94 (d, *J*=8.89 Hz, 1 H). HRMS (ESI) calcd for $C_{26}H_{40}N_3O_{10}S_2Na$: [M-]: 641.2053. Found: 641.2051.

Sodium (2S)-2-((S)-3-cyclohexyl-2-(octylsulfonamido)propanamido)-1-hydroxy-3-(2-oxopyrrolidin-3-yl)propane-1-sulfonate (7m). Yield (65%), mp 58-60 ^{0}C. ^{1}H NMR (400 MHz, DMSO-d_6) δ ppm 0.82 - 0.92 (m, 4 H) 1.04 - 1.19 (m, 2 H) 1.24 (br. s., 6 H) 1.36 - 1.50 (m, 2 H) 1.63 (d, *J*=11.42 Hz, 6 H) 1.77 (d, *J*=10.84 Hz, 2 H) 1.86 - 2.04 (m, 2 H) 2.05 - 2.14 (m, 3 H) 2.15 - 2.25 (m, 1 H) 2.83 - 2.96 (m, 2 H) 3.00 - 3.08 (m, 2 H) 3.14 (t, *J*=8.35 Hz, 2 H) 3.76 (d, *J*=8.30 Hz, 1 H) 3.85 (t, *J*=4.88 Hz, 2 H) 3.92 - 4.06 (m, 1 H) 4.22 (t, *J*=9.62 Hz, 1 H) 5.41 (d, *J*=5.86 Hz, 1 H) 7.21 - 7.29 (m, 1 H) 7.47 (d, *J*=5.47 Hz, 1 H) 7.62 (d, *J*=9.08 Hz, 1 H) 7.88 (d, *J*=8.98 Hz, 1 H). HRMS (ESI) calcd for $C_{24}H_{44}N_3O_8S_2Na$: [M-]: 589.2468. Found: 589.2466.

Synthesis of esters *9a-c*. General procedure. To a solution of the hydrochloride salt of ester **3** (10 mmol) in anhydrous THF (40 mL) kept at 0 ^{o}C was added slowly N,N-diisopropylethylamine (DIEA) (2.6 mL,20 mmol, 2 eq) with stirring. The appropriate chloroformate (11 mmol, 1.1 eq) was added to the solution and the reaction mixture was stirred for 16 h at room temperature. The solvent was removed and the residue was dissolved in ethyl acetate (100 mL) and washed with water (2 x 50 mL). The ethyl acetate layer was further washed with 5% HCl (2 x 50 mL) and saturated NaCl (50 mL). The organic layer was dried over anhydrous sodium sulfate, filtered and concentrated to yield a crude product which was purification by flash chromatography to yield esters ***9a-c***.

methyl (2S)-2-((S)-2-(((3-chlorophenethoxy)carbonyl)amino)-3-cyclohexylpropanamido)-3-(2-oxopyrrolidin-3-yl)propanoate (9a). Yield (73%), mp 43-45 ^{0}C. ^{1}H NMR (400 MHz, $CDCl_3$-*d*) δ ppm 0.84 - 1.02 (m, 2 H) 1.09 - 1.23 (m, 3 H) 1.38 (d, *J*=2.64 Hz, 1 H) 1.45 - 1.53 (m, 1 H) 1.69 (d, *J*=10.20 Hz, 6 H) 1.79 - 1.95 (m, 2 H) 2.12 - 2.22 (m, 1 H) 2.36 - 2.46 (m, 2 H) 2.87 - 2.94 (m, 2 H) 3.34 (d, *J*=6.88 Hz, 2 H) 3.73 (s, 3 H) 4.20 - 4.35 (m, 3 H) 4.48 (ddd, *J*=11.12, 7.07, 3.88 Hz, 1 H) 5.29 (d, *J*=8.25 Hz, 1 H) 6.18 (s, 1 H) 7.08 - 7.13 (m, 1 H) 7.19 - 7.26 (m, 3 H) 7.84 (d, *J*=5.52 Hz, 1 H). HRMS (ESI) calcd for $C_{26}H_{37}ClN_3O_6$: [M+H]: 522.2371 Found: 522.2372.

methyl (8S,11S)-8-(cyclohexylmethyl)-6,9-dioxo-11-((2-oxopyrrolidin-3-yl)methyl)-1-phenyl-2,5-dioxa-7,10-diazadodecan-12-oate (9b). Yield (67%), mp 59-61 ^{0}C. ^{1}H NMR (400 MHz, $CDCl_3$-*d*) δ ppm 0.86 - 1.03 (m, 2 H) 1.09 - 1.29 (m, 4 H) 1.34 - 1.44 (m, 2 H) 1.45 - 1.55 (m, 1 H) 1.60 - 1.73 (m, 5 H) 1.75 - 1.95 (m, 2 H) 2.10 - 2.22 (m, 1 H) 2.35 - 2.46 (m, 2 H) 3.30 (d, *J*=8.40 Hz, 2 H) 3.67 (q, *J*=4.65 Hz, 2 H) 3.72 (s, 3 H) 4.18 - 4.28 (m, 2 H) 4.32 (d, *J*=5.66 Hz, 1 H) 4.49 (ddd, *J*=11.05, 7.02, 3.95 Hz, 1 H) 4.56 (s, 2 H) 5.40 (d, *J*=8.30 Hz, 1 H) 6.11 (s, 1 H) 7.28 - 7.31 (m, 1 H) 7.34 (s, 4 H) 7.76 (d, *J*=6.83 Hz, 1 H). HRMS (ESI) calcd for $C_{27}H_{39}N_3O_7$: [M+H]: 518.2866 Found: 518.2874.

methyl (2S)-2-((S)-3-cyclohexyl-2-(((decyloxy)carbonyl)amino)propanamido)-3-(2-oxopyrrolidin-3-yl)propanoate (9c). Yield (60%), mp 67-68 ^{0}C. ^{1}H NMR (400 MHz, $CDCl_3$-*d*) δ ppm 0.88 (t, *J*=6.44 Hz, 4 H) 0.91 - 1.03 (m, 2 H) 1.10 - 1.21 (m, 2 H) 1.23 - 1.36 (m, 14 H) 1.37 - 1.44 (m, 1 H) 1.45 - 1.54 (m, 1 H) 1.57 - 1.66 (m, 2 H) 1.70 (d, *J*=8.59 Hz, 2 H) 1.78 - 1.98 (m, 5 H) 2.11 - 2.26 (m, 2 H) 2.37 - 2.48 (m, 2 H) 3.35 (d, *J*=7.81 Hz, 2 H) 3.73 (s, 3 H) 3.98 - 4.12 (m, 2 H) 4.33 (d, *J*=4.78 Hz, 1 H) 4.46 - 4.56 (m,

1 H) 5.21 (d, *J*=7.91 Hz, 1 H) 6.23 (s, 2 H) 7.77 (d, *J*=5.66 Hz, 1 H). HRMS (ESI) calcd for $C_{28}H_{49}N_3O_6$: [M+H]: 524.3700 Found: 524.3712.

Synthesis of alcohols 10a-c. General procedure. To a solution of ester **9** (5 mmol) in anhydrous THF (30 mL) was added dropwise lithium borohydride (2M in THF, 7.5 mL, 15 mmol), followed by absolute ethyl alcohol (15 mL), and the reaction mixture was stirred at room temperature overnight. The reaction mixture was acidified with 5% HCl and the pH adjusted to ~2. Removal of the solvent left a residue which was taken up in ethyl acetate (100 mL). The organic layer was washed with brine (25 mL), dried over anhydrous sodium sulfate, filtered, and concentrated to yield compounds **10a-c.**

3-chlorophenethyl ((2S)-3-cyclohexyl-1-(((2S)-1-hydroxy-3-(2-oxopyrrolidin-3-yl)propan-2-yl)amino)-1-oxopropan-2-yl)carbamate (10a). Yield (93%), mp 55-56 ^{0}C. ^{1}H NMR (400 MHz, $CDCl_3$-*d*) δ ppm 0.86 - 0.96 (m, 2 H) 1.18 (d, *J*=17.43 Hz, 3 H) 1.29 - 1.37 (m, 2 H) 1.39 - 1.52 (m, 1 H) 1.66 (br. s., 6 H) 1.76 - 1.88 (m, 2 H) 2.00 (br. s., 1 H) 2.34 - 2.49 (m, 2 H) 2.84 - 2.94 (m, 2 H) 3.33 (d, *J*=8.18 Hz, 2 H) 3.61 (d, *J*=15.55 Hz, 2 H) 3.94 - 4.02 (m, 1 H) 4.19 - 4.31 (m, 3 H) 5.36 (d, *J*=7.23 Hz, 1 H) 6.20 (s, 1 H) 7.10 (d, *J*=6.47 Hz, 1 H) 7.17 - 7.25 (m, 3 H) 7.77 (d, *J*=7.80 Hz, 1 H). HRMS (ESI) calcd for $C_{25}H_{36}ClN_3O_5$: [M+H]: 494.2422 Found: 494.2412.

2-(benzyloxy)ethyl ((2S)-3-cyclohexyl-1-(((2S)-1-hydroxy-3-(2-oxopyrrolidin-3-yl) propan-2-yl)amino)-1-oxopropan-2-yl)carbamate (10b). Yield (97%), mp 68-69 ^{0}C. ^{1}H NMR (400 MHz, $CDCl_3$-*d*) δ ppm 0.83 - 1.04 (m, 2 H) 1.11 - 1.24 (m, 3 H) 1.31 - 1.41 (m, 1 H) 1.51 (dd, *J*=8.59, 5.27 Hz, 2 H) 1.68 (d, *J*=9.28 Hz, 6 H) 1.80 (d, *J*=8.79 Hz, 2 H) 2.02 (br. s., 1 H) 2.33 - 2.46 (m, 2 H) 3.23 - 3.34 (m, 2 H) 3.55 - 3.61 (m, 3 H) 3.66 (s, 2 H) 3.94 - 4.05 (m, 1 H) 4.24 (s, 2 H) 4.55 (s, 2 H) 5.59 (d, *J*=5.66 Hz, 1 H) 6.33 (s, 1 H)

7.28 - 7.41 (m, 5 H) 7.64 (d, *J*=6.44 Hz, 1 H). HRMS (ESI) calcd for $C_{26}H_{39}N_3O_6$: [M+H]: 490.2917 Found: 490.2907.

decyl ((2S)-3-cyclohexyl-1-(((2S)-1-hydroxy-3-(2-oxopyrrolidin-3-yl)propan-2-yl) amino)-1-oxopropan-2-yl)carbamate (10c). Yield (97%), mp 78-80 ^{0}C. ^{1}H NMR (400 MHz, $CDCl_3$-*d*) δ ppm 0.88 (t, *J*=6.20 Hz, 3 H) 0.96 (d, *J*=10.94 Hz, 2 H) 1.09 - 1.19 (m, 3 H) 1.20 - 1.34 (m, 14 H) 1.51 (d, *J*=7.42 Hz, 1 H) 1.58 - 1.73 (m, 10 H) 1.80 (d, *J*=10.15 Hz, 2 H) 2.03 (br. s., 1 H) 2.36 - 2.55 (m, 2 H) 3.30 - 3.41 (m, 2 H) 3.63 (s, 3 H) 4.04 (t, *J*=7.00 Hz, 2 H) 4.19 - 4.28 (m, 1 H) 5.34 (d, *J*=7.80 Hz, 1 H) 6.45 (s, 1 H) 7.67 (d, *J*=5.60 Hz, 1 H). HRMS (ESI) calcd for $C_{27}H_{49}N_3O_5$: [M+H]: 496.3750 Found: 496.3745.

Synthesis of aldehydes 11a-c. General procedure. Compound **10** (5 mmol) was dissolved in anhydrous dichloromethane (50 mL) under a nitrogen atmosphere and cooled to 0^{o}C. Dess-Martin periodinane reagent (3.18 g, 7.5 mmol, 1.5 eq) was added to the reaction mixture with stirring. The ice bath was removed and the reaction mixture was stirred at room temperature for 3 h (monitoring by TLC indicated complete disappearance of the starting material). A solution of 10% aqueous sodium thiosulfate (20 mL) was added and the solution was stirred for another 15 minutes. The aqueous layer was removed and the organic layer was washed with 10% aqueous sodium thiosulfate (20 mL), followed by saturated aqueous sodium bicarbonate (2 x 20 mL), water (2 x 20 mL) and brine (20 mL). The organic layer was dried over anhydrous sodium sulfate, filtered and concentrated. The yellow residue was purified by flash chromatography (silica gel/methylene chloride/ethyl acetate/methanol) to yield aldehydes ***11a-c***.

3-chlorophenethyl ((2S)-3-cyclohexyl-1-oxo-1-(((2S)-1-oxo-3-(2-oxopyrrolidin-3-yl) propan-2-yl)amino)propan-2-yl)carbamate (11a). Yield (76%), mp 45-47 ^{0}C. ^{1}H NMR

(400 MHz, $CDCl_3$-*d*) δ ppm 0.86 - 1.01 (m, 2 H) 1.10 - 1.27 (m, 2 H) 1.30 - 1.45 (m, 2 H) 1.47 - 1.58 (m, 1 H) 1.60 - 1.89 (m, 6 H) 1.92 - 2.00 (m, 2 H) 2.01 - 2.10 (m, 1 H) 2.36 - 2.51 (m, 2 H) 2.91 (t, *J*=6.69 Hz, 2 H) 3.31 - 3.43 (m, 2 H) 4.16 - 4.37 (m, 4 H) 5.25 (d, *J*=8.20 Hz, 1 H) 5.96 (br. s., 1 H) 7.10 (d, *J*=6.35 Hz, 1 H) 7.17 - 7.25 (m, 3 H) 8.36 (d, *J*=5.57 Hz, 1 H) 9.49 (s, 1 H). HRMS (ESI) calcd for $C_{25}H_{34}ClN_3O_5$: [M-]: 491.2187. Found: 491.2198.

2-(benzyloxy)ethyl ((2S)-3-cyclohexyl-1-oxo-1-(((2S)-1-oxo-3-(2-oxopyrrolidin-3-yl) propan-2-yl)amino)propan-2-yl)carbamate (11b). Yield (78%), mp 38-40 ^{0}C. ^{1}H NMR (400 MHz, $CDCl_3$-*d*) δ ppm 0.84 - 1.04 (m, 2 H) 1.11 - 1.30 (m, 2 H) 1.39 (d, *J*=3.22 Hz, 1 H) 1.48 - 1.57 (m, 1 H) 1.71 (dd, *J*=13.57, 8.69 Hz, 6 H) 1.78 - 1.88 (m, 2 H) 1.93 - 1.98 (m, 1 H) 2.01 - 2.09 (m, 1 H) 2.32 - 2.52 (m, 2 H) 3.25 - 3.36 (m, 2 H) 3.67 (t, *J*=4.54 Hz, 4 H) 4.25 (d, *J*=2.93 Hz, 1 H) 4.30 - 4.39 (m, 1 H) 4.51 - 4.62 (m, 2 H) 5.37 (d, *J*=8.01 Hz, 1 H) 5.99 (br s, 1 H) 7.34 (s, 5 H) 8.24 (d, *J*=4.88 Hz, 1 H) 9.49 (s, 1 H). HRMS (ESI) calcd for $C_{26}H_{37}N_3O_6$: [M-]: 487.2682. Found: 487.2683.

Decyl ((2S)-3-cyclohexyl-1-oxo-1-(((2S)-1-oxo-3-(2-oxopyrrolidin-3-yl)propan-2-yl)amino) propan-2-yl)carbamate (11c). Yield (71%), sticky solid. ^{1}H NMR (400 MHz, $CDCl_3$-*d*) δ ppm 0.88 (t, *J*=6.71 Hz, 2 H) 0.91 - 1.01 (m, 2 H) 1.07 - 1.36 (m, 16 H) 1.49 - 1.64 (m, 4 H) 1.69 (d, *J*=5.71 Hz, 6 H) 1.77 - 1.90 (m, 2 H) 1.91 - 1.99 (m, 1 H) 2.02 - 2.14 (m, 1 H) 2.27 - 2.58 (m, 3 H) 3.31 - 3.42 (m, 2 H) 3.94 - 4.12 (m, 2 H) 4.28 - 4.39 (m, 1 H) 4.41 - 4.53 (m, 1 H) 5.20 - 5.27 (m, 1 H) 6.16 - 6.24 (m, 1 H) 8.21 - 8.28 (m, 1 H) 9.57 (s, 1 H). HRMS (ESI) calcd for $C_{27}H_{47}N_3O_5$: [M-]: 493.3516. Found: 493.3518.

Synthesis of bisulfite adducts 12a-c*.* General procedure. To a solution of aldehyde **11** (5 mmol) in dry ethyl acetate (20 mL) was added absolute ethanol (12 mL) with stirring, followed by a solution of sodium bisulfite (540 mg; 5 mmol) in water (5 mL). The reaction

mixture was stirred for 3 h at 50 ^{0}C. The reaction mixture was allowed to cool to room temperature and then vacuum filtered. The solid was thoroughly washed with absolute ethanol and the filtrate was dried over anhydrous sodium sulfate, filtered, and concentrated to yield a yellowish oil. The oily product was treated with ethyl ether (2 x 50 mL) to form white solid. The white solid was stirred with ethyl ether (30 mL) and ethyl acetate (15 mL) for 5 minutes. Careful removal of the solvent using a pipette yielded compounds ***12a-c*.**

Sodium (2S)-2-((S)-2-(((3-chlorophenethoxy)carbonyl)amino)-3-cyclohexylpropanamido)-1-hydroxy-3-(2-oxopyrrolidin-3-yl)propane-1-sulfonate (12a). Yield (68%), mp 76-78 ^{0}C. ^{1}H NMR (400 MHz, DMSO-d_6) δ ppm 0.76 - 0.92 (m, 2 H) 1.02 - 1.17 (m, 3 H) 1.25 (d, *J*=13.38 Hz, 1 H) 1.40 (d, *J*=4.69 Hz, 2 H) 1.51 - 1.75 (m, 6 H) 1.80 - 2.02 (m, 1 H) 2.03 - 2.23 (m, 2 H) 2.87 (d, *J*=3.81 Hz, 2 H) 2.99 - 3.08 (m, 1 H) 3.08 - 3.20 (m, 1 H) 3.69 - 3.87 (m, 2 H) 3.88 - 4.04 (m, 1 H) 4.14 (d, *J*=6.54 Hz, 3 H) 5.43 - 5.48 (m, 1 H) 7.19 - 7.38 (m, 4 H) 7.47 (br s, 1 H) 7.55 (dd, *J*=14.94, 9.08 Hz, 2 H). HRMS (ESI) calcd for $C_{25}H_{35}ClN_3O_8SNa$: [M-]: 595.1731. Found: 595.1733.

Sodium (8S,11S)-8-(cyclohexylmethyl)-12-hydroxy-6,9-dioxo-11-((2-oxopyrrolidin-3-yl)methyl)-1-phenyl-2,5-dioxa-7,10-diazadodecane-12-sulfonate (12b). Yield (73%), mp 47-50 ^{0}C. ^{1}H NMR (400 MHz, DMSO-d_6) δ ppm 0.78 - 0.94 (m, 2 H) 1.01 - 1.22 (m, 4 H) 1.32 (br s, 1 H) 1.39 - 1.51 (m, 2 H) 1.53 - 1.72 (m, 6 H) 1.86 - 1.94 (m, 1 H) 2.00 - 2.34 (m, 2 H) 2.99 - 3.18 (m, 2 H) 3.60 (d, *J*=3.71 Hz, 4 H) 3.75 (q, *J*=7.13 Hz, 1 H) 4.00 - 4.22 (m, 2 H) 4.50 (s, 2 H) 7.25 - 7.38 (m, 5 H) 7.43 (d, *J*=7.13 Hz, 1 H) 7.54 (br s, 1 H) 7.64 (br s, 1 H) 8.47 (d, *J*=7.03 Hz, 1 H). HRMS (ESI) calcd for $C_{26}H_{38}N_3O_9SNa$: [M-]: 591.2226. Found: 591.2227.

sodium (2S)-2-((S)-3-cyclohexyl-2-(((decyloxy)carbonyl)amino)propanamido)-1-hydroxy-3-(2-oxopyrrolidin-3-yl)propane-1-sulfonate (12c). Yield (67%), mp 53-55 ^{0}C. ^{1}H NMR (400 MHz, DMSO-d_6) δ ppm 0.86 (t, J=6.13 Hz, 2 H) 1.07 - 1.14 (m, 2 H) 1.25 (br s, 16 H) 1.39 (d, J=19.72 Hz, 2 H) 1.52 (br s, 5 H) 1.62 (br. s., 6 H) 1.87 - 2.02 (m, 2 H) 2.12 (d, J=7.23 Hz, 2 H) 3.01 - 3.20 (m, 2 H) 3.82 - 4.00 (m, 2 H) 4.05 (br. s., 1 H) 4.17 - 4.29 (m, 1 H) 5.29 - 5.36 (m, 1 H) 5.73 - 5.78 (m, 1 H) 7.14 - 7.19 (m, 1 H) 7.47 (d, J=9.15 Hz, 1 H) 7.58 (s, 1 H). HRMS (ESI) calcd for $C_{27}H_{48}N_3O_7SNa$: [M-]: 597.3060. Found: 597.3063.

3.3.2 FRET Protease Assays

These were carried out as described on page 68.

3.3.3 Cell-Based Inhibition Assays

These were carried out as described on page 69.

3.3.4 Nonspecific Cytotoxicity Effects

The toxic dose for 50% cell death (TD_{50}) for each compound was determined for HG23 cells used in this study. Confluent cells grown in 96-well plates were treated with various concentrations (1 to 500 μM) of each compound for 72 h. Cell cytotoxicity was measured by a CytoTox 96 nonradioactive cytotoxicity assay kit (Promega, Madison, WI) and crystal violet staining. The in vitro therapeutic index was calculated by dividing the TD_{50} by the EC_{50}.

3.3.5 X-ray Crystallographic Studies. Crystallization and Data Collection

Purified norovirus 3CL Protease (NV 3CLpro) in 100 mM NaCl, 20 mM Tris pH 8.0 (11 mg/mL) was used for preparation of the inhibitor complexes. Stock solutions (100 mM) of each inhibitor were prepared in DMSO and added to NV 3CLpro by mixing 7 μL of the inhibitor (3 mM) with 243 μL (0.5 mM) of NV 3CLpro and incubating on ice for 1 hour. All crystallization experiments were conducted Compact Jr. (Rigaku Reagents) sitting drop vapor diffusion plates at 20 ^{o}C using equal volumes of protein and crystallization solution equilibrated against 75 μL of the latter. Hexagonal NV 3CLpro:***6l*** (h) and orthorhombic crystals NV 3CLpro:***6l*** (o) were obtained for the NV 3CLpro:***6l*** complex in 2-3 days from the Index HT screen (Hampton Research) condition G5 (25% (w/v) PEG 3350, 100 mM Tris pH 8.5, 200 mM lithium sulfate) and Wizard 3-4 screen

(Rigaku Reagents) condition A10 (20% (w/v) PEG 3350, 200 mM sodium thiocyanate) respectively. Crystals of the complex with inhibitor ***6m*** (NV 3CLpro**:6m**) were also obtained from the Index HT G5 condition. Samples were transferred to a fresh drop composed of 80% crystallization solution and 20% (v/v) PEG 200 and stored in liquid nitrogen. X-ray diffraction data were collected at the Advanced Photon Source beamline 17-ID using a Dectris Pilatus 6M pixel array detector.

3.3.6 Structure Solution and Refinement

Intensities were integrated using XDS[141-142] via Autoproc[161] and the Laue class analysis and data scaling were performed with Aimless.[143] Structure solution was conducted by molecular replacement with Phaser[145] using a previously determined structure of inhibitor bound to NV 3CLpro (PDB: 3UR9)[140] as the search model. Each crystal form contained two molecules in the asymmetric unit. Structure refinement and manual model building were conducted with Phenix[146] and Coot,[147] respectively. Disordered side chains were truncated to the point for which electron density could be observed. Structure validation was conducted with Molprobity[148] and figures were prepared using the CCP4MG package.[149] Structure superposition was conducted with GESAMT.[162]

3.4 Results and Discussion

The inhibitory activity of the synthesized compounds against NV 3CLpro and their anti-norovirus activity in a cell-based replicon system, were evaluated as described in the experimental section.[140] The determined IC_{50}, EC_{50} and CC_{50} values are listed in Tables 3.1 and 3.2 and they are the average of at least two determinations.

Inspection of the results in Table 3.1 permit the following inferences to be drawn: (a) the potency of the aldehyde bisulfite adducts is comparable to those of the precursor aldehydes, an observation noted previously.[151c,158] Advantages accrued through the use of aldehyde bisulfite adducts include higher solubility and metabolic stability, as well as low cytotoxicity.[160] Whether the bisulfite adducts exert their action by functioning as transition state mimics or latent precursors of the aldehyde functionality, or both, has not been established as yet and is currently under investigation; (b) a significant increase in potency (15-fold) was observed when the phenyl ring is moved further into the S_4 pocket (Table 3.1, compare the EC_{50} values of compounds ***7a, 7b*** and ***7c***) and an additional 4-fold gain in potency was realized by extending the linker further (Table 3.1, compound ***7l***).

TABLE 3.1 ACTIVITY OF COMPOUNDS ***6A-M*** AND ***7A-M*** AGAINST NV 3CL PROTEASE AND NOROVIRUS IN CELL-BASED REPLICON CELLS

Compound	R	IC_{50} (μM)	EC_{50} (μM)	CC_{50} (μM)
6a	C_6H_5	8.5	9.5	> 100
7a		13.5	12.3	> 100
6b	(C_6H_5) CH_2	4.5	4.1	> 100
7b		4.3	4.3	> 100
6c	(C_6H_5) CH_2CH_2	1.8	0.7	> 100
7c		2.1	0.8	> 100
6d	*p*-F (C_6H_4)	4.8	2	> 100
7d		6.2	2.1	> 100
6e	*m*-Cl (C_6H_4)	5.5	2.3	> 100
7e		5.7	1.9	> 100
6f	*p*-Cl (C_6H_4)	5.8	3.5	> 100
7f		5.1	7.2	> 100
6g	*p*-Cl (C_6H_4) CH_2	1.8	2.4	> 100
7g		1.2	2.2	> 100
6h	*m*-Cl (C_6H_5) CH_2CH_2	2.3	1.1	> 100
7h		1.9	0.8	> 100
6i	2-Thiophene	10.4	8.5	> 100
7i		8.5	8.1	> 100
6j	Biphenyl-4-	1.3	1.3	> 100
7j		1.1	1.2	> 100
6k	2-Phthalimidoethane	2.5	2.3	> 100
7k		2.6	2.1	> 100
6l	p-$CH_3O(C_6H_4)O(CH_2)_3$	1.8	0.5	> 100
7l		1.6	0.3	> 100
6m	$CH_3(CH_2)_7$	1.2	0.3	33.8
7m		1.1	0.2	35.4

TABLE 3.2 ACTIVITY OF COMPOUNDS ***11A-C*** AND ***12A-C*** AGAINST NV 3CL PROTEASE AND NOROVIRUS IN CELL-BASED REPLICON CELLS

Compound	R	IC_{50} (μM)	EC_{50} (μM)	CC_{50}
11a	*m-Cl* $(C_6H_4)CH_2CH_2$	0.6	0.1	43.2
12a		0.5	0.1	46.7
11b	$(C_6H_5)CH_2O(CH_2)_2$	2.1	0.2	> 100
12b		1.6	0.3	> 100
11c	CH_3 $(CH_2)_9$	0.3	0.1	32.1
12c		0.4	0.2	34.5

These observations are congruent with the results of X-ray crystallographic studies with inhibitor ***7l*** (Table 3.3). Crystallization of NV 3CLpro with inhibitor ***7l*** yielded hexagonal and orthorhombic crystals and the electron density clearly shows the sulfur atom of the active site Cys139 residue bound covalently to the carbonyl carbon of the P_1 residue of inhibitor ***7l***, thereby establishing the mechanism of action of this class of inhibitors (Figure 3.1). The electrostatic surface representation shows the aryl ring to be optimally nestled in the hydrophobic S_4 pocket of the enzyme and engaged in hydrophobic interactions with Ile109, Val168, Ala160 and Ala159 (Figure 3.2). Inhibitor ***7l*** is bound to the active site of the enzyme via a network of hydrogen bonds in the manner of an antiparallel β-sheet and includes inhibitor backbone H-bonds with Gln110 and Ala158 which serve to position and orient the inhibitor correctly with respect to the catalytic residues (Figures 3.3 and 3.4).

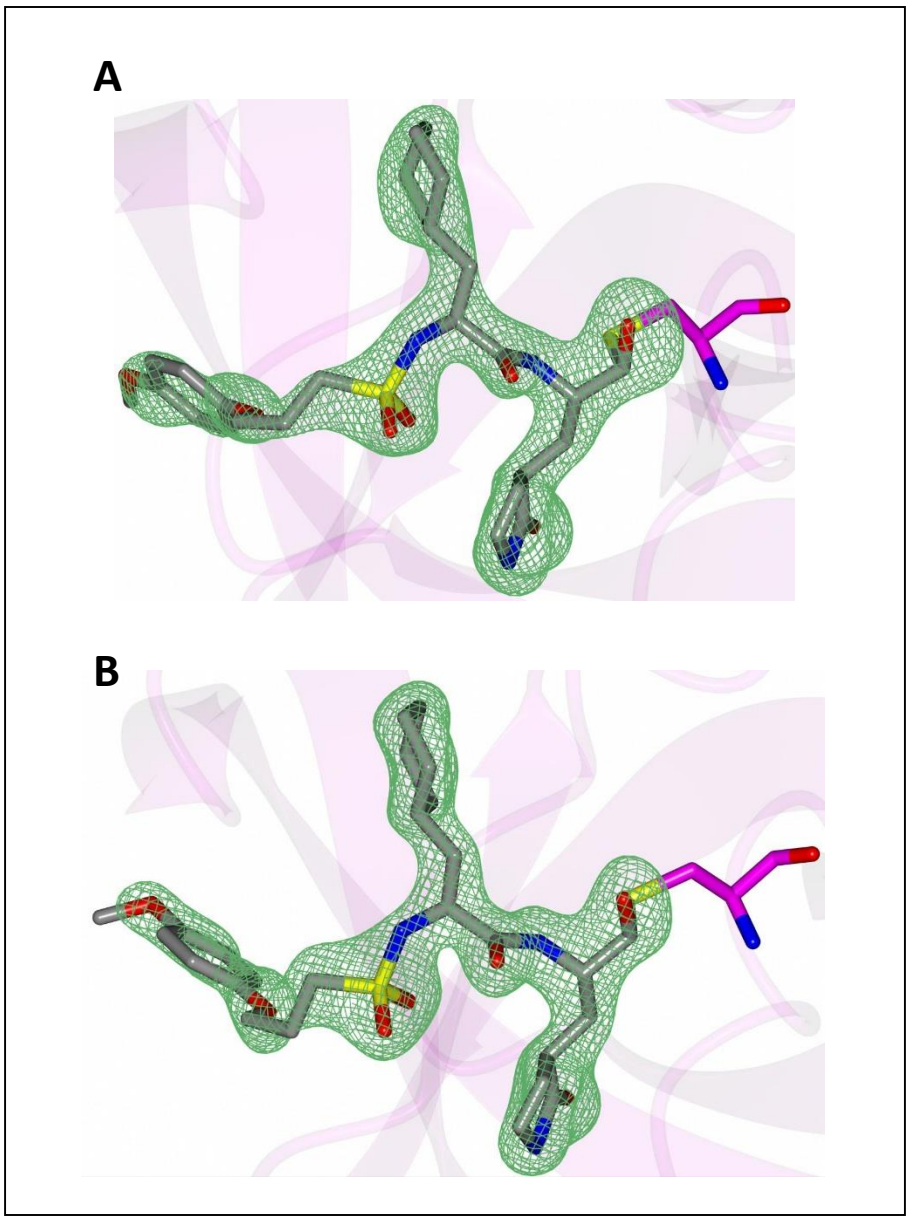

Figure 3.1 Fo-Fc omit map of inhibitor ***7l*** (green mesh) contoured at 3σ for (**A**) NV 3CLpro:***7l*** (hexagonal) and **B**) NV 3CLpro:***7l*** (orthorhombic).

Additionally, a H-bond with His30 serves to stabilize the tetrahedral adduct and two critical H-bonds involving the P_1 Gln surrogate ring oxygen with His157 and Thr134 are clearly evident; (c) halogen substitutions in the aromatic ring were generally beneficial (Table 3.1, compounds ***6d/7d, 6e/7e*** and ***6g/7g***); (d) potency also improved when a 4-

biphenyl or 2-pthalimidoethane moiety was used (Table 3.1, compounds ***6j/7j*** and ***6k/7k***); (e) the significance of hydrophobic interactions involving R and the S_4 subsite was further probed by using an n-octyl chain cap, resulting in inhibitors displaying submicromolar ED_{50} values (Table 3.1, compounds ***6m/7m).*** The structural determinants accounting for the higher potency of compounds ***6m/7m*** were identified by obtaining a high resolution X-ray crystal structure of the NV 3CLpro:***7m*** complex (Figure 3.5) (Table 3.3).

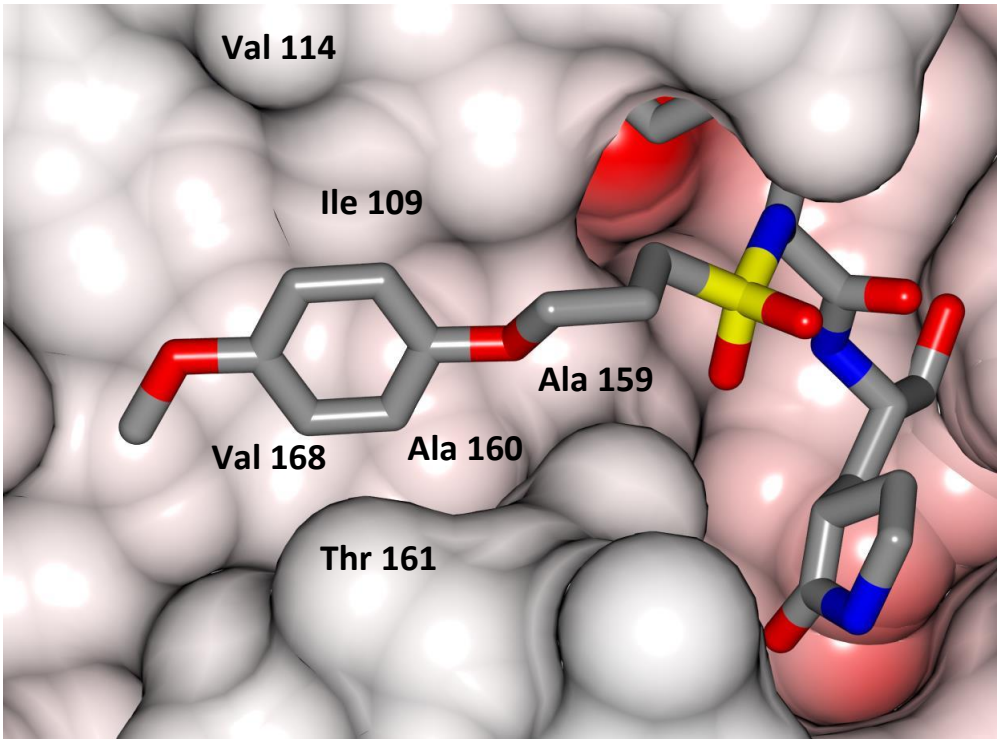

Figure 3.2 Electrostatic surface representation of NV 3CLpro showing the aryl ring region of inhibitor ***7l*** positioned in the hydrophobic S_4 pocket.

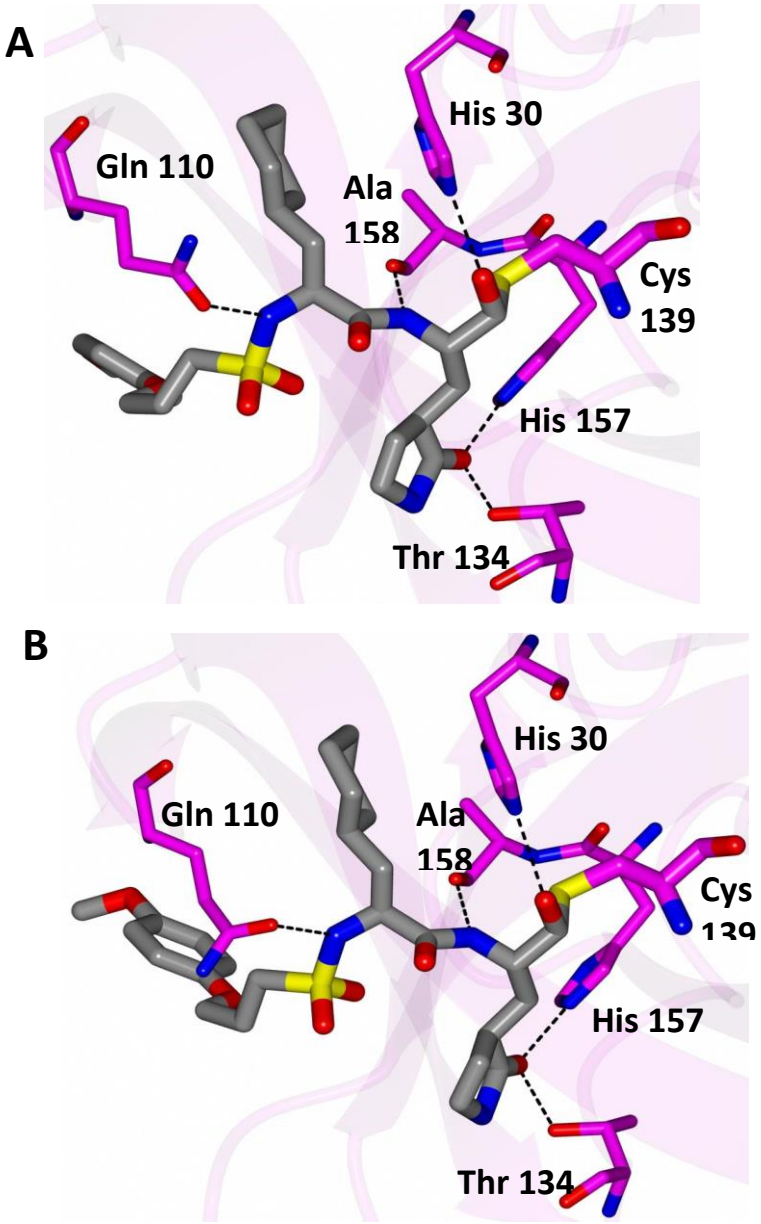

Figure 3.3 Hydrogen bond interactions (dashed lines) for (**A**) NV 3CLpro:***7l*** (hexagonal) and **B**) NV 3CLpro:***7l*** (orthorhombic).

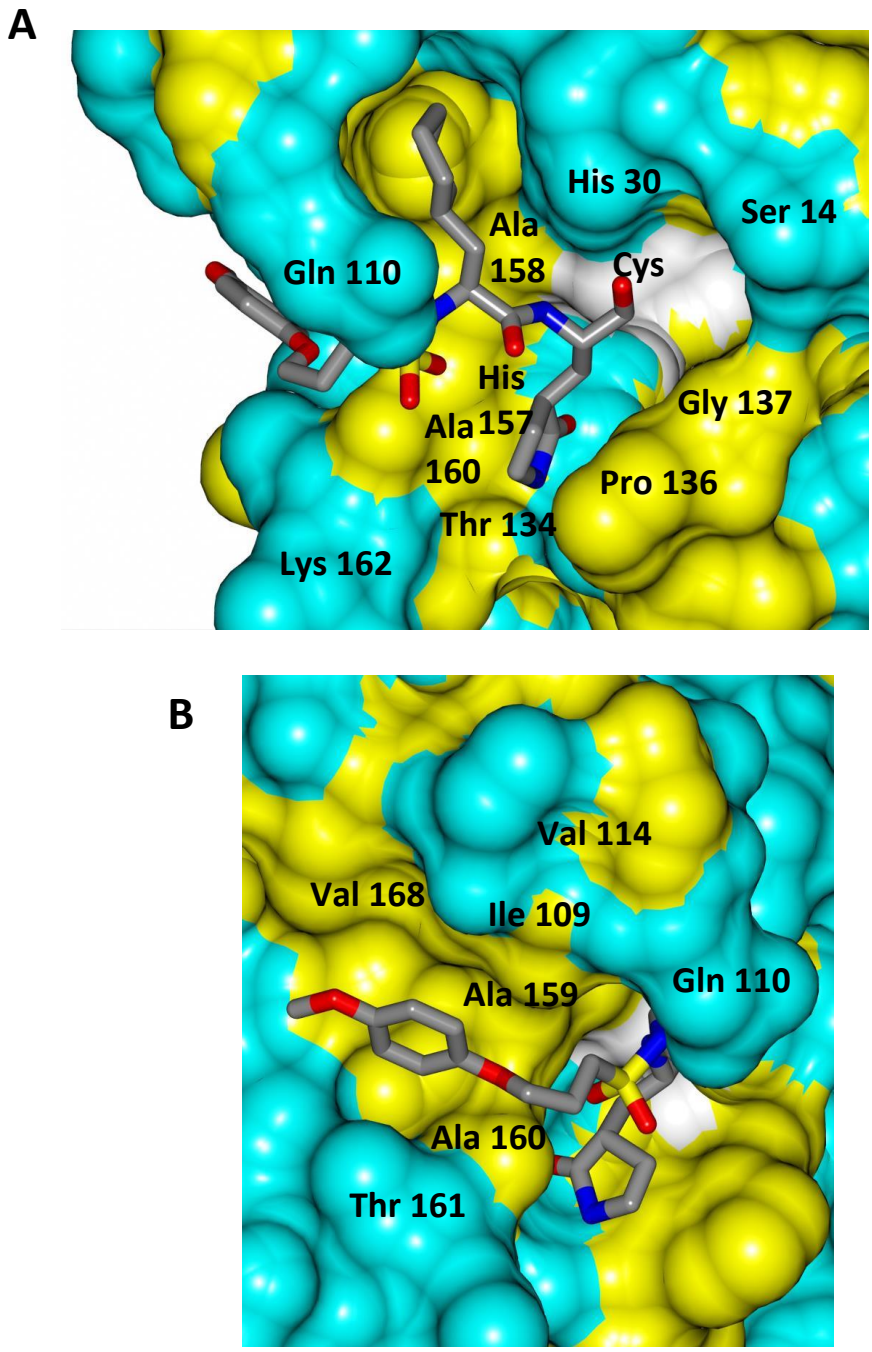

Figure 3.4 Surface representation of NV 3CLpro:***7l*** (hexagonal) with neighboring residues colored yellow (nonpolar), cyan (polar), and white (weakly polar). **A**) View of the inhibitor in the S_1/S_2 pocket and **B**) the S_4 pocket.

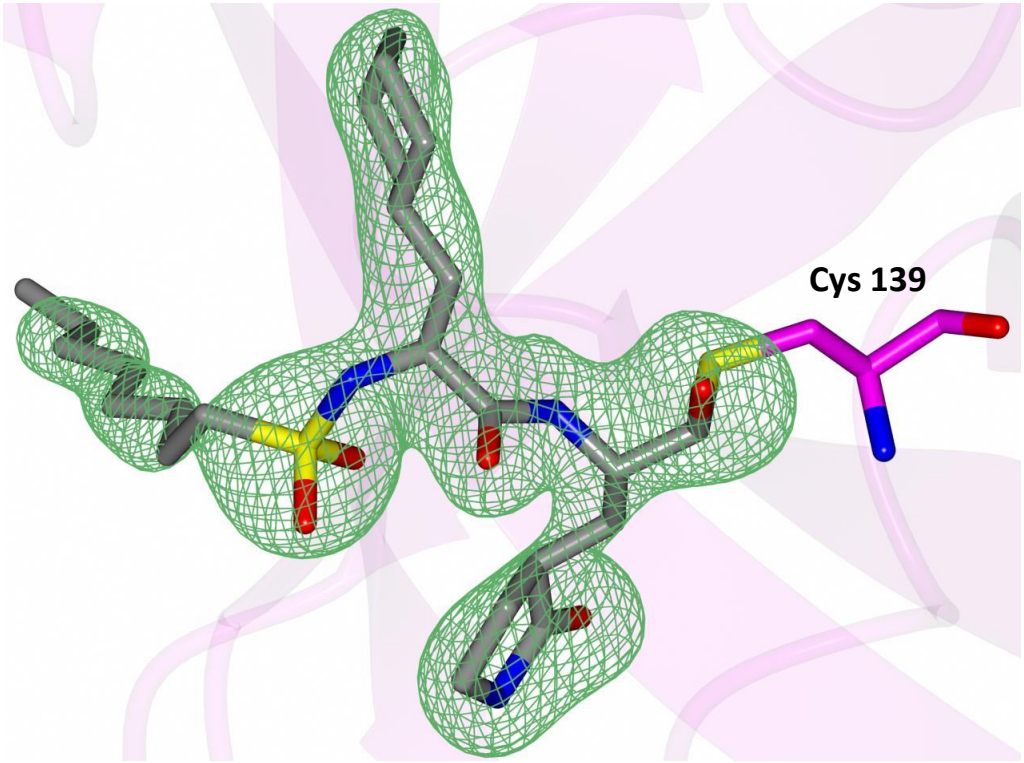

Figure 3.5 Fo-Fc omit map of inhibitor ***7m*** (green mesh) contoured at 3σ

Inhibitor ***7m*** adopts a binding mode in the active site similar to ***7l*** (Figure 3.6) which is clearly evident from the superposition of the two inhibitors in the active site of the enzyme (Figure 3.7). Furthermore, inhibitor ***7m*** engages in identical H-bond interactions as inhibitor ***7l*** (Figure 3.8), hence the comparable potencies. Importantly, the n-octyl chain encompasses the S_4 subsite and participates in hydrophobic interactions with the string of hydrophobic amino acids that make up the S_4 pocket (Figure 3.9).

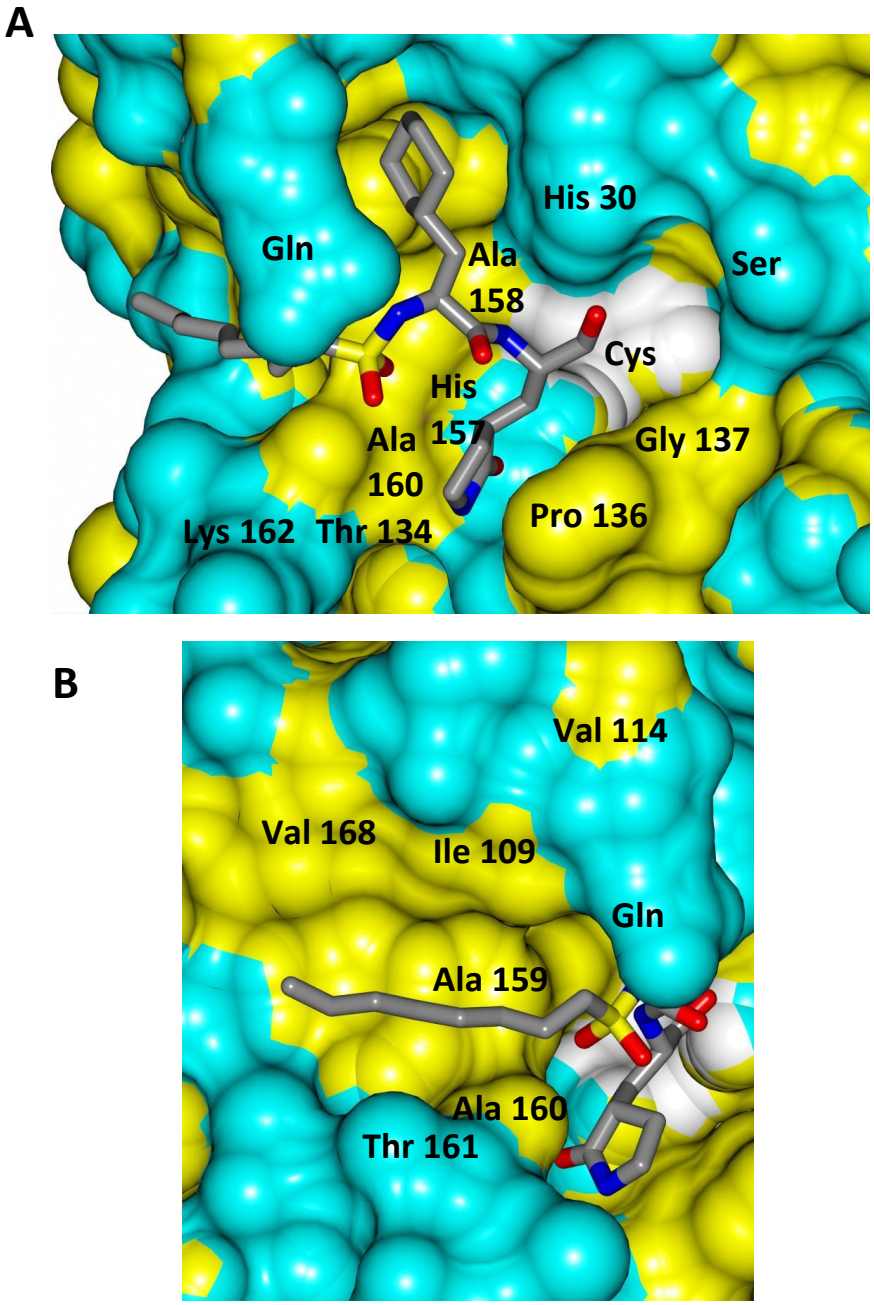

Figure 3.6 Surface representation of NV 3CLpro:***7m*** with neighboring residues colored yellow (nonpolar), cyan (polar), and white (weakly polar). **A**) View of the inhibitor in the S_1/S_2 pocket and **B**) the S_4 pocket.

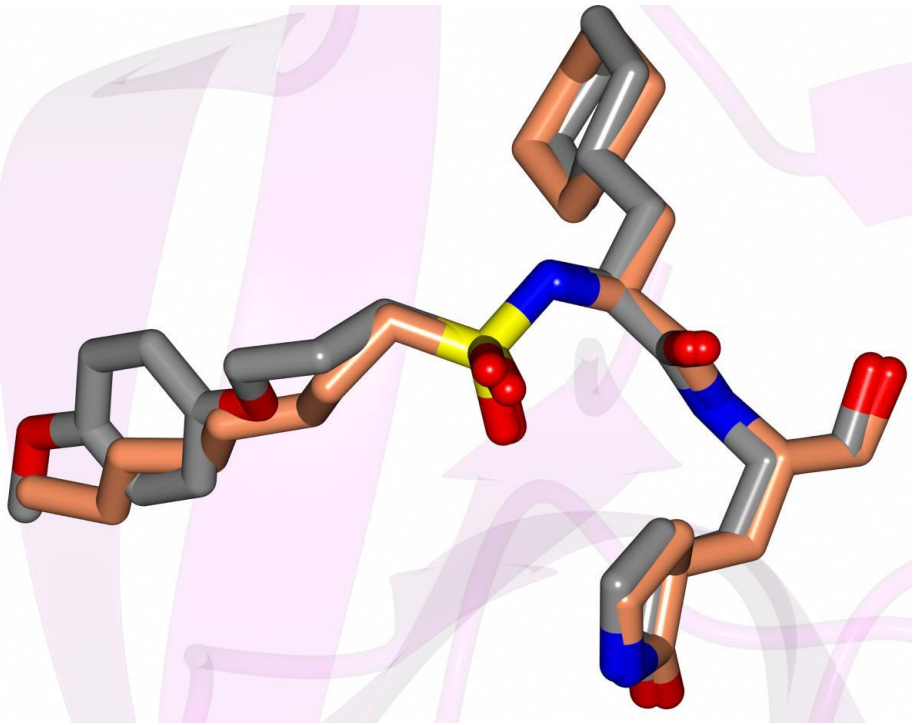

Figure 3.7 Superposition of inhibitor ***7l*** (gray) and ***7m*** (coral) which adopt similar binding modes in the NV 3CLpro active site

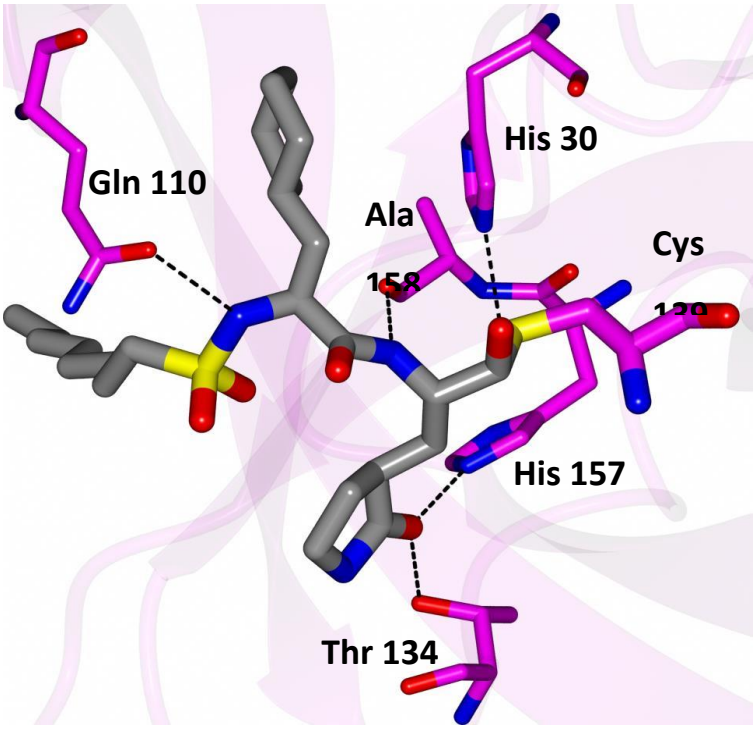

Figure 3.8 Hydrogen bond interactions (dashed lines) for NV 3CLpro:***7m***

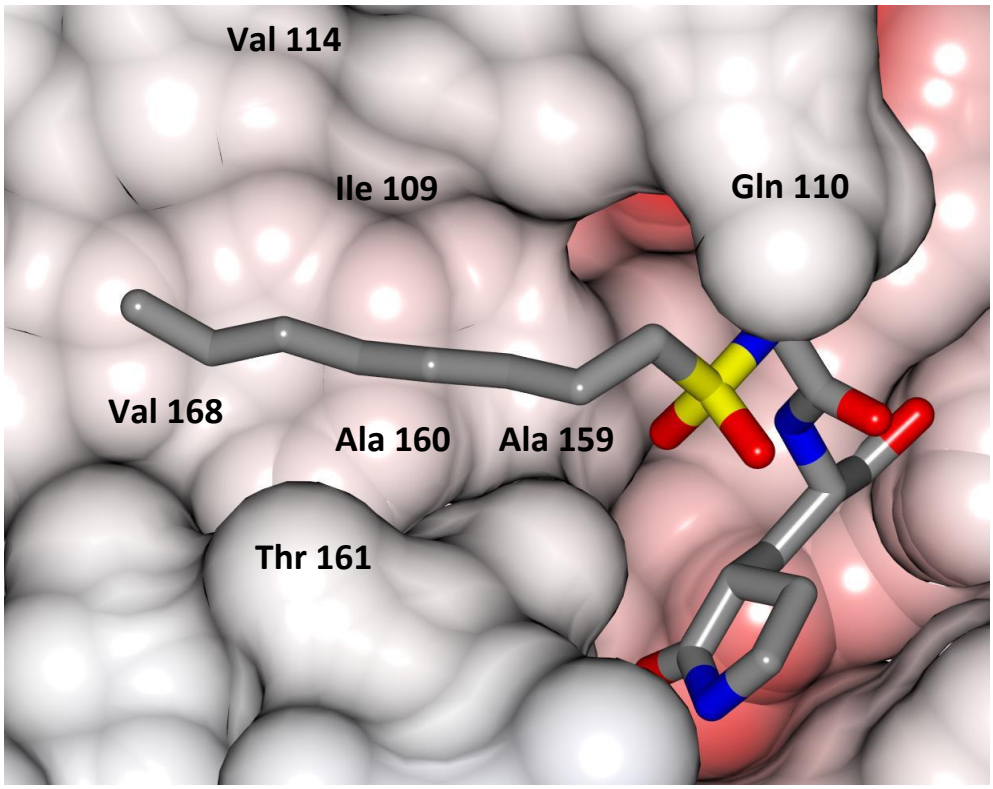

Figure 3.9 Electrostatic surface representation of NV 3CLpro showing the aliphatic chain of inhibitor ***7m*** positioned in a hydrophobic S_4 pocket

The importance of hydrophobic interactions is similarly evident in carbamate derivatives ***11c/12c*** (Table 3.2); and, (f) an eight to ten-fold increase in potency was realized when the sulfonamide linkage was replaced by a carbamate moiety (Table 3.2, compounds ***11a/12a*** versus compounds ***6h/7h*** in Table 3.1).

TABLE 3.3 CRYSTALLOGRAPHIC DATA FOR NV 3CL PROTEASE-INHIBITOR STRUCTURES

	NV 3CLpro:7l (h)	NV 3CLpro:7l (o)	NV 3CLPro:7m
Data Collection			
Unit-cell parameters (Å, °)	*a*=*b*=59.53, *c*=356.80	*a*=37.51, *b*=64.80, *c*=125.37	*a*=*b*=59.58, *c*=357.70
Space group	$P6_122$	$P2_12_12_1$	$P6_122$
Resolution (Å)[1]	49.53-2.10 (2.16-2.10)	45.05-1.90 (1.94-1.90)	49.57-2.45 (2.55-2.45)
Wavelength (Å)	1.0000	1.0000	1.0000
Temperature (K)	100	100	100
Observed reflections	434,656	158,261	276,664
Unique reflections	23,382	24,911	15,076
$<I/\sigma(I)>$[1]	13.4 (1.9)	13.7 (2.1)	13.2 (1.9)
Completeness (%)[1]	100 (99.9)	99.9 (100)	100 (100)
Multiplicity[1]	18.6 (18.9)	6.4 (5.8)	18.4 (19.5)
R_{merge} (%)[1, 2]	20.7 (186.3)	9.9 (92.6)	25.1 (197.3)
R_{meas} (%)[1, 4]	21.3 (191.5)	10.7 (101.8)	25.8 (202.6)
R_{pim} (%)[1, 4]	4.9 (43.8)	4.2 (41.6)	6.0 (45.5)
$CC_{1/2}$ [1, 5]	0.998 (0.897)	0.999 (0.834)	0.997 (0.714)
Refinement			
Resolution (Å) [1]	47.30-2.10	35.94-1.90	49.57-2.45
Reflections (working/test)[1]	22,094/1,115	23,626/1,210	14,228/727
R_{factor} / R_{free} (%)[1,3]	19.3/24.3	19.4/24.9	18.8/26.1
No. of atoms (Protein/Ligand/Water)	2,440/74/108	2,400/63/104	2,473/63/74
Model Quality			
R.m.s deviations			
Bond lengths (Å)	0.010	0.010	0.008
Bond angles (°)	1.040	1.031	0.924
Average *B*-factor (Å^2)			

TABLE 3.3 (continued)

All Atoms	32.6	35.4	38.1
Protein	32.3	35.3	38.1
Ligand	35.5	38.3	36.7
Water	38.2	37.2	39.7
Coordinate error(maximum likelihood) (Å)	0.23	0.22	0.28
Ramachandran Plot			
Most favored (%)	96.9	96.0	94.9
Additionally allowed (%)	3.1	3.7	4.8

3.5 Conclusion

Structural, synthetic, biochemical, and cell-based studies have been employed to illuminate the S_4 subsite of NV 3CLpro and to gain insight and understanding into the significance and impact of hydrophobic interactions on pharmacological activity. In principle, further gains in potency can be realized through the use of constrained R moieties that mitigate the entropic penalty incurred in using long aliphatic chains. The results reported herein provide a sound framework and a solid foundation for conducting further studies aimed at identifying anti-norovirus drug candidates.

CHAPTER IV

DESIGN, SYNTHESIS AND EVALUATION OF NOVEL PRODRUGS OF TRANSITION STATE INHIBITORS OF NOROVIRUS 3CL PROTEASE

4.1 Inhibitor Design Rationale

Peptidyl and non-peptidyl aldehydes, α-ketoamides, α-ketoheterocycles, α-ketoesters and others, are frequently employed as transition state inhibitors of mammalian, viral, and parasitic serine and cysteine proteases of clinical relevance,[163-165] however, the therapeutic potential of these inhibitors, particularly aldehyde-based inhibitors, is adversely impacted by their sub-optimal pharmacokinetics and low oral bioavailability.[166] These considerations provided the impetus for conducting further studies to identify structural variants that display improved physicochemical properties and are likely to be **orally-bioavailable**. Thus, we initially explored the utilization of bisulfite adducts as a latent form of the warheads used in TS inhibitors.[151c] In order to further optimize the PK characteristics of the aldehyde bisulfite adducts, it was envisaged that further structural modifications would likely result in additional improvements in the physicochemical and PK characteristics of these compounds. Specifically, the hydroxyl group in bisulfite adducts provided a convenient site for further derivatization to yield ester (I) and carbamate (II) prodrugs (Figure 4.1).[167-168] Thus, the design and mechanism of action of prodrugs (I-II), entails enzyme-mediated[41-43] or non-enzymatic hydrolysis that converts prodrugs (I-II) into the aldehyde bisulfite adduct which subsequently reverts to the precursor aldehyde (Figure 4.2).

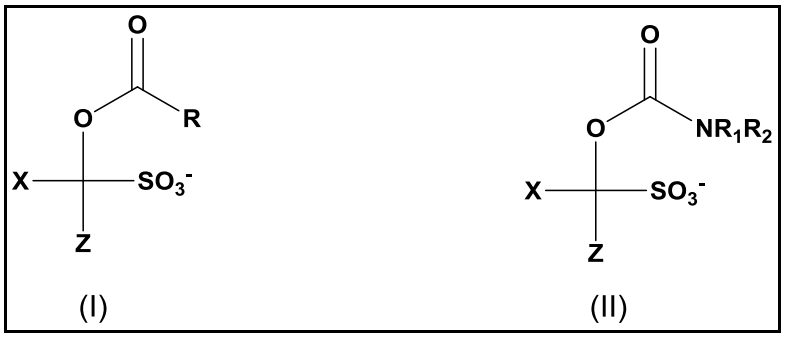

Figure 4.1 General structures of prodrugs (I-II).

Although this has not been demonstrated as yet, it is possible that the aldehyde bisulfite adduct itself may have intrinsic inhibitory activity toward NV 3CLpro by functioning as a transition state mimic.[165] Subsequent reaction with the catalytic cysteine (Cys139) of norovirus 3CLpro leads to inactivation of the enzyme via the formation of a tetrahedral adduct.[63],[158,169-171]

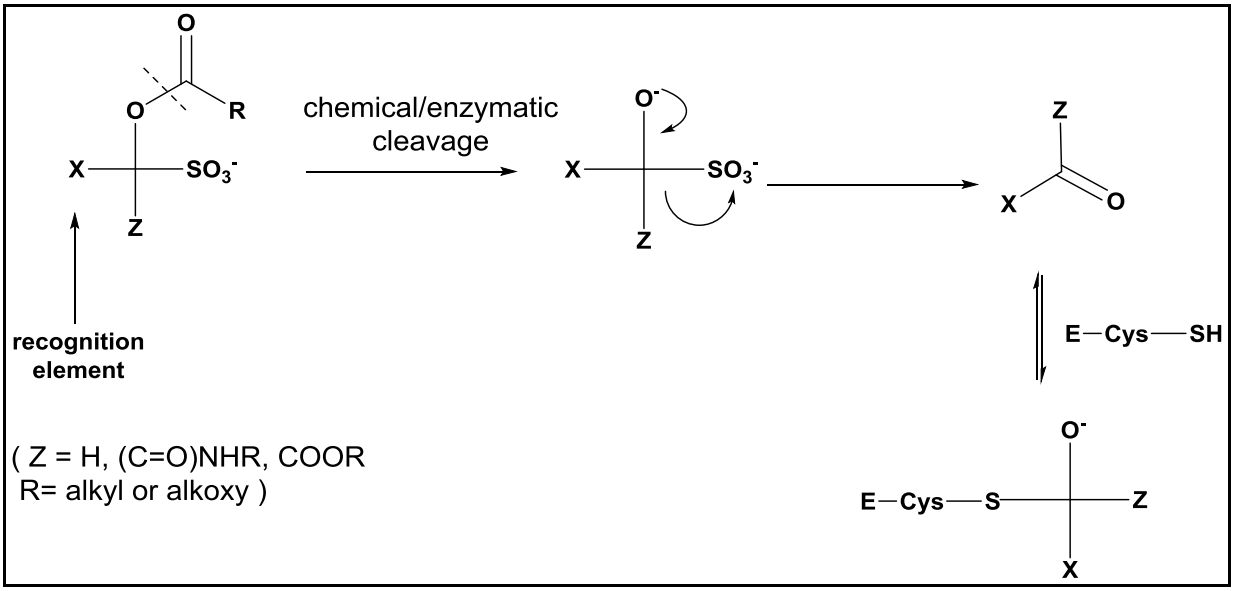

Figure 4.2 Postulated mechanism of action of prodrugs (I-II).

The increased lipophilicity of ester prodrugs (I) was anticipated to result in enhanced absorption, and the rate and extent of absorption of (I) can be conveniently modulated by varying the hydrophobic component (R). Furthermore, the rate of non-enzymatic activation of prodrugs (I) can also be conveniently controlled through the use of appropriate esters and strategies.[172-173] Lastly, carbamate prodrugs (II) derived from amino acids offer additional advantages, including control of the hydrolysis rate via the use of natural and unnatural amino acids.[174]

4.2 Chemistry

Prodrugs (I-II) were readily synthesized by refluxing the peptidyl aldehyde bisulfite adduct with an appropriate anhydride, chloroformate or amino acid-derived isocyanate in dry acetonitrile (Schemes 4.1 and 4.2) and are listed in Tables 4.1 and 4.2.

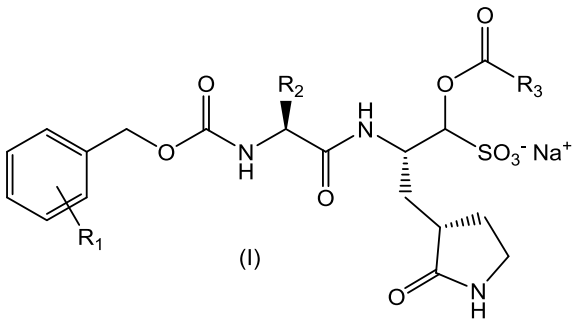

(I)

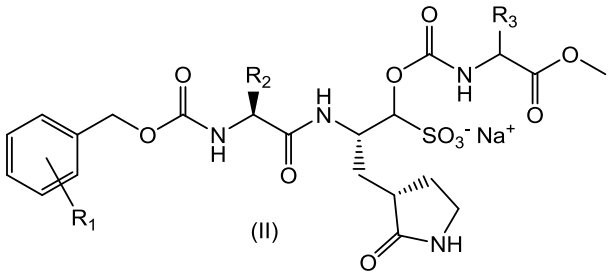

(II)

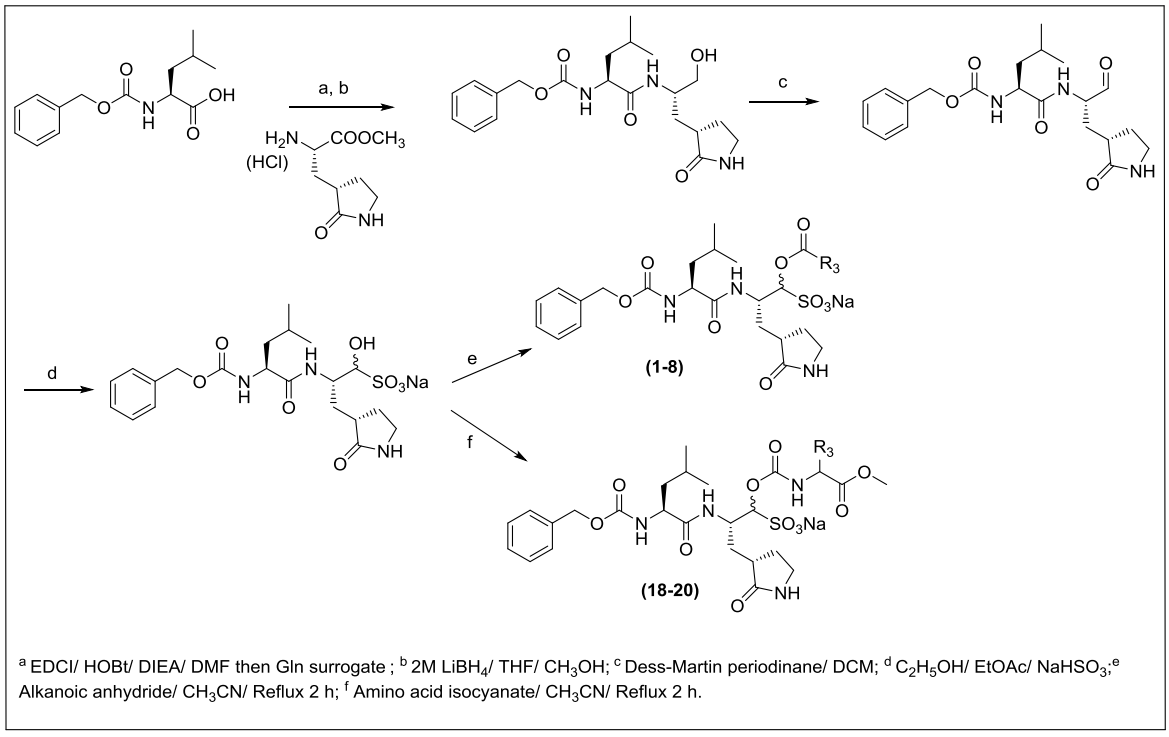

[a] EDCI/ HOBt/ DIEA/ DMF then Gln surrogate ; [b] 2M $LiBH_4$/ THF/ CH_3OH; [c] Dess-Martin periodinane/ DCM; [d] C_2H_5OH/ EtOAc/ $NaHSO_3$;[e] Alkanoic anhydride/ CH_3CN/ Reflux 2 h; [f] Amino acid isocyanate/ CH_3CN/ Reflux 2 h.

Scheme 4.1 Synthesis of Inhibitors ***1-8*** and ***18-20***.

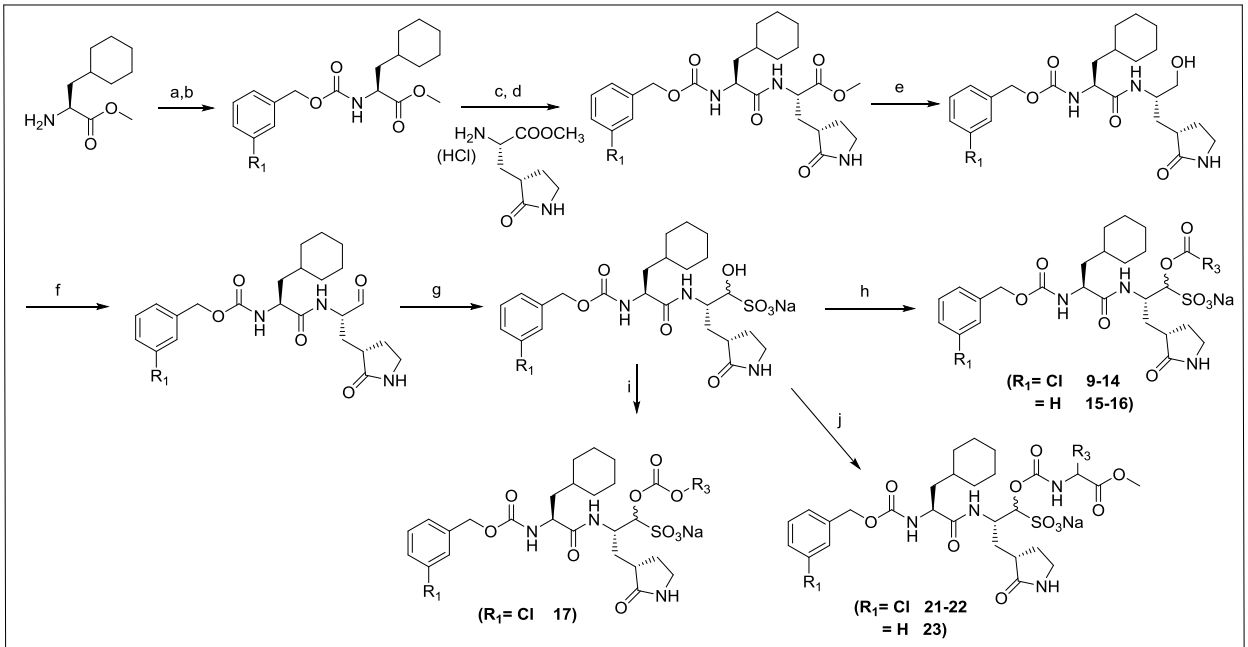

[a] Trichloromethyl chloroformate/ 1,4-dioxane/ Reflux 16 h; [b] $ArCH_2OH$/ TEA/ CH_3CN/ Reflux 2 h; [c] 1M LiOH/ THF/ RT 3 h; [d] EDCI/ HOBt/ DIEA/ DMF then Gln surrogate ; [e] 2M $LiBH_4$/ THF/ CH_3OH; [f] Dess-Martin periodinane/ DCM; [g] C_2H_5OH/ EtOAc/ $NaHSO_3$;[h] Alkanoic anhydride/ CH_3CN/ Reflux 2 h; [i] Chloroformate/ CH_3CN/ Reflux 2 h; [j] amino acid isocyanate/ CH_3CN/ Reflux 2 h.

Scheme 4.2 Synthesis of Inhibitors ***9-17***, and ***21-23***.

4.3 Experimental Section

4.3.1 General

Reagents and dry solvents were purchased from various chemical suppliers (Aldrich, Acros Organics, Chem-Impex, TCI America, Oakwood chemicals, Bachem, and Fisher) and were used as obtained. Silica gel (230-450 mesh) used for flash chromatography was purchased from Sorbent Technologies (Atlanta, GA). The ^{1}H spectra were recorded in $CDCl_3$ or DMSO-d_6 on a Varian XL-400 NMR spectrometer. High resolution mass spectra (HRMS) were performed at the University of Kansas Mass Spectrometry lab using an LCT Premier mass spectrometer (Waters, Milford, MA) equipped with a time of flight mass analyzer and an electrospray ion source. Thin layer chromatography was performed using Analtech silica gel plates and visualization was accomplished using UV light and/ or iodine.

Synthesis of compounds 1-15: General Procedure. Alkanoic anhydride (1 mmol) was added to a solution of dipeptidyl bisulfite salt (1 mmol) in dry acetonitrile 10 mL and the reaction mixture was refluxed for 2 h with stirring. The solvent was removed *in vacuo*. The residue was washed thoroughly with ethyl ether until a white precipitate formed. The supernatant was carefully removed using pipette and the white precipitate was dried *in vacuo.*

(5S,8S)-5-Isobutyl-3,6,11-trioxo-8-(((S)-2-oxopyrrolidin-3-yl)methyl)-1-phenyl-2,10-dioxa-4,7-diazadodecane-9-sulfonate (1). Yield (67 %), mp 94-97 ^{0}C. ^{1}H NMR (400 MHz, DMSO-d_6) δ ppm 7.86 - 7.93 (m, 1H), 7.62 - 7.71 (m, 1H), 7.48 (br. s., 1H), 7.23 - 7.40 (m, 5H), 5.30 (d, *J* = 2.34 Hz, 1H), 4.96 - 5.07 (m, 2H), 4.08 - 4.20 (m, 1H), 3.93 (d, *J* = 8.30 Hz, 1H), 3.09 (br. s., 2H), 2.05 - 2.20 (m, 1H), 2.02 (s, 3H), 1.87 - 1.95 (m, 2H),

1.66 - 1.73 (m, 1H), 1.51 - 1.64 (m, 2H), 1.27 - 1.49 (m, 2H), 0.79 - 0.88 (m, 6H). HRMS (ESI) calcd for $C_{23}H_{32}N_3O_9S$: [M-]: 526.1865. Found: 526.1857. HPLC purity 96.4% (Method A).

(5S,8S)-5-Isobutyl-3,6,11-trioxo-8-(((S)-2-oxopyrrolidin-3-yl)methyl)-1-phenyl-2,10-dioxa-4,7-diazatridecane-9-sulfonate (2). Yield (63 %), mp 83-85 ^{0}C. ^{1}H NMR (400 MHz, DMSO-d_6) δ ppm 7.83 - 7.91 (m, 1H), 7.55 (t, *J* = 7.62 Hz, 1H), 7.45 - 7.51 (m, 1H), 7.35 (d, *J* = 4.30 Hz, 5H), 5.58 - 5.67 (m, 1H), 4.93 - 5.08 (m, 2H), 4.14 - 4.28 (m, 1H), 3.90 - 4.12 (m, 1H), 2.93 - 3.19 (m, 2H), 2.00 - 2.26 (m, 2H), 1.83 - 1.96 (m, 1H), 1.74 - 1.82 (m, 2H), 1.54 - 1.71 (m, 4H), 1.31 - 1.52 (m, 1H), 0.95 (t, *J* = 7.42 Hz, 3H), 0.75 - 0.90 (m, 6H). HRMS (ESI) calcd for $C_{24}H_{34}N_3O_9S$: [M-]: 540.2021. Found: 540.2013. HPLC purity 95.8% (Method A).

(5S,8S)-5-Isobutyl-3,6,11-trioxo-8-(((S)-2-oxopyrrolidin-3-yl)methyl)-1-phenyl-2,10-dioxa-4,7-diazatetradecane-9-sulfonate (3) : Yield (68 %), mp 77-79 ^{0}C. ^{1}H NMR (400 MHz, DMSO-d_6) δ ppm 8.60 - 8.66 (m, 1H), 8.49 - 8.55 (m, 1H), 7.62 - 7.71 (m, 1H), 7.26 - 7.57 (m, 5H), 5.60 - 5.68 (m, 1H), 4.94 - 5.18 (m, 2H), 3.83 - 4.05 (m, 1H), 3.74 (d, *J* = 7.03 Hz, 1H), 2.98 - 3.18 (m, 2H), 2.12 (br. s., 2H), 1.99 (br. s., 1H), 1.60 (br. s., 3H), 1.46 (d, *J* = 7.23 Hz, 6H), 1.11 (t, *J* = 6.74 Hz, 3H), 0.85 (br. s., 6H). HRMS (ESI) calcd for $C_{25}H_{36}N_3O_9S$: [M-]: 554.2178. Found: 554.2166. HPLC purity 98.2% (Method A).

(5S,8S)-5-Isobutyl-3,6,11-trioxo-8-(((S)-2-oxopyrrolidin-3-yl)methyl)-1-phenyl-2,10-dioxa-4,7-diazapentadecane-9-sulfonate (4): Yield (52 %), mp 80-83 ^{0}C. ^{1}H NMR (400 MHz, DMSO-d_6) δ ppm 8.45 - 8.51 (m, 1H), 7.61 - 7.66 (m, 1H), 7.44 - 7.53 (m, 1H), 7.35 (br. s., 5H), 5.10 - 5.15 (m, 1H), 4.98 - 5.07 (m, 2H), 4.17 - 4.26 (m, 1H), 4.03 - 4.13 (m, 1H), 3.00 - 3.17 (m, 2H), 2.16 - 2.22 (m, 2H), 1.86 - 1.94 (br. s., 1H), 1.60 - 1.70 (m, 2H),

1.43 - 1.54 (m, 4H), 1.23 - 1.35 (m, 5H), 1.10 (t, *J* = 7.78 Hz, 3H), 0.80 - 0.91 (m, 6H). HRMS (ESI) calcd for $C_{26}H_{38}N_3O_9S$: [M-]: 568.2334. Found: 568.2336. HPLC purity 94.7% (Method A).

(5S,8S)-5-Isobutyl-3,6,11-trioxo-8-(((S)-2-oxopyrrolidin-3-yl)methyl)-1-phenyl-2,10-dioxa-4,7-diazahexadecane-9-sulfonate (5): Yield (62 %), mp 72-75 ^{0}C. ^{1}H NMR (400 MHz, DMSO-d_6) δ ppm 7.58 - 7.68 (m, 1H), 7.50 (d, *J* = 8.20 Hz, 1H), 7.44 (d, *J* = 3.91 Hz, 1H), 7.28 - 7.40 (m, 5H), 5.06 (s, 1H), 4.99 - 5.04 (m, 2H), 3.91 - 4.00 (m, 1H), 3.81 - 3.85 (m, 1H), 2.97 - 3.15 (m, 2H), 2.07 - 2.20 (m, 2H), 1.87 - 1.91 (m, 1H), 1.57 - 1.64 (m, 2H), 1.40 - 1.49 (m, 7H), 1.28 (br. s., 4H), 1.10 (t, *J* = 6.20 Hz, 3H), 0.80 - 0.91 (m, 6H). HRMS (ESI) calcd for $C_{27}H_{40}N_3O_9S$: [M-]: 582.2491. Found: 582.2487. HPLC purity 97.2% (Method A).

(5S,8S)-5-Isobutyl-3,6,11-trioxo-8-(((S)-2-oxopyrrolidin-3-yl)methyl)-1-phenyl-2,10-dioxa-4,7-diazaoctadecane-9-sulfonate (6): Yield (61 %), mp 74-77 ^{0}C. ^{1}H NMR (400 MHz, DMSO-d_6) δ ppm 8.45 - 8.51 (m, 1H), 7.62 - 7.66 (m, 1H), 7.46 - 7.54 (m, 1H), 7.28 - 7.42 (m, 5H), 5.31 - 5.34 (m, 1H), 4.96 - 5.06 (m, 2H), 4.16 - 4.22 (m, 1H), 4.05 - 4.11 (m, 1H), 3.00 - 3.17 (m, 2H), 2.09 - 2.20 (m, 5H), 1.40 - 1.54 (m, 6H), 1.20 - 1.32 (m, 9H), 1.11 (t, *J* = 6.70 Hz, 3H), 0.86 (br. s., 6H). HRMS (ESI) calcd for $C_{29}H_{44}N_3O_9S$: [M-]: 610.2804. Found: 610.2817. HPLC purity 95.8% (Method A).

(5S,8S)-5-Isobutyl-3,6,11-trioxo-8-(((S)-2-oxopyrrolidin-3-yl)methyl)-1,11-diphenyl-2,10-dioxa-4,7-diazaundecane-9-sulfonate (7): Yield (51 %), mp 84-87 ^{0}C. ^{1}H NMR (400 MHz, DMSO-d_6) δ ppm 8.51 - 8.56 (m, 1H), 8.15 (d, *J* = 7.13 Hz, 1H), 7.93 (d, *J* = 7.03 Hz, 2H), 7.60 - 7.70 (m, 1H), 7.46 - 7.57 (m, 3H), 7.25 - 7.43 (m, 5H), 5.33 - 5.38 (m, 1H), 4.97 - 5.09 (m, 2H), 4.14 - 4.35 (m, 1H), 3.82 - 4.11 (m, 1H), 2.93 - 3.20 (m, 2H),

1.97 - 2.35 (m, 3H), 1.74 - 1.95 (m, 1H), 1.54 - 1.69 (m, 2H), 1.28 - 1.51 (m, 2H), 0.74 - 0.92 (m, 6H). HRMS (ESI) calcd for $C_{28}H_{34}N_3O_9S$: [M-]: 588.2021. Found: 588.2017. HPLC purity 96.7% (Method A).

(5S,8S)-5-Isobutyl-12-methyl-3,6,11-trioxo-8-(((S)-2-oxopyrrolidin-3-yl)methyl)-1-phenyl-2,10-dioxa-4,7-diazatridecane-9-sulfonate (8): Yield (69 %), mp 71-73 ^{0}C. ^{1}H NMR (400 MHz, DMSO-d_6) δ ppm 8.46 - 8.52 (m, 1H), 7.59 - 7.63 (m, 1H), 7.46 - 7.54 (m, 1H), 7.32 (d, *J* = 1.56 Hz, 5H), 4.93 - 5.05 (m, 3H), 4.14 - 4.23 (m, 1H), 4.01 - 4.08 (m, 1H), 3.27 - 3.38 (m, 2H), 3.03 - 3.12 (m, 2H), 2.11 - 2.21 (m, 1H), 1.52 - 1.65 (m, 2H), 1.38 - 1.50 (m, 2H), 1.01 - 1.12 (m, 2H), 0.95 (d, *J* = 6.93 Hz, 6H), 0.84 (d, *J* = 7.23 Hz, 6H). HRMS (ESI) calcd for $C_{25}H_{36}N_3O_9S$: [M-]: 554.2178. Found: 554.2158. HPLC purity 94.6% (Method A).

(5S,8S)-1-(3-Chlorophenyl)-5-(cyclohexylmethyl)-3,6,11-trioxo-8-(((S)-2-oxopyrrolidin-3-yl)methyl)-2,10-dioxa-4,7-diazadodecane-9-sulfonate (9): Yield (69 %), mp 94-96 ^{0}C. ^{1}H NMR (400 MHz, DMSO-d_6) δ ppm 8.46 - 8.52 (m, 1H), 7.61 - 7.64 (m, 1H), 7.54 - 7.58 (m, 1H), 7.46 - 7.51 (m, 1H), 7.34 - 7.43 (m, 2H), 7.27 - 7.32 (m, 1H), 5.28 - 5.32 (m, 1H), 5.04 (d, *J* = 5.66 Hz, 2H), 4.14 - 4.22 (m, 1H), 4.06 - 4.13 (m, 1H), 3.01 - 3.20 (m, 2H), 2.22 - 2.36 (m, 1H), 1.99 - 2.19 (m, 4H), 1.97 (s, 3H), 1.54 - 1.74 (m, 6H), 1.49 (br. s., 1H), 1.06 - 1.21 (m, 4H), 0.76 - 0.96 (m, 2H). HRMS (ESI) calcd for $C_{26}H_{35}ClN_3O_9S$: [M-]: 600.1788. Found: 600.1758. HPLC purity 98.3% (Method A).

(5S,8S)-1-(3-chlorophenyl)-5-(cyclohexylmethyl)-3,6,11-trioxo-8-((2-oxopyrrolidin-3-yl)methyl)-2,10-dioxa-4,7-diazatridecane-9-sulfonate (10): Yield (75 %), mp 74-77 ^{0}C. ^{1}H NMR (400 MHz, DMSO-d_6) δ ppm 8.47 - 8.52 (m, 1 H), 7.74 - 7.79 (m, 1 H), 7.66 (d, *J*=8.40 Hz, 1 H), 7.49 (d, *J*=8.98 Hz, 1 H), 7.33 - 7.45 (m, 2 H), 7.29 (br. s., 1 H), 5.03

(br. s., 2 H), 4.67 (br. s., 1 H), 4.01 (d, *J*=6.44 Hz, 1 H), 3.68 - 3.79 (m, 1 H), 3.09 (d, *J*=8.40 Hz, 2 H), 2.99 (d, *J*=7.81 Hz, 2 H), 2.17 - 2.30 (m, 2 H), 2.10 (br. s., 2 H), 1.74 - 1.84 (m, 1 H), 1.48 - 1.72 (m, 4 H), 1.34 - 1.46 (m, 2 H), 1.30 (d, *J*=6.05 Hz, 1 H), 0.95 - 1.16 (m, 6 H), ppm 0.85 (br. s., 3 H). HRMS (ESI) calcd for $C_{27}H_{37}ClN_3O_9S$: [M-]: 614.1945. Found: 614.1947. HPLC purity 98.2% (Method A).

(5S,8S)-1-(3-Chlorophenyl)-5-(cyclohexylmethyl)-3,6,11-trioxo-8-(((S)-2-oxopyrrolidin-3-yl)methyl)-2,10-dioxa-4,7-diazahexadecane-9-sulfonate (11): Yield (71 %), mp 72-74 ^{0}C. ^{1}H NMR (400 MHz, DMSO-d_6) δ ppm 8.52 (d, *J* = 7.71 Hz, 1H), 7.68 (s, 1H), 7.57 (dd, *J* = 3.91, 7.91 Hz, 1H), 7.49 (d, *J* = 8.89 Hz, 1H), 7.34 - 7.47 (m, 2H), 7.31 (d, *J* = 6.54 Hz, 1H), 5.32 - 5.35 (m, 1H), 4.98 - 5.08 (m, 2H), 4.15 - 4.28 (m, 1H), 3.90 - 4.13 (m, 1H), 2.97 - 3.19 (m, 2H), 2.03 - 2.28 (m, 4H), 1.87 - 1.96 (m, 2H), 1.62 (d, *J* = 8.59 Hz, 7H), 1.39 - 1.52 (m, 4H), 1.21 - 1.35 (m, 6H), 1.05 - 1.15 (m, 4H), 0.81 - 0.93 (m, 2H). HRMS (ESI) calcd for $C_{30}H_{43}ClN_3O_9S$: [M-]: 656.2414. Found: 656.2403. HPLC purity 98.9% (Method A).

(5S,8S)-1-(3-Chlorophenyl)-5-(cyclohexylmethyl)-3,6,11-trioxo-8-(((S)-2-oxopyrrolidin-3-yl)methyl)-2,10-dioxa-4,7-diazaoctadecane-9-sulfonate (12): Yield (71 %), mp 71-73 ^{0}C. ^{1}H NMR (400 MHz, DMSO-d_6) δ ppm 8.47 (d, *J* = 7.41 Hz, 1H), 7.53 - 7.62 (m, 1H), 7.49 (d, *J* = 8.49 Hz, 2H), 7.33 - 7.46 (m, 3H), 5.06 (br. s., 1H), 5.03 (s, 2H), 4.07 - 4.18 (m, 1H), 3.81 - 3.87 (m, 1H), 2.97 - 3.14 (m, 2H), 2.33 (br. s, 4H), 1.63 (d, *J* = 6.25 Hz, 6H), 1.38 - 1.47 (m, 4H), 1.19 - 1.31 (m, 10H), 1.10 (td, *J* = 7.10, 7.50 Hz, 6H), 0.86 (t, *J* = 6.54 Hz, 3H). HRMS (ESI) calcd for $C_{32}H_{47}ClN_3O_9S$: [M-]: 684.2727. Found: 684.2706. HPLC purity 97.3% (Method A).

(5S,8S)-1-(3-Chlorophenyl)-5-(cyclohexylmethyl)-12-methyl-3,6,11-trioxo-8-(((S)-2-oxopyrrolidin-3-yl)methyl)-2,10-dioxa-4,7-diazatridecane-9-sulfonate (13): Yield (41 %), mp 76-78 ^{0}C. ^{1}H NMR (400 MHz, DMSO-d_6) δ ppm 8.50 (d, *J* = 7.71 Hz, 1H), 7.62 (s, 1H), 7.56 (d, *J* = 7.71 Hz, 1H), 7.34 - 7.45 (m, 3H), 7.30 (d, *J* = 4.59 Hz, 1H), 5.33 - 5.39 (m, 1H), 5.04 (d, *J* = 4.98 Hz, 2H), 4.15 - 4.23 (m, 1H), 4.10 (q, *J* = 7.94 Hz, 1H), 3.01 - 3.18 (m, 2H), 2.08 - 2.27 (m, 1H), 1.84 - 1.95 (m, 2H), 1.56 - 1.76 (m, 8H), 1.44 - 1.52 (m, 2H), 1.09 - 1.17 (m, 4H), 1.06 (d, *J* = 6.93 Hz, 6H), 0.82 - 0.93 (m, 2H). HRMS (ESI) calcd for $C_{28}H_{39}ClN_3O_9S$: [M-]: 628.2101. Found: 628.2115. HPLC purity 95.8% (Method A).

(5S,8S)-1-(3-Chlorophenyl)-11-cyclohexyl-5-(cyclohexylmethyl)-3,6,11-trioxo-8-(((S)-2-oxopyrrolidin-3-yl)methyl)-2,10-dioxa-4,7-diazaundecane-9-sulfonate (14): Yield (53 %), mp 86-88 ^{0}C. ^{1}H NMR (400 MHz, DMSO-d_6) δ ppm 8.48 - 8.52 (m, 1H), 7.50 (d, *J* = 8.20 Hz, 1H), 7.44 (d, *J* = 3.91 Hz, 1H), 7.28 - 7.40 (m, 4H), 5.06 (s, 1H), 4.99 - 5.04 (m, 2H), 3.91 - 4.00 (m, 1H), 3.81 - 3.85 (m, 1H), 2.97 - 3.15 (m, 2H), 2.07 - 2.20 (m, 4H), 1.87 - 1.91 (m, 2H), 1.57 - 1.64 (m, 2H), 1.40 - 1.49 (m, 5H), 1.28 (s, 4H), 1.10 (td, *J* = 6.20, 6.50 Hz, 4H), 0.80 - 0.91 (m, 8H). HRMS (ESI) calcd for $C_{31}H_{43}ClN_3O_9S$: [M-]: 668.2414. Found: 668.2403. HPLC purity 97.7% (Method A).

(5S,8S)-5-(Cyclohexylmethyl)-3,6,11-trioxo-8-(((S)-2-oxopyrrolidin-3-yl)methyl)-1-phenyl-2,10-dioxa-4,7-diazadodecane-9-sulfonate (15) : Yield (62 %), mp 92-94 ^{0}C. ^{1}H NMR (400 MHz, DMSO-d_6) δ ppm 8.34 (d, *J* = 8.79 Hz, 1H), 7.47 - 7.53 (m, 1H), 7.34 (br. s., 5H), 5.68 - 5.76 (m, 1H), 5.02 (s, 2H), 4.64 - 4.71 (m, 1H), 3.97 - 4.09 (m, 1H), 3.73 (q, *J* = 7.13 Hz, 1H), 2.96 - 3.15 (m, 2H), 2.04 - 2.26 (m, 2H), 1.99 (s, 3H), 1.79 (d, *J* = 11.03 Hz, 2H), 1.53 - 1.72 (m, 6H), 1.38 - 1.48 (m, 3H), 1.22 - 1.34 (m, 1H), 1.04 -

1.20 (m, 2H), 0.86 (d, *J* = 11.33 Hz, 2H). HRMS (ESI) calcd for $C_{26}H_{36}N_3O_9S$: [M-]: 566.2178. Found: 566.2147. HPLC purity 95.8% (Method A).

(5S,8S)-11-Cyclohexyl-5-(cyclohexylmethyl)-3,6,11-trioxo-8-(((S)-2-oxopyrrolidin-3-yl)methyl)-1-phenyl-2,10-dioxa-4,7-diazaundecane-9-sulfonate (16) : Yield (52 %), mp 83-85 ^{0}C. ^{1}H NMR (400 MHz, DMSO-d_6) δ ppm 8.43 - 8.52 (m, 1H), 7.64 (d, *J* = 8.49 Hz, 1H), 7.48 - 7.54 (m, 1H), 7.34 (br. s., 5H), 5.69 - 5.76 (m, 1H), 5.02 (s, 2H), 3.96 - 4.12 (m, 1H), 3.69 - 3.81 (m, 1H), 2.96 - 3.17 (m, 2H), 2.18 (t, *J* = 7.37 Hz, 4H), 2.13 (br. s., 2H), 1.48 - 1.71 (m, 7H), 1.35 - 1.46 (m, 2H), 1.27 (d, *J* = 4.00 Hz, 4H), 1.04 - 1.19 (m, 4H), 0.85 (qd, *J* = 5.20, 5.60 Hz, 6H). HRMS (ESI) calcd for $C_{26}H_{36}N_3O_9S$: [M-]: 634.2804. Found: 634.2818. HPLC purity 98.1% (Method A).

Synthesis of compounds 17: General procedure. Hexyl chloroformate (1.1 mmol) was added to a solution of dipeptidyl bisulfite salt (1 mmol) in dry acetonitrile (10 mL) and the reaction mixture was refluxed for 2 h with stirring. The solvent was removed *in vacuo* and the oily residue was treated with ether/hexane until a white precipitate formed. The supernatant was carefully removed using a pipette and the white solid was dried *in vacuo*.

(5S,8S)-1-(3-chlorophenyl)-5-(cyclohexylmethyl)-3,6,11-trioxo-8-((2-oxo pyrrolidin-3-yl)methyl)-2,10,12-trioxa-4,7-diazaoctadecane-9-sulfonate (17): Yield (61 %), mp 77-79 ^{0}C. ^{1}H NMR (400 MHz, DMSO-d_6) δ ppm 8.53 (d, *J* = 7.74 Hz, 1H), 7.68 (s, 1H), 7.57 (dd, *J* = 3.91, 7.91 Hz, 1H), 7.49 (d, *J* = 8.89 Hz, 1H), 7.34 - 7.47 (m, 2H), 7.31 (d, *J* = 6.54 Hz, 1H), 5.32 - 5.35 (m, 1H), 4.98 - 5.08 (m, 2H), 4.15 - 4.28 (m, 1H), 3.90 - 4.13 (m, 1H), 3.60 (t, J=8.54 Hz, 2 H), 2.97 - 3.19 (m, 2H), 2.03 - 2.28 (m, 4H), 1.87 - 1.96 (m, 2H), 1.62 (d, *J* = 8.59 Hz, 7H), 1.39 - 1.52 (m, 4H), 1.21 - 1.35 (m, 6H), 1.05 - 1.15 (m,

4H), 0.81 - 0.93 (m, 2H). HRMS (ESI) calcd for $C_{31}H_{45}ClN_3O_{10}S$: [M-]: 709.2412. Found: 709.2408. HPLC purity 98.9% (Method A).

Synthesis of compounds 18-21: General procedure. Isocyanate of amino acid (1.1 mmol) was added to a solution of dipeptidyl bisulfite salt (1 mmol) in dry acetonitrile (10 mL) and the reaction mixture was refluxed for 2 h with stirring. The solvent was removed *in vacuo* and the oily residue was treated with ether until a white precipitate formed. The supernatant was carefully removed using a pipette and the white solid was dried *in vacuo*.

(5S,8S)-5-Isobutyl-3,6,11,14-tetraoxo-8-(((S)-2-oxopyrrolidin-3-yl)methyl)-1-phenyl-2,10,15-trioxa-4,7,12-triazahexadecane-9-sulfonate (18) : Yield (67 %), mp 83-86 ^{0}C. ^{1}H NMR (400 MHz, DMSO-d_6) δ ppm 8.43 (d, *J* = 8.31 Hz, 1H), 7.59 (s, 1H), 7.40 - 7.52 (m, 1H), 7.28 - 7.37 (m, 5H), 6.48 (t, *J* = 6.91 Hz, 1H), 4.98 - 5.07 (m, 2H), 4.15 - 4.28 (m, 1H), 3.87 - 4.03 (m, 1H), 3.74 (s, 3H), 3.68 (d, *J* = 7.13 Hz, 1H), 3.35 (d, *J* = 7.03 Hz, 1H), 3.11 (dd, *J* = 8.84, 18.43 Hz, 2H), 2.02 - 2.26 (m, 2H), 1.53 - 1.74 (m, 2H), 1.37 - 1.54 (m, 3H), 1.05 - 1.16 (m, 2H), 0.86 (d, *J* = 7.33 Hz, 6H).HRMS (ESI) calcd for $C_{25}H_{35}N_4O_{11}S$: [M-]: 599.2029. Found: 599.2019. HPLC purity 96.3% (Method B).

(5S,8S)-5-Isobutyl-13-methyl-3,6,11,14-tetraoxo-8-(((S)-2-oxopyrrolidin-3-yl) methyl)-1-phenyl-2,10,15-trioxa-4,7,12-triazahexadecane-9-sulfonate (19) : Yield (70 %), mp 63-65 ^{0}C. ^{1}H NMR (400 MHz, DMSO-d_6) δ ppm 8.45 (d, *J* = 7.52 Hz, 1H), 7.60 (s, 1H), 7.46 (d, *J* = 7.81 Hz, 1H), 7.28 - 7.37 (m, 5H), 6.39 (d, *J* = 7.62 Hz, 1H), 5.01 (s, 2H), 4.34 - 4.41 (m, 1H), 4.13 - 4.25 (m, 1H), 4.06 (q, *J* = 7.20 Hz, 1H), 3.72 (s, 3H), 3.00 - 3.16 (m, 2H), 2.26 (dd, *J* = 3.66, 9.03 Hz, 1H), 1.87 (ddd, *J* = 4.05, 10.69, 14.35 Hz, 2H), 1.54 - 1.67 (m, 3H), 1.38 - 1.49 (m, 2H), 1.21 (d, *J* = 7.32 Hz, 3H), 1.07 (dt, *J* = 4.39, 7.08

Hz, 1H), 0.84 (d, *J* = 7.60 Hz, 6H). HRMS (ESI) calcd for $C_{26}H_{37}N_4O_{11}S$: [M-]: 613.2185. Found: 613.2174. HPLC purity 95.9% (Method B).

(5S,8S)-5-Isobutyl-13-isopropyl-3,6,11,14-tetraoxo-8-(((S)-2-oxopyrrolidin-3-yl) methyl)-1-phenyl-2,10,15-trioxa-4,7,12-triazahexadecane-9-sulfonate (20) : Yield (73 %), mp 85-87 ^{0}C. ^{1}H NMR (400 MHz, DMSO-d_6) δ ppm 8.48 (d, *J* = 7.52 Hz, 1H), 7.61 - 7.67 (m, 1H), 7.46 - 7.53 (m, 1H), 7.27 - 7.42 (m, 5H), 6.38 - 6.43 (m, 1H), 4.95 - 5.08 (m, 2H), 4.15 - 4.24 (m, 1H), 4.03 - 4.12 (m, 1H), 3.90 - 4.01 (m, 1H), 3.67 (s, 3H), 3.11 (dd, *J* = 6.35, 13.28 Hz, 2H), 2.31 - 2.35 (m, 1H), 2.07 - 2.15 (m, 3H), 1.96 - 2.05 (m, 2H), 1.91 (dd, *J* = 8.70, 14.20 Hz, 3H), 1.39 - 1.71 (m, 6H), 1.10 (dt, *J* = 4.49, 7.08 Hz, 1H), 0.76 - 0.92 (m, 6H). HRMS (ESI) calcd for $C_{28}H_{41}N_4O_{11}S$: [M-]: 641.2498. Found: 641.2464. HPLC purity 98.5% (Method B).

(5S,8S)-1-(3-Chlorophenyl)-5-(cyclohexylmethyl)-13-methyl-3,6,11,14-tetraoxo-8-(((S)-2-oxopyrrolidin-3-yl)methyl)-2,10,15-trioxa-4,7,12-triazahexadecane-9-sulfonate (21): Yield (66 %), mp 64-66 ^{0}C. ^{1}H NMR (400 MHz, DMSO-d_6) δ ppm 8.50 (d, *J* = 7.81 Hz, 1H), 7.61 - 7.69 (m, 1H), 7.48 - 7.57 (m, 1H), 7.34 - 7.44 (m, 2H), 7.30 (d, *J* = 2.93 Hz, 1H), 6.42 (d, *J* = 7.42 Hz, 1H), 5.69 - 5.77 (m, 1H), 4.94 - 5.12 (m, 2H), 4.19 - 4.29 (m, 1H), 4.06 - 4.17 (m, 1H), 3.81 - 4.00 (m, 1H), 3.63 (s, 3H), 2.96 - 3.20 (m, 2H), 2.01 - 2.29 (m, 2H), 1.82 - 1.96 (m, 1H), 1.62 (d, *J* = 8.59 Hz, 6H), 1.38 - 1.52 (m, 4H), 1.23 (d, *J* = 7.23 Hz, 3H), 1.06 - 1.14 (m, 4H), 0.76 - 0.94 (m, 2H). HRMS (ESI) calcd for $C_{29}H_{40}ClN_4O_{11}S$: [M-]: 687.2108. Found: 687.2131. HPLC purity 97.4% (Method B).

(5S,8S)-1-(3-Chlorophenyl)-5-(cyclohexylmethyl)-13-isopropyl-3,6,11,14-tetraoxo-8-(((S)-2-oxopyrrolidin-3-yl)methyl)-2,10,15-trioxa-4,7,12-triazahexadecane-9-sulfonate (22): Yield (62 %), mp 82-84 ^{0}C. ^{1}H NMR (400 MHz, DMSO-d_6) δ ppm 8.45 (d,

J = 7.72 Hz, 1H), 7.63 - 7.71 (m, 1H), 7.48 - 7.55 (m, 1H), 7.31 - 7.42 (m, 2H), 7.20 (d, *J* = 3.56 Hz, 1H), 6.47 (d, *J* = 7.61 Hz, 1H), 5.62 - 5.74 (m, 1H), 4.94 - 5.12 (s, 2H), 4.19 - 4.31 (m, 1H), 4.06 - 4.17 (m, 1H), 3.81 - 4.02 (m, 1H), 3.63 (s, 3H), 2.96 - 3.17 (m, 2H), 2.01 - 2.29 (m, 2H), 1.82 - 1.96 (m, 1H), 1.62 (m, 6H), 1.38 - 1.52 (m, 4H), 1.10 (dt, *J* = 4.49, 7.08 Hz, 1H), 1.06 - 1.14 (m, 4H), 0.97-1.04 (d, *J*= 7.48 Hz, 6H), 0.76 - 0.94 (m, 2H). HRMS (ESI) calcd for $C_{31}H_{44}ClN_4O_{11}S$: [M-]: 715.2421. Found: 715.2413. HPLC purity 98.3% (Method B).

(5S,8S)-5-(Cyclohexylmethyl)-13-methyl-3,6,11,14-tetraoxo-8-(((S)-2-oxopyrrolidin-3-yl)methyl)-1-phenyl-2,10,15-trioxa-4,7,12-triazahexadecane-9-sulfonate (23) : Yield (72 %), mp 61-63 ^{0}C. ^{1}H NMR (400 MHz, DMSO-d_6) δ ppm 8.47 (s, 1H), 7.63 (s, 1H), 7.42 - 7.54 (m, 1H), 7.37 (s, 1H), 7.28 - 7.40 (m, 5H), 6.52 (t, *J* = 5.91 Hz, 1H), 4.98 - 5.04 (m, 2H), 4.15 - 4.28 (m, 1H), 3.87 - 4.03 (m, 1H), 3.77 (s, 3H), 3.74 (d, *J* = 7.13 Hz, 1H), 3.11 (dd, *J* = 8.84, 19.67 Hz, 2H), 2.02 - 2.22 (m, 2H), 1.53 - 1.70 (m, 4H), 1.34 - 1.52 (m, 4H), 1.05 - 1.13 (d, *J* = 7.24 Hz, 3H), 0.87 - 0.98 (m, 6H), 0.76 - 0.84 (m, 2H). HRMS (ESI) calcd for $C_{29}H_{41}N_4O_{11}S$: [M-]: 653.2498. Found: 653.2483. HPLC purity 97.7% (Method B).

4.3.2 FRET Protease Assays

The FRET protease assay (3CLpro) was performed by preparing stock solutions of the substrate (Edans-DFHLQ/GP-Dabcyl) and inhibitor in DMSO and diluting into assay buffer which was comprised of 20 mM HEPES buffer, pH 8, containing NaCl (200 mM), 0.4 mM EDTA, glycerol (60%), and 6 mM dithiothreitol (DTT). The protease was mixed with serial dilutions of each compound up to 100 µM or with DMSO in 25 µL of assay buffer and incubated at 37^{o}C for 30 min, followed by the addition of 25 µL of assay buffer containing substrate. Fluorescence readings were obtained using an excitation wavelength of 360 nm and an emission wavelength of 460 nm on a fluorescence microplate reader (FLx800; Biotec, Winoosk, VT) 1 h following the addition of substrate. Relative fluorescence units (RFU) were determined by subtracting background values (substrate-containing well without protease) from the raw fluorescence values, as described previously.[140,158, 175-176] The dose-dependent FRET inhibition curves were fitted with a variable slope by using GraphPad Prism software (GraphPad, La Jolla, CA) in order to determine the IC_{50} values of the inhibitors.

4.3.3 Cell-Based Inhibition Assays

The effects of each inhibitor on virus replication were examined against NV in the NV replicon harboring cells (HG23 cells).[158] Briefly, confluent and semi-confluent HG23 cells were incubated with medium containing DMSO (<0.1%) or each compound (up to 20 μM) for 48 h. After the incubation, total RNA was extracted and viral genome was quantitated with real-time quantitative RT-PCR (qRT-PCR). The EC_{50} values were determined by GraphPadPrism software.[158]

4.3.4 Cytotoxicity Studies

The cytotoxicity of a select number of compounds was determined using human HeLa cells and the MTT assay as described previously.[177] This assay measures the viability of a population of cells after a 72 h incubation with the test compound. The CC_{50} was calculated as the concentration at which cell viability was at 50% of the untreated controls.

4.3.5 Liver Microsomes Stability.

Liver microsomes stability was determined by incubating 25 μM compound in a solution with mouse or human liver microsomes (Xenotech), NADPH (Sigma Aldrich) 50 mM phosphate buffer (pH 7.4) and 3 mM $MgCl_2$ for 1 h at 37ºC, as described previously,[178] quenching the sample with 1% trifluoroacetic acid in acetonitrile and then analyzing the quantity of the parent compound present in the sample using LC/MS (Thermo Scientific LCQ Fleet).

4.3.6 Plasma Protein-Binding

Protein binding studies were performed using a 96-well equilibrium dialysis apparatus (Pierce Biochemicals) according to a published protocol.[179] Mouse or human serum samples (55%) were incubated at 37 ºC for 24 h in the presence of 25 µM compound prior to LC/MS quantitation of the post-dialysis material.

4.3.7 High Performance Liquid Chromatography (HPLC)

Method A: Prodrug compound 1 mg was dissolved in 100 µL of acetonitrile: dichloromethane (2:3) mixture. Then 10 µL of solution (10 g/L) was injected into HPLC (Varian Pro-star) with mobile phase isocratic 40 mode with 40% acetonitrile and 60% dichloromethane. The flow rate of mobile phase is 1.0 mL/min through the normal phase column stationary phase (Kinetex 2.6u HILIC 100A, 75x4.6mm).

Method B: Prodrug compound 1 mg was dissolved in 100 µL of acetonitrile: dichloromethane (2:3) mixture. Then 10 µL of solution (10 g/L) was injected into HPLC (Varian Pro-star) with mobile phase isocratic 20 mode with 20% acetonitrile and 80% dichloromethane. The flow rate of moile phase is 1.0 mL/min through the normal phase column stationary phase (Kinetex 2.6u HILIC 100A, 75x4.6mm).

4.4 Results and Discussion

The inhibitory activity of the synthesized compounds against NV 3CLpro and their anti-norovirus activity in a cell-based replicon system were evaluated as described in the experimental section.[140,158] The determined IC_{50} values in enzyme assay and EC_{50} values against NV in replicon harboring cells (HG23 cells) are listed in Tables 4.1 and 4.2 and they are the average of at least two determinations.

The results listed in Table 4.1 clearly demonstrate that prodrugs ***1-17*** display significant anti-norovirus activity in replicon cells. Furthermore, these compounds were found to exhibit comparable inhibitory activity against norovirus 3CLpro, as well as norovirus in replicon cells, as the precursor bisulfite adducts and corresponding aldehydes. As anticipated, the *m*-Cl phenyl substituted derivatives with a cyclohexylalanine (Cha) as the P_2[180] residue (compounds ***9-14***, Table 4.1), displayed higher potency because the Cha side chain optimally fills the hydrophobic S_2 subsite and the chlorine substituent engages in additional binding interactions.[160] The prime subsites (S_n') of norovirus 3CLpro are shallow, consequently, prodrugs ***1-17*** are presumed to be devoid of intrinsic inhibitory activity toward 3CLpro or norovirus, however, under the conditions used to assay the enzyme or in conducting the replicon harboring cells studies, hydrolysis of the esters yields the corresponding TS inhibitor bisulfite adducts which then revert to the corresponding aldehydes, the putative inhibitory species. This hypothesis is supported by the results of structural studies where incubation of a peptidyl aldehyde bisulfite adduct with norovirus 3CLpro 20 mM Tris buffer, pH 8.0, resulted in reversal of the bisulfite adduct to the precursor aldehyde, followed by reaction with the active site cysteine (Cys139), ultimately leading to the formation of an enzyme-aldehyde inhibitor

adduct. The high-resolution structure of the enzyme-inhibitor complex provides cogent confirmation of this hypothesis.[158]

TABLE 4.1 ANTI-NV ACTIVITY OF COMPOUNDS ***1-17*** IN ENZYME (IC_{50}) AND CELL-BASED (EC_{50}) ASSAY

Compound	R_1	R_2	R_3	IC_{50} (μM)	EC_{50} (μM)
1	H	Isobutyl	CH_3	10.5	0.6
2			CH_2CH_3	7.5	0.7
3			$(CH_2)_2CH_3$	3.7	1.3
4			$(CH_2)_3CH_3$	3.5	1.4
5			$(CH_2)_4CH_3$	2.8	0.3
6			$(CH_2)_6CH_3$	3.0	0.5
7			C_6H_5	7.2	0.8
8			$CH(CH_3)_2$	3.5	0.3
9	*m*-Cl	Cha	CH_3	0.08	0.03
10			CH_2CH_3	0.1	0.025
11			$(CH_2)_4CH_3$	0.1	0.015
12			$(CH_2)_6CH_3$	0.9	0.03
13			$CH(CH_3)_2$	0.3	0.03
14			C_6H_{11}	0.4	0.02
15	H		CH_3	7.5	0.2
16			$(CH_2)_4CH_3$	0.6	0.06
17	m-Cl		$O(CH_2)_5CH_3$	0.8	0.025

A small number of carbamate prodrugs ***18-23*** (Table 4.2) were also synthesized and shown to exhibit potent anti-norovirus activity (Table 4.2, compounds ***21-22***). The availability of a large number of natural and unnatural amino acids makes possible the fine tuning of the rate and extent of absorption, as well as release in blood plasma, of the inhibitory species. Likewise, the high potency and lower chemical reactivity of carbonate esters can also be exploited (for example, compound ***17*** in Table 4.1).

TABLE 4.2 ANTI-NV ACTIVITY OF COMPOUNDS ***18-23*** IN ENZYME (IC_{50}) AND CELL-BASED (EC_{50}) ASSAY

Compound	R_1	R_2	R_3	IC_{50} (μM)	EC_{50} (μM)
18	H	Isobutyl	H	3.1	0.4
19			CH_3	1.8	0.3
20			$CH(CH_3)_2$	2.5	0.4
21	*m*-Cl	Cha	CH_3	0.8	0.025
22			$CH(CH_3)_2$	0.5	0.04
23	H		CH_3	10.2	0.2

4.4.1 Hydrolysis of Ester Prodrugs to the Aldehyde in Mouse and Human Serum

The hydrolysis of the bisulfite adducts and three prodrug compounds in mouse and human serum was initially determined by incubating the compounds at 37 ^{o}C for 1 h and the results are summarized in Table 4.3. At the end of the incubation period, most of the bisulfite adducts forms of compounds ***24*** and ***26*** were converted to the active aldehyde counterparts in the presence of mouse or human serum. For the prodrug compounds, the hydrolysis of compounds ***9*** and ***10*** was shown to be species specific: complete conversion to the aldehyde in mouse serum versus <50% conversion human serum in 1 h.

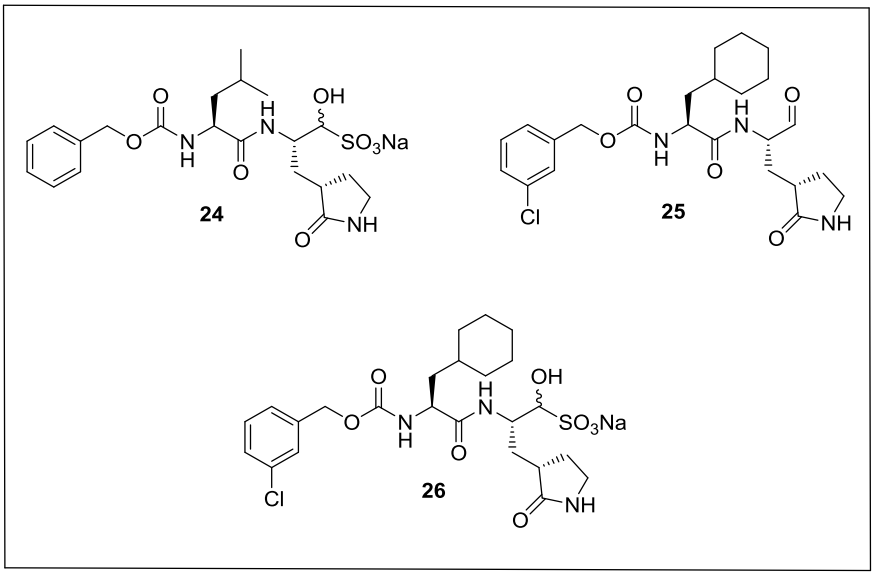

Figure 4.3 Structures of compounds ***24-26***.

To determine detailed kinetics of hydrolysis of the precursor ester prodrugs, compounds ***9***, ***10***, and ***11***, were incubated separately in 55% human serum, aliquots were withdrawn at different time intervals, and the % remaining ester prodrug was plotted over

time (Figure 4.4). Esterified derivatives ***9*** and ***10*** were found to release the putative inhibitory species (aldehyde) rapidly (half-life ~25 minutes), while the hydrolysis of the n-hexanoic acid-derived ester ***11*** was much slower. These results demonstrate that ester prodrugs (I) are capable of releasing the active inhibitory species in blood serum and that the nature of the R group can be used to modulate the rate of release. The hydrolysis of the ester prodrugs could, in principle, proceed through a spontaneous or esterase-mediated hydrolysis (or both).

TABLE 4.3 HYDROLYSIS OF COMPOUNDS ***9-11***, ***24*** AND ***26*** IN MOUSE OR HUMAN SERUM TO YIELD THE PRECURSOR ALDEHYDE

Compound	% of parent remaining after 1 h	
	Mouse Serum	Human Serum
24[b]	18	2
26[b]	0	0
9[c]	0	56
10[c]	0	52
11[c]	60	103

[a]Compounds (25 µM or 100 µM) were incubated with 55% serum for 1 h at 37ºC (detection of aldehyde by LC/MS).
[b]Structures shown in Figure 4.3.
[c]See Table 4.1 for structures.

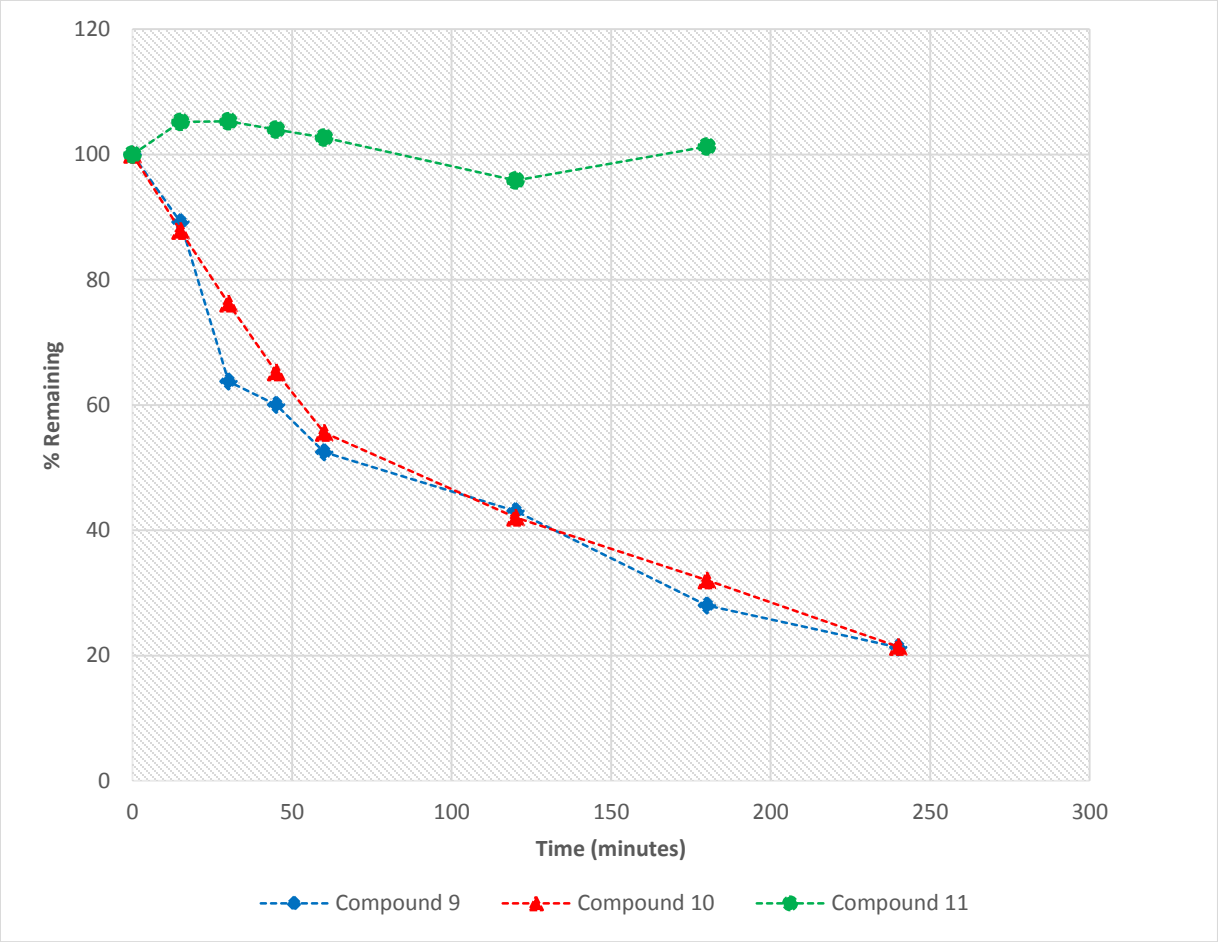

Figure 4.4 Time-dependent hydrolysis of prodrugs ***9, 10*** and ***11*** and conversion to the aldehyde form in 55% human serum.

4.4.2 Cytotoxicity

The potential toxicity to human HeLa cells was determined using a representative set of prodrugs and precursor compounds and the results are summarized Table 4.4. The prodrugs, as well as the precursor aldehyde and aldehyde bisulfite adducts were all relatively nontoxic in this assay, with CC_{50} values ranging from 50 to >200 µM. The selectivity index was calculated as the ratio between toxicity and potency (CC_{50} HeLa/EC_{50}) and the values ranged from >667 to >6,667, demonstrating an excellent selectivity for the viral target.

TABLE 4.4 CYTOTOXICITY AND SELECTIVITY INDEX OF COMPOUNDS ***9-11*** AND ***24-26***

Compound[a]	CC_{50} (µM)	EC_{50} (µM)	Selectivity Index
24[b]	>200	0.3	>667
25[b]	56.1	0.02	2,800
26[b]	49.6	0.02	2,480
9[c]	>200	0.03	>6,667
10[c]	112	0.025	4480
11[c]	82	0.015	5,467

[a]HeLa cells were exposed to compound during a 72-h incubation and cytotoxicity was determined using the MTT assay.
[b]Structures shown in Figure 4.3
[c]See Table 4.1 for structures

4.4.3 Liver Microsomes Stability

The stability of a select number of compounds in liver microsomes was determined. The stability of the aldehyde form of ***24*** (Figure 4.3) was high when exposed to mouse and human liver microsomes (Table 4.5), a desirable property for an active compound.

TABLE 4.5 METABOLIC STABILITY OF COMPOUNDS ***9-11*** AND ***25-27*** WITH HUMAN AND MOUSE LIVER MICROSOMES

Compound	% of parent remaining after 1 h	
	Mouse Microsomes[a]	Human Microsomes[a]
24[b]	82	92
25[b]	40	63
26[b]	35	54
9[c]	14	17
10[c]	17	11
11[c]	38	76
Warfarin (high stability control)	99.6	95
Verapamil (low stability control)	30	41

[a]Compounds (25 µM or 100 µM) were incubated with mouse or human liver microsomes in the presence of NADPH for 1 h at 37ºC (detection of aldehyde by LC/MS).

[b]Structures listed in Figure 4.3.

[c]See Table 4.1 for structures.

The chloro-substituted analogs, ***25*** and ***26***, were both present in solution as the aldehyde form prior to the addition of microsomes. As expected, both compounds behaved similarly (40 and 35% remaining, respectively) in the presence of mouse microsomes. In the presence of mouse liver microsomes prodrug ***11*** was converted to the aldehyde form ***25*** (Figure 4.3) and to other forms, with 38% remaining after 1 h. Importantly, compound ***11*** was only moderately metabolized (76% remaining) by human liver microsomes after 1 h.

4.4.4 Plasma Protein Binding

Binding to albumin, α_1-glycoprotein and red blood cells impacts drug distribution, PK parameters and exposure to the target. Consequently, the extent of binding to plasma proteins of a select number of compounds was also investigated. Compounds were tested for their ability to bind to plasma proteins over a 4-h time period. Chloro-substituted analogs ***11, 25,*** and ***26*** were strongly bound to mouse and human serum (Table 4.6), whereas the aldehyde form of ***24*** demonstrated only moderate binding (65-71%).

TABLE 4.6 PLASMA PROTEIN BINDING OF COMPOUNDS ***9-11*** AND ***24-26***

Compound	% bound to serum protein	
	Mouse Serum[a]	Human Serum[a]
24[b]	71	65
25[b]	98	98
26[b]	97	96
9[c]	ND[d]	ND[d]
10[c]	ND[d]	ND[d]
11[c]	100	100
Atenolol (weak binding control)	0	4
Warfarin (strong binding control)	96	99

[a]Compound (25 µM or 100 µM) was incubated with 55% mouse or human serum in an equilibrium dialysis chamber for 4 h at 37ºC (detection of aldehyde by LC/MS).
[b]Structures shown in Figure 4.3.
[c]See Table 4.1 for structures.
[d]ND, not detected due to low serum stability over 4 h.

4.5 Conclusions

A general approach toward the optimization of the pharmacokinetics of peptidyl and non-peptidyl transition state inhibitors via the synthesis of ester and carbamate prodrugs of aldehyde bisulfite adducts is reported. The ester prodrugs were found to undergo hydrolysis in blood plasma with a half-life of ~0.25 h. The rate of hydrolysis was dependent on the ester alkyl chain. The generated prodrugs also exhibited low cytotoxicity and satisfactory liver microsomes stability and plasma protein binding. The approach has wide applicability and provides an effective means of augmenting the therapeutic potential of these classes of inhibitors. It should be noted that the prodrug approach expounded herein can be extended to other transition state inhibitors, such as α-ketoamides. Lastly, previously reported peptidyl or nonpeptidyl TS inhibitors of mammalian, viral, and parasitic serine and cysteine proteases such as, for example, cathepsins L and S, calpains, and falcipain-2, can all be transformed to the corresponding ester and carbamate prodrugs. We have indeed demonstrated this using known cathepsin L, falcipain-2, and calpain inhibitors.

CHAPTER V

PEPTIDYL KETOPHOSPHONATE INHIBITORS OF NOROVIRUS 3CL PROTEASE: SAR, BIOCHEMICAL, STRUCTURAL AND IN VITRO CELL-BASED STUDIES

5.1 Inhibitor Design Rationale

The design of protease inhibitors typically involves the attachment of a warhead (or transition state mimic) to a recognition element that is congruent with the known substrate specificity of the target enzyme. A critical consideration of the design process is the selection of a warhead capable of reacting with the active site cysteine to form a stable tetrahedral intermediate *(vide infra)*. The reactivity of a carbonyl-based warhead is dependent on the electrophilicity of the C=O carbon. Consequently, a warhead that displays low to moderate chemical reactivity would be anticipated to exhibit higher selectivity toward human proteases and diminished off-target effects. Furthermore, a warhead that is structurally-amenable to exploiting favorable binding interactions with the S' subsites,[180] would provide additional advantages. In continuing our foray in this area,[140,151c-g,158,160] and based on the aforementioned considerations, we describe herein the results of exploratory studies related to the inhibition of NV 3CLpro by α-ketophosphonates (structure (I), Figure 5.1).

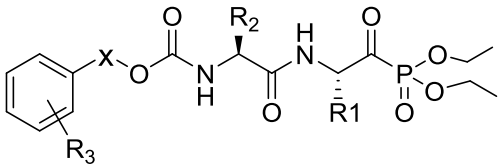

Figure 5.1 General structure (I) of 3CL protease inhibitor.

Inhibitor (I) was envisaged to function as a transition state inhibitor resulting in the inactivation of the enzyme via the formation of a stable tetrahedral adduct (Figure 5.2). To our knowledge, this is the first time that α-ketophosphonates have been used in the inhibition of a viral cysteine protease.

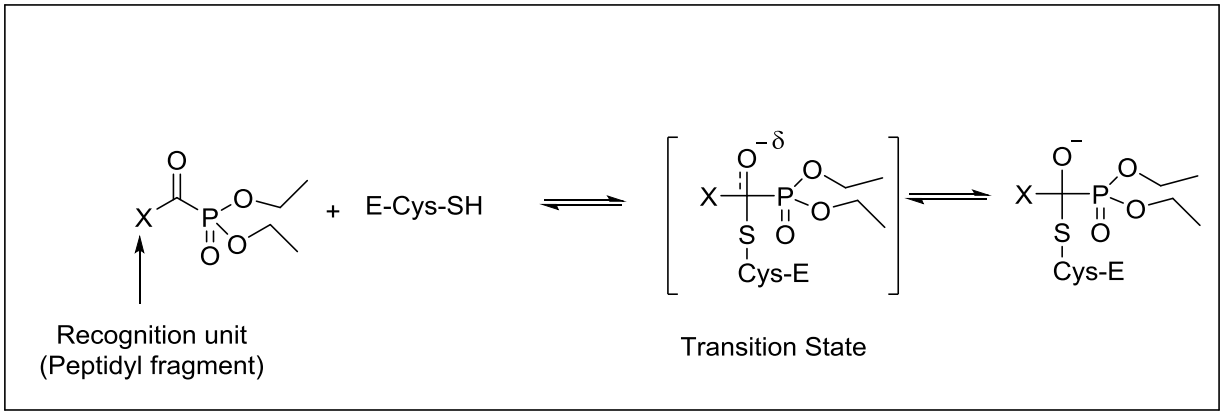

Figure 5.2 Transition state tetrahedral adduct.

5.2 Chemistry

The synthesis of α-ketophosphonates ***9a-h*** was carried out as shown in Scheme 5.1. Thus, the appropriate amino acid was converted to the corresponding amino acid ester ***1*** via treatment with thionyl chloride/dry methanol and the generated esters were treated with trichloromethyl chloroformate to form the corresponding isocyanates. Refluxing with an appropriate alcohol in acetonitrile in the presence of trimethylamine yielded the corresponding carbamates ***3.*** Subsequent hydrolysis yielded the acids which were coupled to glutamine surrogate ***12*** to yield intermediates ***5*****.** Sequential reduction and oxidation with lithium borohydride and Dess-Martin periodinane reagent,

respectively, yielded aldehydes ***7*** which were reacted with diethyl phosphite in the presence of diisopropyl ethyl amine in dichloromethane to yield the corresponding α-hydroxyphosphonates which, upon treatment with Dess-Martin reagent, yielded final products ***9a-h.***

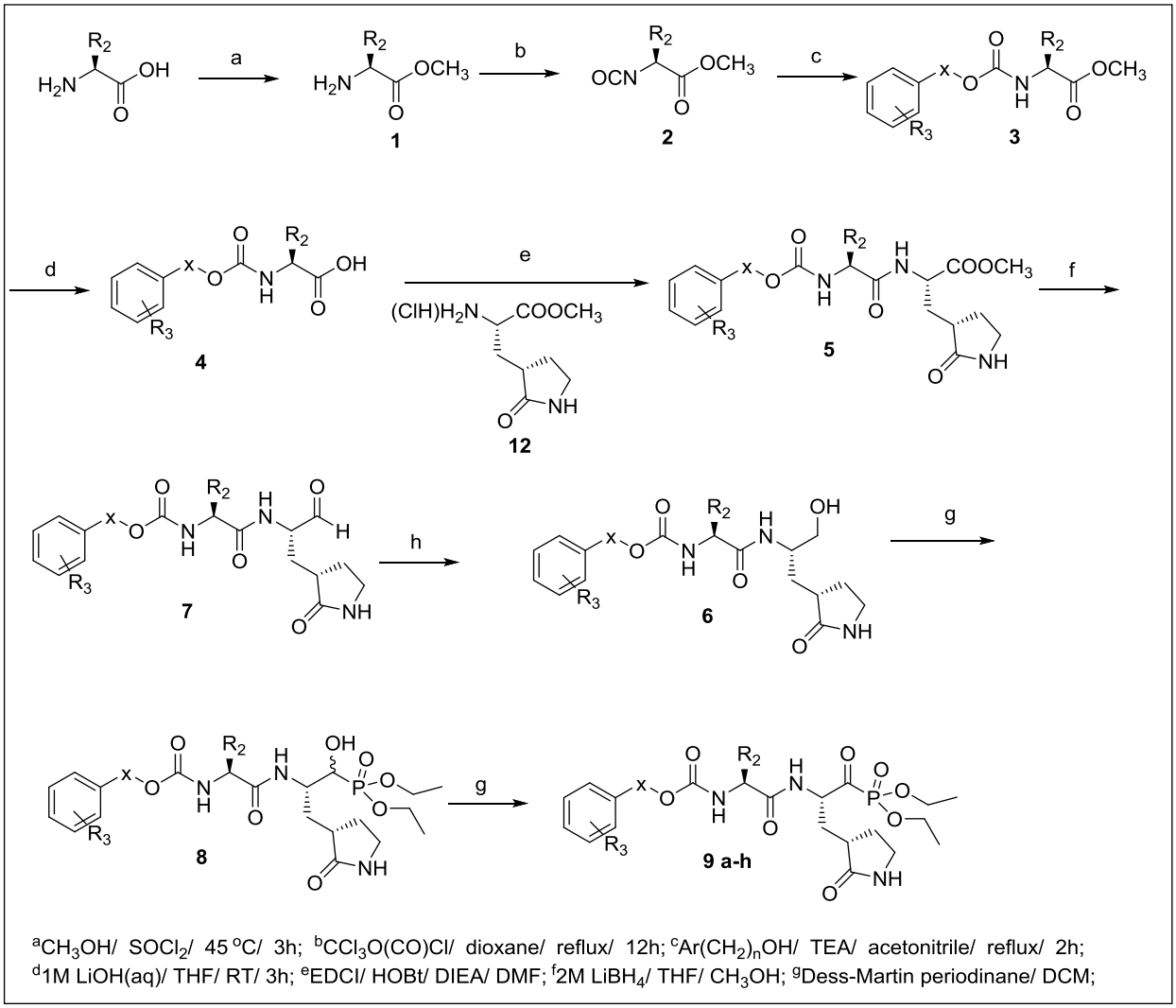

Scheme 5.1 Synthesis of inhibitors ***9a-9h***

5.3 Experimental Section

5.3.1 General

Reagents and dry solvents were purchased from various chemical suppliers (Chem-Impex, Acros Organics, TCI America, Aldrich, and Bachem) and were used as obtained. Silica gel (230-450 mesh) used for flash chromatography was purchased from Sorbent Technologies (Atlanta, GA). Thin layer chromatography was performed using Analtech silica gel plates (Newark, DE). Visualization was accomplished using UV light and/or iodine. NMR spectra were recorded in $CDCl_3$ or DMSO-d_6 using a Varian XL-400 spectrometer. Melting points were recorded on a Mel-Temp apparatus and are uncorrected. High resolution mass spectrometry (HRMS) was performed at the University of Kansas Mass Spectrometry lab using an LCT Premier mass spectrometer (Waters, Milford, MA) equipped with a time of flight mass analyzer and an electrospray ion source or in-house using a G6230B TOF MS (Agilent Technologies, Santa Clara, CA). The purity of the synthesized compounds was established using HPLC and was >95%.

Synthesis of amino acid methyl esters 1. General procedure. To a 250 mL RB flask (oven dried and purged with nitrogen) was added absolute methanol (30 mL) and the solution was cooled to 0 ^{0}C in an ice bath while kept under a nitrogen atmosphere. Thionyl chloride (8 mL) was added to the cooled methanol with stirring, followed by the addition of the amino acid (100 mmol). The ice bath was replaced by a water bath and the reaction mixture was heated to ~50 ^{0}C for 3 h with stirring. Removal of the solvent left a white residue which was washed with diethyl ether (250 mL) and collected by vacuum filtration to yield the amino acid methyl ester hydrochloride ***1*** as a white solid (yield ~90%).

Synthesis of amino acid methyl ester isocyanates. General procedure. Amino acid methyl ester hydrochloride (100 mmol) was placed in a dry 500-mL RB flask and then dried overnight on the vacuum pump. The flask was flushed with nitrogen and dry dioxane (200 mL) was added followed by trichloromethyl chloroformate (29.67 g, 150 mmol), and the reaction mixture was refluxed for 10 h. The solvent was removed on the rotary evaporator and the residue was vacuum distilled to yield pure isocyanate ***2*** as a colorless oil (yield ~85%).

Synthesis of substituted benzyl carbamates 3. General procedure. A solution of substituted benzyl alcohol (20 mmol) in dry acetonitrile (15 mL) was treated with triethylamine (4.05 g, 40 mmol) followed by the amino acid methyl ester isocyanate (20 mmol). The resulting solution was refluxed for 2 h and then allowed to cool to room temperature. The solution was concentrated and the residue was taken up in ethyl acetate (75 mL). The organic layer was washed with 5% HCl (2 x 20 mL) and brine (20 mL). The organic layer was dried over anhydrous sodium sulfate, filtered and concentrated, leaving a colorless oil (compound ***3***) (yield ~92%).

Synthesis of acids 4. General procedure. A solution of ester ***3*** (20 mmol) in tetrahydrofuran (30 mL) was treated with 1M LiOH (40 mL). The reaction mixture was stirred for 3 h at room temperature and the disappearance of the ester was monitored by TLC. Most of the solvent was evaporated off and the residue was diluted with water (25 mL). The solution was acidified to pH ~3 using 5% hydrochloride acid (20 mL) and the aqueous layer was extracted with ethyl acetate (3 x 100 mL). The combined organic layers were dried over anhydrous sodium sulfate, filtered, and concentrated to yield compound **4** as a colorless sticky solid or oil (yield ~100%).

Synthesis of compounds 5. General Procedure. To a solution of compound ***4*** (10 mmol) in dry DMF (20 mL) was added EDCI (2.40 g, 12.5 mmol, 1.25 eq), HOBt (1.92 g, 12.5 mmol, 1.25 eq) and the mixture was stirred for 30 minutes at room temperature. In a separate flask, a solution of deprotected glutamine surrogate ***12*** (2.23 g, 10 mmol) in DMF (15 mL) cooled to 0-5 ^{o}C was treated with diisopropylethylamine (DIEA) (9.5 g, 40 mmol, 4 eq), stirred for 30 minutes, and then added to the reaction mixture containing acid. The reaction mixture was stirred for 12 h while monitoring the reaction by TLC. The solvent was removed and the residue was partitioned between ethyl acetate (200 mL) and 10% citric acid (2 x 40 mL). The ethyl acetate layer was further washed with saturated aqueous $NaHCO_3$ (40 mL), followed by saturated NaCl (50 mL). The organic layer was dried over anhydrous sodium sulfate, filtered and concentrated to yield a yellow-colored oily product. Purification by flash chromatography yielded ester compound ***5*** as a white solid (yield ~65-70%)**.**

Synthesis of alcohols 6. General procedure. To a solution of ester ***5*** (5 mmol) in anhydrous THF (30 mL) was added lithium borohydride (2M in THF, 7.5 mL, 15 mmol) dropwise, followed by absolute ethyl alcohol (15 mL), and the reaction mixture was stirred at room temperature overnight. The reaction mixture was then acidified by adding 5% HCl and the pH adjusted to ~2. Removal of the solvent left a residue which was taken up in ethyl acetate (100 mL). The organic layer was washed with brine (25 mL), dried over anhydrous sodium sulfate, filtered, and concentrated to yield compound ***6*** as a white solid (yield ~90%).

Synthesis of aldehydes 7. General procedure. Compound ***6*** (5 mmol) was dissolved in anhydrous dichloromethane (50 mL) under a nitrogen atmosphere and cooled to 0^{o}C.

Dess-Martin periodinane reagent (3.18 g, 7.5 mmol, 1.5 eq) was added to the reaction mixture with stirring. The ice bath was removed and the reaction mixture was stirred at room temperature for 3 h (monitoring by TLC indicated complete disappearance of the starting material). A solution of 10% aqueous sodium thiosulfate (20 mL) was added and the solution was stirred for another 15 minutes. The aqueous layer was removed and the organic layer was washed with 10% aqueous sodium thiosulfate (20 mL), followed by saturated aqueous sodium bicarbonate (2 x 20 mL), water (2 x 20 mL) and brine (20 mL). The organic layer was dried over anhydrous sodium sulfate, filtered and concentrated. The yellow residue was purified by flash chromatography (silica gel/methylene chloride/ethyl acetate/methanol) to yield a white solid ***7*** (yield ~70-80%).

Synthesis of α-Hydroxyphosphonates *8*. General procedure. To a solution of diethylphosphite (135 mg, 1 mmol) in dry dichloromethane (3.5 mL) was added DIEA (129 mg, 1 mmol) followed by a solution of aldehyde ***7*** (1 mmol) in dichloromethane (5 mL). The reaction mixture was stirred at room temperature for 20 h. The reaction mixture was diluted with dichloromethane (100 mL) and washed with 5% HCl (2 x 20 mL), and brine (30 mL). The organic layer was dried over anhydrous sodium sulfate, filtered and concentrated, leaving a light yellow solid which was purified by flash chromatography to yield compound ***8*** as a white solid (yield ~65%).

Synthesis of α-ketophosphonates *9*. General procedure. Compound ***8*** (5 mmol) was dissolved in anhydrous dichloromethane (50 mL) under a nitrogen atmosphere and cooled to 0^{o}C. Dess-Martin periodinane reagent (3.18 g, 7.5 mmol, 1.5 eq) was added to the reaction mixture with stirring. The ice bath was removed and the reaction mixture was stirred at room temperature for 3 h (monitoring by TLC indicated complete disappearance

of the starting material). A solution of 10% aqueous sodium thiosulfate (20 mL) was added and the solution was stirred for another 15 minutes. The aqueous layer was removed and the organic layer was washed with 10% aqueous sodium thiosulfate (20 mL), followed by saturated aqueous sodium bicarbonate (2 x 20 mL), water (2 x 20 mL) and brine (20 mL). The organic layer was dried over anhydrous sodium sulfate, filtered and concentrated. The yellow residue was purified by flash chromatography (silica gel/methylene chloride/ethyl acetate/methanol) to yield a white solid ***9*** (yield ~60-80%).

benzyl ((S)-1-(((S)-1-(diethoxyphosphoryl)-1-oxo-3-((S)-2-oxopyrrolidin-3-yl)propan-2-yl)amino)-4-methyl-1-oxopentan-2-yl)carbamate (9a): Yield (67 %), mp 53-54 ^{0}C. ^{1}H NMR (400 MHz, $CDCl_3$-*d*) δ ppm 0.80 - 1.01 (m, 6 H) 1.23 - 1.28 (m, 6 H) 1.31 - 1.41 (m, 2 H) 1.48 - 1.60 (m, 1 H) 1.63 - 1.79 (m, 2 H) 1.87 - 1.96 (m, 1 H) 2.27 - 2.54 (m, 2 H) 3.26 - 3.38 (m, 2 H) 4.10 - 4.28 (m, 5 H) 4.31 (dd, *J*=8.54, 4.78 Hz, 1 H) 5.10 (d, *J*=3.81 Hz, 2 H) 7.34 (br. s., 5 H) 7.53 (dd, *J*=5.69, 3.30 Hz, 1 H) 7.71 (dd, *J*=5.69, 3.30 Hz, 1 H) 8.43 - 8.47 (m, 1 H). ^{31}P NMR (162 MHz, DMSO-d_6) δ ppm -2.31 (s, major isomer, 86%) -2.21 (s, minor isomer, 14%). HRMS (ESI) calcd for $C_{25}H_{38}N_3O_8P$: [M+H]: 540.25. Found: 540.25. (HPLC %).

phenethyl ((S)-1-(((S)-1-(diethoxyphosphoryl)-1-oxo-3-((S)-2-oxopyrrolidin-3-yl)propan-2-yl)amino)-4-methyl-1-oxopentan-2-yl)carbamate (9b): Yield (61 %), mp 51-52 ^{0}C. ^{1}H NMR (400 MHz, DMSO-d_6) δ ppm 0.83 (d, *J*=6.49 Hz, 6 H) 1.18 - 1.26 (m, 6 H) 1.34 - 1.45 (m, 2 H) 1.58 (d, *J*=6.49 Hz, 2 H) 1.74 - 1.91 (m, 1 H) 2.10 (d, *J*=6.20 Hz, 2 H) 2.19 - 2.34 (m, 1 H) 2.82 (br. s., 2 H) 2.99 - 3.15 (m, 2 H) 3.95 - 4.05 (m, 1 H) 4.06 - 4.20 (m, 5 H) 4.64 (br. s., 2 H) 7.14 - 7.31 (m, 5 H) 7.49 (br. s., 1 H) 7.59 (d, *J*=7.66 Hz, 1 H) 8.40 (d, *J*=7.57 Hz, 1 H). ^{31}P NMR (162 MHz, DMSO-d_6) δ ppm -2.30 (s, major

isomer, 86%) -2.24 (s, minor isomer, 14%). HRMS (ESI) calcd for $C_{26}H_{40}N_3O_8P$: [M+H]: 554.26. Found: 554.25.

3-chlorobenzyl ((S)-1-(((S)-1-(diethoxyphosphoryl)-1-oxo-3-((S)-2-oxopyrrolidin-3-yl)propan-2-yl)amino)-4-methyl-1-oxopentan-2-yl)carbamate (9c): Yield (77 %), mp 65-67 ^{0}C. ^{1}H NMR (400 MHz, DMSO-d_6) δ ppm 0.84 - 0.92 (m, 6 H) 1.26 (td, *J*=6.93, 4.69 Hz, 6 H) 1.42 - 1.52 (m, 2 H) 1.59 - 1.78 (m, 2 H) 1.85 - 1.96 (m, 1 H) 1.99 - 2.18 (m, 2 H) 2.33 - 2.44 (m, 1 H) 3.01 - 3.19 (m, 2 H) 4.03 - 4.19 (m, 6 H) 5.04 (d, *J*=6.64 Hz, 2 H) 7.26 - 7.33 (m, 1 H) 7.37 (br. s., 2 H) 7.40 (d, *J*=6.64 Hz, 1 H) 7.50 - 7.54 (m, 1 H) 7.68 - 7.71 (m, 1 H) 8.58 - 8.65 (m, 1 H). ^{31}P NMR (162 MHz, DMSO-d_6) δ ppm -2.29 (s, major isomer, 92%) -2.23 (s, minor isomer, 8%). HRMS (ESI) calcd for $C_{25}H_{37}ClN_3O_8P$: [M+H]: 574.21. Found: 574.21. (HPLC %).

3-chlorophenethyl ((S)-1-(((S)-1-(diethoxyphosphoryl)-1-oxo-3-((S)-2-oxopyrrolidin-3-yl)propan-2-yl)amino)-4-methyl-1-oxopentan-2-yl)carbamate (9d): Yield (63 %), mp 55-57 ^{0}C. ^{1}H NMR (400 MHz, DMSO-d_6) δ ppm 0.85 (d, *J*=5.91 Hz, 6 H) 1.20 - 1.29 (m, 6 H) 1.44 (br. s., 2 H) 1.51 - 1.70 (m, 2 H) 1.80 - 1.93 (m, 1 H) 2.08 - 2.20 (m, 2 H) 2.35 - 2.44 (m, 1 H) 2.86 (br. s., 2 H) 3.04 - 3.20 (m, 2 H) 3.98 - 4.07 (m, 1 H) 4.07 - 4.26 (m, 5 H) 4.73 (d, *J*=8.59 Hz, 2 H) 7.22 (d, *J*=5.81 Hz, 1 H) 7.25 - 7.30 (m, 1 H) 7.32 (d, *J*=4.35 Hz, 2 H) 7.69 (br. s., 1 H) 8.22 (d, *J*=7.47 Hz, 1 H) 8.52 (d, *J*=7.08 Hz, 1 H). ^{31}P NMR (162 MHz, DMSO-d_6) δ ppm -2.31 (s, major isomer, 85%) -2.24 (s, minor isomer, 15%). HRMS (ESI) calcd for $C_{26}H_{39}ClN_3O_8P$: [M+H]: 588.22. Found: 588.21.

benzyl ((S)-3-cyclohexyl-1-(((S)-1-(diethoxyphosphoryl)-1-oxo-3-((S)-2-oxopyrrolidin-3-yl)propan-2-yl)amino)-1-oxopropan-2-yl)carbamate (9e): Yield (76 %), mp 62-64 ^{0}C. ^{1}H NMR (400 MHz, DMSO-d_6) δ ppm 0.75 - 0.91 (m, 3 H) 1.08 (br. s., 2 H) 1.23

(td, *J*=6.88, 4.69 Hz, 6 H) 1.38 - 1.48 (m, 2 H) 1.51 - 1.73 (m, 6 H) 1.79 - 1.90 (m, 1 H) 1.94 - 2.02 (m, 1 H) 2.03 - 2.16 (m, 1 H) 2.16 - 2.27 (m, 1 H) 2.29 - 2.39 (m, 1 H) 2.97 - 3.17 (m, 2 H) 4.08 (dt, *J*=10.13, 7.63 Hz, 6 H) 4.99 (s, 2 H) 7.31 (br. s., 5 H) 7.36 - 7.40 (m, 1 H) 7.65 (s, 1 H) 8.49 - 8.57 (m, 1 H). ^{31}P NMR (162 MHz, DMSO-d_6) δ ppm -2.31 (s, major isomer, 91%) -2.24 (s, minor isomer, 9%). HRMS (ESI) calcd for $C_{28}H_{42}N_3O_8P$: [M+H]: 580.28. Found: 580.28. (HPLC %).

phenethyl ((S)-3-cyclohexyl-1-(((S)-1-(diethoxyphosphoryl)-1-oxo-3-((S)-2-oxopyrrolidin-3-yl)propan-2-yl)amino)-1-oxopropan-2-yl)carbamate (9f): Yield (59 %), mp 58-59 ^{0}C. ^{1}H NMR (400 MHz, DMSO-d_6) δ ppm 0.86 (dd, *J*=11.86, 6.79 Hz, 3 H) 1.12 (br. s., 2 H) 1.21 - 1.33 (m, 6 H) 1.37 - 1.51 (m, 2 H) 1.57 - 1.76 (m, 6 H) 1.82 - 1.95 (m, 1 H) 2.15 (d, *J*=3.91 Hz, 2 H) 2.22 - 2.30 (m, 1 H) 2.35 - 2.42 (m, 1 H) 2.81 - 2.90 (m, 2 H) 3.03 - 3.20 (m, 2 H) 3.97 - 4.04 (m, 1 H) 4.06 - 4.21 (m, 5 H) 4.72 (s, 2 H) 7.19 - 7.33 (m, 5 H) 7.52 (br. s., 1 H) 7.69 (s, 1 H) 8.52 (d, *J*=7.13 Hz, 1 H). ^{31}P NMR (162 MHz, DMSO-d_6) δ ppm -2.31 (s, major isomer, 90%) -2.24 (s, minor isomer, 10%). HRMS (ESI) calcd for $C_{29}H_{44}N_3O_8P$: [M+H]: 594.29. Found: 594.29. (HPLC %).

3-chlorobenzyl ((S)-3-cyclohexyl-1-(((S)-1-(diethoxyphosphoryl)-1-oxo-3-((S)-2-oxopyrrolidin-3-yl)propan-2-yl)amino)-1-oxopropan-2-yl)carbamate (9g): Yield (81 %), mp 64-65 ^{0}C. ^{1}H NMR (400 MHz, $CDCl_3$-*d*) δ ppm 0.84 - 1.01 (m, 3 H) 1.11 - 1.29 (m, 4 H) 1.33 - 1.43 (m, 6 H) 1.50 (br. s., 2 H) 1.67 (br. s., 4 H) 1.81 - 1.98 (m, 2 H) 2.15 - 2.24 (m, 1 H) 2.28 - 2.55 (m, 2 H) 3.36 (d, *J*=8.93 Hz, 2 H) 4.05 - 4.16 (m, 1 H) 4.18 - 4.29 (m, 4 H) 4.34 (d, *J*=4.30 Hz, 1 H) 5.08 (s, 2 H) 5.33 (d, *J*=8.30 Hz, 1 H) 5.88 (br. s., 1 H) 7.22 (d, *J*=4.10 Hz, 1 H) 7.25 - 7.30 (m, 2 H) 7.36 (br. s., 1 H) 8.46 (br. s., 1 H). ^{31}P NMR

(162 MHz, $CDCl_3$-*d*) δ ppm -2.33 (s, major isomer, 88%) -2.24 (s, minor isomer, 12%). HRMS (ESI) calcd for $C_{28}H_{41}ClN_3O_8P$: [M+H]: 614.24. Found: 614.24. (HPLC %).

3-chlorophenethyl ((S)-3-cyclohexyl-1-(((S)-1-(diethoxyphosphoryl)-1-oxo-3-((S)-2-oxopyrrolidin-3-yl)propan-2-yl)amino)-1-oxopropan-2-yl)carbamate (9h): Yield (72 %), mp 56-58 ^{0}C. ^{1}H NMR (400 MHz, DMSO-d_6) δ ppm 0.75 - 0.88 (m, 3 H) 1.04 - 1.16 (m, 2 H) 1.23 (d, *J*=4.30 Hz, 6 H) 1.36 - 1.46 (m, 2 H) 1.50 - 1.74 (m, 6 H) 1.80 - 1.91 (m, 1 H) 1.92 - 2.04 (m, 1 H) 2.08 - 2.16 (m, 1 H) 2.18 - 2.27 (m, 1 H) 2.30 - 2.40 (m, 1 H) 2.80 - 2.87 (m, 2 H) 3.04 - 3.17 (m, 2 H) 3.98 - 4.20 (m, 6 H) 4.68 (s, 2 H) 7.17 - 7.21 (m, 1 H) 7.22 - 7.27 (m, 2 H) 7.28 - 7.32 (m, 1 H) 7.38 - 7.39 (m, 1 H) 7.65 - 7.67 (m, 1 H) 8.46 - 8.51 (m, 1 H). ^{31}P NMR (162 MHz, $CDCl_3$-*d*) δ ppm -2.30 (s, major isomer, 90%) -2.23 (s, minor isomer, 10%). HRMS (ESI) calcd for $C_{29}H_{43}ClN_3O_8P$: [M+H]: 628.26. Found: 628.25. (HPLC %).

5.3.2 FRET Protease Assays/Enzyme Assays and Inhibition Studies

The FRET protease assay was performed by preparing stock solutions of the substrate (Edans-DFHLQ/GP-Dabcyl and inhibitor in DMSO and diluting into assay buffer which was comprised of 20mM HEPES buffer, pH 8, containing NaCl (200 mM), 0.4 mM EDTA, glycerol (60%), and 6 mM dithiothreitol (DTT). The protease was mixed with serial dilutions of each compound or with DMSO in 25 µL of assay buffer and incubated at 37^{o}C for 30 min, followed by the addition of 25 µL of assay buffer containing substrate. Fluorescence readings were obtained using an excitation wavelength of 360 nm and an emission wavelength of 460 nm on a fluorescence microplate reader (FLx800; Biotec, Winoosk, VT) 1 h following the addition of substrate. Relative fluorescence units (RFU) were determined by subtracting background values (substrate-containing well without protease) from the raw fluorescence values, as described previously.[140,158,160] The dose-dependent FRET inhibition curves were fitted with a variable slope by using GraphPad Prism software (GraphPad, La Jolla, CA) in order to determine the IC_{50} values of the inhibitors.

5.3.3 Cell-based inhibition assays

These were carried out as previously described on page 69.

5.3.4 Nonspecific cytotoxicity effects

These were carried out as previously described on page 117.

5.4 Results and Discussion

The inhibitory activity of the synthesized compounds against NV 3CLpro and their anti-norovirus activity in a cell-based replicon system were evaluated as described in the experimental section.[140,158] The determined IC_{50} values in enzyme assay and EC_{50} values against NV in replicon harboring cells (HG23 cells) are listed in Table 5.1 and they are the average of at least two determinations.

Inspection of the results shown in Table 5.1 reveals that, in general, α-ketophosphonates exhibit potent anti-norovirus activity in a cell-based replicon system. Consistent with previous findings,[151a-g,158,175,181] the replacement of the P2 leucine residue with cyclohexyl alanine augmented the inhibitory activity of the compounds (compare ***9b/9f***, ***9c/9g***, and ***9d/9h*** in Table 5.1). The effect of ring substituents was also explored to further enhance pharmacological activity. Compounds with a chlorine at the meta position[158] were particularly effective (compounds ***9c, 9d, 9g, and 9h***). Importantly, cell cytotoxicity was found to be minimal.

TABLE 5.1 ANTI-NV ACTIVITY OF COMPOUNDS ***9A-9H*** IN ENZYME (IC_{50}) AND CELL-BASED (EC_{50}) ASSAY

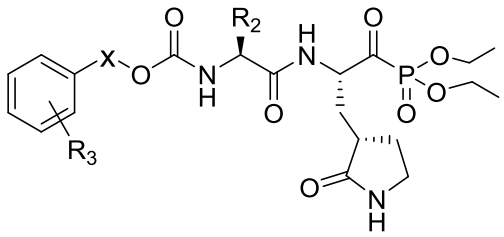

Compound	R_3	X	R_2	IC_{50} (µM)	EC_{50} (µM)	CC_{50} (µM)
9a	H	CH_2	Isobutyl	2.8	2.4	> 100
9b		CH_2CH_2		42.5	14.7	> 100
9c	m-Cl	CH_2		3.2	1.3	> 100
9d		CH_2CH_2		17.5	8.2	> 100
9e	H	CH_2	Cyclohexyl methyl	3.2	2.5	> 100
9f		CH_2CH_2		12.4	3.3	> 100
9g	m-Cl	CH_2		1.7	0.8	> 100
9h		CH_2CH_2		4.3	1.8	> 100

5.5 Conclusions

The design of a novel series of dipeptidyl transition state inhibitors of NV 3CL protease that incorporate their structure an α-ketophosphonate warhead is described for the first time. The limited structure-activity relationship studies described herein reveal that peptidyl α-ketophosphonate inhibitors are a promising class of inhibitors of viral cysteine proteases of potential therapeutic value.

CHAPTER VI

CONCLUSIONS

The studies described in this dissertation have focus on norovirus 3CL and MERS-CoV 3CL proteases. Structural, synthetic, biochemical, and in vivo studies have been carried out in order to delineate the role of NV 3CLpro in norovirus infection. Specifically, a structure-based approach was used to design a novel series of potent and selective dipeptidyl TS inhibitors and TS mimics of norovirus 3CL protease. Proof of principle has been demonstrated in an animal model (mouse model) of norovirus infection (in vivo studies in gnotobiotic pigs are ongoing), thereby establishing that NV 3CLp is a druggable target for developing anti-norovirus therapeutics.

High resolution X-ray crystal structures established the mechanism of action of the inhibitors and revealed the key amino acid residues involved in binding. These studies have laid a solid structural framework for designing more effective inhibitors of the enzyme. Furthermore, a general approach toward the optimization of the pharmacokinetics of peptidyl and non-peptidyl transition state inhibitors via the synthesis of ester and carbamate prodrugs of aldehyde bisulfite adducts is reported. The approach has wide applicability and can be extended to transition state inihibitors of other cysteine and seriene proteases of clinical relevance. Specifically, it provides an effective means of augmenting the therapeutic potential of these classes of inhibitors.

More importantly, an inhibitor of feline infectious peritonitis virus (FIPV) has been identified and shown in clinical trials to be effective in curing FIPV infection (in clinical development). **This is the first demonstration of clinical efficacy of a coronavirus**

protease inhibitor. This approach could, in principle, be extended to other coronaviruses such as SARS and MERS-CoV (unpublished data and ongoing studies).

In conclusion, norovirus and MERS-CoV 3CL proteases are druggable targets for the development of therapeutics and prophylactics for norovirus and MERS-CoV infections.

REFERENCES

REFERENCES

1. Koo, H. L.; Ajami, N.; Atmar, R. L.; DuPont, H. L. Noroviruses: the leading cause of gastroenteritis worldwide. *Discov. Med.* **2010**, *10*: 61-70.

2. Hall, A. J.; Lopman, B. A.; Payne, D. C.; Patel, M. M.; Gastanaduy, P. A.; Vinje, J.; Parashar, U. D. Norovirus disease in the United States. *Emerg. Infect. Dis.* **2013**, *19*: 1198-1205.

3. Lee, B.E.; Pang, X-L. New strains of norovirus and the mystery of viral gastroenteritis epidemics. *Can Med Assoc J*. **2013**, 185:1381-1382.

4. White, P.A. Evolution of norovirus. Clin Microbiol Infect. **2014**, 20:741-745.

5. Lopman, B.A.; Steele, D.; Kirkwood, C.D.; Parashar, U.D. The vast and varied global burden of norovirus: Prospects for prevention and control. PLoS Medicine. 2016, 13(4): e1001999.

6. Bartsch, S.M.; Lopman, B.A.; Ozawa, S.; Hall, A.J.; Lee, B.Y. Global economic burden of norovirus gastroenteritis. *PLoS One*. **2016**, 11(4): e0151219.

7. Cates, S.C.; Kosa, K.M.; Brophy, J.E.; Hall, A.J.; Fraser, A. Consumer education needed on norovirus prevention and control: findings from a nationally representative survey of U.S. adults. *J. Food. Prot*. **2015**, 78(3):484-490.

8. http://www.cdc.gov/norovirus (accessed on August 16, 2016)

9. Hall, A.J.; Wikswo, M.E.; Pringle, K.; Gould, L.H.; Parashar U.D. Division of viral disease NCfl, vital signs: foodborne norovirus Outbreaks-United States, 2009-2012. *MMWR Morb Mortal Wkly Rep*. **2014**, 63(22): 491-495.

10. Lanata, C.F.; Fischer-Walker, C.L.; Olascoaga, A.C.; Torres, C.X.; Aryee, M.J.; Black, R.E.; Child Health Epidemiology Reference Group of the World Health Organization and UNICEF. Global cause of diarrheal disease mortality in children <5 years of age: a systematic review. *PLoS One*. **2013**, 8(9): e72788.

11. Huang, P.; Farkas, T.; Zhong, W.;Tan, M.;Thornton, S.; Morrow, A.L.; Jiang X. Norovirus and Histo-Blood Group Antigens: Demonstration of a Wide Spectrum of Strain Specificities and Classification of Two Major Binding Groups among Multiple Binding Patterns. *J. Virol*. **2005**, 79(11): 6714-6722.

12. Fankhauser, R.L.; Monroe, S.S.; Noel, J.S.; Humphrey, C.D.; Bresee, J.S.; Parashar, U.D.; Ando, T.; Glass, R.I. Epidemiologic and molecular trends of “Norwalk-like viruses” associated with outbreaks of gastroenteritis in United States. *J. Infect. Dis*. **2002**, 186: 1-7.

13. Phillips, G.; Tam, C.C.; Rodrigues, L.C.; Lopman, B. Risk factors for symptomatic and asymptomatic norovirus infection in the community. *Epidemiol. Infect.* **2010**,139(11): 1-11.

14. Gotz, H.; Hannelore Götz, H.; Ekdahl, K.; Lindbäck, J.; Jong, B.D.; Hedlund, K.O.; Giesecke, J. Clinical spectrum and transmission characteristics of infection with Norwalk-like virus: findings from a large community outbreak in Sweden. *Clin. Infect. Dis*. **2001**, 33(5): 622-628.

15. Chapin, A.R.; Carpenter, C.M.; Dudley, W.C.; Gibson, L.C.; Pratdesaba, R.; Torres. O.; Sanchez, D.; Belkind-Gerson, J.; Nyquist, I.; Kärnell, A.; Gustafsson, B.; Halpern, J.L.; Bourgeois, A.L.; Schwab, K.J. Prevalence of norovirus among visitors from the United States to Mexico and Guatemala who experience traveler's diarrhea. *J. Clin. Microbiol*. **2005**, 43(3): 1112-1117.

16. Green, K. Y. Caliciviridae: The Noroviruses in *Green's Virology* (Knipe, D. M. and Howley, P. M., eds), Lippincott Williams & Wilkins: Philadelphia. **2007**, 1: 949-979.

17. Kambhampati, A.; Koopmans, M.; Lopman, B.A. Burden of norovirus in healthcare facilities and strategies for outbreak control. *J Hosp. Infect*. **2015**, 89(4): 296-301.

18. Shioda, K.; Kambhampati, A.; Hall, A.J.; Lopman, B.A. Global Age Distribution of Pediatric Norovirus Cases. *Vaccine*. **2015**, 33(33): 4065-4068.

19. Lopman, B.A.; Simmons, K.; Gambhir, M.; Vinjé, J.; Parashar, U.D. Epidemiologic implications of asymptomatic reinfection: a mathematical modeling study of norovirus. *Am. J. Epidemiol*. **2014**, 179(4): 507-512.

20. Parashar, U.D.; Quiroz, E.S.; Mounts, A.W. Norwalk-like viruses. Public health consequences and outbreak management. *Morbidity and Mortality Weekly Report*. **2001**, 50 :1-7.

21. Kendall, M.; Mody, R.; Mahon, B.; Doyle, M.; Herman, K.; Tauxe, R. Emergence of salsa and guacamole as frequent vehicles of foodborne disease outbreaks in the United States, 1973-2008. *Foodborne Patholg. Dis*. **2013**, 10(4): 316-322.

22. Treanor, J.J.; Dolin, R. Norwalk virus and Other Calciviruses. In: Mandell G.L.; Bennett, J.E. 5th Edition ed. *Principles and Practice of Infectious Diseases*. Philadelphia: Churchill Livingstone. **2000**, 2: 1949-1956.

23. Lopman, B.A.; Gastanaduy, P.; Park, G.W; Hall, A,J.; Parashar, U.D.; Vinjé, J. Environmental transmission of norovirus gastroenteritis. *Curr. Opin. Virol*. **2012**, 2(1): 96-102.

24. Bentley, K.; Dove, B.K.; Parks, S.R.; Walker, J.T.; Bennett, A.M. Hydrogen peroxide vapor decontamination of surfaces artificially contaminated with norovirus surrogate feline calcivirus. *J. Hosp. Infect*. **2012**, 80(2): 16-121.

25. Zhang, Y.; Yao, Q.; Xia, C.; Jiang, X.; Wang, P.G. Trapping norovirus by glycosylated hydrogels: a potential oral antiviral drug. *Chem. Med. Chem*. **2006**, 1(12): 1361-1366.

26. Farkas, T.; Sestak, K.; Wei, C.; Jiang, X. Characterization of a rhesus monkey calicivirus representing a new genus of Caliciviridae. *J. Virol*. **2008**, 82: 5408-5416.

27. Caddy, S.; Breiman, A.; Pendu, J.L.; Goodfellow**,** I. Genogroup IV and VI Canine Noroviruses Interact with Histo-Blood Group Antigens. *J. Virol*. **2014**, 88(18): 10377-10391.

28. Muhaxhiri, Z.; Deng, L.; Shanker, S.; Sankaran, B.; Estes, M.K.; Palzkill, T.; Song, Y.; Prasad, B.V.V. Structural basis of substrate specificity and protease inhibition in Norwalk virus. *J. Virol*. **2013**, 87(8): 4281-4292.

29. Galasiti Kankanamalage, A.C.; Weerawarna, P.M.; Kim, Y.; Chang, K.O.; Groutas, W.C. Anti-norovirus therapeutics: a patent review (2010-2015). *Exp. Opin. Ther. Pat*. **2016**, 26(3): 297-308.

30. Tan, M.; Huang, P.; Meller, J.; Zhong, W.; Farkas, T.; Jiang, X. Mutations within the P2 domain of norovirus capsid affect binding to human histo-blood group antigens: evidence for a binding pocket*. J Virol*, **2003**. 77(23): 12562-71.

31. Chen, R.; Neill, J.D.; Noel, J.S.; Hutson, A.M.; Glass, R.I.; Estes, M.K.; Prasad, B.V. Inter- and intragenus structural variations in caliciviruses and their functional implications*. J Virol*. **2004**, 78(12): 6469-79.

32. Lindesmith, L.C.; Donaldson, E.F.; Lobue, A.D.; Cannon, J.L.; Zheng, D.P.; Vinje, J.; Baric, R.S. Mechanisms of GII.4 norovirus persistence in human populations*. PLoS Med*. **2008**, 5(2): e31.

33. Thorne, L.G.; Goodfellow, I. Norovirus gene expression and replication. *J. Gen. Virol*. **2014**, 95:278–291.

34. Bull, R.A.; White, P.A. Mechanisms of GII.4 norovirus evolution*. Trends Microbiol*, **2011**, 19(5): 233-240.

35. Hardy, M.E. Norovirus protein structure and function. *Microbiol Lett*. **2005**, 253:1-8.

36. Vinjé, J. Advances in laboratory methods for detection and typing of norovirus. *J. Clin. Microbiol*. **2015**, 53(2):373-81.

37. Subba-Reddy, C.V.; Yunus, M.A.; Goodfellow, I.; Kao, C.C. Norovirus RNA Synthesis is Modulated by an Interaction Between the Viral RNA-Dependent RNA Polymerase and the Major Capsid Protein, VP1. *J. Virol*. **2012**, 86: 10138-10149.

38. Liu, W.; Chen, Y.; Jiang, X.; Xia, M.; Yang, Y.; Tan, M.; Li, X.; Rao, Z. A Unique Human Norovirus Lineage with a Distinct HBGA Binding Interface. *PLoS Pathog*. **2015**, 11 (7): e1005025.

39. Tan, M.; Jiang, X. Norovirus gastroenteritis, carbohydrate receptors and animal models. *PLoS Pathog*. **2010**, 6 (8): e1000983.

40. Han, L.; Kitova, E.N.; Tan, M.; Jiang, X.; Pluvinage, B.; Boraston, A.B.; Klassen, J.S. Affinities of Histo-blood Group Antigens for Norovirus Capsid Protein Complexes. *Glycobiology* **2015**, 25: 170-180.

41. Alhatlani, B.; Vashist, S.; Goodfellow, I. Functions of the 5′ and 3′ Ends of Calicivirus Genomes. *Virus. Res*. **2015**, 206: 134-143.

42. Wobus, C.E.; Karst, S.M.; Thackray, L.B.; Chang, K.O.; Sosnovtsev, S.V.; Belliot, G.; Krug, A.; Mackenzie,J.M.; Green, K.Y.; Virgin, H.W. Replication of Norovirus in Cell Culture Reveals a Tropism for Dendritic Cells and Macrophages. *PLoS Biol*. **2004**, 2(12): e432.

43. Kim, Y.; Galasiti Kankanamalage, A.C.; Chang, K.O.; Groutas, W.C. Recent Advances in the Discovery of Norovirus Therapeutics. *J. Med. Chem*. **2015**, 58(24): 9438-9450.

44. Lay, M.K.; Atmar, R.L.; Guix, S.; Bharadwaj, U.; He, H.; Neill, F.H.; Sastry, K.J.; Yao, Q.; Estes, M.K. Norwalk virus does not replicate in human macrophages or dendritic cells derived from the peripheral blood of susceptible humans. *Virology*. **2010**, 406(1):1-11.

45. Jones, M.K.; Grau, K.R.; Costantini, V.; Kolawole, A.O.; de Graaf, M.; Freiden, P.; Graves, C.L.; Koopmans, M.; Wallet, S.M.; Tibbetts, S.A.; Schultz-Cherry, S.; Wobus, C.E.; Vinjé, J.; Karst, S.M. Human norovirus culture in B cells. *Nat Protoc*. **2015**, 10(12):1939-1947.

46. (a) Dolin, R.; Levy, A.G.; Wyatt, R.G.; Thornhill, T.S.; Gardner, J.D. Viral gastroenteritis induced by the Hawaii agent. Jejunal histopathology and serologic response. *Am J Med*. **1975**, 59(6):761-768. (b) Troeger, H.; Loddenkemper, C.; Schneider, T.; Schreier, E.; Epple, H.J.; Zeitz, M.; Fromm, M.; Schulzke, J.D. Structural and functional changes of the duodenum in human norovirus infection. *Gut*. **2009**, 58(8):1070-1077. (c) Acute infectious nonbacterial gastroenteritis: etiology and pathogenesis. *Ann Intern Med*. **1972**, 76(6):993-1008. (d) Schreiber, D.S.; Blacklow, N.R.; Trier, J.S. The small intestinal lesion induced by Hawaii agent acute infectious nonbacterial gastroenteritis. *J Infect Dis*. **1974**, 129(6):705-708.

47. Mercer, J.; Schelhaas, M.; Helenius, A. Virus entry by endocytosis. *Annu Rev Biochem*. **2010**, 79: 803-833.

48. Miller, H.; Zhang, J.; Kuolee, R.; Patel, G.B.; Chen, W. Intestinal M cells: the fallible sentinels? *World J Gastroenterol*. **2007**, 13: 1477-1486.

49. Karst, S.M.; Wobus, C.E. A Working Model of How Noroviruses Infect the Intestine. *PLoS Pathog*. **2015**, 11(2): e1004626.

50. Bragazzi Cunha, J.; Wobus, C.E. Select membrane proteins modulate MNV-1 infection of macrophages and dendritic cells in a cell type-specific manner. *Virus Res*. **2016**, 222:64-70.

51. Jones, M.K.; Watanabe, M.; Zhu, S.; Graves, C.L.; Keyes, L.R.; Grau, K.R.; Gonzalez-Hernandez, M.B.; Iovine, N.M.; Wobus, C.E.; Vinjé, J.; Tibbetts, S.A.; Wallet, S.M.; Karst, S.M. Enteric bacteria promote human and mouse norovirus infection of B cells. *Science*. **2014**, 346(6210):755-759.

52. Teunis, P.F.; Sukhrie, F.H.; Vennema, H.; Bogerman, J.; Beersma, M.F.; Koopmans, M.P. Shedding of norovirus in symptomatic and asymptomatic infections. *Epidemiol Infect*. **2014**, 143(8), 1710-1717.

53. Grove, J.; Marsh, M. The cell biology of receptor-mediated virus entry. *J Cell Biol.* **2011**, 195(7):1071-1082.

54. Karst, S. M.; Wobus, C. E.; Goodfellow, I. G.; Green, Y. K.; Virgin, H. W. Advances in Norovirus Biology. *Cell Host Microbe* **2014**, 15: 668-680.

55. Ball, J.M.; Mitchell, D.M.; Gibbons, T.F.; Parr, R.D. Rotavirus NSP4: a multifunctional viral enterotoxin. *Viral Immunol*. **2005**, 18: 27-40.

56. Muller, P.A.; Koscso, B.; Rajani, G.M.; Stevanovic, K.; Berres, M.L.; Hashimoto, D.; Mortha, A.; Leboeuf, M.; Li, X.M.; Mucida, D.; Stanley, E.R.; Dahan, S.; Margolis, K.G.; Gershon, M.D.; Merad, M.; Bogunovic, M. Crosstalk between muscularis macrophages and enteric neurons regulates gastrointestinal motility. *Cell*. **2014**, 158: 300-313.

57. Wouters, M.M.; Boeckxstaens, G.E. Neuroimmune mechanisms in functional bowel disorders. Neth J Med. **2011**, 69: 55-61.

58. Wehner, S.; Behrendt, F.F.; Lyutenski, B.N.; Lysson, M.; Bauer, A.J.; Hirner, A.; Kalff, J.C. Inhibition of macrophage function prevents intestinal inflammation and postoperative ileus in rodents. *Gut*. **2007**, 56: 176-185.

59. Zeitler, C.E.; Esters, M.K.; Venkataram Prasad, B.V.; X-ray crystallographic structure of the Norwalk virus protease at 1.5 ^{0}A resolution. *J. Virol*. **2006**, 80(10): 5050-5058.

60. Someya. Y.; Takeda, N.; Miyamura, T. Identification of active-site amino acid residues in the Chiba virus 3C-like protease. *J. Virol*. **2002**, 76(12): 5949-5958.

61. Schechter, I.; Berger, A. On the size of the active site in protease. I. Papain. *Biochem. Biophys. Res. Comm*. **1967**, 27(2): 57-162.

62. Rawling, N.D. A large and accurate collection of peptidase cleavages in the MEROPS database. *Database*. **2009**, DOI:10.1093/database/bap015.

63. Hussey, R.J.; Coates, L.; Gill, R.S.; Erskine, P.T.; Coker, S-F.; Mitchell, E.; Cooper, J.B.; Wood, S.; Broadbridge, R.; Clarke, I.N.; Lambden, P.R.; Shoolingin-Jordan, P.M. A Structural Study of Norovirus 3C Protease Specificity: Binding of a Designed Active Site-Directed Peptide Inhibitor. *Biochemistry*. **2011**, 50: 240–249.

64. Robilotti, E.; Deresinski, S.; Pinsky, B. A. Norovirus. *Clin. Microbiol. Rev.* **2015**, 28: 134-164.

65. Chang, K. O.; Takahashi, D.; Prakash, O.; Kim, Y. Characterization and Inhibition of Norovirus Proteases of Genogroups I and II Using a Fluorescence Resonance Energy Transfer Assay. *Virology* **2012**, 423: 125-133.

66. Lee, J-H.; Alam, I.; Han, K. R.; Cho, S.; Shin, S.; Kang, S.; Yang, J. M.; Kim, K. H. Crystal Structures of Murine Norovirus-1 RNA-dependent RNA Polymerase. J. Gen. Virol. **2011**, 92: 1607-1616.

67. Adam, I.; Lee, J-H.; Cho, K. J.; Han, K. R.; Yang, J. M.; Chung, M. S.; Kim, K. H. Crystal Structures of Murine Norovirus-1 RNA-dependent RNA Polymerase in Complex with 2-Thiouridine or Ribavirin. *Virology* **2012**, 426: 143-151.

68. Croci, R.; Pezzullo, M.; Tarantino, D.; Milani, M.; Tsay, S-C.; Surshbabu, R.; Tsai, Y-J.; Mastrangelo, E.; Rohayem, J.; Bolognesi, M.; Hwu, J. R. Structural Bases of Norovirus RNA Dependent RNA Polymerase InhibitIon by Novel Suramin-Related Compounds. *PLoS One* **2014**, 9: e91765.

69. Rocha-Pereira, J.; Jochmans, D.; Debing, Y.; Verbeken, E.; Nascimento, M. S. J.; Neyts, J. The Viral Polymerase Inhibitor 2'-C-Methylcytidine Inhibits Norwalk Virus Replication and Protects Against Norovirus-Induced Diarrhea and Mortality in a Mouse Model. *J. Virol.* **2013**, 87: 11798-11805.

70. Constantini, V. P.; Whitaker, T.; Barclay, L.; Lee, D.; McBrayer, T. R.; Schinazi, R. F.; Vinje, J. Antiviral Activity of Nucleoside Analogues Against Norovirus. *Antiviral Ther.* **2012**, 17: 981-991.

71. Rocha-Pereira, J.; Jochmans, D.; Dallmeir, K.; Leyssen, P.; Nascimento, M. S.; Neyts, J. Favipiravir (T-705) Inhibits In Vitro Norovirus Replication. *Biochem. Biophys. Res. Comm.* **2012**, 424: 777-780.

72. Zhang, X.; Tan, M.; Chhabra, M.; Dai, Y.; Meller, J.; Jiang, X. Inhibition of Blood Group Antigen Binding as a Novel Strategy to Block Norovirus Infections. PLoS One **2013**, 8: e69379.

73. Guiard, J.; Kitov, P. I.; Fiege, B.; Peters, T.; Bundle, D. R. "Double-Click" Protocol for Synthesis of Heterobifunctional Multivalent Ligands: Toward a Focused Library of Specific Norovirus Inhibitors. *Chem. Eur. J.* **2011**, 17: 7438-7441.

74. Rademacher, C.; Guiard, J.; Kitov, P. I.; Fiege, B.; Dalton, K. P.; Parra, F.; Bundle, D. R.; Peters, T. Targeting Norovirus Infection – Multivalent Entry Inhibitor Design Based on NMR Experiments. *Chem. Eur. J.* **2011**, 17: 7442-7453.

75. Zhang, X-F.; Tan, M.; Chhabra, M.; Dai, Y-C.; Meller, J.; Jiang, X. Inhibition of Histo-blood Group Antigen Binding as a Novel Strategy to Block Norovirus Infections. *PLoS One* **2013**, 8: e69379.

76. El-Hawiet, A.; Shoemaker, G. K.; Daneshfar, R.; Kitova, E. N.; Klassen, J. S. Applications of a Catch and Release Electrospray Ionization Mass Spectrometry Assay for Carbohydrate Library Screening. *Anal. Chem.* **2012**, 84: 50-58.

77. Feng, X.; Jiang, X. Library Screen for Inhibitors Targeting Norovirus Binding to Histo-blood Group Antigen Receptors. *Antimicrob. Agents Chemother.* **2007**, 51: 324-331.

78. Shivanna, V.; Kim, Y.; Chang, K. O. Endosomal Acidification and Cathepsin L Activity is Required for Calicivirus Replication. *Virology* **2014**, 0, 287-295.

79. Karst, S. M.; Zhu, S.; Goodfellow, I. G. The Molecular Pathology of Noroviruses. *J. Pathol.* **2015**, 235: 206-216.

80. Nagy, P. D.; Pogany, J. The Dependence of viral RNA Replication on Co-Opted Host Factors. *Nat. Rev. Microbiol.* **2012**, 10: 137-149.

81. Vashist, S.; Urena, L.; Chaudhry, Y.; Goodfellow, I. Identification of RNA-Protein Interaction Networks Involved in the Norovirus Life Cycle. *J. Virol.* **2012**, 86: 11977-11990.

82. Chang, K. O. Role of Cholesterol Pathways in Norovirus Replication. *J. Virol.* **2009**, 83: 8587-8595.

83. Vashist, S.; Urena, L.; Gonzalez-Hernandez, M. B.; Choi, J.; de Rougemont, A.; Rocha-Pereira, J.; Neyts, J.; Hwang, S.; Wobus, C. E.; Goodfellow, I. The Molecular Chaperone HSP90 is a Therapeutic Target for Noroviruses. *J. Virol.* **2015**, 89: 6352-6363.

84. Rossignol, J. F.; El-Gohary, Y. Nitazoxanide in Treatment of Viral Gastroenteritis: a Randomized, Double-Blind, Placebo-Controlled Clinical Trial. *Aliment. Pharmacol. Ther.* **2006**, 24*:* 1423-1430.

85. Rossignol, J. F. Nitazoxanide: A First-in-Class Broad-Spectrum Antiviral Agent. *Antiviral Res.* **2014**, 110: 94-103.

86. http://www.who.int/emergencies/mers-cov/en (accessed on December 17, 2016)

87. Drexler, J.F.; Corman, V.M.; Drosten, C. Ecology, evolution and classification of bat coronaviruses in the aftermath of SARS. *Antiviral Res*. **2014**, 101: 45-56.

88. Nowotny, N.; Kolodziejek, J. Middle East respiratory syndrome coronavirus (MERS-CoV) in dromedary camels, Oman, 2013. *Euro Surveill*. **2014**, 19 (16): 20781.

89. Hijawi, B.; Abdallat, M.; Sayaydeh, A.; Alqasrawi, S.; Haddadin, A.; Jaarour, N.; Alsheikh, S.; Alsanouri, T. Novel coronavirus infections in Jordan, April 2012: epidemiological findings from a retrospective investigation. *East Mediterr Health J*. **2013**, 19: S12-18.

90. de Groot, R.J.; Baker, S.C.; Baric, R.S.; Brown, C.S.; Drosten, C.; Enjuanes, L.; Fouchier R.A.M.; Galiano, M.; Gorbalenya, A.E.; Memish, Z.A.; Perlmen, S.; Poon, L.L.M.; Snijder E.J.; Stephens, G.M.; Woo, P.C.Y.; Zaki, A.M.; Zambon, M.; Ziebuhr, J. Middle East respiratory syndrome coronavirus (MERS-CoV): announcement of the Coronavirus Study Group. *J Virol*. **2013**, 87(14): 7790-7792.

91. https://www.cdc.gov/coronavirus/mers/about/symptoms.html (accessed on December 21, 2016)

92. Drosten, C.; Seilmaier, M.; Corman, V.M.; Hartmann, W.; Scheible, G.; Sack, S.; Guggemos, W.; Kallies, R.; Muth, D.; Junglen, S.; Müller, M.A.; Haas, W.; Guberina, H.; Röhnisch, T.; Schmid-Wendtner, M.; Aldabbagh, S.; Dittmer, U.; Gold, H.; Graf, P.; Bonin, F.; Rambaut, A.; Wendtner, C.M. Clinical features and virological analysis of a case of Middle East respiratory syndrome coronavirus infection. *Lancet Infect Dis*. **2013**, 13: 745-751.

93. Zulma, A.; Hui, D.S.; Perlman, S. Middle East respiratory syndrome. *Lancet*. **2015**, 386: 995-1007.

94. Al-Abdallat, M.M.; Payne, D.C.; Alqasrawi, S.; Rha, B.; Tohme, R.A.; Abedi, G.R.; Al Nsour, M.; Iblan, I.; Jarour, N.; Farag, N.H.; Haddadin, A.; Al-Sanouri, T.; Tamin, A.; Harcourt, J.L.; Kuhar, D.T.; Swerdlow, D.L.; Erdman, D.D.; Pallansch, M.A.; Haynes, L.M.; Gerber, S.I.; Jordan MERS-CoV Investigation Team. Hospital-associated outbreak of Middle East respiratory syndrome coronavirus: a serologic, epidemiologic, and clinical description. *Clin. Infect. Dis.* **2014**, 59: 1225-1233.

95. Alraddadi, B.M.; Watson, J.T.; Almarashi, A.; Abedi, G.R.; Turkistani, A.; Sadran, M.; Housa, A.; Almazroa, M.A.; Alraihan, N.; Banjar, A.; Albalawi, E.; Alhindi, H.; Choudhry, A.J.; Meiman, J.G.; Paczkowski, M.; Curns, A.; Mounts, A.; Feikin, D.R.; Marano, N.; Swerdlow, D.L.; Gerber, S.I.; Hajjeh, R.; Madani, T.A. Risk Factors for Primary Middle East Respiratory Syndrome Coronavirus Illness in Humans, Saudi Arabia, 2014. *Emerg Infect Dis*. **2016**, 22(1):49-55.

96. World Health Organization. WHO statement on the eighth meeting of the IHR Emergency Committee regarding MERS-CoV. http://www.who.int/mediacentre/ (accessed on January 2, 2017)

97. Reusken, C.B.; Haagmans, B.L.; Müller, M.A.; Gutierrez, C.; Godeke, G.J.; Meyer, B.; Muth, D.; Raj, V.S.; Smits-De Vries, L.; Corman, V.M.; Drexler, .J.;, Smits, S.L.; El Tahir, Y.E.; De Sousa, R.; van Beek, J.; Nowotny, N.; van Maanen, K.; Hidalgo-Hermoso, E.; Bosch, B.J.; Rottier, P.; Osterhaus, A.; Gortázar-Schmidt, C.; Drosten, C.; Koopmans, M.P. Middle East respiratory syndrome coronavirus neutralizing serum antibodies in dromedary camels: a comparative serological study. *Lancet Infect. Dis.* **2013**, 13: 859-866.

98. De Wit, E.; Van Doremalen, N.; Falzarano, D.; Munster, V.J. SARS and MERS: recent insights into emerging coronaviruses. *Nat Rev Microbiol*. **2016**, 14(8): 523-34.

99. Al-Tawfiq, J.A.; Memish, Z.A. Managing MERS-CoV in the healthcare setting. *Hosp Pract. 1995*. **2015**, 43: 158–63.

100. Canadian Agency for Drugs and Technologies in Health. Respiratory Precautions for Protection from Bioaerosols or Infectious Agents: A Review of the Clinical Effectiveness and Guidelines. Ottowa, ON: CADTH Rapid Response Report, **2014**.

101. Chan, J.F.; Lau, S.K.; To, K.K.; Cheng, V.C.; Woo, P.C.; Yuen, K.Y. Middle East respiratory syndrome coronavirus: another zoonotic betacoronavirus causing SARS-like disease. *Clin Microbiol Rev*. **2015**, 28(2): 465-522.

102. Fehr, A.R.; Perlman, S. Coronaviruses: an overview of their replication and pathogenesis. *Methods Mol. Biol.* **2015**, 1282: 1–23.

103. Needle, D.; Lountos, G.T.; Waugh, D.S. Structures of the Middle East respiratory syndrome coronavirus 3C-like protease reveal insights into substrate specificity. *Acta Crystallogr D Biol Crystallogr*. **2015**, D71: 1102-1111.

104. Wang, N.; Shi, X.; Jiang, L.; Zhang, S.; Wang, D.; Tong, P.; Guo, D.; Fu, L.; Cui, Y.; Liu, X.; Arledge, K.C.; Chen, Y.H.; Zhang, L.; Wang, X. Structure of MERS-CoV spike receptor-binding domain complexed with human receptor DPP4. *Cell Res*. **2013**, 23: 986-993.

105. Perlman, S.; Netland, J. Coronaviruses post-SARS: update on replication and pathogenesis. *Nat Rev Microbiol*. **2009**, 7: 439-450.

106. Sawicki, S.G.; Sawicki, D.L.; Siddell, S.G. A contemporary view of coronavirus transcription. *J Virol*. **2007**, 81: 20-29.

107. Lee, H.; Lei, H.; Santarsiero, B.D.; Gatuz, J.L.; Cao, S.; Rice, A.J.; Patel, K.; Szypulinski, M.Z.; Ojeda, I.; Ghosh, A.K.; Johnson, M.E. Inhibitor recognition specificity of MERS-CoV papain-like protease may differ from that of SARS-CoV. *ACS Chem Biol*. **2015**, 10: 1456-1465.

108. De Haan, C.A.; Rottier, P.J. Molecular interactions in the assembly of coronaviruses. *Adv Virus Res*. **2005**, 64: 165-230.

109. Kuo, C.J.; Liang, P.H. Characterization and Inhibition of the Main Protease of Severe Acute Respiratory Syndrome Coronavirus. *ChemBioEng Rev*. **2015**, 2: 118-132.

110. Kumar, V.; Jung, Y.S.; Liang, P.H. Anti-SARS coronavirus agents: a patent review (2008 - present). *Expert. Opin. Ther. Pat*. **2008**, 23: 1337-1348.

111. Hilgenfeld, R.; Peiris, M. From SARS to MERS: 10 years of research on highly pathogenic human coronaviruses. *Antivir. Res*. **2013**, 100: 286-295.

112. Anand, K.; Pam, G.J.; Mesters, J.R.; Siddell, S.G.; Ziebuhr, J.; Hilgenfeld, R. Structure of coronavirus main protease reveals combination of a chymotrypsin fold with an extra α-helical domain. *EMBO J*. **2002**, 21(13): 3213-3224.

113. Tomar, S.; Johnston, M.L.; St John, S.E.; Osswald, H.L.; Nyalapatla, P.R.; Paul, L.N.; Ghosh, A.K.; Denison, M.R.; Mesecar, A.D. Ligand-induced Dimerization of Middle East Respiratory Syndrome (MERS) Coronavirus nsp5 Protease (3CLpro): Implications FOR nsp5 Regulation and the Development of Antivirals. *J Biol Chem*. **2015**, 290(32): 19403-19422.

114. Hegyi, A.; Ziebuhr, J. Conservation of substrate specificities among coronavirus main proteases. *J Gen Virol*. **2002**, 83: 595-599.

115. Berry, M.; Fielding B.C.; Gamieldien, J. Potential broad spectrum inhibitors of the coronavirus 3CLpr: A virtual screening and structure-based drug design study. *Viruses*. **2015**, 7: 6642-6660.

116. Wu, A.; Wang, Y.; Zeng, C.; Huang, X.; Xu, S.; Su, C.; Wang, M.; Chen, Y.; Guo, D. Prediction and biochemical analysis of putative cleavage sites of the 3C-like protease of Middle East respiratory syndrome coronavirus. *Virus Res*. **2015**, 208: 56-65.

117. Chan, J.F.; Li, K.S.; To, K.K.; Cheng, V.C.; Chen, H.; Yuen, K.Y. Is the discovery of the novel human betacoronavirus 2c EMC/2012 (HCoV-EMC) the beginning of another SARS-like pandemic? *J. Infect.* **2012**, 65: 477-489.

118. Zielecki, F.; Weber, M.; Eickmann, M.; Spiegelberg, L.; Zaki, A.M.; Matrosovich, M.; Becker, S.; Weber, F. Human cell tropism and innate immune system interactions of human respiratory coronavirus EMC compared to those of severe acute respiratory syndrome coronavirus. *J. Virol.* **2013**, 87: 5300-5304.

119. Kindler, E.; Jónsdóttir, H.R.; Muth, D.; Hamming, O.J.; Hartmann, R.; Rodriguez, R.; Geffers, R.; Fouchier, R.A.; Drosten, C.; Müller, M.A.; Dijkman, R.; Thiel, V. Efficient replication of the novel human betacoronavirus EMC on primary human epithelium highlights its zoonotic potential. *MBio*. **2013**, 4: e00611-00612.

120. de Wilde, A.H.; Raj, V.S.; Oudshoorn, D.; Bestebroer, T.M.; van Nieuwkoop, S.; Limpens, R.W.; Posthuma, C.C.; van der Meer, Y. Bárcena, M.; Haagmans, B.L.; Snijder, E.J.; van den Hoogen, B.G. MERS-coronavirus replication induces severe in vitro cytopathology and is strongly inhibited by cyclosporin A or interferon-α treatment. *J. Gen. Virol.* **2013**, 94: 1749–1760.

121. Falzarano, D.; de Wit, E.; Martellaro, C.; Callison, J.; Munster, V.J.; Feldmann, H. Inhibition of novel β coronavirus replication by a combination of interferon-α2b and ribavirin. *Sci Rep*. **2013**, 3: 1686.

122. Guberina, H.; Witzke, O.; Timm, J.; Dittmer, U.; Müller, M.A.; Drosten, C.; Bonin, F. A patient with severe respiratory failure caused by novel human coronavirus. *Infection*. **2013**, 42(1): 203-206.

123. Josset, L.; Menachery, V.D.; Gralinski, L.E.; Agnihothram, S.; Sova, P.; Carter, V.S.; Yount, B.L.; Graham, R.L.; Baric, R.S.; Katze, M.G. Cell host response to infection with novel human coronavirus EMC predicts potential antivirals and important differences with SARS coronavirus. *MBio*. **2013**, 4: e00165-00113.

124. Zhao, G.; Du, L.; Ma, C.; Li, Y.; Li, L.; Poon, V.K.M.; Wang, L.; Yu, F.; Zheng, B.; Jiang, S.; Zhou, Y. A safe and convenient pseudovirus-based inhibition assay to detect neutralizing antibodies and screen for viral entry inhibitors against the novel human coronavirus MERS-CoV. *Virol. J.* **2013**, 10: 266.

125. Gierer, S.; Bertram, S.; Kaup, F.; Wrensch, F.; Heurich, A.; Krämer-Kühl, A.; Welsch, K.; Winkler, M.; Meyer, B.; Drosten, C.; Dittmer, U.; von Hahn, T.; Simmons, G.; Hofmann, H.; Pöhlmann, S. The spike protein of the emerging betacoronavirus EMC uses a novel coronavirus receptor for entry, can be activated by TMPRSS2, and is targeted by neutralizing antibodies. *J. Virol.* **2013**, 87: 5502–5511.

126. Ren, Z.; Yan, L.; Zhang, N.; Guo, Y.; Yang, C.; Lou, Z.; Rao, Z. The newly emerged SARS-like coronavirus HCoV-EMC also has an 'Achilles' heel': current effective inhibitor targeting a 3C-like protease. *Protein Cell*. **2013**, 4: 248-250.

127. Kilianski, A; Mielech, A.; Deng, X.; Baker, S.C. Assessing Activity and Inhibition of MERS-CoV Papain-like and 3C-like Proteases Using Luciferase-based Biosensors. *J. Virol.* **2013**, 87(21): 11955-11962.

128. Chen, Y.; Rajashankar, K.R.; Yang, Y.; Agnihothram, S.S.; Liu, C.; Lin, Y.L.; Baric, R.S.; Li, F. Crystal structure of the receptor-binding domain from newly emerged Middle East respiratory syndrome coronavirus. *J. Virol.* **2013**, 87(19): 10777-10783.

129. Dixon, M**.** Determination of Enzyme Inhibitor Constants*. Biochem J*. **1953**, 55:170-171.

130. Morrison, J.F.; Walsh, C.T. The Behavior and Significance of Slow Binding Inhibitors*. Adv Enzymol*. **1988**, 61:201-301.

131. Brown, S.; Bernardo, M.; Li, Z.H.; Kotra, L.P.; Tanaka, Y.; Fridman, R.; Mobashery, S. Potent and Selective Mechanism-Based Inhibition of Gelatinases*. J Am Chem Soc*. **2000**, 122:6799-6800.

132. Perni, R.B.; Almquist, S.J.; Byrn, R.A.; Chandorkar, G.; Chaturvedi, P.R.; Courtney, L.F.; Decker, C.J.; Dinehart, K.; Gates, C.A.; Harbeson, S.L.; Heiser, A.; Kalkeri, G.; Kolaczkowski, E.; Lin, K.; Luong, Y.P.; Rao, B.G.; Taylor, W.P.; Thomson, J.A.; Tung, R.D.; Wei, Y.; Kwong, A.D.; Lin, C. Preclinical Profile of VX-950, a Potent, Selective, and Orally Bioavailable Inhibitor of Hepatitis C NS3/4A Serine Protease. *Antimicrob Agents Chemother*. **2006**, 50:899-909.

133. Copeland RA. Evaluation of Enzyme Inhibitors in Drug Discovery. John Wiley & Sons, Hoboken NJ. (2005).

134. Rajopalan, R.; Misialek, S.; Stevens, S.K.; Myszka, D.G.; Brandhuber, B.; Ballard, J.A.; Andrews, S.W.; Seiwert, S.D.; Kossen, K. Inhibition and Binding Kinetics of the Hepatitis C Virus NS3 Protease Inhibitor ITMN 191 Reveals Tight Binding and Slow Dissociative Behavior. *Biochemistry*. **2009**, 48:2559-2568.

135. Dou, D.; Tie, K.-C.; He, G.; Mandadapu, S. R.; Aravapalli, S.; Alliston, K. R.; Kim, Y.; Chang, K- O; Groutas, W. C. Potent Inhibition of Norwalk Virus by Cyclic Sulfamide Derivatives *Bioorg. Med. Chem*. **2011**, 19: 5975−5983.

136. Webber, S. E.; Okano, K.; Little, T. L.; Reich, S. H.; Xin, Y.; Fuhrman, S. A.; Matthews, D. A.; Love, R. A.; Hendrickson, T. F.; Patick, A. K.; Meador, J. W.; Ferre, R. A.; Brown, E. L.; Ford, C. E.; Binford, S. L.; Worland, S. T. Tripeptide Aldehyde Inhibitors of Human Rhinovirus 3C Protease: Design, Synthesis, Biological Evaluation, and Cocrystal Structure Solution of P1 Glutamine Isosteric Replacements. *J. Med. Chem*. **1998**, 41: 2786−2805.

137. (a) Lu, Y.; Liu, Y.; Xu, Z.; Li, H.; Liu, H.; Zhu, W. Halogen Bonding for Rational Drug Design and New Drug Discovery. *Expert Opin. Drug Discovery*, **2012**, 7: 375-383. (b) Scholfield, M. R.; Vander Zanden, C. M.; Carter, M.; Ho, P. S. Halogen Bonding (X-bonding): A Biological Perspective. *Protein Sci*. **2013**, 22: 139-152. (c) Zhou, P.; Huang, J.; Tian, F. Specific Noncovalent Interactions at Protein−Ligand Interface: Implications for Rational Drug Design. *Curr. Med. Chem*. **2012**, 19: 226-238.

138. Patel, D. V.; Rielly-Gauvin, K.; Ryono, D. E.; Free, C. A.; Rogers, W. L.; Smith, S. A.; DeForrest, J. M.; Oehl, R. S.; Petrillo, E. W. α-Hydroxy Phosphinyl-Based Inhibitors of Human Renin. *J. Med. Chem*. **1995**, 38: 4557-4569.

139. Kjell, D. P.; Slattery, B. J.; Semo, M. J. A Novel Nonaqueous Method for Regeneration of Aldehydes from Bisulfite Adducts. *J. Org. Chem*. **1999**, 64: 5722-5724.

140. Kim, Y.; Lovell, S.; Tiew, K.-C.; Mandadapu, S. R.; Alliston, K. R.; Battaille, K. P.; Groutas, W. C.; Chang, K.-O. Broad Spectrum Antivirals Against 3C or 3C-Like Proteases of Picornaviruses, Noroviruses and Coronaviruses. *J. Virol*. **2012**, 6: 11754-11762.

141. Kabsch, W. Automatic indexing of rotation diffraction patterns. *J. Appl. Crystallogr*. **1988**, 21: 67-72.

142. Kabsch, W. XDS. *Acta Crystallogr., Sect. D: Biol. Crystallogr*. **2010**, 66: 125-132.

143. Evans, P. R. An introduction to data reduction: space-group determination, scaling and intensity statistics. *Acta Crystallogr., Sect. D: Biol. Crystallogr*. **2011**, 67: 282-292.

144. Matthews, B. W. Solvent content of protein crystals. *J. Mol. Biol*. **1968**, 33: 491-497.

145. McCoy, A. J.; Grosse-Kunstleve, R. W.; Adams, P. D.; Winn, M. D.; Storoni, L. C.; Read, R. J. Phaser crystallographic software. *J. Appl. Crystallogr*. **2007**, 40: 658-674.

146. Adams, P. D.; Afonine, P. V.; Bunkóczi, G.; Chen, V. B.; Davis, I. W.; Echols, N.; Headd, J. J.; Hung, L.-W.; Kapral, G. J.; Grosse-Kunstleve, R. W.; McCoy, A. J.; Moriarty, N. W.; Oeffner, R.; Read, R. J.; Richardson, D. C.; Richardson, J. S.; Terwilliger, T. C.; Zwart, P. H. PHENIX: A Comprehensive Python-based System for Macromolecular Structure Solution. *Acta Crystallogr., Sect. D: Biol. Crystallogr*. **2010**, 66: 213-221.

147. Emsley, P.; Lohkamp, B.; Scott, W. G.; Cowtan, K. Features and Development of Coot. *Acta Crystallogr., Sect. D: Biol. Crystallogr*. **2010**, 66: 486-501.

148. Chen, V. B.; Arendall, W. B., III; Headd, J. J.; Keedy, D. A.; Immormino, R. M.; Kapral, G. J.; Murray, L. W.; Richardson, J. S.; Richardson, D. C. MolProbity: All-Atom Structure Validation for Macromolecular Crystallography. *Acta Crystallogr., Sect. D: Biol. Crystallogr*. **2010**, 66: 12-21.

149. Potterton, L.; McNicholas, S.; Krissinel, E.; Gruber, J.; Cowtan, K.; Emsley, P.; Murshudov, G. N.; Cohen, S.; Perrakis, A.; Noble, M. Developments in the CCP4Molecular Graphics Project. *Acta Crystallogr., Sect. D: Biol. Crystallogr*. **2004**, 60: 2288-2294.

150. Perry, J. W.; Ahmed, M.; Chang, K. O.; Donato, N. J.; Showalter, H. D.; Wobus, C. E. Antiviral Activity of a Small Molecule Deubiquitinase Inhibitor Occurs via Induction of the Unfolded Protein Response. *PLoS Pathog*. **2012**, 8 (7): e1002783.

151. (a) Tiew, K-C.; He, G.; Aravapalli, S.; Mandadapu, S. R.; Gunnam, M. R.; Alliston KR, Lushington GH, Kim Y, Chang K-O, Groutas WC. Design, Synthesis, and Evaluation of Inhibitors of Norwalk Virus 3C Protease *Bioorg. Med. Chem. Lett.* **2011**, 21, 5315-5319; (b) Mandadapu, S. R.; Weerawarna, P. M.; Gunnam, M. R.; Alliston, K. R.; Lushington, G. H.; Kim, Y.; Chang, K-O; Groutas, W. C. Potent Inhibition of Norovirus 3CL Protease by Peptidyl α-Ketoamides and α-Ketoheterocycles*. Bioorg. Med. Chem. Lett.* **2012**, 22, 4820-4826; (c) Mandadapu, S. R.; Gunnam, M. R.; Tiew, K-C.; Uy, R. A. Z.; Prior, A. M.; Alliston, K. R.; Hua, D. H.; Kim, Y.; Chang, K-O.; Groutas, W. C. Inhibition of Norovirus mue3CL Protease by Bisulfite Adducts of Transition State Inhibitors. *Bioorg. Med. Chem. Lett.* **2013**, 23, 62-65; (d) Prior, A. M.; Kim, Y.; Weerasekara, S.; Moroze, M.; Alliston, K. R.; Uy, R. A. Z.; Groutas, W. C.; Chang, K-O.; Hua, D. H. Design, Synthesis, and Bioevaluation of Viral 3C and 3C-like Protease Inhibitors. *Bioorg. Med. Chem. Lett.* **2013**, 23, 6317-6320; (e) Mandadapu, S. R.; Gunnam, M. R.; Kankanamalage, A. C. G.; Uy, R. A. Z.; Alliston, K. R.; Lushington, G.H.; Kim, Y.; Chang, K-O.; Groutas, W. C. Potent Inhibition of Norovirus by Dipeptidyl α- Hydroxyphosphonate Transition State Mimics *Bioorg. Med. Chem. Lett.* **2013**, 23, 5941-5944; (f) Mandadapu, S. R.; Weerawarna, P. M.; Prior, A. M.; Uy, R. A. Z.; Aravapalli, S.; Alliston, K. R.; Lushington, G. H.; Kim, Y.; Hua, D. H.; Chang, K-O.; Groutas, W. C. Macrocyclic Inhibitors of 3C and 3C-like Proteases of Picornavirus, Norovirus and Coronavirus*. Bioorg. Med. Chem. Lett.* **2013**, 23, 3709-3712; (g) Takahashi, D.; Kim, Y.; Lovell, S.; Prakash, O.; Groutas, W. C.; Chang, K-O. Structural and Inhibitor Studies of Norovirus 3C-Like Proteases*. Virus Res.* **2013**, 178, 437-444.

152. ***Trypsin***: De Fenza, A.; Hiene, A.; Koert, U.; Klebe, G. Understanding the Binding Selectivity Toward Trypsin and Factor Xa. *ChemMedChem* **2007**, 2: 297-308. ***Thrombin***: Sidhu, P. S.; Liang, A.; Mehta, A. Y.; Abdel Aziz, M. H.; Zhou, Q.; Desai, U. R. Rational Design of potent, Small, Synthetic Allosteric Inhibitors of Thrombin. *J. Med. Chem*. **2011**, 54: 5522-5531. ***Cathepsins***: Taggart, C. C.; Lowe, G. J.; Greene, C. M.; Mulgrew, A. T.; O'Neill, S. J.; Levine, R. L.; McElvaney, N. G.; Cathepsin, B. L, and S Cleave and Inactivate Secretory Leukoprotease Inhibitor. *J. Biol. Chem*. **2001**, 276: 33345-33352. ***Human neutrophil elastase***: Groutas, W. C.; Kuang, R.; Venkataraman, R.; Epp, J. B.; Ruan, S.; Prakash, O. Structure-Based Design of a General Class of Mechanism-Based Inhibitors of the Serine Proteinases Employing a Novel Amino Acid-Derived Heterocyclic Scaffold. *Biochemistry* **1997**, 36: 4739-4750. ***Carboxypeptidase A***: Tanaka, Y.; Grapsas, I.; Dakoji, S.; Cho, Y. J.; Mobashery, S. Conscripting the Active Site Zinc Ion in Carboxypeptidase A in Inactivation Chemistry by a New Type of Irreversible Enzyme Inactivator. *J. Am. Chem. Soc*. **1994**, 116: 7475-7480.

153. Evans, P.R. Scaling and Assessment of Data Quality. *Acta Crystallogr., Sect. D: Biol. Crystallogr*. **2006**, 62: 72-82.

154. Diederichs, K.; Karplus, P. A. Improved R-factors for Diffraction Data Analysis in Macromolecular Crystallography. *Nature Struct. Biol*. **1997**, 4: 269-275.

155. Weiss, M. S. Global Indicators of X-ray Data Quality. *J. Appl. Crystallogr*. **2001**, 34: 130-135.

156. Karplus, P. A.; K. Diederichs, K. Linking Crystallographic Model and Data Quality. *Science*. **2012**, 336: 1030-1033.

157. Evans, P.R. Biochemistry. Resolving Some Old Problems in Protein Crystallography. *Science*. **2012**, 336: 986-987.

158. Galasiti Kankanamalage, A. C.; Kim, Y.; Weerawarna, P. M.; Uy, R. A.; Damalanka, V. C.; Mandadapu, S. R.; Alliston, K. R.; Mehzabeen, N.; Battaille, K. P.; Lovell, S.; Chang, K-O.; Groutas, W. C. Structure-guided design and optimization of norovirus 3CL protease. Structure-activity relationships and biochemical, X-ray crystallographic, cell-based and in vivo studies. *J. Med. Chem.* **2015**, 58: 3144-3155.

159. Webster, S. E.; Okano, K.; Little, T. L.; Reich, S. H.; Xin, Y.; Fuhrman, S. A.; Matthews, D. A.; Love, R. A.; Hendrickson, T. F.; Patick, A. K.; Meador, J. W.; Ferre, R. A.; Brown, E. L.; Ford, C. E.; Binford, S. L.; Worland, S. T. Tripeptide aldehyde inhibitors of human rhinovirus 3C protease: design, synthesis, biological evaluation, and cocrystal structure solution of P1 glutamine isosteric replacements. *J. Med. Chem.* **1998**, 41: 2786-2805.

160. Kim, Y.; Liu, H.; Galasiti Kankanamalage, A. C.; Weerasekara, S.; Hua, D. H.; Groutas, W. C.; Chang, K-O.; Pedersen, N. C. Reversal of the progression of fatal coronavirus infection in cats by a broad-spectrum coronavirus protease inhibitor. *PLoS Pathog.* **2016**, 12(3):e1005531.

161. Vonrhein, C. et al. Data processing and analysis with the autoPROC toolbox. *Acta Crystallogr. D Biol. Crystallogr.* **2011**, 67(Pt 4): 293-302.

162. E. Krissinel, Enhanced fold recognition using efficient short fragment clustering, *J. Mol. Biochem*. **2012**, 1: 76e85.

163. Chen, K. X.; Njoroge, F. G. A Review of HCV protease inhibitors. *Curr. Opin. Investig. Drugs.* **2009**, *10*, 821-837.

164. Murkin, A. S.; Moynihan, M. M. Transition state-guided drug design for treatment of parasitic neglected tropical diseases. *Curr. Med. Chem.* **2014**, *21*, 1781-1793.

165. Schramm, V. L. Transition states, analogues, and drug development. *Chem. Biol.* **2013**, *8*, 71-81.

166. Kerns, E. H.; Di, L. Drug-like properties: concepts, structure, design and methods. Academic Press, San Diego, CA. **2008**.

167. Clas, S-D.; Sanchez, R. I.; Nofsinger, R. Chemistry-enabled drug delivery (prodrugs): recent progress and challenges. *Drug Discov. Today* **2014**, *19*, 79-87.

168. Jana, S.; Mandlekar, S.; Marathe, P. Prodrug design to improve pharmacokinetic and drug delivery properties: challenges to the discovery scientists. *Curr. Med. Chem.* **2010**, *17*, 3874-3908.

169. Muhazhiri, Z.; Deng, L.; Shanker, S.; Sankaran, B.; Estes, M. K.; Palzkill, T.; Song, Y.; Venkataraman Prasad, B. V. Structural basis of substrate specificity and protease inhibition in Norwalk virus. *J. Virol.* **2013**, 87, 4281-4292.

170. Allaire, M.; Chernaia, M. M.; Malcolm, B. A.; James, M. N. Picornaviral 3C cysteine proteinases have a fold similar to chymotrypsin-like serine proteinases. *Nature* **1994**, *369*, 72-76.

171. Malcolm, B. A. The picornaviral 3C proteinases: Cysteine nucleophiles in serine proteinase folds. *Protein Sci.* **1995**, *4*, 1439-1445.

172. Bender, D. M.; Peterson, J. A.; McCarthy, J. R.; Gunaydin, H.; Takano, Y.; Houk, K. N. Cyclopropane carboxylic acid esters as potential prodrugs with enhanced hydrolytic stability. *Org. Lett.* **2008**, *10*, 509-511.

173. Levine, M. N.; Raines, R. T. Trimethyl lock: a trigger for molecular release in Chemistry, Biology, and Pharmacology. *Chem. Sci*. **2012**, *3*, 2412-2420.

174. Vacondio, F.; Bassi, M.; Silva, C.; Castelli, R.; Carmi, C.; Scalvini, L.; Lodola, A.; Vivo, V.; Flammini, L.; Barocelli, E.; Mor, M.; Rivara, S. Amino acid derivatives as palmitoylethanolamide prodrugs: Synthesis, in vitro metabolism and in vivo plasma profile in rats. *PLoS One* **2015**, *10*, e0128699.

175. Weerawarna, P. M.; Kim, Y.; Galasiti Kankanamalage, A. C.; Damalanka, V. C.; Lushington, G. H.; Alliston, K. R.; Mehzabeen, N.; Battaille, K. P.; Lovell, S.; Chang, K-O.; Groutas, W. C. Structure-based design and synthesis of triazole-based macrocyclic inhibitors of norovirus protease: structural, biochemical, spectroscopic and antiviral studies. *Eur. J. Med. Chem.* **2016**, *25*, 300-318.

176. Tiew, K-C.; He, G.; Aravapalli, S.; Mandadapu, S. R.; Gunnam, M. R.; Alliston K. R, Lushington GH, Kim Y, Chang K-O, Groutas WC. Design, synthesis, and evaluation of inhibitors of Norwalk virus 3C protease. *Bioorg. Med. Chem. Lett.* **2011**, 21, 5315-5319.

177. Marshall, N.J.; Goodwin, C.J.; Holt, S.J. A critical assessment of the use of microculture tetrazolium assays to measure cell growth and function. *Growth Regul*. **1995**, 5, 69-84.

178. Houston, J.B. Utility of in vitro drug metabolism data in predicting in vivo metabolic clearance. *Biochem Pharmacol*, **1994**, 47, 1469-1479.

179. Banker, M.J.; Clark, T.H.; Williams, J.A. Development and validation of a 96-well equilibrium dialysis apparatus for measuring plasma protein binding. *J Pharm Sci,* **2003**, 92, 967-974.

180. The nomenclature used is that of Schechter, I. & Berger, A. *Biochem. Biophys. Res. Comm.* **1967**, *27*, 157-162 where the residues on the N-terminus side of the peptide bond that is cleaved are designated as P_1-P_n and those on the C-terminus side are designated P_1'-P_n'. The corresponding active site subsites are designated S_1-S_n and S_1'-S_n'. S_1 is the primary substrate specificity subsite and P_1-P_1' is the scissile bond.

181. Galasiti Kankanamalage, A.C.; Kim, Y.; Rathnayake, A.D.; Damalanka, V.C.; Weerawarna, P.M.; Doyle, S.T.; Alsoudi, A.F.; Dissanayake, D.M.; Lushington, G.H.; Mehzabeen, N.; Battaile, K.P.; Lovell, S.; Chang, K-O.; Groutas, W.C. Structure-based exploration and exploitation of the S4 subsite of norovirus 3CL protease in the design of potent and permeable inhibitors. *Eur J Med Chem*. **2017**, 126: 502-516.

182. Tao, M.; Bihovsky, R.; Wells, G.J.; Mallamo, J.P. Novel peptide phosphorous derivatives as Inhibitors of Human Calpain I. *J Med Chem*. **1998**, 41: 3912-3916.

183. Tao, M.; Bihovsky, R.; Kauer, J.C. Inhibition of calpain by peptidyl heterocycles. *Bioorg Med Chem Lett*. **1996**, 6: 3009-3012.